Fundamental Theories of Physics 189

Francisco S.N. Lobo *Editor*

Wormholes, Warp Drives and Energy Conditions

Springer

Fundamental Theories of Physics

Volume 189

The international monograph series “Fundamental Theories of Physics” aims to stretch the boundaries of mainstream physics by clarifying and developing the theoretical and conceptual framework of physics and by applying it to a wide range of interdisciplinary scientific fields. Original contributions in well-established fields such as Quantum Physics, Relativity Theory, Cosmology, Quantum Field Theory, Statistical Mechanics and Nonlinear Dynamics are welcome. The series also provides a forum for non-conventional approaches to these fields. Publications should present new and promising ideas, with prospects for their further development, and carefully show how they connect to conventional views of the topic. Although the aim of this series is to go beyond established mainstream physics, a high profile and open-minded Editorial Board will evaluate all contributions carefully to ensure a high scientific standard.

More information about this series at http://www.springer.com/series/6001

Francisco S.N. Lobo
Editor

Wormholes, Warp Drives and Energy Conditions

Springer

Editor
Francisco S.N. Lobo
Departamento de Física da FCUL
Lisbon
Portugal

ISSN 0168-1222 ISSN 2365-6425 (electronic)
Fundamental Theories of Physics
ISBN 978-3-319-55181-4 ISBN 978-3-319-55182-1 (eBook)
DOI 10.1007/978-3-319-55182-1

Library of Congress Control Number: 2017936326

Printed on acid-free paper

This Springer imprint is published by Springer Nature
The registered company is Springer International Publishing AG
The registered company address is: Gewerbestrasse 11, 6330 Cham, Switzerland

Preface

The General Theory of Relativity is an extremely successful theory, with a well-established experimental footing, at least for weak gravitational fields. Its predictions range from the existence of black holes, gravitational radiation (now confirmed) to the cosmological models, predicting a primordial beginning, namely the big-bang. All these solutions have been obtained by first considering a plausible distribution of matter, and through the Einstein field equation, the spacetime metric of the geometry is determined. However, one may solve the Einstein field equation in the reverse direction, namely one first considers an interesting and exotic spacetime metric and then finds the matter source responsible for the respective geometry. In this manner, it was found that some of these solutions possess a peculiar property, namely "exotic matter," involving a stress-energy tensor that violates the null energy condition. These geometries also allow closed timelike curves, with the respective causality violations. It is thus perhaps important to emphasize that these solutions are primarily useful as "gedanken-experiments" and as a theoretician's probe of the foundations of general relativity, and include traversable wormholes and superluminal "warp drive" spacetimes. This book, in addition to extensively exploring interesting features, in particular, the physical properties and characteristics of these "exotic spacetimes," is meant to present a state of the art of wormhole physics, warp drive spacetimes and recent research on the energy conditions. The ideal audience is intended for undergraduate and postgraduate students, with a knowledge of general relativity, and researchers in the field, who are interested in exploring new avenues of research in these topics.

More specifically, in this book, general relativistic rotating wormhole solutions, supported by a phantom scalar field, are presented. The properites of these rotating wormhole solutions including their mass, angular momentum, quadrupole moment, and ergosphere are discussed, and the stability issues are explored. Concerning the astrophysical signatures, physical properties and characteristics of matter forming thin accretion disks in wormhole geometries are analyzed. It is shown that specific signatures appear in the electromagnetic spectrum of thin disks around wormhole spacetimes, thus leading to the possibility of distinguishing these geometries by using astrophysical observations of the emission spectra from accretion disks.

Explicit examples of globally regular static, spherically symmetric solutions in general relativity are also constructed with scalar and electromagnetic fields, describing traversable wormholes with flat and AdS asymptotics and regular black holes, in particular, black universes. (A black universe is a regular black hole with an expanding, asymptotically isotropic spacetime beyond the horizon.) Such objects exist in the presence of scalar fields with negative kinetic energy ("phantoms," or "ghosts"), which are not observed under usual physical conditions. To account for that, "trapped ghosts" (scalars whose kinetic energy is only negative in a strong-field region of spacetime) are considered, as well as "invisible ghosts," i.e., phantom scalar fields sufficiently rapidly decaying in the weak-field region. Self-sustained traversable wormholes, which are configurations sustained by their own gravitational quantum fluctuations, are also considered. The investigation is evaluated by means of a variational approach with Gaussian trial wave functionals to one loop, and the graviton quantum fluctuations are interpreted as a kind of *exotic energy*. It is shown that for every framework, the self-sustained equation will produce a Wheeler wormhole of Planckian size. Some consequences on topology change are discussed together with the possibility of obtaining an enlarged wormhole radius.

In the context of modified theories of gravity, it is shown that the higher-order curvature terms, interpreted as a gravitational fluid, can effectively sustain wormhole geometries, while the matter threading the wormhole can be imposed to satisfy the energy conditions. In this context, a systematic analysis of static spherically symmetric solutions describing a wormhole geometry in a Horndeski model with Galileon shift symmetry is presented. In addition to this, working in a metric-affine framework, explicit models are explored in four and higher dimensions. It is shown that these solutions represent explicit realizations of the concept of geon introduced by Wheeler, interpreted as topologically nontrivial self-consistent bodies generated by an electromagnetic field without sources. Several of their properties are discussed. Furthermore, using exactly solvable models, it is shown that black hole singularities in different electrically charged configurations can be cured. These solutions describe black hole spacetimes with a wormhole giving structure to the otherwise point-like singularity. It is shown that geodesic completeness is satisfied despite the existence of curvature divergences at the wormhole throat. In some cases, physical observers can go through the wormhole, and in other cases, the throat lies at an infinite affine distance. The removal of singularities occurs in a nonperturbative way.

Quantum field theory violates all the classical energy conditions of general relativity. Nonetheless, it turns out that quantum field theories satisfy remnants of the classical energy conditions, known as quantum energy inequalities (QEIs), that have been developed by various authors since the original pioneering work of Ford in 1978. Here, an introduction to QEIs is introduced, as well as to some of the techniques of quantum field theory in curved spacetime (particularly, the use of microlocal analysis together with the algebraic formulation of QFT) that enable rigorous and general QEIs to be derived. Specific examples are computed for the free scalar field, and their consequences are discussed. QEIs are also derived for the

class of unitary, positive energy conformal field theories in two spacetime dimensions. In that setting, it is also possible to determine the probability distribution for individual measurements of certain smearings of the stress-energy tensor in the vacuum state. Semiclassical quantum effects also typically violate the energy conditions. The characteristics of a nonlinear energy condition and the flux energy condition (FEC) are also studied, and a quantum version of this energy condition (QFEC) is presented, which is satisfied even in more situations of physical interest. Other possible nonlinear energy conditions are introduced, namely the "trace-of-square" (TOSEC) and "determinant" (DETEC) energy conditions.

While General Relativity (GR) ranks undoubtedly among the best physical theories ever developed, it is also among those with the most striking implications. In particular, GR admits solutions that allow faster-than-light motion and consequently allow closed timelike curves, with the respective causality violations, such as warp drive spacetimes. The basic definition and interesting aspects of these spacetimes are extensively discussed, such as the violation of the energy conditions associated with these spacetimes, the appearance of horizons for the superluminal case, and the possibility of using a warp drive to create closed timelike curves. Applying linearized gravity to the weak-field warp drive, it is found that the energy condition violations in this class of spacetimes are generic to these geometries and are not simply a side effect of the superluminal properties. Furthermore, a "preemptive" chronology protection mechanism is considered that destabilizes superluminal warp drives via quantum matter back-reaction and hence forbids even the conceptual possibility to use these solutions for building a time machine. This result will be considered both in standard quantum field theory in curved spacetime and in the case of a quantum field theory with Lorentz invariance breakdown at high energies. Some lessons and future perspectives will be finally discussed.

Lisbon, Portugal
December 2016

Francisco S.N. Lobo

Acknowledgements

I would like to thank all those who have accompanied me in the elaboration of this book, in particular, Miguel Alcubierre, Carlos Barceló, Kirill A. Bronnikov, Christopher J. Fewster, Remo Garattini, Tiberiu Harko, Burkhard Kleihaus, Zoltán Kovács, Jutta Kunz, Stefano Liberati, Prado Martín-Moruno, Gonzalo J. Olmo, Diego Rubiera-Garcia, Sergey Sushkov, and Matt Visser, for their excellent contributions and for their patience and understanding.

I am grateful to the Instituto de Astrofísica e Ciências do Espaço, Universidade de Lisboa and the Departamento de Física da Faculdade de Ciências da Universidade de Lisboa, where this work was carried out, for the use of the physical resources available. Many of the figures and calculations in this work were done with the aid of the Maple and grtensor software programs. I also acknowledge financial support of the Fundação para a Ciência e Tecnologia through an Investigador FCT Research contract, with reference IF/00859/2012, funded by FCT/MCTES (Portugal).

Contents

Acronyms

AFEC	Averaged flux energy condition
AGN	Active galactic nuclei
ANCC	Averaged null convergence condition
ANEC	Averaged null energy condition
ASEC	Averaged strong condition
ATCC	Averaged timelike convergence condition
AWEC	Averaged weak energy condition
CCC	Closed chronological curve
CFT	Conformal field theory
CTC	Closed timelike curve
DEC	Dominant energy condition
DETEC	Determinant energy condition
FEC	Flux energy condition
FTL	Faster than light
GR	General Relativity
NCC	Null convergence condition
NEC	Null energy condition
NED	Nonlinear electrodynamics
QDEC	Quantum dominant energy condition
QDEI	Quantum Dominated Energy Inequality
QEI	Quantum Energy Inequality
QFEC	Quantum flux energy condition
QFT	Quantum field theory
QG	Quantum gravity
QNEI	Quantum Null Energy Inequality
QWEC	Quantum weak energy condition
QWEI	Quantum Weak Energy Inequality
RSET	Renormalized stress-energy tensor
SAWEC	Spacetime averaged weak energy condition
SEC	Strong energy condition

SET	Stress-energy tensor
TCC	Timelike convergence condition
TM	Time machine
TOSEC	Trace-of-square energy condition
UV	Ultra-violet
WEC	Weak energy condition

Chapter 1
Introduction

Francisco S.N. Lobo

1.1 Historical Background

Traversable wormholes and "warp drive" spacetimes are solutions to the Einstein field equation that violate the classical energy conditions and are primarily useful as "gedanken-experiments" and as a theoretician's probe of the foundations of general relativity. They are obtained by solving the Einstein field equation in the reverse direction, namely, one first considers an interesting and exotic spacetime metric, then finds the matter source responsible for the respective geometry. It is interesting to note that they allow "effective" superluminal travel, although the speed of light is not surpassed *locally*, and generate closed timelike curves, with the associated causality violations.

Wormhole physics can originally be tentatively traced back to Flamm in 1916 [1, 2], where his aim was to render the conclusions of the Schwarzschild solution in a clearer manner. Recall that Schwarzschild published two remarkable papers in 1916, where the first is related to the exterior static and spherically symmetric vacuum solution [3], and the second to the interior solution of a general relativistic incompressible fluid [4]. Flamm in his paper showed through sketches of an equatorial plane that the spatial sections of Schwarzschild's interior solution possess the geometry of a portion of a round sphere. Furthermore, he showed that the surface of revolution is isometric to a planar section of the Schwarzschild exterior solution. Now, he considered that the meridional curve is a parabola, where the surface of revolution joins two asymptotically flat sheets, which in a modern terminology can be considered as a tunnel. However, we emphasize that he was not contemplating the possibility of bridge-like, or wormhole-like, solutions [2].

It was only in 1935, that specific wormhole-type solutions were considered by Einstein and Rosen [5]. Their motivation was to construct an elementary particle

F.S.N. Lobo (✉)
Faculdade de Ciências, Instituto de Astrofísica e Ciências do Espaço,
Universidade de Lisboa, 1749-016 Campo Grande, Lisboa, Portugal
e-mail: fslobo@fc.ul.pt

F.S.N. Lobo (ed.), *Wormholes, Warp Drives and Energy Conditions*,
Fundamental Theories of Physics 189, DOI 10.1007/978-3-319-55182-1_1

model represented by a "bridge" connecting two identical sheets. This mathematical representation of physical space being connected by a wormhole-type solution was subsequently denoted as an "Einstein–Rosen bridge". In fact, the neutral version of the Einstein–Rosen bridge is an observation that a suitable coordinate change seems to make the Schwarzschild (coordinate) singularity disappear, at $r = 2M$. In particular, Einstein and Rosen discovered that certain coordinate systems naturally cover only two asymptotically flat regions of the maximally extended Schwarzschild spacetime. Thus, the key ingredient of the bridge construction is the existence of an event horizon, and the Einstein–Rosen bridge is a coordinate artefact arising from choosing a coordinate patch, which is defined to double-cover the asymptotically flat region exterior to the black hole event horizon.

The field lay dormant for approximately two decades after the work by Einstein and Rosen, and it was only in 1955 that John Wheeler began to be interested in topological issues in General Relativity [6]. More specifically, in a multiply-connected spacetime, where two widely separated regions were connected by a tunnel, and taking into account the coupled Einstein–Maxwell field equations, Wheeler constructed hypothesized "geon" solutions. These denote a "gravitational-electromagnetic entity" and in modern language, the geon may be considered as a hypothetical "unstable gravitational-electromagnetic quasisoliton" [7]. Building on this work, in 1957, Misner and Wheeler presented an extensive analysis, where Riemannian geometry of manifolds of nontrivial topology was investigated with an ambitious view to explain all of physics [8]. Their objective was essentially to use the source-free Maxwell equations, coupled to Einstein gravity, in the context of nontrivial topology, to build models for classical electrical charges and all other particle-like entities in classical physics. Indeed, this work was one of the first uses of abstract topology, homology, cohomology, and differential geometry in physics [7] and their point of view is best summarized by the phrase: "Physics is geometry". It is interesting to note that this is also the first paper [8] that introduces the term "wormhole". In fact, Misner and Wheeler considered that the existing well-established "already unified classical theory" allows one to describe in terms of empty curved space [8] the following concepts: *gravitation without gravitation*; *electromagnetism without electromagnetism*; *charge without charge*; and *mass without mass* (where around the mouth of the "wormhole" lies a concentration of electromagnetic energy that gives mass to this region of space).

Despite of the fact that considerable effort was invested in attempting to understand the "geon" concept, the geonlike-wormhole structures seem to have been considered a mere curiosity and after the solutions devised by Wheeler and Misner, there is a 30-year gap between their original work and the 1988 Morris–Thorne renaissance of wormhole physics [9]. However, isolated pieces of work appeared in the 1970s, such as the Homer Ellis' drainhole [10, 11] concept and Bronnikov's tunnel-like solutions [12]. It is only in 1988 that a renaissance of wormhole physics took place, through the seminal paper by Morris and Thorne [9]. In 1995, Matt Visser wrote a full-fledged treatise on wormhole physics and we refer the reader to [13] for a more recent review on wormhole physics and warp drive spacetimes.

1.2 State of the Art: Wormhole Geometries and Warp Drive Spacetimes

The purpose of the present book is to provide an update on the state of the art on several topics of research in wormhole physics and warp drive spacetimes. Although rather incomplete in all the existing topics, we present the relevant fields of modern research in this interesting topic throughout the book.

In Chap. 2, the basics of wormhole physics are briefly reviewed, where the interesting properties and characteristics of static spherically symmetric traversable wormholes are considered, such as, the mathematics of embedding, equations of structure for the wormhole, the traversability conditions, the necessity of exotic matter to support these geometries and wormhole solutions in modified gravity. Furthermore, recent advances are presented on dynamic spherically symmetric thin-shell traversable wormholes. More specifically, a novel approach is considered in the stability analysis of thin-shell wormholes, by reversing the logic flow and the surface mass is determined as a function of the potential. This procedure implicitly makes demands on the equation of state of the matter residing on the transition layer, and demonstrates in full generality that the stability of thin-shell wormholes is equivalent to choosing suitable properties for the material residing on the thin shell.

In Chap. 3, rotating wormholes in General Relativity are presented in four and five dimensions. Their nontrivial topology is supported by a phantom field, and it is shown that the wormhole solutions depend on three parameters, which are associated with the size of the throat, the magnitude of the rotation, and the symmetry of the two asymptotic regions. The physical properties of these wormholes are discussed in detail. Their global charges are derived, including the mass formulae for the symmetric and nonsymmetric cases, and their geometry is discussed, a definition of their throat is presented in the nonsymmetric case, and their ergoregions are investigated. Furthermore, the existence of limiting configurations are demonstrated, which correspond to extremal rotating vacuum black holes. Since a stability analysis of rotating wormholes in four dimensions is very involved, a stability analysis of five-dimensional rotating wormholes is performed, with equal magnitude of the angular momenta only, where the investigation is restricted to the unstable radial modes. It is interesting to note that when the rotation is sufficiently fast, the radial instability disappears for these five dimensional wormholes.

In Chap. 4, the observational and astrophysical features are considered and the physical properties of matter forming thin accretion disks in static spherically symmetric and stationary axially symmetric wormhole spacetimes are discussed. The time averaged energy flux, the disk temperature and the emission spectra of the accretion disks are obtained for these exotic geometries, and are compared with the Schwarzschild and Kerr solutions, respectively. For static and spherically symmetric wormholes it is shown that more energy is emitted from the disk than in the case of the Schwarzschild potential and the conversion efficiency of the accreted mass into radiation is more than a factor of two higher for wormholes than for static black holes. For axially symmetric wormhole spacetimes, by comparing the mass accretion

with the one of a Kerr black hole, it is verified that the intensity of the flux emerging from the disk surface is greater for wormholes than for rotating black holes with the same geometrical mass and accretion rate. Furthermore, it is shown that the rotating wormholes provide a much more efficient engine for the transformation of the accretion mass into radiation than the Kerr black holes. It is then concluded that specific signatures appear in the electromagnetic spectrum, thus leading to the possibility of distinguishing wormhole geometries by using astrophysical observations of the emission spectra from accretion disks.

In Chap. 5, wormhole geometries in modified gravity are considered, in particular, a systematic analysis of static spherically symmetric solutions describing a wormhole geometry in a specific Horndeski model with Galileon shift symmetry is presented. The Lagrangian of the theory contains the term $(\varepsilon g^{\mu\nu} + \eta G^{\mu\nu})\phi_{,\mu}\phi_{,\nu}$ and represents a particular case of the general Horndeski lagrangian, which leads to second-order equations of motion. The Rinaldi approach is used to construct analytical solutions describing wormholes with nonminimal kinetic coupling. It is shown that wormholes exist only if $\varepsilon = -1$ (phantom case) and $\eta > 0$. The wormhole throat connects two anti-de Sitter spacetimes. The wormhole metric has a coordinate singularity at the throat. However, since all curvature invariants are regular, there is no curvature singularity there.

In Chap. 6, *self sustained* traversable wormholes are considered, which are configurations sustained by their own gravitational quantum fluctuations. The analysis is evaluated by means of a variational approach with Gaussian trial wave functionals to one loop, and the graviton quantum fluctuations are interpreted as a kind of *exotic energy*. Since these fluctuations usually produce ultra-violet divergences, two procedures to keep them under control are introduced. The first consists of a zeta function regularization and a renormalization process that is introduced to obtain a finite one loop energy. The second approach considers the case of *distorted gravity*, namely, when either Gravity's Rainbow or a noncommutative geometry is used as a tool to keep under control the ultra-violet divergences. In this context, it is shown that for every framework, the self-sustained equation will produce a Wheeler wormhole of Planckian size. Some consequences on topology change are discussed together with the possibility of obtaining an enlarged wormhole radius.

Chapter 7 reviews the properties of static and spherically symmetric configurations of general relativity with a minimally coupled scalar field ϕ, whose kinetic energy is negative in a restricted (strong-field) region of space and positive outside it. This "trapped ghost" concept may, in principle, explain why no ghosts are observed under usual weak-field conditions. The configurations considered are wormholes and regular black holes without a center in particular, black universes (black holes with an expanding cosmology beyond the event horizon). Spherically symmetric perturbations of these objects are considered, and it is stressed that, due to the universal shape of the effective potential near a transition surface from canonical to phantom behavior of the scalar field, such surfaces restrict the possible perturbations and play a stabilizing role.

In Chap. 8, an explicit implementation of geons in the context of gravitational theories extending General Relativity is discussed in detail. Such extensions are

formulated in the *Palatini* approach, where the metric and affine connection are regarded as independent entities. This formulation is inspired on the macroscopic description of the physics of crystalline structures with defects in the context of solid state physics. Several theories for the gravitational field are discussed, including additional contributions of the Ricci tensor in four and higher dimensions. As opposed to the standard metric approach, which generically develops higher order derivative field equations and ghost-like instabilities, the Palatini formulation generates ghost-free and second-order equations that reduce to the general relativistic equations in vacuum. In this context, static and spherically symmetric solutions with electric fields generate a plethora of wormhole solutions satisfying the classical energy conditions, and whose properties allow to identify them with the concept of the geon, originally introduced by Wheeler. These solutions provide new insights on the avoidance of spacetime singularities in classical effective geometries.

The standard energy conditions of classical general relativity are (mostly) linear in the stress–energy tensor, and have clear physical interpretations in terms of geodesic focussing, but suffer the significant drawback that they are often violated by semi-classical quantum effects. In contrast, it is possible to develop non-standard energy conditions that are intrinsically non-linear in the stress–energy tensor, and which exhibit much better well-controlled behavior when semi-classical quantum effects are introduced, at the cost of a less direct applicability to geodesic focussing. In Chap. 9, a review of the standard energy conditions and their various limitations is presented. (Including the connection to the Hawking–Ellis type I, II, III, and IV classification of stress-energy tensors). One then turns to the averaged, nonlinear, and semi-classical energy conditions, and see how much can be done once semi-classical quantum effects are included.

Chapter 10 surveys the violation of classical energy conditions in quantum field theory (QFT) and the theory of Quantum Energy Inequalities (QEIs). The latter QEIs are lower bounds on local averages of energy densities and related quantities in QFT. They replace the classical energy conditions of classical general relativity. In particular, (a) the main properties of QEIs are indicated using the example of a free scalar field in Minkowski spacetime; (b) a rigorous derivation of a QEI for scalar fields in general curved spacetimes is given; (c) the resulting QEI is evaluated explicitly in some specific cases; (d) further recent developments, including QEIs for conformal field theories and an integrable QFT are presented, along with work on the probability distribution for measurements of averaged energy densities; (e) the status of QEIs in interacting models is discussed; (f) various applications of the QEIs are presented.

Moving on to "warp drive" spacetimes, the basic definition is considered and interesting aspects of these spacetimes are explored, in Chap. 11. In particular, the violation of the energy conditions associated with these spacetimes is discussed, as well as some other interesting properties such as the appearance of horizons for the superluminal case, and the possibility of using a warp drive to create closed timelike curves. Applying linearized gravity to the weak-field warp drive, it is found that the energy condition violations in this class of spacetimes is generic to the form of the geometry under consideration and is not simply a side-effect of the "superluminal"

properties. Fundamental limitations of "warp drive" spacetimes are also found, by proving extremely stringent conditions placed on these geometries.

An interesting aspect of the warp drive resides in the fact that points on the outside front edge of a superluminal bubble are always spacelike separated from the centre of the bubble. This implies that an observer in a spaceship cannot create nor control on demand an Alcubierre bubble. However, causality considerations do not prevent the crew of a spaceship from arranging, by their own actions, to complete a round trip from the Earth to a distant star and back in an arbitrarily short time, as measured by clocks on the Earth, by altering the metric along the path of their outbound trip. Thus, Krasnikov introduced a metric with an interesting property that although the time for a one-way trip to a distant destination cannot be shortened, the time for a round trip, as measured by clocks at the starting point (e.g., Earth), can be made arbitrarily short. Interesting properties of this solution, denoted as the Krasnikov tube are presented such as its four-dimensional generalization, the violations of the energy condition, among other features. Finally, the generation of closed timelike curves are considered in the warp spacetime and the Krasnikov tube.

Faster than light travel and time machines are among the most tantalizing possibilities allowed for by Einstein's General Relativity. In Chap. 12, the main features of these phenomena are reviewed, namely, in which spacetimes they appear to be realized, and it is explained why they are interconnected with the Einsteinian framework. The paradoxes related to the possibility of time travel of the proposed solutions are then briefly discussed. Finally, an explicit example is provided where a purely semi-classical gravity framework seems sufficient to prevent the stability of a spacetime allowing faster than light propagation. It is argued that this supports a sort of "pre-emptive" chronology protection that forbids the generation of the very spacetime structures which could lead to the construction of time machines.

Acknowledgements FSNL acknowledges financial support of the Fundação para a Ciência e Tecnologia through an Investigador FCT Research contract, with reference IF/00859/2012, funded by FCT/MCTES (Portugal).

References

1. Flamm L. Beitrage zur Einsteinschen Gravitationstheorie. Phys Z. 1916;17:448.
2. Gibbons GW. Editorial note to: Ludwig Flamm, Republication of: contributions to Einsteins theory of gravitation. Gen Relativ Gravit. 2015;47:72.
3. Schwarzschild K. Über das Gravitationsfeld eines Massenpunktes nach der Einsteinschen Theorie. Sitzungsberichte der Kööniglich Preussischen Akademie der Wissenschaften zu Berlin. Phys Math Kl. 1916;189–196. (Translated into English in. Gen Relativ Gravit. 2003;35:951–959.
4. Schwarzschild K. Über das Gravitationsfeld einer Kugel aus inkompressible Flüssigkeit nach der Einsteinschen Theorie. Sitzungsberichte der Königlich Preussischen Akademie der Wissenschaften zu Berlin. Phys Math Kl. 1916;424–434.
5. Einstein A, Rosen N. The particle problem in the general theory of relativity. Phys Rev. 1935;48:73–7.

6. Wheeler JA. Geons. Phys Rev. 1955;97:511–36.
7. Visser M. Lorentzian wormholes: from Einstein to Hawking. New York: American Institute of Physics; 1995.
8. Misner CW, Wheeler JA. Classical physics as geometry: gravitation, electromagnetism, unquantized charge, and mass as properties of curved empty space. Annals Phys. 1957;2:525.
9. Morris MS, Thorne KS. Wormholes in space-time and their use for interstellar travel: a tool for teaching general relativity. Am J Phys. 1988;56:395–412.
10. Ellis HG. Ether flow through a drainhole: a particle model in general relativity. J Math Phys. 1973;14:104.
11. Ellis HG. The evolving, flowless drain hole: a nongravitating particle model in general relativity theory. Gen Rel Grav. 1979;10:105–23.
12. Bronnikov KA. Scalar-tensor theory and scalar charge. Acta Phys Pol B. 1973;4:251.
13. Lobo FSN. Exotic solutions in general relativity: traversable wormholes and 'warp drive' spacetimes. Classical and quantum gravity research. New York: Nova Science Publishers; 2008. p. 1–78 ISBN 978-1-60456-366-5.

Part I
Traversable Wormholes

Chapter 2
Wormhole Basics

Francisco S.N. Lobo

2.1 Static and Spherically Symmetric Traversable Wormholes

2.1.1 Spacetime Metric

Throughout this book, unless stated otherwise, we will consider the following spherically symmetric and static wormhole solution [1]

$$ds^2 = -e^{2\Phi(r)}\,dt^2 + \frac{dr^2}{1-b(r)/r} + r^2\,(d\theta^2 + \sin^2\theta\,d\phi^2)\,. \tag{2.1}$$

The metric functions $\Phi(r)$ and $b(r)$ are arbitrary functions of the radial coordinate r. As $\Phi(r)$ is related to the gravitational redshift, it has been denoted the redshift function, and $b(r)$ is called the shape function, as it determines the shape of the wormhole [1–3], which will be shown below using embedding diagrams. The radial coordinate r is non-monotonic in that it decreases from $+\infty$ to a minimum value r_0, representing the location of the throat of the wormhole, where $b(r_0) = r_0$, and then increases from r_0 to $+\infty$. Although the metric coefficient g_{rr} becomes divergent at the throat, which is signalled by the coordinate singularity, the proper radial distance $l(r) = \pm \int_{r_0}^{r} [1 - b(r)/r]^{-1/2}\,dr$ is required to be finite everywhere. The proper distance decreases from $l = +\infty$, in the upper universe, to $l = 0$ at the throat, and then from zero to $-\infty$ in the lower universe. One must verify the absence of horizons,

F.S.N. Lobo (✉)
Faculdade de Ciências, Instituto de Astrofísica e Ciências do Espaço,
Universidade de Lisboa, Campo Grande, 1749-016 Lisboa, Portugal
e-mail: fslobo@fc.ul.pt

F.S.N. Lobo (ed.), *Wormholes, Warp Drives and Energy Conditions*,
Fundamental Theories of Physics 189, DOI 10.1007/978-3-319-55182-1_2

in order for the wormhole to be traversable. This condition must imply that $g_{tt} = -e^{2\Phi(r)} \neq 0$, so that $\Phi(r)$ must be finite everywhere.[1]

Another interesting feature of the redshift function is that its derivative with respect to the radial coordinate also determines the "attractive" or "repulsive" nature of the geometry. In order to verify this, consider the four-velocity of a static observer given by $U^\mu = dx^\mu/d\tau = (e^{-\Phi(r)}, 0, 0, 0)$. The observer's four-acceleration is $a^\mu = U^\mu{}_{;\nu}\, U^\nu$, which has the following components:

$$a^t = 0\,, \qquad a^r = \Phi' \left(1 - \frac{b}{r}\right)\,, \tag{2.2}$$

where the prime denotes a derivative with respect to the radial coordinate r. Now, note that from the geodesic equation, a radially moving test particle which starts from rest initially has the equation of motion

$$\frac{d^2 r}{d\tau^2} = -\Gamma^r_{tt} \left(\frac{dt}{d\tau}\right)^2 = -a^r\,. \tag{2.3}$$

Here, a^r is the radial component of proper acceleration that an observer must maintain in order to remain at rest at constant r, θ, ϕ, so that from Eq. (2.2), a static observer at the throat for generic $\Phi(r)$ is a geodesic observer. In particular, for a constant redshift function, $\Phi'(r) = 0$, static observers are also geodesic. Thus, a wormhole is "attractive" if $a^r > 0$, i.e. observers must maintain an outward-directed radial acceleration to keep from being pulled into the wormhole. If $a^r < 0$, the geometry is "repulsive", i.e. observers must maintain an inward-directed radial acceleration to avoid being pushed away from the wormhole. Indeed, this distinction depends on the sign of Φ', as is transparent from Eq. (2.2).

2.1.2 The Mathematics of Embedding

We can use embedding diagrams to represent a wormhole and extract some useful information for the choice of the shape function, $b(r)$. Due to the spherically symmetric nature of the problem, one may consider an equatorial slice, $\theta = \pi/2$, without loss of generality. The respective line element, considering a fixed moment of time, $t = \text{const}$, is given by

$$ds^2 = \frac{dr^2}{1 - b(r)/r} + r^2\, d\phi^2\,. \tag{2.4}$$

[1] This follows from a result originally due to C.V. Vishveshwara stated as follows: In any asymptotically flat spacetime with a Killing vector ξ ($\xi = \mathbf{e_0}$ for the metric (2.1)) which (i) is the ordinary time-translation Killing vector at spatial infinity and (ii) is orthogonal to a family of three-dimensional surfaces, the 3-surface $\xi \cdot \xi = 0$, i.e. $\mathbf{e_0} \cdot \mathbf{e_0} = g_{tt} = 0$, is a null surface that cannot be crossed by any outgoing, future-directed timelike curves, i.e. a horizon.

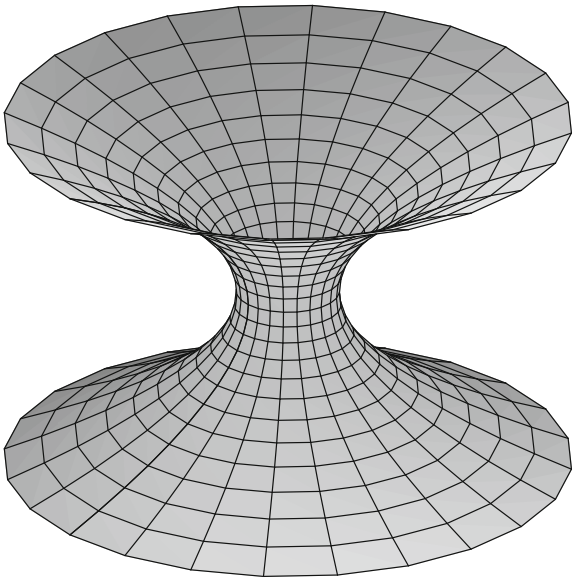

Fig. 2.1 The embedding diagram of a two-dimensional section along the equatorial plane ($t = \text{const}, \theta = \pi/2$) of a traversable wormhole. For a full visualization of the surface sweep through a 2π rotation around the $z-$axis, as can be seen from the graphic on the right

To visualize this slice, one embeds this metric into three-dimensional Euclidean space, in which the metric can be written in cylindrical coordinates, (r, ϕ, z), as

$$ds^2 = dz^2 + dr^2 + r^2\, d\phi^2\,. \tag{2.5}$$

In the three-dimensional Euclidean space the embedded surface has equation $z = z(r)$, so that the metric of the surface can be written as

$$ds^2 = \left[1 + \left(\frac{dz}{dr}\right)^2\right] dr^2 + r^2\, d\phi^2\,. \tag{2.6}$$

Comparing Eq. (2.4) with (2.6), one deduces the equation for the embedding surface, which is given by

$$\frac{dz}{dr} = \pm\left(\frac{r}{b(r)} - 1\right)^{-1/2}\,. \tag{2.7}$$

To be a solution of a wormhole, the geometry has a minimum radius, $r = b(r) = r_0$, denoted as the throat, at which the embedded surface is vertical, i.e. $dz/dr \to \infty$. Far from the throat, one may consider that space is asymptotically flat, $dz/dr \to 0$ as $r \to \infty$.

To be a solution of a wormhole, one also needs to impose that the throat flares out (see Fig. 2.1 for details). This flaring-out condition entails that the inverse of the embedding function $r(z)$ must satisfy $d^2r/dz^2 > 0$ at or near the throat r_0. Differentiating $dr/dz = \pm(r/b(r) - 1)^{1/2}$ with respect to z, we have

$$\frac{d^2r}{dz^2} = \frac{b - b'r}{2b^2} > 0\,. \tag{2.8}$$

This "flaring-out" condition is a fundamental ingredient of wormhole physics, and plays a fundamental role in the analysis of the violation of the energy conditions. At the throat we verify that the form function satisfies the condition $b'(r_0) < 1$. Note, however, that this treatment has the drawback of being coordinate dependent, and we refer the reader to Refs. [4, 5] for a covariant treatment.

2.1.3 Equations of Structure for the Wormhole

From the metric expressed in the form $ds^2 = g_{\mu\nu}\,dx^\mu\,dx^\nu$, one may determine the Christoffel symbols (connection coefficients), $\Gamma^\mu{}_{\alpha\beta}$, defined as

$$\Gamma^\mu{}_{\alpha\beta} = \frac{1}{2}\,g^{\mu\nu}\,\left(g_{\nu\alpha,\beta} + g_{\nu\beta,\alpha} - g_{\alpha\beta,\nu}\right)\,, \tag{2.9}$$

which for the metric (2.1) have the following nonzero components:

$$\begin{gathered}
\Gamma^t{}_{rt} = \Phi'\,, \qquad \Gamma^r{}_{tt} = \left(1 - \frac{b}{r}\right)\Phi'\,e^{2\Phi}\,, \qquad \Gamma^r{}_{rr} = \frac{b'r - b}{2r(r-b)}\,, \\
\Gamma^r{}_{\theta\theta} = -r + b\,, \qquad \Gamma^r{}_{\phi\phi} = -(r-b)\,\sin^2\theta\,, \\
\Gamma^\theta{}_{r\theta} = \Gamma^\phi{}_{r\phi} = \frac{1}{r}\,, \qquad \Gamma^\theta{}_{\phi\phi} = -\sin\theta\,\cos\theta\,, \qquad \Gamma^\phi{}_{\theta\phi} = \tan\theta\,.
\end{gathered} \tag{2.10}$$

The Riemann tensor is defined as

$$R^\alpha{}_{\beta\gamma\delta} = \Gamma^\alpha{}_{\beta\delta,\gamma} - \Gamma^\alpha{}_{\beta\gamma,\delta} + \Gamma^\alpha{}_{\lambda\gamma}\Gamma^\lambda{}_{\beta\delta} - \Gamma^\alpha{}_{\lambda\delta}\Gamma^\lambda{}_{\beta\gamma}\,. \tag{2.11}$$

However, the mathematical analysis and the physical interpretation is simplified using a set of orthonormal basis vectors. These may be interpreted as the proper reference frame of a set of observers who remain at rest in the coordinate system (t, r, θ, ϕ), with (r, θ, ϕ) fixed. Denote the basis vectors in the coordinate system as $(\mathbf{e}_t, \mathbf{e}_r, \mathbf{e}_\theta, \mathbf{e}_\phi)$. Thus, the orthonormal basis vectors are given by

$$\begin{cases}
\mathbf{e}_{\hat{t}} = e^{-\Phi}\,\mathbf{e}_t \\
\mathbf{e}_{\hat{r}} = (1 - b/r)^{1/2}\,\mathbf{e}_r \\
\mathbf{e}_{\hat{\theta}} = r^{-1}\,\mathbf{e}_\theta \\
\mathbf{e}_{\hat{\phi}} = (r\sin\theta)^{-1}\,\mathbf{e}_\phi
\end{cases}\,. \tag{2.12}$$

The nontrivial Riemann tensor components, given in the orthonormal reference frame, take the following form:

$$R^{\hat{t}}{}_{\hat{r}\hat{t}\hat{r}} = -R^{\hat{t}}{}_{\hat{r}\hat{r}\hat{t}} = R^{\hat{r}}{}_{\hat{t}\hat{t}\hat{r}} = -R^{\hat{r}}{}_{\hat{t}\hat{r}\hat{t}} = \left(1-\frac{b}{r}\right)\left[-\Phi'' - (\Phi')^2 + \frac{b'r-b}{2r(r-b)}\Phi'\right], \tag{2.13}$$

$$R^{\hat{t}}{}_{\hat{\theta}\hat{t}\hat{\theta}} = -R^{\hat{t}}{}_{\hat{\theta}\hat{\theta}\hat{t}} = R^{\hat{\theta}}{}_{\hat{t}\hat{t}\hat{\theta}} = -R^{\hat{\theta}}{}_{\hat{t}\hat{\theta}\hat{t}} = -\left(1-\frac{b}{r}\right)\frac{\Phi'}{r}, \tag{2.14}$$

$$R^{\hat{t}}{}_{\hat{\phi}\hat{t}\hat{\phi}} = -R^{\hat{t}}{}_{\hat{\phi}\hat{\phi}\hat{t}} = R^{\hat{\phi}}{}_{\hat{t}\hat{t}\hat{\phi}} = -R^{\hat{\phi}}{}_{\hat{t}\hat{\phi}\hat{t}} = -\left(1-\frac{b}{r}\right)\frac{\Phi'}{r}, \tag{2.15}$$

$$R^{\hat{r}}{}_{\hat{\theta}\hat{r}\hat{\theta}} = -R^{\hat{r}}{}_{\hat{\theta}\hat{\theta}\hat{r}} = R^{\hat{\theta}}{}_{\hat{r}\hat{\theta}\hat{r}} = -R^{\hat{\theta}}{}_{\hat{r}\hat{r}\hat{\theta}} = \frac{b'r-b}{2r^3}, \tag{2.16}$$

$$R^{\hat{r}}{}_{\hat{\phi}\hat{r}\hat{\phi}} = -R^{\hat{r}}{}_{\hat{\phi}\hat{\phi}\hat{r}} = R^{\hat{\phi}}{}_{\hat{r}\hat{\phi}\hat{r}} = -R^{\hat{\phi}}{}_{\hat{r}\hat{r}\hat{\phi}} = \frac{b'r-b}{2r^3}, \tag{2.17}$$

$$R^{\hat{\theta}}{}_{\hat{\phi}\hat{\theta}\hat{\phi}} = -R^{\hat{\theta}}{}_{\hat{\phi}\hat{\phi}\hat{\theta}} = R^{\hat{\phi}}{}_{\hat{\theta}\hat{\phi}\hat{\theta}} = -R^{\hat{\phi}}{}_{\hat{\theta}\hat{\theta}\hat{\phi}} = \frac{b}{r^3}, \tag{2.18}$$

where, as before, a prime denotes a derivative with respect to the radial coordinate r.

The Ricci tensor, $R_{\hat{\mu}\hat{\nu}}$, is given by the contraction $R_{\hat{\mu}\hat{\nu}} = R^{\hat{\alpha}}{}_{\hat{\mu}\hat{\alpha}\hat{\nu}}$, and the nonzero components are the following:

$$R_{\hat{t}\hat{t}} = \left(1-\frac{b}{r}\right)\left[\Phi'' + (\Phi')^2 - \frac{b'r-3b+4r}{2r(r-b)}\Phi'\right], \tag{2.19}$$

$$R_{\hat{r}\hat{r}} = -\left(1-\frac{b}{r}\right)\left[\Phi'' + (\Phi')^2 + \frac{b-b'r}{2r(r-b)}\Phi' + \frac{b-b'r}{r^2(r-b)}\right], \tag{2.20}$$

$$R_{\hat{\theta}\hat{\theta}} = R_{\hat{\phi}\hat{\phi}} = \left(1-\frac{b}{r}\right)\left[\frac{b'r+b}{2r^2(r-b)} - \frac{\Phi'}{r}\right]. \tag{2.21}$$

The curvature scalar or Ricci scalar, defined by $R = g^{\hat{\mu}\hat{\nu}}\,R_{\hat{\mu}\hat{\nu}}$, is given by

$$R = -2\left(1-\frac{b}{r}\right)\left[\Phi'' + (\Phi')^2 - \frac{b'}{r(r-b)} - \frac{b'r+3b-4r}{2r(r-b)}\,\Phi'\right]. \tag{2.22}$$

Thus, the Einstein tensor, given in the orthonormal reference frame by $G_{\hat{\mu}\hat{\nu}} = R_{\hat{\mu}\hat{\nu}} - \frac{1}{2}R\,g_{\hat{\mu}\hat{\nu}}$, yields for the metric (2.1), the following nonzero components:

$$G_{\hat{t}\hat{t}} = \frac{b'}{r^2}, \tag{2.23}$$

$$G_{\hat{r}\hat{r}} = -\frac{b}{r^3} + 2\left(1-\frac{b}{r}\right)\frac{\Phi'}{r}, \tag{2.24}$$

$$G_{\hat{\theta}\hat{\theta}} = \left(1-\frac{b}{r}\right)\left[\Phi'' + (\Phi')^2 - \frac{b'r-b}{2r(r-b)}\Phi' - \frac{b'r-b}{2r^2(r-b)} + \frac{\Phi'}{r}\right], \tag{2.25}$$

$$G_{\hat{\phi}\hat{\phi}} = G_{\hat{\theta}\hat{\theta}}, \tag{2.26}$$

respectively.

2.1.4 Stress–Energy Tensor

Through the Einstein field equation, $G_{\hat{\mu}\hat{\nu}} = 8\pi T_{\hat{\mu}\hat{\nu}}$, one verifies that the stress–energy tensor $T_{\hat{\mu}\hat{\nu}}$ has the same algebraic structure as $G_{\hat{\mu}\hat{\nu}}$, Eqs. (2.23)–(2.26), and the only nonzero components are precisely the diagonal terms $T_{\hat{t}\hat{t}}$, $T_{\hat{r}\hat{r}}$, $T_{\hat{\theta}\hat{\theta}}$ and $T_{\hat{\phi}\hat{\phi}}$. Using the orthonormal basis, these components carry a simple physical interpretation, i.e.

$$T_{\hat{t}\hat{t}} = \rho(r)\,, \qquad T_{\hat{r}\hat{r}} = -\tau(r)\,, \qquad T_{\hat{\theta}\hat{\theta}} = T_{\hat{\phi}\hat{\phi}} = p(r)\,, \tag{2.27}$$

where $\rho(r)$ is the energy density, $\tau(r)$ is the radial tension, with $\tau(r) = -p_r(r)$, i.e. it is the negative of the radial pressure, $p(r)$ is the pressure measured in the tangential directions, orthogonal to the radial direction.

Thus, the Einstein field equation provides the following stress–energy scenario:

$$\rho(r) = \frac{1}{8\pi}\frac{b'}{r^2}\,, \tag{2.28}$$

$$\tau(r) = \frac{1}{8\pi}\left[\frac{b}{r^3} - 2\left(1-\frac{b}{r}\right)\frac{\Phi'}{r}\right], \tag{2.29}$$

$$p(r) = \frac{1}{8\pi}\left(1-\frac{b}{r}\right)\left[\Phi'' + (\Phi')^2 - \frac{b'r-b}{2r^2(1-b/r)}\Phi' - \frac{b'r-b}{2r^3(1-b/r)} + \frac{\Phi'}{r}\right]. \tag{2.30}$$

Note that one now has three equations with five unknown functions of the radial coordinate. Several strategies to solve these equations are available, for instance, one can impose an equation of state [6–10] and consider a specific choice of the shape function or of the redshift function.

Note that the sign of the energy density depends on the sign of $b'(r)$. One often comes across the misleading statement, in the literature, that wormholes should necessarily be threaded by negative energy densities, or negative matter; however, this is not necessarily the case. Note, however, that due to the flaring-out condition, observers traversing the wormhole with sufficiently high velocities, $v \to 1$, will measure a negative energy density. This will be shown below. Furthermore, one should perhaps correctly state that it is the radial pressure that is necessarily negative at the throat, which is transparent for the radial tension at the throat, which is given by $p_r(r) = -\tau(r_0) = -(8\pi r_0^2)^{-1}$.

By taking the derivative with respect to the radial coordinate r, of Eq. (2.29), and eliminating b' and Φ'', given in Eqs. (2.28) and (2.30), respectively, we obtain the following equation:

$$\tau' = (\rho - \tau)\Phi' - \frac{2}{r}(p+\tau)\,. \tag{2.31}$$

Equation (2.31) is the relativistic Euler equation, or the hydrostatic equation for equilibrium for the material threading the wormhole, and can also be obtained using the conservation of the stress–energy tensor, $T^{\hat{\mu}\hat{\nu}}{}_{;\hat{\nu}} = 0$, inserting $\hat{\mu} = r$.

The effective mass, $m(r) = b(r)/2$ contained in the interior of a sphere of radius r, can be obtained by integrating Eq. (2.28), which yields

$$m(r) = \frac{r_0}{2} + \int_{r_0}^{r} 4\pi\, \rho(r')\, r'^2\, dr' \,. \tag{2.32}$$

Therefore, the form function has an interpretation which depends on the mass distribution of the wormhole.

2.1.5 Exotic Matter and Modified Gravity

2.1.5.1 Exoticity Function

To gain some insight into the matter threading the wormhole, Morris and Thorne defined the dimensionless function $\xi = (\tau - \rho)/|\rho|$ [1], which taking into account Eqs. (2.28) and (2.29) yields

$$\xi = \frac{\tau - \rho}{|\rho|} = \frac{b/r - b' - 2r(1 - b/r)\Phi'}{|b'|} \,. \tag{2.33}$$

Combining the flaring-out condition, given by Eq. (2.8), with Eq. (2.33), the exoticity function takes the form

$$\xi = \frac{2b^2}{r|b'|}\,\frac{d^2r}{dz^2} - 2r\left(1 - \frac{b}{r}\right)\frac{\Phi'}{|b'|} \,. \tag{2.34}$$

Now, taking into account the finite character of ρ, and consequently of b', and the fact that $(1 - b/r)\Phi' \to 0$ at the throat, we have the following relationship:

$$\xi(r_0) = \frac{\tau_0 - \rho_0}{|\rho_0|} > 0 \,. \tag{2.35}$$

The restriction $\tau_0 > \rho_0$ is a somewhat troublesome condition, depending on one's point of view, as it states that the radial tension at the throat should exceed the energy density. Thus, Morris and Thorne coined matter constrained by this condition "exotic matter" [1]. We shall verify below that this is defined as matter that violates the null energy condition (in fact, it violates all the energy conditions) [1, 2].

Exotic matter is particularly troublesome for measurements made by observers traversing through the throat with a radial velocity close to the speed of light. Consider a Lorentz transformation, $x^{\hat{\mu}'} = \Lambda^{\hat{\mu}'}{}_{\hat{\nu}}\, x^{\hat{\nu}}$, with $\Lambda^{\hat{\mu}}{}_{\hat{\alpha}'}\, \Lambda^{\hat{\alpha}'}{}_{\hat{\nu}} = \delta^{\hat{\mu}}{}_{\hat{\nu}}$ and $\Lambda^{\hat{\mu}}{}_{\hat{\nu}'}$ defined as

$$(\Lambda^{\hat{\mu}}{}_{\hat{\nu}'}) = \begin{bmatrix} \gamma & 0 & 0 & \gamma v \\ 0 & 1 & 0 & 0 \\ 0 & 0 & 1 & 0 \\ \gamma v & 0 & 0 & \gamma \end{bmatrix} . \tag{2.36}$$

The energy density measured by these observers is given by $T_{\hat{0}'\hat{0}'} = \Lambda^{\hat{\mu}}{}_{\hat{0}'}\, \Lambda^{\hat{\nu}}{}_{\hat{0}'}\, T_{\hat{\mu}\hat{\nu}}$, i.e.

$$T_{\hat{0}'\hat{0}'} = \gamma^2 \left(\rho_0 - v^2 \tau_0\right), \tag{2.37}$$

with $\gamma = (1 - v^2)^{-1/2}$. For sufficiently high velocities, $v \to 1$, the observer will measure a negative energy density, $T_{\hat{0}'\hat{0}'} < 0$.

This feature also holds for any traversable, nonspherical and nonstatic wormhole. To see this, one verifies that a bundle of null geodesics that enters the wormhole at one mouth and emerges from the other must have a cross-sectional area that initially increases, and then decreases. This conversion of decreasing to increasing is due to the gravitational repulsion of matter through which the bundle of null geodesics traverses.

2.1.5.2 The Violation of the Energy Conditions

The exoticity function (2.33) is closely related to the null energy condition (NEC), which asserts that for any null vector k^μ, we have $T_{\mu\nu}k^\mu k^\nu \geq 0$. For a diagonal stress–energy tensor, this implies $\rho - \tau \geq 0$ and $\rho + p \geq 0$. Using the Einstein field equations (2.28) and (2.29), evaluated at the throat r_0, and taking into account the finite character of the redshift function so that $(1 - b/r)\Phi'|_{r_0} \to 0$, we verify the condition $(\rho - \tau)|_{r_0} < 0$. This violates the NEC. In fact, it implies the violation of all the pointwise energy condition. Although classical forms of matter are believed to obey the energy conditions, it is a well-known fact that they are violated by certain quantum fields, amongst which we may refer to the Casimir effect. Thus, the flaring-out condition (2.8) entails the violation of the NEC, at the throat. Note that negative energy densities are not essential, but negative pressures are necessary to sustain the wormhole throat.

It is interesting to note that the violations of the pointwise energy conditions led to the averaging of the energy conditions over timelike or null geodesics [11]. The averaged energy conditions permit localized violations of the energy conditions, as long on average the energy conditions hold when integrated along timelike or null geodesics. Now, as the averaged energy conditions involve averaging over a line integral, with dimensions (mass)/(area), not a volume integral, they do not provide useful information regarding the "total amount" of energy condition violating matter. In order to overcome this shortcoming, the "volume integral quantifier" was proposed [12]. Thus, the amount of energy condition violations is then the extent that these integrals become negative.

2.1.5.3 Wormholes in Modified Theories of Gravity

Generally, the NEC arises when one refers back to the Raychaudhuri equation, which is a purely geometric statement, without the need to refer to any gravitational field equations. Now, in order for gravity to be attractive, the positivity condition $R_{\mu\nu}k^\mu k^\nu \geq 0$ is imposed in the Raychaudhuri equation. In general relativity, contracting both sides of the Einstein field equation $G_{\mu\nu} = \kappa^2 T_{\mu\nu}$ (where $\kappa^2 = 8\pi$) with any null vector k^μ, one can write the above condition in terms of the stress–energy tensor given by $T_{\mu\nu}k^\mu k^\nu \geq 0$, which is the statement of the NEC.

In modified theories of gravity the gravitational field equations can be rewritten as an effective Einstein equation, given by $G_{\mu\nu} = \kappa^2 T^{\rm eff}_{\mu\nu}$, where $T^{\rm eff}_{\mu\nu}$ is an effective stress–energy tensor containing the matter stress–energy tensor $T_{\mu\nu}$ and the curvature quantities, arising from the specific modified theory of gravity considered [13]. Now, the positivity condition $R_{\mu\nu}k^\mu k^\nu \geq 0$ in the Raychaudhuri equation provides the *generalized* NEC, $T^{\rm eff}_{\mu\nu}k^\mu k^\nu \geq 0$, through the modified gravitational field equation.

Therefore, the necessary condition to have a wormhole geometry is the violation of the generalized NEC, i.e. $T^{\rm eff}_{\mu\nu}k^\mu k^\nu < 0$. In classical general relativity this simply reduces to the violation of the usual NEC, i.e. $T_{\mu\nu}k^\mu k^\nu < 0$. However, in modified theories of gravity, one may in principle impose that the matter stress–energy tensor satisfies the standard NEC, $T_{\mu\nu}k^\mu k^\nu \geq 0$, while the respective generalized NEC is necessarily violated, $T^{\rm eff}_{\mu\nu}k^\mu k^\nu < 0$, in order to ensure the flaring-out condition.

More specifically, consider the generalized gravitational field equations for a large class of modified theories of gravity, given by the following field equation: [13]

$$g_1(\Psi^i)(G_{\mu\nu} + H_{\mu\nu}) - g_2(\Psi^j)\, T_{\mu\nu} = \kappa^2\, T_{\mu\nu}\,, \tag{2.38}$$

where $H_{\mu\nu}$ is an additional geometric term that includes the geometrical modifications inherent in the modified gravitational theory under consideration; $g_i(\Psi^j)$ $(i = 1, 2)$ are multiplicative factors that modify the geometrical sector of the field equations, and Ψ^j denote generically curvature invariants or gravitational fields such as scalar fields; the term $g_2(\Psi^i)$ covers the coupling of the curvature invariants or the scalar fields with the matter stress–energy tensor, $T_{\mu\nu}$.

It is useful to rewrite this field equation as an effective Einstein field equation, as mentioned above, with the effective stress–energy tensor, $T^{\rm eff}_{\mu\nu}$, given by

$$T^{\rm eff}_{\mu\nu} \equiv \frac{1 + \bar{g}_2(\Psi^j)}{g_1(\Psi^i)}\, T_{\mu\nu} - \bar{H}_{\mu\nu}\,, \tag{2.39}$$

where $\bar{g}_2(\Psi^j) = g_2(\Psi^j)/\kappa^2$ and $\bar{H}_{\mu\nu} = H_{\mu\nu}/\kappa^2$ are defined for notational convenience.

In modified gravity, the violation of the generalized NEC, $T^{\rm eff}_{\mu\nu}k^\mu k^\nu < 0$, implies the following restriction:

$$\frac{1+\bar{g}_2(\Psi^j)}{g_1(\Psi^i)}\,T_{\mu\nu}k^\mu k^\nu < \bar{H}_{\mu\nu}k^\mu k^\nu\,. \tag{2.40}$$

For general relativity, with $g_1(\Psi^j)=1$, $g_2(\Psi^j)=0$, and $H_{\mu\nu}=0$, we recover the standard violation of the NEC for the matter threading the wormhole, i.e. $T_{\mu\nu}k^\mu k^\nu < 0$.

If the additional condition $[1+\bar{g}_2(\Psi^j)]/g_1(\Psi^i) > 0$ is met, then one obtains a general bound for the normal matter threading the wormhole, in the context of modified theories of gravity, given by

$$0 \leq T_{\mu\nu}k^\mu k^\nu < \frac{g_1(\Psi^i)}{1+\bar{g}_2(\Psi^j)}\,\bar{H}_{\mu\nu}k^\mu k^\nu\,. \tag{2.41}$$

2.1.6 Traversability Conditions

In constructing traversable wormhole geometries, we will be interested in specific solutions by imposing specific traversability conditions. Assume that a traveller of an absurdly advanced civilization begins the trip in a space station in the lower universe, at proper distance $l=-l_1$, and ends up in the upper universe, at $l=l_2$. Furthermore, consider that the traveller has a radial velocity $v(r)$, as measured by a static observer positioned at r. One may relate the proper distance travelled dl, radius travelled dr, coordinate time lapse dt, and proper time lapse as measured by the observer $d\tau$, by the following relations:

$$v = e^{-\Phi}\,\frac{dl}{dt} = \mp\, e^{-\Phi}\left(1-\frac{b}{r}\right)^{-1/2}\frac{dr}{dt}\,, \tag{2.42}$$

$$v\,\gamma = \frac{dl}{d\tau} = \mp\left(1-\frac{b}{r}\right)^{-1/2}\frac{dr}{d\tau}\,. \tag{2.43}$$

It is also important to impose certain conditions at the space stations [1]. First, consider that space is asymptotically flat at the stations, i.e. $b/r \ll 1$. Second, the gravitational redshift of signals sent from the stations to infinity should be small, i.e. $\Delta\lambda/\lambda = e^{-\Phi}-1 \approx -\Phi$, so that $|\Phi| \ll 1$. The condition $|\Phi| \ll 1$ imposes that the proper time at the station equals the coordinate time. Third, the gravitational acceleration measured at the stations, given by $g=-(1-b/r)^{-1/2}\,\Phi' \simeq -\Phi'$, should be less than or equal to the Earth's gravitational acceleration, $g \leq g_\oplus$, so that the condition $|\Phi'| \leq g_\oplus$ is met.

For a convenient trip through the wormhole, certain conditions should also be imposed [1]. First, the entire journey should be done in a relatively short time as measured both by the traveller and by observers who remain at rest at the stations. Second, the acceleration felt by the traveller should not exceed the Earth's

gravitational acceleration, $g_{\oplus}$. Finally, the tidal accelerations between different parts of the traveller's body should not exceed, once again, Earth's gravity.

2.1.6.1 Total Time in a Traversal

The trip should take a relatively short time, for instance, Morris and Thorne considered 1 year, as measured by the traveller and for observers that stay at rest at the space stations, $l = -l_1$ and $l = l_2$, i.e.

$$\Delta\tau_{\text{traveller}} = \int_{-l_1}^{+l_2} \frac{dl}{v\gamma} \leq 1 \text{ year}, \tag{2.44}$$

$$\Delta t_{\text{space station}} = \int_{-l_1}^{+l_2} \frac{dl}{ve^{\Phi}} \leq 1 \text{ year}, \tag{2.45}$$

respectively.

2.1.6.2 Acceleration Felt by a Traveller

An important traversability condition required is that the acceleration felt by the traveller should not exceed Earth's gravity [1]. Consider an orthonormal basis of the traveller's proper reference frame, $(\mathbf{e}_{\hat{0}'}, \mathbf{e}_{\hat{1}'}, \mathbf{e}_{\hat{2}'}, \mathbf{e}_{\hat{3}'})$, given in terms of the orthonormal basis vectors of Eq. (2.12) of the static observers, by a Lorentz transformation, i.e.

$$\mathbf{e}_{\hat{0}'} = \gamma\, \mathbf{e}_{\hat{t}} \mp \gamma\, v\, \mathbf{e}_{\hat{r}}\ , \qquad \mathbf{e}_{\hat{1}'} = \mp\gamma\, \mathbf{e}_{\hat{r}} + \gamma\, v\, \mathbf{e}_{\hat{t}}\ , \qquad \mathbf{e}_{\hat{2}'} = \mathbf{e}_{\hat{\theta}}\ , \qquad \mathbf{e}_{\hat{3}'} = \mathbf{e}_{\hat{\phi}}\ , \tag{2.46}$$

where $\gamma = (1 - v^2)^{-1/2}$, and $v(r)$ being the velocity of the traveller as he passes r, as measured by a static observer positioned there. Thus, the traveller's four-acceleration expressed in his proper reference frame, $a^{\hat{\mu}'} = U^{\hat{\nu}'} U^{\hat{\mu}'}{}_{;\hat{\nu}'}$, yields the following restriction:

$$|\mathbf{a}| = \left| \left(1 - \frac{b}{r}\right)^{1/2} e^{-\Phi} \left(\gamma\, e^{\Phi}\right)' \right| \leq g_{\oplus}\,. \tag{2.47}$$

2.1.6.3 Tidal Acceleration Felt by a Traveller

It is also convenient that an observer traversing through the wormhole should not be ripped apart by enormous tidal forces. Thus, another of the traversability conditions required is that the tidal accelerations felt by the traveller should not exceed, for instance, the Earth's gravitational acceleration [1]. The tidal acceleration felt by the traveller is given by

$$\Delta a^{\hat{\mu}'} = -R^{\hat{\mu}'}_{\ \hat{\nu}'\hat{\alpha}'\hat{\beta}'}\, U^{\hat{\nu}'} \eta^{\hat{\alpha}'} U^{\hat{\beta}'}, \tag{2.48}$$

where $U^{\hat{\mu}'} = \delta^{\hat{\mu}'}_{\hat{0}'}$ is the traveller's four-velocity and $\eta^{\hat{\alpha}'}$ is the separation between two arbitrary parts of his body. Note that $\eta^{\hat{\alpha}'}$ is purely spatial in the traveller's reference frame, as $U^{\hat{\mu}'}\eta_{\hat{\mu}'} = 0$, so that $\eta^{\hat{0}'} = 0$. For simplicity, assume that $|\eta^{\hat{i}'}| \approx 2\,\mathrm{m}$ along any spatial direction in the traveller's reference frame. Taking into account the antisymmetric nature of $R^{\hat{\mu}'}_{\ \hat{\nu}'\hat{\alpha}'\hat{\beta}'}$ in its first two indices, we verify that $\Delta a^{\hat{\mu}'}$ is purely spatial with the components

$$\Delta a^{\hat{i}'} = -R^{\hat{i}'}_{\ \hat{0}'\hat{j}'\hat{0}'}\, \eta^{\hat{j}'} = -R_{\hat{i}'\hat{0}'\hat{j}'\hat{0}'}\, \eta^{\hat{j}'}. \tag{2.49}$$

Using a Lorentz transformation of the Riemann tensor components in the static observer's frame, $(\mathbf{e}_{\hat{t}}, \mathbf{e}_{\hat{r}}, \mathbf{e}_{\hat{\theta}}, \mathbf{e}_{\hat{\phi}})$, to the traveller's frame, $(\mathbf{e}_{\hat{0}'}, \mathbf{e}_{\hat{1}'}, \mathbf{e}_{\hat{2}'}, \mathbf{e}_{\hat{3}'})$, the nonzero components of $R_{\hat{i}'\hat{0}'\hat{j}'\hat{0}'}$ are given by

$$\begin{aligned} R_{\hat{1}'\hat{0}'\hat{1}'\hat{0}'} &= R_{\hat{r}\hat{t}\hat{r}\hat{t}} \\ &= -\left(1-\frac{b}{r}\right)\left[-\Phi'' - (\Phi')^2 + \frac{b'r-b}{2r(r-b)}\Phi'\right], \end{aligned} \tag{2.50}$$

$$\begin{aligned} R_{\hat{2}'\hat{0}'\hat{2}'\hat{0}'} &= R_{\hat{3}'\hat{0}'\hat{3}'\hat{0}'} \;=\; \gamma^2\, R_{\hat{\theta}\hat{t}\hat{\theta}\hat{t}} + \gamma^2 v^2\, R_{\hat{\theta}\hat{r}\hat{\theta}\hat{r}} \\ &= \frac{\gamma^2}{2r^2}\left[v^2\left(b' - \frac{b}{r}\right) + 2(r-b)\Phi'\right]. \end{aligned} \tag{2.51}$$

Thus, Eq. (2.49) takes the form

$$\Delta a^{\hat{1}'} = -R_{\hat{1}'\hat{0}'\hat{1}'\hat{0}'}\, \eta^{\hat{1}'}, \qquad \Delta a^{\hat{2}'} = -R_{\hat{2}'\hat{0}'\hat{2}'\hat{0}'}\, \eta^{\hat{2}'}, \qquad \Delta a^{\hat{3}'} = -R_{\hat{3}'\hat{0}'\hat{3}'\hat{0}'}\, \eta^{\hat{3}'}. \tag{2.52}$$

The constraint $|\Delta a^{\hat{\mu}'}| \leq g_{\oplus}$ provides the tidal acceleration restrictions as measured by a traveller moving radially through the wormhole, given by the following inequalities:

$$\left|\left(1-\frac{b}{r}\right)\left[\Phi'' + (\Phi')^2 - \frac{b'r-b}{2r(r-b)}\Phi'\right]\right| \left|\eta^{\hat{1}'}\right| \leq g_{\oplus}, \tag{2.53}$$

$$\left|\frac{\gamma^2}{2r^2}\left[v^2\left(b' - \frac{b}{r}\right) + 2(r-b)\Phi'\right]\right| \left|\eta^{\hat{2}'}\right| \leq g_{\oplus}. \tag{2.54}$$

The radial tidal constraint, Eq. (2.53), constrains the redshift function, and the lateral tidal constraint, Eq. (2.54), constrains the velocity with which observers traverse the wormhole. These inequalities are particularly simple at the throat, r_0,

$$|\Phi'(r_0)| \leq \frac{2g_\oplus r_0}{(1-b')\,|\eta^{\hat{1}'}|}\,, \tag{2.55}$$

$$\gamma^2 v^2 \leq \frac{2g_\oplus r_0^2}{(1-b')\,|\eta^{\hat{2}'}|}\,, \tag{2.56}$$

For the particular case of a constant redshift function, $\Phi' = 0$, the radial tidal acceleration is zero, and Eq. (2.54) reduces to

$$\frac{\gamma^2 v^2}{2r^2}\left|\left(b' - \frac{b}{r}\right)\right| |\eta^{\hat{2}'}| \leq g_\oplus\,. \tag{2.57}$$

For this specific case one verifies that stationary observers with $v = 0$ measure null tidal forces.

2.2 Dynamic Spherically Symmetric Thin-Shell Traversable Wormholes

An interesting and efficient manner to minimize the violation of the null energy condition is to construct thin-shell wormholes using the thin-shell formalism [2, 14] and the cut-and-paste procedure as described in [2, 15–18]. Motivated in minimizing the usage of exotic matter, the thin-shell construction was generalized to nonspherically symmetric cases [2, 15], and in particular, it was found that a traveller may traverse through such a wormhole without encountering regions of exotic matter. In the context of a linearized stability analysis [16], two Schwarzschild spacetimes were surgically grafted together in such a way that no event horizon is permitted to form. This surgery concentrates a nonzero stress energy on the boundary layer between the two asymptotically flat regions and a dynamical stability analysis (with respect to spherically symmetric perturbations) was explored. In the latter stability analysis, constraints were found on the equation of state of the exotic matter that comprises the throat of the wormhole. Indeed, the stability of the latter thin-shell wormholes was considered for certain specially chosen equations of state [2, 16], where the analysis addressed the issue of stability in the sense of proving bounded motion for the wormhole throat.

This dynamical analysis was generalized to the stability of spherically symmetric thin-shell wormholes by considering linearized radial perturbations around some assumed static solution of the Einstein field equations, without the need to specify an equation of state [18]. This linearized stability analysis around a static solution was soon generalized to the presence of charge [19], and of a cosmological constant [20], and was subsequently extended to a plethora of individual scenarios (see [21] and references therein). The key point of the present section is to develop an extremely general, flexible, and robust framework that can quickly be adapted to general spherically symmetric traversable wormholes in $3+1$ dimensions see [21].

We shall consider standard general relativity, with traversable wormholes that are spherically symmetric, with all of the exotic material confined to a thin shell.

2.2.1 Generic Static Spherically Symmetric Spacetimes

To set the stage, consider two distinct spacetime manifolds, $\mathcal{M}_+$ and $\mathcal{M}_-$, with metrics given by $g^+_{\mu\nu}(x^\mu_+)$ and $g^-_{\mu\nu}(x^\mu_-)$, in terms of independently defined coordinate systems x^μ_+ and x^μ_-. A single manifold $\mathcal{M}$ is obtained by gluing together the two distinct manifolds, $\mathcal{M}_+$ and $\mathcal{M}_-$, i.e. $\mathcal{M} = \mathcal{M}_+ \cup \mathcal{M}_-$, at their boundaries. The latter are given by Σ_+ and Σ_-, respectively, with the natural identification of the boundaries $\Sigma = \Sigma_+ = \Sigma_-$.

Consider two generic static spherically symmetric spacetimes given by the following line elements:

$$ds^2 = -e^{2\Phi_\pm(r_\pm)}\left[1 - \frac{b_\pm(r_\pm)}{r_\pm}\right]dt^2_\pm + \left[1 - \frac{b_\pm(r_\pm)}{r_\pm}\right]^{-1} dr^2_\pm + r^2_\pm d\Omega^2_\pm, \quad (2.58)$$

on $\mathcal{M}_\pm$, respectively. Using the Einstein field equation, $G_{\mu\nu} = 8\pi\, T_{\mu\nu}$ (with $c = G = 1$), the (orthonormal) stress–energy tensor components are given by

$$\rho(r) = \frac{1}{8\pi r^2} b', \quad (2.59)$$

$$\bar{\tau}(r) = \frac{1}{8\pi r^2}\left[2\Phi'(b - r) + b'\right], \quad (2.60)$$

$$p_t(r) = -\frac{1}{16\pi r^2}\big[(-b + 3rb' - 2r)\Phi' + 2r(b - r)(\Phi')^2 + 2r(b - r)\Phi'' + b''r\big], \quad (2.61)$$

where we have denoted the quantity $\bar{\tau}(r)$ here as the radial tension (the variable τ in this section denotes the proper time, as measured by a comoving observer on the thin shell). The $\pm$ subscripts were (temporarily) dropped so as not to overload the notation.

2.2.2 Extrinsic Curvature

The manifolds are bounded by hypersurfaces Σ_+ and Σ_-, respectively, with induced metrics g^+_{ij} and g^-_{ij}. The hypersurfaces are isometric, i.e. $g^+_{ij}(\xi) = g^-_{ij}(\xi) = g_{ij}(\xi)$, in terms of the intrinsic coordinates, invariant under the isometry. As mentioned above, a single manifold $\mathcal{M}$ is obtained by gluing together $\mathcal{M}_+$ and $\mathcal{M}_-$ at their boundaries, i.e. $\mathcal{M} = \mathcal{M}_+ \cup \mathcal{M}_-$, with the natural identification of the boundaries

$\Sigma = \Sigma_+ = \Sigma_-$. The three holonomic basis vectors $\mathbf{e}_{(i)} = \partial/\partial\xi^i$ tangent to Σ have the following components $e^{\mu}_{(i)}|_{\pm} = \partial x^{\mu}_{\pm}/\partial\xi^i$, which provide the induced metric on the junction surface by the following scalar product $g_{ij} = \mathbf{e}_{(i)} \cdot \mathbf{e}_{(j)} = g_{\mu\nu} e^{\mu}_{(i)} e^{\nu}_{(j)}|_{\pm}$. The intrinsic metric to Σ is thus provided by

$$ds^2_{\Sigma} = -d\tau^2 + a^2(\tau)\,(d\theta^2 + \sin^2\theta\, d\phi^2), \tag{2.62}$$

where τ is the proper time of an observer comoving with the junction surface, as mentioned above.

Thus, for the static and spherically symmetric spacetime considered in this section, the single manifold, $\mathscr{M}$, is obtained by gluing $\mathscr{M}_+$ and $\mathscr{M}_-$ at Σ, i.e. at $f(r,\tau) = r - a(\tau) = 0$. The position of the junction surface is given by

$$x^{\mu}(\tau,\theta,\phi) = (t(\tau), a(\tau), \theta, \phi)\,, \tag{2.63}$$

and the respective 4-velocities (as measured in the static coordinate systems on the two sides of the junction) are

$$U^{\mu}_{\pm} = \left(\frac{e^{-\Phi_{\pm}(a)}\sqrt{1 - \frac{b_{\pm}(a)}{a} + \dot{a}^2}}{1 - \frac{b_{\pm}(a)}{a}},\ \dot{a}, 0, 0 \right), \tag{2.64}$$

where the overdot denotes a derivative with respect to τ.

We shall consider a timelike junction surface Σ, defined by the parametric equation of the form $f(x^{\mu}(\xi^i)) = 0$. The unit normal 4−vector, n^{μ}, to Σ is defined as

$$n_{\mu} = \pm \left| g^{\alpha\beta} \frac{\partial f}{\partial x^{\alpha}} \frac{\partial f}{\partial x^{\beta}} \right|^{-1/2} \frac{\partial f}{\partial x^{\mu}}\,, \tag{2.65}$$

with $n_{\mu}\, n^{\mu} = +1$ and $n_{\mu} e^{\mu}_{(i)} = 0$. The Israel formalism requires that the normals point from $\mathscr{M}_-$ to $\mathscr{M}_+$ [14]. Thus, the unit normals to the junction surface, determined by Eq. (2.65), are given by

$$n^{\mu}_{\pm} = \pm \left(\frac{e^{-\Phi_{\pm}(a)}}{1 - \frac{b_{\pm}(a)}{a}}\, \dot{a}, \sqrt{1 - \frac{b_{\pm}(a)}{a} + \dot{a}^2}, 0, 0 \right). \tag{2.66}$$

Note that the above expressions can also be deduced from the contractions $U^{\mu} n_{\mu} = 0$ and $n^{\mu} n_{\mu} = +1$. The extrinsic curvature, or the second fundamental form, is defined as $K_{ij} = n_{\mu;\nu} e^{\mu}_{(i)} e^{\nu}_{(j)}$. Taking into account the differentiation of $n_{\mu} e^{\mu}_{(i)} = 0$ with respect to ξ^j, the extrinsic curvature is given by

$$K_{ij}^{\pm} = -n_{\mu}\left(\frac{\partial^2 x^{\mu}}{\partial\xi^i\,\partial\xi^j} + \Gamma^{\mu\pm}_{\alpha\beta}\,\frac{\partial x^{\alpha}}{\partial\xi^i}\,\frac{\partial x^{\beta}}{\partial\xi^j}\right). \tag{2.67}$$

Note that for the case of a thin shell K_{ij} is not continuous across Σ, so that for notational convenience, the discontinuity in the second fundamental form is defined as $\kappa_{ij} = K_{ij}^{+} - K_{ij}^{-}$.

Thus, using Eq. (2.67), the nontrivial components of the extrinsic curvature can easily be computed to be

$$K^{\theta\,\pm}_{\theta} = \pm\frac{1}{a}\sqrt{1 - \frac{b_{\pm}(a)}{a} + \dot{a}^2}\,, \tag{2.68}$$

$$K^{\tau\,\pm}_{\tau} = \pm\left\{\frac{\ddot{a} + \frac{b_{\pm}(a) - b'_{\pm}(a)a}{2a^2}}{\sqrt{1 - \frac{b_{\pm}(a)}{a} + \dot{a}^2}} + \Phi'_{\pm}(a)\sqrt{1 - \frac{b_{\pm}(a)}{a} + \dot{a}^2}\right\}, \tag{2.69}$$

where the prime now denotes a derivative with respect to the coordinate a.

2.2.3 *Lanczos Equations: Surface Stress–Energy*

The Lanczos equations follow from the Einstein equations applied to the hypersurface joining the four-dimensional spacetimes, and are given by

$$S^{i}_{\ j} = -\frac{1}{8\pi}\left(\kappa^{i}_{\ j} - \delta^{i}_{\ j}\kappa^{k}_{\ k}\right), \tag{2.70}$$

where $S^{i}_{\ j}$ is the surface stress–energy tensor on Σ. In particular, because of spherical symmetry considerable simplifications occur, namely $\kappa^{i}_{\ j} = \text{diag}\left(\kappa^{\tau}_{\tau}, \kappa^{\theta}_{\theta}, \kappa^{\theta}_{\theta}\right)$. The surface stress–energy tensor may be written in terms of the surface energy density, σ, and the surface pressure, $\mathscr{P}$, as $S^{i}_{\ j} = \text{diag}(-\sigma, \mathscr{P}, \mathscr{P})$. The Lanczos equations then reduce to

$$\sigma = -\frac{1}{4\pi}\,\kappa^{\theta}_{\theta}\,, \tag{2.71}$$

$$\mathscr{P} = \frac{1}{8\pi}(\kappa^{\tau}_{\tau} + \kappa^{\theta}_{\theta})\,. \tag{2.72}$$

Taking into account the computed extrinsic curvatures, Eqs. (2.68) and (2.69), we see that Eqs. (2.71) and (2.72) provide us with the following expressions for the surface stresses:

$$\sigma = -\frac{1}{4\pi a}\left[\sqrt{1-\frac{b_+(a)}{a}+\dot{a}^2}+\sqrt{1-\frac{b_-(a)}{a}+\dot{a}^2}\right], \tag{2.73}$$

$$\mathscr{P} = \frac{1}{8\pi a}\left[\frac{1+\dot{a}^2+a\ddot{a}-\frac{b_+(a)+ab'_+(a)}{2a}}{\sqrt{1-\frac{b_+(a)}{a}+\dot{a}^2}}+\sqrt{1-\frac{b_+(a)}{a}+\dot{a}^2}\,a\Phi'_+(a)\right.$$
$$\left.+\frac{1+\dot{a}^2+a\ddot{a}-\frac{b_-(a)+ab'_-(a)}{2a}}{\sqrt{1-\frac{b_-(a)}{a}+\dot{a}^2}}+\sqrt{1-\frac{b_-(a)}{a}+\dot{a}^2}\,a\Phi'_-(a)\right]. \tag{2.74}$$

Note that the surface energy density σ is always negative, consequently violating the energy conditions. The surface mass of the thin shell is given by $m_s = 4\pi a^2\sigma$, which will be used below.

2.2.4 Conservation Identity

The first contracted Gauss–Codazzi equation is given by

$$G_{\mu\nu}\,n^\mu\,n^\nu = \frac{1}{2}\left(K^2 - K_{ij}K^{ij} - {}^3R\right), \tag{2.75}$$

which combined with the Einstein equations provides the evolution identity

$$S^{ij}\,\overline{K}_{ij} = -\left[T_{\mu\nu}n^\mu n^\nu\right]^+_- . \tag{2.76}$$

The convention $[X]^+_- \equiv X^+|_\Sigma - X^-|_\Sigma$ and $\overline{X} \equiv \frac{1}{2}(X^+|_\Sigma + X^-|_\Sigma)$ is used.

The second contracted Gauss–Codazzi equation is

$$G_{\mu\nu}e^\mu_{(i)}n^\nu = K^j_{i|j} - K_{,i}\ , \tag{2.77}$$

which together with the Lanczos equations provides the conservation identity

$$S^i_{j|i} = \left[T_{\mu\nu}\,e^\mu_{(j)}n^\nu\right]^+_- . \tag{2.78}$$

When interpreting the conservation identity Eq. (2.78), consider the momentum flux defined by

$$\left[T_{\mu\nu}\,e^\mu_{(\tau)}\,n^\nu\right]^+_- = \left[T_{\mu\nu}\,U^\mu\,n^\nu\right]^+_- = \left[\pm\left(T_{\hat{t}\hat{t}}+T_{\hat{r}\hat{r}}\right)\frac{\dot{a}\sqrt{1-\frac{b(a)}{a}+\dot{a}^2}}{1-\frac{b(a)}{a}}\right]^+_-, \tag{2.79}$$

where $T_{\hat{t}\hat{t}}$ and $T_{\hat{r}\hat{r}}$ are the four-dimensional stress–energy tensor components given in an orthonormal basis. This flux term corresponds to the net discontinuity in the momentum flux $F_\mu = T_{\mu\nu}\, U^\nu$ which impinges on the shell. Applying the Einstein equations, we have

$$\left[T_{\mu\nu}\, e^{\mu}_{(\tau)}\, n^\nu\right]^+_- = \frac{\dot{a}}{4\pi a}\left[\Phi'_+(a)\sqrt{1-\frac{b_+(a)}{a}+\dot{a}^2}+\Phi'_-(a)\sqrt{1-\frac{b_-(a)}{a}+\dot{a}^2}\right]. \tag{2.80}$$

It is useful to define the quantity

$$\Xi = \frac{1}{4\pi a}\left[\Phi'_+(a)\sqrt{1-\frac{b_+(a)}{a}+\dot{a}^2}+\Phi'_-(a)\sqrt{1-\frac{b_-(a)}{a}+\dot{a}^2}\right]. \tag{2.81}$$

and to let $A = 4\pi a^2$ be the surface area of the thin shell. Then in the general case, the conservation identity provides the following relationship:

$$\frac{d(\sigma A)}{d\tau} + \mathscr{P}\frac{dA}{d\tau} = \Xi\, A\, \dot{a}\,. \tag{2.82}$$

The first term represents the variation of the internal energy of the shell, the second term is the work done by the shell's internal force, and the third term represents the work done by the external forces.

If we assume that the equations of motion can be integrated to determine the surface energy density as a function of radius a, that is, assuming the existence of a suitable function $\sigma(a)$, then the conservation equation can be written as

$$\sigma' = -\frac{2}{a}\left(\sigma + \mathscr{P}\right) + \Xi\,, \tag{2.83}$$

where $\sigma' = d\sigma/da$. Note that the flux term Ξ is zero whenever $\Phi_\pm = 0$, which is actually a quite common occurrence, for instance in either Schwarzschild or Reissner–Nordström geometries, or more generally whenever $\rho + p_r = 0$. In particular, for a vanishing flux $\Xi = 0$ one obtains the so-called "transparency condition", $\left[G_{\mu\nu}\, U^\mu\, n^\nu\right]^+_- = 0$ [22]. The conservation identity, Eq. (2.78), then reduces to the simple relationship $\dot{\sigma} = -2\,(\sigma + \mathscr{P})\dot{a}/a$, which is extensively used in the literature.

2.2.5 Equation of Motion

To qualitatively analyse the stability of the wormhole, it is useful to rearrange Eq. (2.73) into the thin-shell equation of motion given by

$$\frac{1}{2}\dot{a}^2 + V(a) = 0\,, \tag{2.84}$$

where the potential $V(a)$ is given by

$$V(a) = \frac{1}{2}\left\{1 - \frac{\bar{b}(a)}{a} - \left[\frac{m_s(a)}{2a}\right]^2 - \left[\frac{\Delta(a)}{m_s(a)}\right]^2\right\}. \tag{2.85}$$

Here $m_s(a) = 4\pi a^2\,\sigma(a)$ is the mass of the thin shell. The quantities $\bar{b}(a)$ and $\Delta(a)$ are defined, for simplicity, as

$$\bar{b}(a) = \frac{b_+(a) + b_-(a)}{2}, \qquad \Delta(a) = \frac{b_+(a) - b_-(a)}{2}, \tag{2.86}$$

respectively. This gives the potential $V(a)$ as a function of the surface mass $m_s(a)$. By differentiating with respect to a, we see that the equation of motion implies $\ddot{a} = -V'(a)$.

It is useful to reverse the logic flow and determine the surface mass as a function of the potential. Following the techniques used in [23], suitably modified for the present wormhole context, we have

$$m_s^2(a) = 2a^2\left[1 - \frac{\bar{b}(a)}{a} - 2V(a) + \sqrt{1 - \frac{b_+(a)}{a} - 2V(a)}\sqrt{1 - \frac{b_-(a)}{a} - 2V(a)}\right], \tag{2.87}$$

and in fact

$$m_s(a) = -a\left[\sqrt{1 - \frac{b_+(a)}{a} - 2V(a)} + \sqrt{1 - \frac{b_-(a)}{a} - 2V(a)}\right], \tag{2.88}$$

with the negative root now being necessary for compatibility with the Lanczos equations. Note the novel approach used here, namely, by specifying $V(a)$ dictates the amount of surface mass that needs to be inserted on the wormhole throat. This implicitly makes demands on the equation of state of the exotic matter residing on the wormhole throat.

In a completely analogous manner, after imposing the equation of motion for the shell one has

$$\sigma(a) = -\frac{1}{4\pi a}\left[\sqrt{1 - \frac{b_+(a)}{a} - 2V(a)} + \sqrt{1 - \frac{b_-(a)}{a} - 2V(a)}\right], \tag{2.89}$$

$$\begin{aligned}\mathscr{P}(a) = \frac{1}{8\pi a}\Bigg[&\frac{1 - 2V(a) - aV'(a) - \frac{b_+(a) + ab'_+(a)}{2a}}{\sqrt{1 - \frac{b_+(a)}{a} - 2V(a)}} + \sqrt{1 - \frac{b_+(a)}{a} - 2V(a)}\,a\Phi'_+(a)\\ &+ \frac{1 - 2V(a) - aV'(a) - \frac{b_-(a) + ab'_-(a)}{2a}}{\sqrt{1 - \frac{b_-(a)}{a} - 2V(a)}} + \sqrt{1 - \frac{b_-(a)}{a} - 2V(a)}\,a\Phi'_-(a)\Bigg].\end{aligned} \tag{2.90}$$

and the flux term is given by

$$\Xi(a) = \frac{1}{4\pi a}\left[\Phi'_{+}(a)\sqrt{1-\frac{b_{+}(a)}{a}-2V(a)}+\Phi'_{-}(a)\sqrt{1-\frac{b_{-}(a)}{a}-2V(a)}\right]. \tag{2.91}$$

The three quantities $\{\sigma(a),\ \mathscr{P}(a),\ \Xi(a)\}$ are related by the differential conservation law, so at most two of them are independent.

2.2.6 Linearized Equation of Motion

Consider a linearization around an assumed static solution a_0 to the equation of motion $\frac{1}{2}\dot{a}^2 + V(a) = 0$, and so also a solution of $\ddot{a} = -V'(a)$. A Taylor expansion of $V(a)$ around a_0 to second order yields

$$V(a) = V(a_0) + V'(a_0)(a-a_0) + \frac{1}{2}V''(a_0)(a-a_0)^2 + O[(a-a_0)^3], \tag{2.92}$$

and since we are expanding around a static solution, $\dot{a}_0 = \ddot{a}_0 = 0$, we automatically have $V(a_0) = V'(a_0) = 0$, which reduces Eq. (2.92) to

$$V(a) = \frac{1}{2}V''(a_0)(a-a_0)^2 + O[(a-a_0)^3]. \tag{2.93}$$

The assumed static solution at a_0 is stable if and only if $V(a)$ has a local minimum at a_0, which requires $V''(a_0) > 0$, which is the primary criterion for wormhole stability.

For instance, it is extremely useful to express $m'_s(a)$ and $m''_s(a)$ by the following expressions:

$$m'_s(a) = +\frac{m_s(a)}{a} + \frac{a}{2}\left\{\frac{(b_{+}(a)/a)' + 2V'(a)}{\sqrt{1-b_{+}(a)/a-2V(a)}} + \frac{(b_{-}(a)/a)' + 2V'(a)}{\sqrt{1-b_{-}(a)/a-2V(a)}}\right\}, \tag{2.94}$$

and

$$\begin{aligned} m''_s(a) = {} & \left\{\frac{(b_{+}(a)/a)' + 2V'(a)}{\sqrt{1-b_{+}(a)/a-2V(a)}} + \frac{(b_{-}(a)/a)' + 2V'(a)}{\sqrt{1-b_{-}(a)/a-2V(a)}}\right\} \\ & + \frac{a}{4}\left\{\frac{[(b_{+}(a)/a)' + 2V'(a)]^2}{[1-b_{+}(a)/a-2V(a)]^{3/2}} + \frac{[(b_{-}(a)/a)' + 2V'(a)]^2}{[1-b_{-}(a)/a-2V(a)]^{3/2}}\right\} \\ & + \frac{a}{2}\left\{\frac{(b_{+}(a)/a)'' + 2V''(a)}{\sqrt{1-b_{+}(a)/a-2V(a)}} + \frac{(b_{-}(a)/a)'' + 2V''(a)}{\sqrt{1-b_{-}(a)/a-2V(a)}}\right\}. \end{aligned} \tag{2.95}$$

Doing so allows us to easily study linearized stability, and to develop a simple inequality on $m''_s(a_0)$ using the constraint $V''(a_0) > 0$. Similar formulae hold for

$\sigma'(a)$, $\sigma''(a)$, for $\mathscr{P}'(a)$, $\mathscr{P}''(a)$, and for $\Xi'(a)$, $\Xi''(a)$. In view of the redundancies coming from the relations $m_s(a) = 4\pi\sigma(a)a^2$ and the differential conservation law, the only interesting quantities are $\Xi'(a)$, $\Xi''(a)$.

For practical calculations, it is extremely useful to consider the dimensionless quantity $m_s(a)/a$ and then to express $[m_s(a)/a]'$ and $[m_s(a)/a]''$. It is similarly useful to consider $4\pi\,\Xi(a)a$, and then evaluate $[4\pi\,\Xi(a)\,a]'$ and $[4\pi\,\Xi(a)\,a]''$ (see Ref. [21] for more details). We shall evaluate these quantities at the assumed stable solution a_0.

2.2.7 The Master Equations

For practical calculations it is more useful to work with $m_s(a)/a$, so that in view of the above, in order to have a stable static solution at a_0 we must have

$$m_s(a_0)/a_0 = -\left\{\sqrt{1-\frac{b_+(a_0)}{a_0}}+\sqrt{1-\frac{b_-(a_0)}{a_0}}\right\}, \tag{2.96}$$

while

$$[m_s(a)/a]'\big|_{a_0} = +\frac{1}{2}\left\{\frac{(b_+(a)/a)'}{\sqrt{1-b_+(a)/a}}+\frac{(b_-(a)/a)'}{\sqrt{1-b_-(a)/a}}\right\}\Bigg|_{a_0}, \tag{2.97}$$

and the stability condition $V''(a_0) \geq 0$ is translated into

$$\begin{aligned}[m_s(a)/a]''\big|_{a_0} \geq {} & +\frac{1}{4}\left\{\frac{[(b_+(a)/a)']^2}{[1-b_+(a)/a]^{3/2}}+\frac{[(b_-(a)/a)']^2}{[1-b_-(a)/a]^{3/2}}\right\}\Bigg|_{a_0}\\ & +\frac{1}{2}\left\{\frac{(b_+(a)/a)''}{\sqrt{1-b_+(a)/a}}+\frac{(b_-(a)/a)''}{\sqrt{1-b_-(a)/a}}\right\}\Bigg|_{a_0}.\end{aligned} \tag{2.98}$$

In the absence of external forces this inequality (or the equivalent one for $m_s''(a_0)$ above) is the only stability constraint one requires. However, once one has external forces ($\Phi_\pm \neq 0$), there is additional information:

$$\begin{aligned}[4\pi\,\Xi(a)\,a]'\big|_{a_0} = {} & +\left\{\Phi_+''(a)\sqrt{1-b_+(a)/a}+\Phi_-''(a)\sqrt{1-b_-(a)/a}\right\}\Big|_{a_0}\\ & -\frac{1}{2}\left\{\Phi_+'(a)\frac{(b_+(a)/a)'}{\sqrt{1-b_+(a)/a}}+\Phi_-'(a)\frac{(b_-(a)/a)'}{\sqrt{1-b_-(a)/a}}\right\}\Bigg|_{a_0},\end{aligned} \tag{2.99}$$

and (provided $\Phi_\pm'(a_0) \geq 0$)

$$
\begin{aligned}
[4\pi\, \Xi(a)\, a]''\big|_{a_0} \leq & \left\{\Phi_+'''(a)\sqrt{1-b_+(a)/a}+\Phi_-'''(a)\sqrt{1-b_-(a)/a}\right\}\Big|_{a_0} \\
& -\left\{\Phi_+''(a)\frac{(b_+(a)/a)'}{\sqrt{1-b_+(a)/a}}+\Phi_-''(a)\frac{(b_-(a)/a)'}{\sqrt{1-b_-(a)/a}}\right\}\Big|_{a_0} \\
& -\frac{1}{4}\left\{\Phi_+'(a)\frac{[(b_+(a)/a)']^2}{[1-b_+(a)/a]^{3/2}}+\Phi_-'(a)\frac{[(b_-(a)/a)']^2}{[1-b_-(a)/a]^{3/2}}\right\}\Big|_{a_0} \\
& -\frac{1}{2}\left\{\Phi_+'(a)\frac{(b_+(a)/a)''}{\sqrt{1-b_+(a)/a}}+\Phi_-'(a)\frac{(b_-(a)/a)''}{\sqrt{1-b_-(a)/a}}\right\}\Big|_{a_0}. \qquad (2.100)
\end{aligned}
$$

If $\Phi_\pm'(a_0) \leq 0$, we simply have

$$
\begin{aligned}
[4\pi\, \Xi(a)\, a]''\big|_{a_0} \geq & \left\{\Phi_+'''(a)\sqrt{1-b_+(a)/a}+\Phi_-'''(a)\sqrt{1-b_-(a)/a}\right\}\Big|_{a_0} \\
& -\left\{\Phi_+''(a)\frac{(b_+(a)/a)'}{\sqrt{1-b_+(a)/a}}+\Phi_-''(a)\frac{(b_-(a)/a)'}{\sqrt{1-b_-(a)/a}}\right\}\Big|_{a_0} \\
& -\frac{1}{4}\left\{\Phi_+'(a)\frac{[(b_+(a)/a)']^2}{[1-b_+(a)/a]^{3/2}}+\Phi_-'(a)\frac{[(b_-(a)/a)']^2}{[1-b_-(a)/a]^{3/2}}\right\}\Big|_{a_0} \\
& -\frac{1}{2}\left\{\Phi_+'(a)\frac{(b_+(a)/a)''}{\sqrt{1-b_+(a)/a}}+\Phi_-'(a)\frac{(b_-(a)/a)''}{\sqrt{1-b_-(a)/a}}\right\}\Big|_{a_0}. \qquad (2.101)
\end{aligned}
$$

Note that these last three equations are entirely vacuous in the absence of external forces, which is why they have not appeared in the literature until now.

In discussing specific examples one now merely needs to apply the general formalism described above. Several examples are particularly important, some to emphasize the features specific to possible asymmetry between the two universes used in traversable wormhole construction, some to emphasize the importance of NEC nonviolation in the bulk, and some to assess the simplifications due to symmetry between the two asymptotic regions [21, 24].

2.2.8 *Discussion*

These linearized stability conditions reflect an extremely general, flexible and robust framework, which is well-adapted to general spherically symmetric thin-shell traversable wormholes and, in this context, the construction confines the exotic material to the thin shell. The latter, while constrained by spherical symmetry, is allowed to move freely within the four-dimensional spacetimes, which permits a fully dynamic analysis. Note that to this effect, the presence of a flux term has been, although widely ignored in the literature, considered in great detail. This flux term corresponds to the net discontinuity in the conservation law of the surface stresses of the bulk momentum flux, and is physically interpreted as the work done by external forces on the thin shell.

Relative to the linearized stability analysis, we have reversed the logic flow typically considered in the literature, and introduced a novel approach to the analysis. We recall that the standard procedure extensively used in the literature is to define a parametrization of the stability of equilibrium, so as not to specify an equation of state on the boundary surface [18–20]. More specifically, the parameter $\eta(\sigma) = d\mathcal{P}/d\sigma$ is usually defined, and the standard physical interpretation of η is that of the speed of sound. In this section, rather than adopting the latter approach, we considered that the stability of the wormhole is fundamentally linked to the behaviour of the surface mass $m_s(a)$ of the thin shell of exotic matter, residing on the wormhole throat, via a pair of stability inequalities.

More specifically, we have considered the surface mass as a function of the potential. This novel procedure implicitly makes demands on the equation of state of the matter residing on the transition layer, and demonstrates in full generality that the stability of thin-shell wormholes is equivalent to choosing suitable properties for the material residing on the thin shell. Furthermore, specific applications were explored and we refer the reader to Ref. [21] for more details.

Acknowledgements FSNL acknowledges financial support of the Fundação para a Ciência e Tecnologia through an Investigador FCT Research contract, with reference IF/00859/2012, funded by FCT/MCTES (Portugal).

References

1. Morris MS, Thorne KS. Wormholes in space-time and their use for interstellar travel: a tool for teaching general relativity. Am J Phys. 1988;56:395–412.
2. Visser M. Lorentzian wormholes: from Einstein to Hawking. New York: American Institute of Physics; 1995.
3. Lobo FSN. Exotic solutions in General Relativity: Traversable wormholes and 'warp drive' spacetimes, Classical and Quantum Gravity Research, 1– 78, (2008), Nova Sci. Pub. ISBN 978-1-60456-366-5.
4. Hochberg D, Visser M. Null energy condition in dynamic wormholes. Phys Rev Lett. 1998;81:746.
5. Hochberg D, Visser M. Geometric structure of the generic static traversable wormhole throat. Phys Rev D. 1997;56:4745.
6. Sushkov SV. Wormholes supported by a phantom energy. Phys Rev D. 2005;71:043520. arXiv:gr-qc/0502084.
7. Lobo FSN. Phantom energy traversable wormholes. Phys Rev D. 2005;71:084011. arXiv:gr-qc/0502099.
8. Lobo FSN. Stability of phantom wormholes. Phys Rev D. 2005;71:124022. arXiv:gr-qc/0506001.
9. Lobo FSN. Chaplygin traversable wormholes. Phys Rev D. 2006;73:064028. arXiv:gr-qc/0511003.
10. Lobo FSN. Van der Waals quintessence stars. Phys Rev D. 2007;75:024023. arXiv:gr-qc/0610118.
11. Tipler FJ. Energy conditions and spacetime singularities. Phys Rev D. 1978;17:2521.
12. Visser M, Kar S, Dadhich N. Traversable wormholes with arbitrarily small energy condition violations. Phys Rev Lett. 2003;90:201102. arXiv:gr-qc/0301003.

13. Harko T, Lobo FSN, Mak MK, Sushkov SV. Modified-gravity wormholes without exotic matter. Phys Rev D. 2013;87:067504.
14. Israel W. Singular hypersurfaces and thin shells in general relativity, Nuovo Cimento **44**B, 1 (1966); and corrections in *ibid.***48**B, 463 (1966).
15. Visser M. Traversable wormholes: some simple examples. Phys Rev D. 1989;39:3182.
16. Visser M. Traversable wormholes from surgically modified Schwarzschild spacetimes. Nucl Phys B. 1989;328:203.
17. Visser M. Quantum mechanical stabilization of Minkowski signature wormholes. Phys Lett B. 1990;242:24.
18. Poisson E, Visser M. Thin shell wormholes: linearization stability. Phys Rev D. 1995;52:7318 [arXiv:gr-qc/9506083].
19. Eiroa EF, Romero GE. Linearized stability of charged thin-shell wormoles. Gen Rel Grav. 2004;36:651–9.
20. Lobo FSN, Crawford P. Linearized stability analysis of thin shell wormholes with a cosmological constant. Class Quant Grav. 2004;21:391.
21. Garcia NM, Lobo FSN, Visser M. Generic spherically symmetric dynamic thin-shell traversable wormholes in standard general relativity. Phys Rev D. 2012;86:044026.
22. Ishak M, Lake K. Stability of transparent spherically symmetric thin shells and wormholes. Phys Rev D. 2002;65:044011.
23. Visser M, Wiltshire DL. Stable gravastars: an alternative to black holes? Class Quant Grav. 2004;21:1135–52.
24. Bouhmadi-Lpez M, Lobo FSN, Martn-Moruno P. Wormholes minimally violating the null energy condition. JCAP. 2014;1411(11):007.

Chapter 3
Rotating Wormholes

Burkhard Kleihaus and Jutta Kunz

3.1 Introduction

As discussed in the previous section, General Relativity (GR) allows for traversable Lorentzian wormholes, which were first obtained by Ellis [1, 2] and Bronnikov [3] (see also [4]). These wormholes need the presence of an exotic matter field, a phantom field, coupled to gravity. Carrying the reverse sign in front of its kinetic term, a phantom field has an energy-momentum tensor that violates the null energy condition [5, 6]. In recent years phantom fields have also been considered in cosmology, since they give rise to an accelerated expansion of the Universe [7]. On the other hand, e.g. when gravity theories with higher curvature terms are considered [8–14], wormholes can be constructed without the need for a phantom field.

From an astrophysical point of view wormholes have been searched for observationally [15–17]. They have been considered as gravitational lenses [18, 19], including their Einstein rings [20], their shadows have been studied [21, 22] and also the iron line profiles of thin accretion disks surrounding them [23]. So far most investigations have been performed for static wormholes. However, astrophysical objects typically rotate. Therefore one would like to know and understand the properties of rotating wormholes. Moreover, the static Ellis wormholes of GR are known to be unstable [24–27], and the presence of rotation might possibly stabilize them [28, 29].

In this chapter we consider rotating wormholes in GR supported by a phantom field. These Ellis wormholes represent solutions of the coupled Einstein-phantom field equations, which read in D dimensions

$$R_{\mu\nu} = -2\partial_\mu\psi\,\partial_\nu\psi \ , \tag{3.1}$$

B. Kleihaus (✉) · J. Kunz
Institut für Physik, Universität Oldenburg, Postfach 2503,
26111 Oldenburg, Germany
e-mail: b.kleihaus@uni-oldenburg.de

J. Kunz
e-mail: jutta.kunz@uni-oldenburg.de

F.S.N. Lobo (ed.), *Wormholes, Warp Drives and Energy Conditions*,
Fundamental Theories of Physics 189, DOI 10.1007/978-3-319-55182-1_3

$$\partial_\mu \left(\sqrt{-g} g^{\mu\nu} \partial_\nu \psi\right) = 0 \,. \tag{3.2}$$

They are obtained from the D-dimensional action

$$S = \frac{1}{16\pi G_D} \int d^D x \sqrt{-g} \left(R + 2 g^{\mu\nu} \partial_\mu \psi \partial_\nu \psi\right) \,. \tag{3.3}$$

Our main interest concerns rotating wormholes in four dimensions. Here slowly rotating perturbative wormhole solutions have been obtained analytically some time ago [30, 31], while their rapidly rotating counterparts have been constructed numerically only recently [32, 33]. While many of their features have been studied already, a central property yet to be analyzed is their stability. Clearly, their traversability but also their viability as astrophysical objects would require a certain degree of stability. (We remark, that the well-known rotating Teo wormhole [34] only represents a metric, which was not obtained as the solution of a given set of Einstein-matter equations.)

As a first attempt to tackle the question whether rotation could stabilize wormholes, we here consider wormholes in five dimensions, since when both angular momenta are equal the problem simplifies, and one only has to deal with ordinary differential equations. Rapidly rotating wormholes in five dimensions have been constructed numerically in [29], where also many of their properties have been analyzed. In particular, a stability analysis of the unstable radial modes has been performed. Interestingly, this analysis has revealed the disappearance of the unstable radial modes beyond a critical rotational velocity. Since crucial properties of rotating black holes in four and five dimensions show qualitative agreement, this result indicates, that rotation may also stabilize rotating wormholes in four dimensions.

In Sects. 3.2 and 3.3 we discuss the currently known properties of rotating Ellis wormholes in four and five dimensions, respectively. We always begin with the theoretical setting, including the Ansatz, the boundary conditions, the global charges, and mass formulae. Subsequently, we present the results of the numerical calculations, showing a number of interesting wormhole properties such as the global charges, and the wormhole geometry. We also demonstrate that these wormhole solutions approach an extremal rotating black hole, as their angular momentum tends toward its maximal value. Moreover, we address the geodesics in wormhole spacetimes, and we discuss the properties of nonsymmetric wormholes, i.e., wormholes whose mass differs in the two asymptotic regions. Finally, in the case of the five-dimensional wormholes we present a stability analysis of the radial modes. We end with our conclusions in Sect. 3.4.

3.2 Rotating Wormholes in Four Dimensions

3.2.1 Theoretical Setting

Here our aim is to construct four-dimensional stationary rotating wormhole spacetimes and to study their properties. To take the symmetries into account, we choose an appropriate coordinate system, where the fields do not depend on the time coordinate and the azimuthal coordinate. We therefore consider the following line element

$$ds^2 = -e^f dt^2 + p^2 e^{-f} \left[e^{\nu} \left(d\eta^2 + h d\theta^2 \right) + h \sin^2\theta \, (d\varphi - \omega dt)^2 \right] . \tag{3.4}$$

Here the functions f, p, ν and ω depend only on the coordinates η and θ, and $h = \eta^2 + \eta_0^2$ is an auxiliary function. In wormhole spacetimes, the radial coordinate η takes positive and negative values, i.e., $-\infty < \eta < \infty$, where the limits $\eta \to \pm\infty$ correspond to two distinct asymptotically flat regions. The phantom field is described by the function ψ, which depends only on the coordinates η and θ, as well.

Substitution of the above line element into the equations of motion leads to a set of nonlinear partial differential equation. The equation for the function p decouples [32]

$$\partial_\eta^2 p + \frac{3\eta}{h} \partial_\eta p + \frac{2\cos\theta}{h \sin\theta} \partial_\theta p + \frac{1}{h} \partial_\theta^2 \, p = 0 \, , \tag{3.5}$$

and is solved by $p = 1$, respecting the boundary conditions $p(\eta \to \infty) = p(\eta \to -\infty) = 1$ and $\partial_\theta p(\theta = 0) = \partial_\theta p(\theta = \pi) = 0$.

On the other hand, under the assumption $\partial_\theta \psi = 0$ the phantom field equation

$$\partial_\eta \left(h \sin\theta \partial_\eta \psi \right) + \partial_\theta \left(\sin\theta \partial_\theta \psi \right) = 0 \, , \tag{3.6}$$

yields a first integral

$$\partial_\eta \psi = \frac{D}{h} \, , \tag{3.7}$$

where the phantom scalar charge is denoted by D. The phantom field can thus be obtained in closed form

$$\psi = D \left(\arctan(\eta/\eta_0) - \pi/2 \right) \, , \tag{3.8}$$

where the integration constant has been chosen such that $\psi(\infty) = 0$.

The Einstein equations $R_{\varphi\varphi} = 0$, $R_{\theta\theta} = 0$, $R_{t\varphi} = 0$, $R_{tt} = 0$ and $R_{\eta\theta} = 0$ are independent of the scalar field, yielding three second order partial differential equations for the functions f, ω and ν, together with a constraint,

$$0 = \partial_\eta \left(h \sin\theta \partial_\eta f\right) + \partial_\theta \left(\sin\theta \partial_\theta f\right) - h \sin^3\theta e^{-2f} \left(h(\partial_\eta\omega)^2 + (\partial_\theta\omega)^2\right) , \quad (3.9)$$

$$0 = \partial_\eta \left(h^2 \sin^3\theta e^{-2f} \partial_\eta\omega\right) + \partial_\theta \left(h \sin^3\theta e^{-2f} \partial_\theta\omega\right) , \quad (3.10)$$

$$0 = \partial_\eta \left(h \sin\theta \partial_\eta \nu\right) + \sin\theta \partial_{\theta\theta} \nu - \cos\theta \partial_\theta \nu - h \sin^3\theta e^{-2f} \left(h(\partial_\eta\omega)^2 - 2(\partial_\theta\omega)^2\right) , \quad (3.11)$$

$$0 = -h \sin\theta \partial_\eta f \partial_\theta f + h \cos\theta \partial_\eta \nu + \eta \sin\theta \partial_\theta \nu + h^2 \sin^3\theta e^{-2f} \partial_\eta\omega \partial_\theta\omega . \quad (3.12)$$

They are solved numerically, subject to suitable boundary conditions. For $\eta \to +\infty$ the metric should approach Minkowski spacetime,

$$f|_{\eta\to\infty} = 0 , \qquad \omega|_{\eta\to\infty} = 0 , \qquad \nu|_{\eta\to\infty} = 0 . \quad (3.13)$$

In contrast, for $\eta \to -\infty$ we allow for finite values of the functions f and ω,

$$f|_{\eta\to-\infty} = \gamma , \qquad \omega|_{\eta\to-\infty} = \omega_{-\infty} , \qquad \nu|_{\eta\to-\infty} = 0 . \quad (3.14)$$

Here a suitable coordinate transformation is necessary to obtain Minkowski spacetime asymptotically. To ensure regularity on the symmetry axis we require

$$\partial_\theta f|_{\theta=0} = 0 , \qquad \partial_\theta \omega|_{\theta=0} = 0 , \qquad \nu|_{\theta=0} = 0 , \quad (3.15)$$

together with the analogous conditions at $\theta = \pi$.

Choosing the parameter $\omega_{-\infty} = 0$, we obtain static wormholes, which are known in closed form,

$$f = \frac{\gamma}{2}\left(1 - \frac{2}{\pi} \arctan\left(\frac{\eta}{\eta_0}\right)\right) , \qquad \omega = 0 , \qquad \nu = 0 . \quad (3.16)$$

The choice of the parameter $\gamma = 0$ leads to symmetric wormholes, whereas wormholes with $\gamma \neq 0$ are nonsymmetric with respect to their mass in the two asymptotically flat regions.

Substituting the solutions of the metric functions f, ω and ν into the expression for $R_{\eta\eta}$ shows that

$$R_{\eta\eta} = -2\frac{D^2}{h^2} , \quad (3.17)$$

and yields for the scalar charge

$$D^2 = \frac{h}{4}\left[h(\partial_\eta f)^2 - (\partial_\theta f)^2\right] - \frac{h}{2}\left(\eta\partial_\eta\nu - \frac{\cos\theta}{\sin\theta}\partial_\theta\nu\right) - \frac{h^2}{4}\sin^2\theta e^{-2f}\left[h(\partial_\eta\omega)^2 - (\partial_\theta\omega)^2\right] + \eta_0^2 . \quad (3.18)$$

Now we can immediately demonstrate the violation of the Null Energy Condition (NEC). For that purpose we consider the quantity

$$\Xi = R_{\mu\nu} k^\mu k^\nu \,, \tag{3.19}$$

with null vector [31]

$$k^\mu = \left(e^{-f/2}, e^{f/2-\nu/2}, 0, \omega e^{-f/2}\right) \,. \tag{3.20}$$

Making use of the field equations shows that Ξ is non-positive

$$\Xi = -2D^2 \frac{e^{f-\nu}}{h^2} \,, \tag{3.21}$$

and the NEC is violated everywhere. To obtain a measure for the amount of the NEC violation one can introduce a global scale invariant quantity Y by integrating over an asymptotically flat hypersurface bounded by the throat.

Let us now consider the mass, the angular momentum, and the quadrupole moment of the wormholes. The global charges are engraved in the asymptotic form of the metric tensor, where

$$g_{tt} \underset{\eta\to+\infty}{\longrightarrow} -\left(1 - \frac{2M_+}{\eta}\right) \,, \qquad g_{t\varphi} \underset{\eta\to+\infty}{\longrightarrow} -\frac{2J_+ \sin^2\theta}{\eta} \,. \tag{3.22}$$

Since in the limit $\eta \to +\infty$ the wormhole metric becomes Minkowskian, we can read off the mass M_+ and the angular momentum J_+ directly from the asymptotic behavior of the metric functions

$$f \underset{\eta\to+\infty}{\longrightarrow} -\frac{2M_+}{\eta} \,, \qquad \omega \underset{\eta\to+\infty}{\longrightarrow} \frac{2J_+}{\eta^3} \,. \tag{3.23}$$

Since for $\eta \to -\infty$ the expansions read

$$f \underset{\eta\to-\infty}{\longrightarrow} \gamma + \frac{2M_-}{\eta} \,, \qquad \omega \underset{\eta\to-\infty}{\longrightarrow} \omega_{-\infty} + \frac{2J_-}{\eta^3} \,, \tag{3.24}$$

a coordinate transformation

$$\bar{t} = e^{\gamma/2} t \,, \qquad \bar{\eta} = e^{-\gamma/2}\eta \,, \qquad \bar{\varphi} = \varphi - \omega_{-\infty} t \,, \tag{3.25}$$

is needed to obtain an asymptotically flat spacetime. The mass $\bar{M}_-$ and the angular $\bar{J}_-$ then enter the asymptotic expansion of the metric in the new coordinates

$$g_{\bar{t}\bar{t}} \underset{\bar{\eta}\to-\infty}{\longrightarrow} -\left(1 + \frac{2\bar{M}_-}{\bar{\eta}}\right) \,, \qquad g_{\bar{t}\bar{\varphi}} \underset{\bar{\eta}\to-\infty}{\longrightarrow} -\frac{2\bar{J}_+ \sin^2\theta}{\bar{\eta}} \,, \tag{3.26}$$

and we obtain the mass $\bar{M}_-$ and the angular $\bar{J}_-$ in terms of the parameters M_- and J_- as follows

$$\bar{J}_- = J_- e^{-2\gamma} , \qquad \bar{M}_- = M_- e^{-\gamma/2} . \tag{3.27}$$

To see that the angular momentum is the same in both asymptotically flat regions,

$$J_+ = e^{-2\gamma} J_- = \bar{J}_- , \tag{3.28}$$

we first note that Eq. (3.10) is in the form of a conservation law, then integrate it over the full range of η and θ, and finally insert the asymptotic expansions for ω and f.

To obtain a mass formula for the wormholes, we multiply Eq. (3.10) by ω and subtract it from Eq. (3.9) to obtain another equation in the form of a conservation law

$$\partial_\eta \left(h \sin\theta \left[\partial_\eta f - e^{-2f} h \sin^2\theta \omega \partial_\eta \omega \right] \right) + \partial_\theta \left(\sin\theta \left[\partial_\theta f - e^{-2f} h \sin^2\theta \omega \partial_\theta \omega \right] \right) = 0 . \tag{3.29}$$

After integration and insertion of the asymptotic expansions of the metric functions, we find the mass formula

$$M_+ + M_- = 2\omega_{-\infty} e^{-2\gamma} J_- = 2\omega_{-\infty} J_+ . \tag{3.30}$$

For symmetric wormholes we find [32]

$$M_+ = \omega_{-\infty} J_+ = 2\omega_0 J_+, \tag{3.31}$$

i.e., a mass formula akin to the Smarr formula [35, 36] for extremal black holes. The Smarr formula is recovered when ω_0 is identified with the horizon angular velocity.

The quadrupole moment Q of rotating wormholes can be obtained from the asymptotic expansion by going to higher order [33].

We now turn to the geometric properties of the wormholes and, in particular, the wormhole throat. For symmetric wormholes it is obvious, that the wormhole throat represents an extremal surface that is located at $\eta = 0$, if it is a minimal surface. If it were a maximal surface, it would correspond to an equator, and there would be two throats located symmetrically with respect to the equator. However, we do not find Ellis wormholes with multiple throats, unless further matter fields are included (see, e.g., [37]).

For nonsymmetric wormholes it is less obvious how their throat should be defined and where it will reside. Thus to define the wormhole throat in the general case, we start by considering the equatorial (or circumferential) radius $R_e(\eta)$ as a function of the radial coordinate

$$R_e(\eta) = \sqrt{\eta^2 + \eta_0^2} \left(e^{-f/2} \right)_{\theta=\pi/2} . \tag{3.32}$$

Clearly, the rotation should deform the wormhole throat from spherical symmetry. Because of the centrifugal force, its circumference should be largest in the equatorial plane. By studying $R_e(\eta)$ therefore the location of the throat in the equatorial plane should be revealed. We now define the wormhole throat as the surface of minimal area, which intersects the equatorial plane at the circle of minimal circumferential radius R_e,

$$R_e = \min_{-\infty \le \eta \le \infty} \left\{ \sqrt{h} e^{-f/2}|_{\theta=\pi/2} \right\} . \tag{3.33}$$

To incorporate the above extremality condition we consider the line element of the surface of the throat

$$d\sigma^2 = e^{-f+\nu} \left(\eta_t'^2 + h\right) d\theta^2 + e^{-f} h \sin^2\theta d\varphi^2 , \tag{3.34}$$

where $\eta_t = \eta_t(\theta)$, $\eta_t' = d\eta_t/d\theta$, and f, ν and h are regarded as functions of η_t and θ. The area of the surface of the throat is then given by

$$A_\sigma = \int L_\sigma d\theta d\varphi \tag{3.35}$$

with the integrand

$$L_\sigma = \sqrt{\eta_t'^2 + h}\sqrt{h} \sin\theta e^{-f+\nu/2} . \tag{3.36}$$

Variation of the area functional leads to the Euler–Lagrange equation for the function $\eta_t(\theta)$

$$\frac{d}{d\theta}\frac{\partial L_\sigma}{\partial \eta_t'} - \frac{\partial L_\sigma}{\partial \eta_t} = 0 \tag{3.37}$$

or explicitly

$$\eta_t'' + h\partial_\eta s - 2\eta_t - \left[\partial_\theta s - \frac{\cos\theta}{\sin\theta}\right]\eta_t' + \left[\partial_\eta s - \frac{3\eta_t}{h}\right]\eta_t'^2 - \left[\partial_\theta s - \frac{\cos\theta}{\sin\theta}\right]\frac{1}{h}\eta_t'^3 = 0 , \tag{3.38}$$

where $s = f - \nu/2$. The appropriate solution of this equation, which represents the throat, should satisfy the following physical conditions: Regularity at the pole requires $\eta_t'(0) = 0$, and in the equatorial plane the throat should reside at $\eta_t(\pi/2) = \eta_e$, where the coordinate value η_e is determined by the minimum condition (3.32) for the circumferential radius.

From the above considerations it follows immediately, that in the symmetric case the throat is indeed found at $\eta_t = 0$, since $\eta_e = 0$ and $\partial_\eta s = 0$ at $\eta = 0$ for all θ. In contrast, in the nonsymmetric case the throat could be described by a function $\eta_t(\theta)$, which is not a constant. Here the function $\eta_t(\theta)$ has to be determined numerically.

Further geometric quantities of interest are the polar radius R_p

$$R_p = \frac{\eta_0}{\pi} \int_0^\pi e^{(\nu-f)/2}\big|_{\eta=\eta_t(\theta)}\, d\theta \ , \tag{3.39}$$

and the areal radius R_A

$$R_A^2 = \frac{\eta_0^2}{2} \int_0^\pi e^{\nu/2-f}\big|_{\eta=\eta_t(\theta)} \sin\theta d\theta \ . \tag{3.40}$$

We further introduce the rotational velocity v_e of the throat in the equatorial plane

$$v_e = R_e \omega_t \ , \tag{3.41}$$

where the angular velocity of the throat is denoted by $\omega_t = \omega(\eta_t, \theta = \pi/2)$. In the symmetric case $\omega_t = \omega_0$.

To visualize the wormhole geometry we employ embedding diagrams. The first kind of embedding diagrams is obtained by considering the wormhole metric in the equatorial plane, $\theta = \pi/2$, for a fixed time coordinate t and embedding it isometrically in the three-dimensional Euclidean space, i.e.,

$$ds^2 = e^{-f+\nu} d\eta^2 + e^{-f} h d\varphi^2 = d\rho^2 + \rho^2 d\varphi^2 + dz^2 \ , \tag{3.42}$$

with $\rho = \rho(\eta)$ and $z = z(\eta)$. Thus $\rho^2 = e^{-f} h$, and

$$\left(\frac{d\rho}{d\eta}\right)^2 + \left(\frac{dz}{d\eta}\right)^2 = e^{-f+\nu} \ , \tag{3.43}$$

which leads to $z(\eta)$. These diagrams show the presence of the throat, connecting two asymptotically flat regions.

The second kind of embedding diagrams visualizes the shape of the throat itself. Restricting to symmetric wormholes, we embed the metric of the hypersurface forming the throat, $\eta = 0,\ t = 0$, in the (pseudo-)Euclidean space

$$ds^2 = e^{-f+\nu} h d\theta^2 + e^{-f} h \sin^2\theta d\varphi^2 = d\rho^2 + \rho^2 d\varphi^2 \pm dz^2 \tag{3.44}$$

with $\rho = \rho(\theta)$ and $z = z(\theta)$. Thus $\rho^2 = e^{-f} h \sin^2\theta$, and

$$\left(\frac{d\rho}{d\theta}\right)^2 \pm \left(\frac{dz}{d\theta}\right)^2 = e^{-f+\nu} h \ , \tag{3.45}$$

which determines $z(\theta)$. Here we have allowed for an embedding in pseudo-Euclidean space as well, since rapidly rotating black holes are known to possess a negative curvature of their horizon near the poles.

Let us finally briefly address the motion of particles and light in rotating wormhole spacetimes, which is governed by the Lagrangian $\mathscr{L}$

$$2\mathscr{L} = g_{\mu\nu}\dot{x}^{\mu}\dot{x}^{\nu} = \varepsilon \ . \tag{3.46}$$

Here the dot denotes the derivative with respect to an affine parameter, and $\varepsilon = -1$ for massive particles, while $\varepsilon = 0$ for massless particles and light. The presence of two cyclic coordinates, t and φ, implies the existence of two associated constants of motion for the orbits, the energy E and the angular momentum L.

It is then straightforward to analyze the motion in the equatorial plane, $\theta = \pi/2$, where

$$2\mathscr{L} = -e^{f}\dot{t}^{2} + e^{-f}\left(e^{\nu}\dot{\eta}^{2} + h\left(\dot{\varphi} - \omega\dot{t}\right)^{2}\right) = \varepsilon \ . \tag{3.47}$$

Making use of the conservation equations

$$E = \dot{t}\left(e^{f} - e^{-f}h\omega^{2}\right) + e^{-f}h\omega\dot{\varphi} \ , \quad L = -e^{-f}h\omega\dot{t} + e^{-f}h\dot{\varphi} \ , \tag{3.48}$$

the Lagrangian becomes

$$2\mathscr{L} = e^{-f}e^{\nu}\dot{\eta}^{2} - e^{-f}\left((E - \omega L)^{2} - e^{f}\frac{L^{2}}{h}\right) = \varepsilon \ . \tag{3.49}$$

For the analysis of the possible orbits it is instructive to solve this equation for $\dot{\eta}^2$ and to introduce effective potentials $V_{\text{eff}}^{\pm}$

$$\dot{\eta}^{2} = e^{-\nu}\left(E - V_{\text{eff}}^{+}(L,\eta)\right)\left(E - V_{\text{eff}}^{-}(L,\eta)\right) \ , \tag{3.50}$$

where

$$V_{\text{eff}}^{\pm} = \omega L \pm \sqrt{e^{2f}\frac{L^{2}}{h} - \varepsilon e^{f}} \ . \tag{3.51}$$

Equation (3.51) implies $V_{\text{eff}}^{+}(L,\eta) \geq V_{\text{eff}}^{-}(L,\eta)$, and the condition $\dot{\eta}^2 \geq 0$ restricts the allowed energies and angular momenta of the orbits, i.e., $E \geq V_{\text{eff}}^{+}(L,\eta)$ or $E \leq V_{\text{eff}}^{-}(L,\eta)$.

3.2.2 Symmetric Wormholes

Let us now inspect the properties of the rotating symmetric Ellis wormholes in four dimensions. By varying the two parameters η_0 and $\omega_{-\infty}$ in principle the full set of solutions can be obtained. In particular, by fixing η_0 and increasing $\omega_{-\infty}$ a family of rotating wormholes emerges from the respective static symmetric Ellis wormhole. Then the mass and the angular momentum increase monotonically from zero, which is

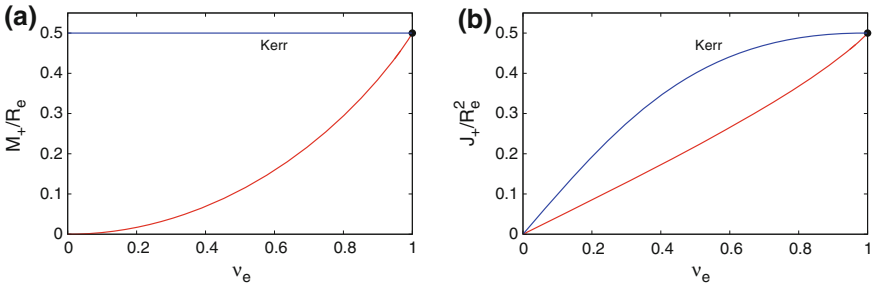

Fig. 3.1 Globel properties of symmetric rotating wormholes at fixed equatorial throat radius R_e: The scaled mass M_+/R_e (**a**) and the scaled angular momentum J_+/R_e^2 (**b**) versus the rotational velocity v_e of the throat in the equatorial plane. The respective curves for the Kerr black holes are shown for comparison. The *black dots* mark the extremal Kerr values

their value in the static case. As the rotational velocity v_e of the throat in the equatorial plane tends to its limiting value of $v_e = 1$, the mass and the angular momentum diverge. Interestingly, at the same time the scalar charge decreases monotonically from its maximal static value and vanishes in the limit $v_e = 1$.

To avoid the divergence of the global charges and get a good physical picture of what happens, as the rotational velocity v_e increases, we now consider instead a family of wormholes, where we keep the equatorial radius R_e fixed. We exhibit in Fig. 3.1 the mass M_+ (a) and the angular momentum J_+ (b), scaled by appropriate powers of the equatorial radius R_e, as functions of the rotational velocity v_e. For comparison we also show the mass and the angular momentum of the respective family of Kerr black holes in the figure, where the equatorial radius of the horizon is kept fixed. Note, that the scaled mass of the Kerr solutions takes a fixed value. Moreover, for $v_e = 1$ the Kerr solutions reach their extremal limit, marked by a black dot in the figure.

Most interestingly, however, we note that for $v_e = 1$ the wormhole solutions reach the same limiting values as the black holes, i.e., those of the respective extremal Kerr solution. Moreover, the mass formula (3.31) for the wormholes looks like the mass formula for extremal black holes. In addition, the scalar charge vanishes in the limit and so does the violation of the NEC, as seen in Fig. 3.2a. All of this indicates, that in the limit $v_e \to 1$ the family of wormholes approaches an extremal Kerr black hole.

To check this hypothesis, the limiting behavior of the metric must be inspected. To that end, we consider a set of solutions at fixed angular velocity $\omega_0 = 1/2$ and increasing rotational velocity, $v_e \to 1$. A comparison of the metric functions with the corresponding functions of the extremal Kerr solution reveals, that the wormholes indeed tend towards an extremal Kerr black hole in the limit $v_e = 1$. This convergence is demonstrated for the function ν in Fig. 3.2b. Note, that the convergence of f and ω is even faster. However, the hypersurface $\eta = 0$ forming the throat of the wormholes must change its character in the limit, since a degenerate horizon must arise.

Kerr black holes are very simple objects, since all their properties are given in terms of just two numbers, the mass and the angular momentum. For instance their

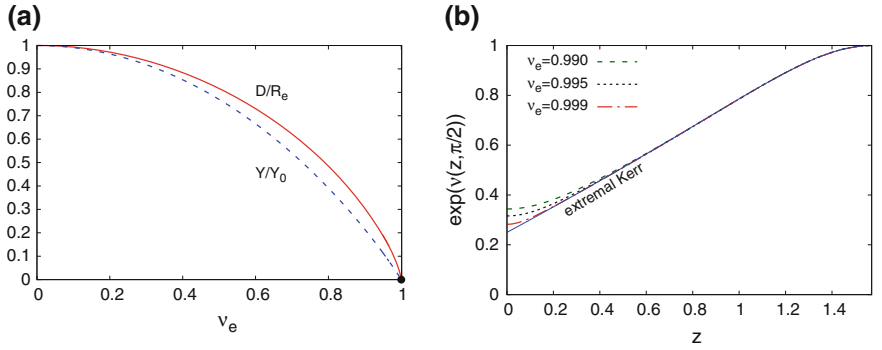

Fig. 3.2 Limiting behavior of symmetric rotating wormholes: **a** The scaled scalar charge D/R_e and the NEC measure Y versus the rotational velocity v_e of the throat in the equatorial plane at fixed equatorial throat radius R_e. **b** The metric function ν versus the radial coordinate $z = \arctan(2\omega_0\eta)$ in the equatorial plane $\theta = \pi/2$ for several values of v_e at fixed $\omega_0 = 1/2$. The respective function of the extremal Kerr solution with horizon angular velocity $\omega_{\rm H} = 1/2$ is also shown

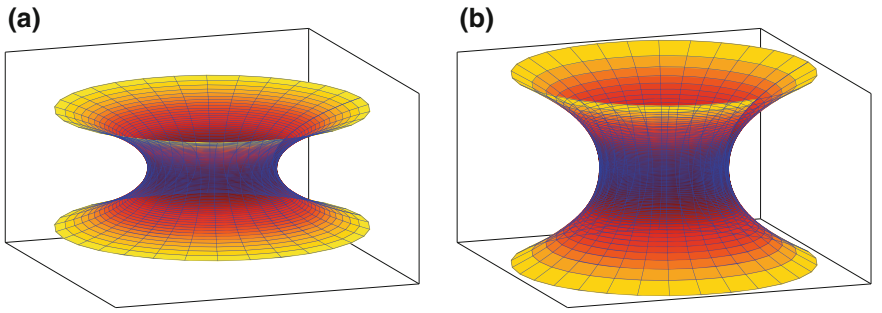

Fig. 3.3 Geometric properties of symmetric rotating wormholes with equatorial throat radius $R_e = 2$: Isometric embeddings of the equatorial plane for rotational velocities $v_e = 0.1$ (**a**) and 0.9 (**b**) of the throat in the equatorial plane

quadrupole moment is given by $Q = J^2/M$. The quadrupole moment of rotating wormholes is always smaller than the corresponding Kerr value, approaching it only in the static and in the extremal limit. The moment of inertia $I = J/\Omega_{\rm H}$ of Kerr black holes satisfies $I/M^3 = 2(1 + \sqrt{1 - j^2})$ with $j = J/M^2$. Also the scaled moment of inertia $I = J_+/\omega_0$ of rotating wormholes is smaller than the corresponding value of the Kerr black holes, except in the extremal limit.

Let us now turn to the discussion of the geometry of rotating wormholes. In Fig. 3.3 we present a first illustration of the effect of the rotation on the wormhole geometry by considering the embeddings of a slowly rotating wormhole (a) and a fast rotating wormhole (b) with the same equatorial throat radius R_e. The embeddings are obtained according to Eq. (3.42), yielding the curve $z(\rho)$, where the figures exploit the axial symmetry.

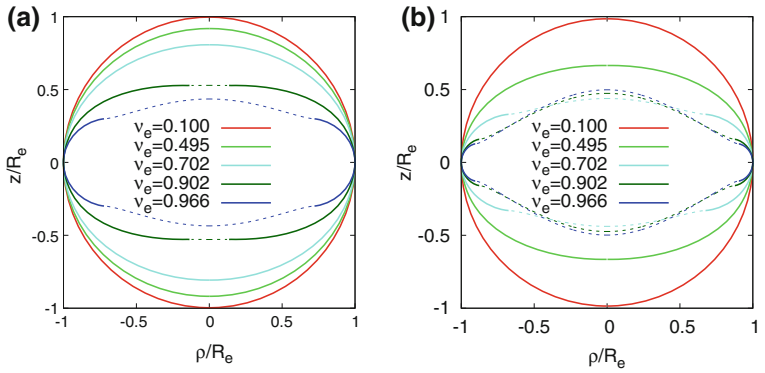

Fig. 3.4 Isometric embeddings of the wormhole throat (**a**) and the Kerr black hole horizon (**b**) according to Eq. (3.44) at fixed equatorial radius $R_e = 2$ for rotational velocities $v_e = 0.966, 0.902, 0.702, 0.495$, and 0.1. Pseudo-Euclidean embeddings are indicated by the *dashed lines*

As the throat starts to rotate its geometry deforms from spherical to oblate, as dictated by the centrifugal force. To demonstrate the geometry of the throat itself, we employ the embedding Eq. (3.44). The deformation of the throat is exhibited in Fig. 3.4a. As the throat velocity v_e increases, the throat flattens at the poles, until a critical velocity $v_e^{\rm cr}$ is reached. This marks the onset of a negative Gaussian curvature at the poles. Thus beyond $v_e^{\rm cr}$ it is no longer possible to use a fully Euclidean embedding, but for a part of the throat surface adjacent to the poles a pseudo-Euclidean embedding must be employed. For rotating Ellis wormholes we find a critical value $v_e^{\rm cr} = 0.9$.

This finding should not surprise us, since Kerr black holes exhibit the analogous feature when their horizon is embedded. Here also a critical value $v_e^{\rm cr,H}$ arises, where the Gaussian curvature changes sign, and thus a pseudo-Euclidean embedding becomes necessary. The critical value for Kerr black holes is, however, much smaller, $v_e^{\rm cr,H} = 0.577$. For comparison, the embedding diagrams for the same set of rotational velocities of the horizon of Kerr black holes is exhibited in Fig. 3.4b.

To quantify how the throat deforms with increasing rotational velocity, we consider the polar throat radius R_p and the areal throat radius R_A at fixed equatorial throat radius R_e, and illustrate both quantities in Fig. 3.5a, b, respectively. Decreasing monotonically, both tend to the respective values of the horizon radius of the extremal Kerr black hole in the limit $v_e \to 1$. We have indicated the critical value $v_e^{\rm cr}$ by a cross in the figures.

For comparison, we also exhibit in Fig. 3.5 the respective curves for the Kerr black holes, marking the critical velocity $v_e^{\rm cr,H}$ as well. Whereas $v_e^{\rm cr,H}$ is much smaller than $v_e^{\rm cr}$, the polar radius R_p assumes the same value at the respective critical velocities of the rotating wormhole and the Kerr black hole. The analogous finding holds true for the areal radius R_A. This remarkable fact is indicated in the figures by the thin horizontal line.

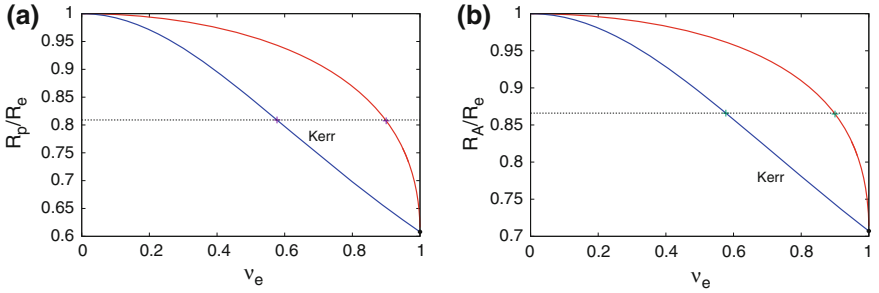

Fig. 3.5 Geometric properties of symmetric rotating wormholes at fixed equatorial throat radius R_e: The scaled polar radius R_p/R_e (**a**) and the scaled areal radius R_A/R_e (**b**) versus v_e. The crosses mark $v_e^{\rm cr}$. The respective curves for the Kerr black holes are also shown

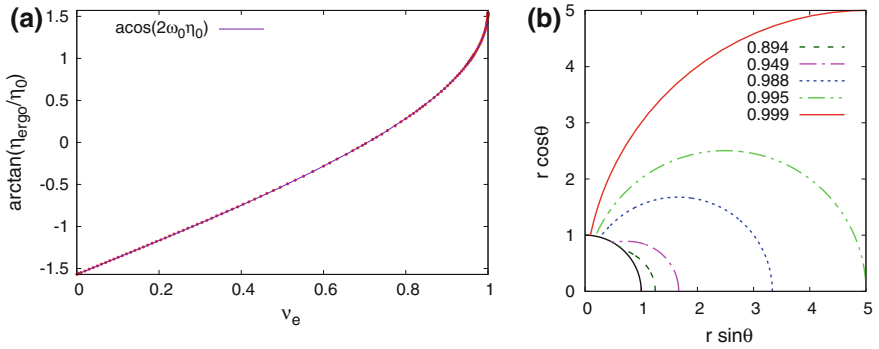

Fig. 3.6 Location of the ergosurface of symmetric rotating wormholes at fixed throat parameter $\eta_0 = 1$: **a** The function $\arctan(\eta_{\rm ergo}/\eta_0)$ in the equatorial plane versus the rotational velocity v_e. Also shown is the function $\arccos(2\omega_0\eta_0)$. **b** One quadrant of the ergosurface and the throat in quasi cartesian coordinates $(r\sin\theta, r\cos\theta)$ where $r = (\eta^2 + \eta_0^2)^{1/2}$ at fixed angle φ for rotational velocities $v_e = 0.894, 0.949, 0.988, 0.995$ and 0.999

Kerr black holes are known to possess ergoregions. Let us therefore inspect, whether rotating wormholes can also possess them. Ergoregions are defined by the condition $g_{tt} \geq 0$ and are bounded by an ergosurface. Interestingly, we find that the location $\eta_{\rm ergo}$ of the ergosurface in the equatorial plane satisfies the following relation with high accuracy: $\arctan(\eta_{\rm ergo}/\eta_0) = \arccos(2\omega_0\eta_0)$, as seen in Fig. 3.6a. Thus the ergosurface touches the throat, $\eta_{\rm ergo} = 0$, in the equatorial plane, when $\omega_0 = 1/2$. This implies for the rotational velocity $v_e = R_e\omega_0 = 1/\sqrt{2}$, when $\eta_0 = 1$.

When the wormhole throat rotates faster than with $v_e = 1/2$, there is an ergoregion in the asymptotically flat spacetime $\eta \geq 0$ which increases in size with increasing rotational velocity v_e. We exhibit embeddings of the ergosurface for a set of rapidly rotating wormholes in the region $\eta \geq 0$ in Fig. 3.6b. Starting with a ring for $v_e = 1/2$, the ergoregion increases in size until it reaches the ergoregion of the extremal Kerr black hole.

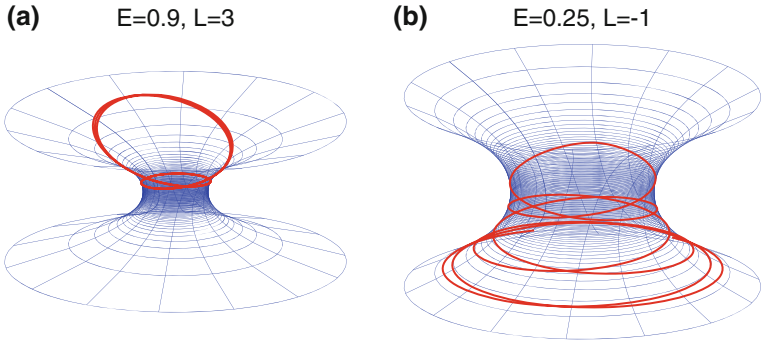

Fig. 3.7 Embedding diagrams of bound orbits for massive test particles in the equatorial plane of a symmetric wormhole with rotational velocity $v_e = 0.78$ and equatorial radius $R_e = 2$ for two values of the particle energy E and angular momentum L

Finally we address the question whether symmetric wormholes can possess stable bound orbits of particles and light. Static Ellis wormholes are known not to possess stable bound orbits, but the inclusion of rotation may change this. We therefore have to analyze the motion of particles and light in these rotating wormhole spacetimes. A full analysis of the general set of geodesic equations might prove difficult, since it is currently unknown, whether in some coordinate system an analog of the Carter constant can be found, necessary to achieve separability.

However, the question can be answered already by restricting the motion to the equatorial plane, as described by Eqs. (3.47)–(3.50). Inspection of the effective potentials then reveals, that massive particles possess even three kinds of bound orbits: (i) orbits within a single universe, (ii) orbits oscillating between the two universes, and (iii) orbits remaining at the throat (for $L = 0$ only). Figure 3.7 shows examples of a single universe bound orbit (a) and a two universe bound orbit (b).

Addressing the innermost stable circular orbits (ISCOs), we find that the ISCO of corotating orbits resides at the throat, whereas the ISCO of the counterrotating orbits changes with the rotation velocity of the wormhole. Moreover, we find that there are unstable bound states for light, which indicates the presence of a photon region to be mapped out by a full analysis.

3.2.3 Nonsymmetric Wormholes

Nonsymmetric wormholes are obtained, when the asymmetry parameter γ assumes a finite value. Only in the static case the nonsymmetric Ellis wormholes are known in closed form, see Eq. (3.16). While the nonsymmetric rotating wormholes have many properties in common with their symmetric counterparts, also new features appear in the nonsymmetric case.

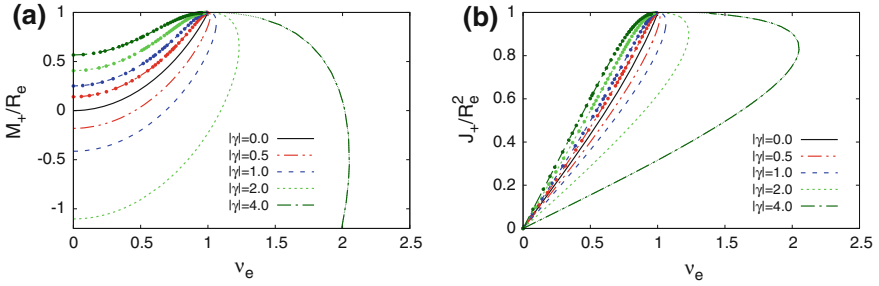

Fig. 3.8 Global properties of nonsymmetric rotating wormholes at fixed equatorial throat radius $R_e = 2$: The scaled mass M_+/R_e (**a**) and the scaled angular momentum J_+/R_e^2 (**b**) versus the rotational velocity v_e of the throat in the equatorial plane. The asymmetry parameter γ is varied in the range $-4 \leq \gamma \leq 4$. Negative values of γ are indicated by *dots*. Extrapolations towards the limiting extremal Kerr black hole are indicated by *thin dotted lines*

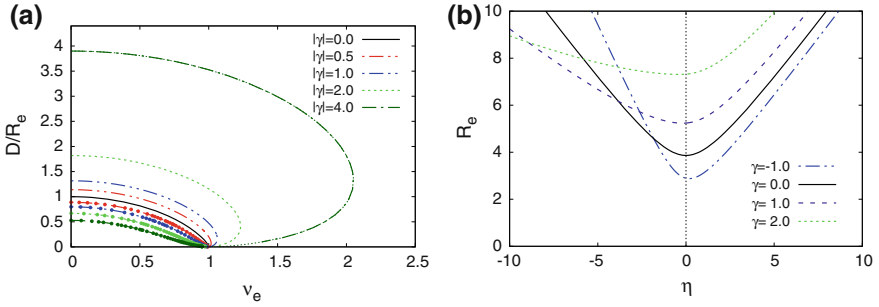

Fig. 3.9 Properties of nonsymmetric rotating wormholes at fixed equatorial throat radius $R_e = 2$: **a** The scaled scalar charge D/R_e versus the rotational velocity v_e of the throat in the equatorial plane. The asymmetry parameter γ is varied in the range $-4 \leq \gamma \leq 4$. Negative values of γ are indicated by *dots*. Extrapolations towards the limiting extremal Kerr black hole are indicated by *thin dotted lines*. **b** The equatorial radius function $R_e(\eta)$ versus the radial coordinate η for spacetimes with $v_e = 0.82$ ($\gamma = -1$), $v_e = 0.97$ ($\gamma = 0$), $v_e = 1.06$ ($\gamma = 1$), and $v_e = 1.10$ ($\gamma = 2$). The minimal value of the function $R_e(\eta)$ determines the location of the throat

To illustrate the effect of the asymmetry parameter γ on the wormhole properties, we first consider families of rotating wormholes with fixed equatorial throat radius R_e, as before in the symmetric case. Figure 3.8 shows the scaled mass (a) and the scaled angular momentum (b) versus the rotational velocity v_e of the throat in the equatorial plane. Similarly, Fig. 3.9a shows the scaled scalar charge versus v_e.

As in the symmetric case, also the families of rotating nonsymmetric wormholes with fixed equatorial throat radius tend to an extremal Kerr black hole, as the rotational velocity v_e of the throat in the equatorial plane tends to the velocity of light. However, in the case of $\gamma > 0$, they approach this limiting value from above, i.e., from rotational velocities greater than the speed of light as seen in the figures. While this may come

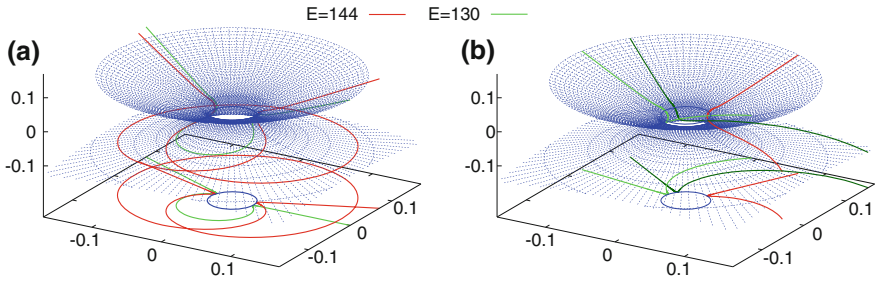

Fig. 3.10 Geodesics in nonsymmetric rotating wormhole spacetimes: Embedding diagrams of escape orbits of massive (**a**) and massless (**b**) particles with vanishing angular momentum for a wormhole solution with $v_e = 8.24$ ($\omega_{-\infty} = 1000$, $\gamma = 10.008$)

as a surprise, there is no objection against it, since it concerns the motion of spacetime itself as viewed by an asymptotic observer.

To see how the asymmetry parameter γ influences the location of the throat of the rotating wormholes, we consider the equatorial radius as a function of the radial coordinate, $R_e(\eta)$. For symmetric wormholes $R_e(\eta)$ has its minimum at $\eta = 0$, which we previously simply denoted by R_e. The asymmetry parameter γ now shifts this minimum. For positive γ the throat then resides at a negative value of η, whereas for negative γ the throat shifts to a positive value of η. This shifting of the location of the throat is demonstrated in Fig. 3.9b.

We finally inspect the geodesics in such nonsymmetric wormhole spacetimes. We retain the three kinds of stable bound orbits of massive particles also for nonsymmetric wormholes in addition to escape orbits. Embedding diagrams of escape orbits of massive particles, which briefly enter the second universe, are illustrated in Fig. 3.10a. But highly rotating asymmetric spacetimes also exhibit rather curiously looking orbits, as exhibited in Fig. 3.10b. Here we see unbound orbits of light moving with vanishing angular momentum from the negative η universe to the positive η universe. While the orbits are strongly dragged along with the rotating spacetime in the negative η universe the orbits continue on almost straight lines after they emerge from the throat in the positive η universe.

3.3 Rotating Wormholes in Five Dimensions

While the study of wormholes in higher dimensions is interesting in its own right, our motivation for their study here is the fact, that by going to higher odd dimensions one can obtain a technically simpler setting and study questions, which would be highly challenging in four dimensions. This concerns, in particular, the question of the stability of rotating wormholes. Here we would like to see how the rotation affects the notoriously unstable radial mode of the static Ellis wormholes. If rotation would make this instability disappear in five-dimensional wormholes, while the global and

geometric properties of rotating wormholes would be completely analogous in four and five dimensions, one would have good reason to believe that rotation would act in an analogously stabilizing way also in four-dimensional wormholes.

3.3.1 Theoretical Setting

In D spacetime dimensions an angular momentum can be associated with each spatial plane, leading to $\lfloor (D-1)/2 \rfloor$ independent angular momenta, in general. Choosing all these angular momenta to be of equal magnitude, the symmetry of odd dimensional spacetimes is strongly enhanced, and the angular dependence factorizes. This leads to a set of coupled ordinary differential equations to be solved for the rotating odd dimensional spacetimes. In contrast, in even dimensions, rotation always results in partial differential equations with dependence on at least two coordinates.

Let us now consider the simplest case, namely, wormholes in five spacetime dimensions, rotating in both spatial planes with equal magnitude angular momenta, $J_1 = J_2 = J$. The line element can then be written as follows [29]

$$\begin{aligned} ds^2 = &- e^{2f} dt^2 + p e^{-f} \left\{ e^{f-q} \left[d\eta^2 + h d\theta^2 \right] \right. \\ &+ e^{q-f} h \left[\sin^2\theta (d\varphi_1 - \omega dt)^2 + \cos^2\theta (d\varphi_2 - \omega dt)^2 \right] \\ &\left. + \left(e^{f-q} - e^{q-f} \right) h \sin^2\theta \cos^2\theta (d\varphi_2 - d\varphi_1)^2 \right\} . \end{aligned} \tag{3.52}$$

where as before $h = \eta^2 + \eta_0^2$, and f, p, q and ω are functions of the coordinate η, $-\infty < \eta < \infty$. The limits $\eta \to \pm\infty$ correspond to two disjoint asymptotically flat regions. The scalar phantom field ψ is also a function of η only.

With this Ansatz, the equation $R^\theta_\theta = 0$ yields a remarkably simple ordinary differential equation for the function p,

$$p'' + \frac{5\eta}{\eta^2 + \eta_0^2} p' - 2 \left(\frac{\eta_0}{\eta^2 + \eta_0^2} \right)^2 p = 0 , \tag{3.53}$$

where the prime denotes differentiation with respect to η. It has the general solution

$$p(\eta) = -c_1 \frac{\eta}{\sqrt{\eta^2 + \eta_0^2}} + c_2 \frac{\eta^2 + \eta_0^2/2}{\eta^2 + \eta_0^2} , \tag{3.54}$$

with the constants c_1 and c_2. We set $c_1 = 0$ and $c_2 = 1$ to obtain asymptotically flat solutions, thus

$$p(\eta) = \frac{\eta^2 + \eta_0^2/2}{\eta^2 + \eta_0^2} . \tag{3.55}$$

The phantom field equation leads immediately to

$$\psi' = \frac{D}{p\sqrt{h^3}} \,, \tag{3.56}$$

with the scalar charge D. Employing Eq. (3.55) for p, we obtain for the scalar field the expression

$$\psi(\eta) = \frac{2D}{\eta_0^2}\left(\arctan\frac{\eta}{\sqrt{\eta^2+\eta_0^2}} - \frac{\pi}{4}\right) \,. \tag{3.57}$$

Here we have chosen the integration constant such that the scalar field vanishes for $\eta \to \infty$.

The equation $\sqrt{-g}R^{\eta}_{\varphi_1} = 0$, i.e.,

$$\left(\sqrt{h^5}p^2 e^{q-4f}\omega'\right)' = 0 \,, \tag{3.58}$$

yields

$$\omega' = \frac{c_\omega}{h^{\frac{5}{2}}p^2 e^{q-4f}} \,, \tag{3.59}$$

with integration constant c_ω.

The equations $R^t_t = 0$ and $R^{\varphi_1}_{\varphi_1} + R^{\varphi_2}_{\varphi_2}$ lead to the set of ordinary differential equations

$$\frac{1}{p(\eta^2+\eta_0^2)^{\frac{3}{2}}}\left(p(\eta^2+\eta_0^2)^{\frac{3}{2}}f'\right)' - \frac{c_\omega^2 e^{4f-q}}{2p^3(\eta^2+\eta_0^2)^4} = 0 \,, \tag{3.60}$$

$$\frac{1}{p(\eta^2+\eta_0^2)^{\frac{3}{2}}}\left(p(\eta^2+\eta_0^2)^{\frac{3}{2}}q'\right)' - \frac{4\left(e^{2(q-f)}-1\right)}{(\eta^2+\eta_0^2)} = 0 \,. \tag{3.61}$$

Having not been able to find a closed form expression for f and q except in the slowly rotating case, we solve these equations numerically. With the boundary conditions

$$f|_{\eta\to\infty} = 0 \,, \qquad \omega|_{\eta\to\infty} = 0 \,, \qquad q|_{\eta\to\infty} = 0 \,, \tag{3.62}$$

we ensure asymptotic flatness for $\eta \to \infty$. Since we again allow for finite values of the functions f, ω and q for $\eta \to -\infty$,

$$f|_{\eta\to-\infty} = \gamma \,, \qquad \omega|_{\eta\to-\infty} = \omega_{-\infty} \,, \qquad q|_{\eta\to-\infty} = \gamma \,, \tag{3.63}$$

a coordinate transformation is again necessary to achieve asymptotic flatness for $\eta \to -\infty$. Note, that the value of $\omega_{-\infty}$ is obtained by integrating Eq. (3.59) with a given integration constant c_ω.

As in four dimensions the constants γ and $\omega_{-\infty}$ represent the asymmetry and the rotation parameter of the wormhole solutions. When $\omega_{-\infty} = 0$, static wormhole solutions are obtained. These can be given in closed form [27, 29]

$$f(\eta) = \frac{M}{\eta_0^2} \arctan\left(\frac{1-\sin z}{1+\sin z}\right) , \tag{3.64}$$

where $z = \arctan(\eta/\eta_0)$, M is an integration constant, and $q = f$.

After eliminating the second derivatives in the equation

$$R_{\eta\eta} = -2\frac{D^2}{h^3 p^2} , \tag{3.65}$$

with the help of Eqs. (3.60) and (3.61), we employ the resulting equation

$$\begin{aligned} 0 = D^2 + \frac{e^{4f-q}c_w^2}{4ph} - \frac{h^3}{4}\left[(4f'^2 - 2f'q' + q'^2)p^2 - 2(f'-q')pp' - 3p'^2\right] \\ - h^2 p\left[(4 - e^{2(q-f)} + (q'-f')\eta)p - 3p'\eta\right] + 3hp^2\eta^2 , \end{aligned} \tag{3.66}$$

as a constraint equation to monitor the quality of the solutions.

We show the violation of the NEC analogously to the four-dimensional case. Choosing the null vector field

$$k^\mu = \left(e^{-f}, \frac{e^{q/2}}{\sqrt{p}}, 0, \omega e^{-f}, \omega e^{-f}\right) , \tag{3.67}$$

we find

$$\Xi = -D^2\frac{e^q}{p^2h^3} \leq 0 . \tag{3.68}$$

After obtaining the solutions, we read off the global charges from their asymptotics analogously to Eq. (3.22) for M_+ and J_+

$$g_{tt} \underset{\eta\to+\infty}{\longrightarrow} -\left(1 - \frac{8M_+}{3\pi\eta^2}\right) , \qquad g_{t\varphi_1} \underset{\eta\to+\infty}{\longrightarrow} -\frac{4J_+\sin^2\theta}{\pi\eta^2} , \tag{3.69}$$

and to Eq. (3.26) for $\bar{M}_-$ and $\bar{J}_-$. Analogously to Eq. (3.70) we find in general

$$\frac{2}{3}M_+ + \frac{2}{3}M_- = 2\omega_{-\infty}e^{-2\gamma}J_- = 2\omega_{-\infty}J_+ . \tag{3.70}$$

For symmetric wormholes $\omega_{-\infty} = 2\omega_0$. Thus, we recover the mass formula,

$$\frac{2}{3}M_+ = \omega_{-\infty}J_+ = 2\omega_0 J_+, \tag{3.71}$$

i.e., a relation akin to the Smarr formula for extremal Myers–Perry black holes in five dimensions. The latter is recovered when the throat angular velocity ω_0 is replaced by the horizon angular velocity.

Addressing briefly the geometry of these wormholes, we define the equatorial radius $R_e(\eta)$ in the planes $\theta = 0$ and $\theta = \pi/2$

$$R_e(\eta) = \sqrt{p(\eta^2 + \eta_0^2)e^{q-2f}} \ , \tag{3.72}$$

and the areal radius $R_A(\eta)$

$$R_A^3(\eta) = \left[(\eta^2 + \eta_0^2)^3 p^3 e^{-(2f+q)}\right]^{\frac{1}{2}} \ . \tag{3.73}$$

To obtain a measure for the deformation of the throat we embed a plane which intersects the planes $\theta = 0$ and $\theta = \pi/2$. To this end, we fix the azimuthal coordinates, $\varphi_i = \varphi_{i,0}$, $\varphi_i = \varphi_{i,0} + \pi \pmod{2\pi}$ for some $\varphi_{i,0}$, $i = 1, 2$. This yields the polar radius $R_p(\eta)$. By taking the ratio R_p/R_e at the throat, we obtain a measure for the deformation of the throat that is induced by the rotation.

3.3.2 Wormholes

We are now ready to investigate the global and geometric properties of these rotating wormholes in five dimensions and compare them with their four-dimensional counterparts to see whether both possess essentially the same features. We start with considering the mass M_+ and the angular momentum J (recall $J_1 = J_2 = J$) of three families of wormholes with fixed equatorial radius R_e of the throat. These quantities are illustrated in Fig. 3.11 for symmetric ($\gamma = 0$) and nonsymmetric ($\gamma = \pm 1$)

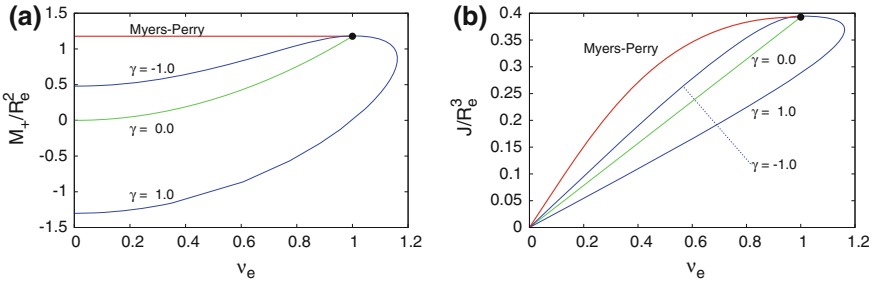

Fig. 3.11 Properties of rotating symmetric and nonsymmetric wormholes in five dimensions at fixed equatorial throat radius R_e: The scaled mass M_+/R_e (**a**) and the scaled angular momentum J/R_e^2 (**b**) versus the rotational velocity v_e of the throat in the equatorial plane. The respective curves for the Myers–Perry black holes are shown for comparison. The *black dots* mark the respective extremal Myers–Perry values

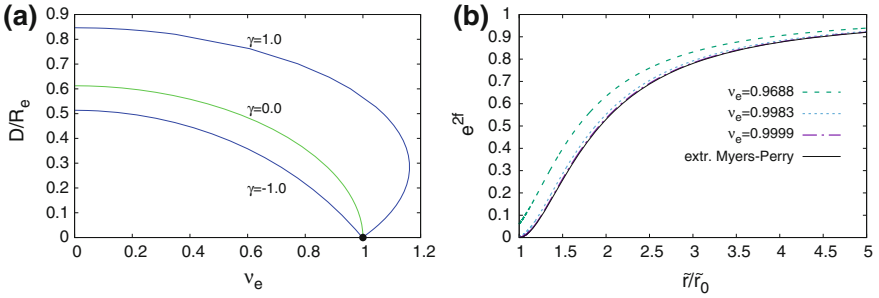

Fig. 3.12 Limiting behavior: **a** The scaled scalar charge D/R_e versus the rotational velocity v_e of the throat in the equatorial plane at fixed equatorial throat radius R_e for symmetric ($\gamma = 0$) and nonsymmetric ($\gamma = \pm 1$) rotating wormholes. The *black dot* marks the extremal Myers–Perry value. **b** The metric function e^{2f} versus the radial coordinate $\tilde{r} = \sqrt{g_{\theta\theta}}$ (where $\tilde{r}_0$ denotes the coordinate at the throat) in the equatorial plane $\theta = \pi/2$ for several values of v_e at fixed $\omega_0 = 1/2$. The respective function of the extremal Myers–Perry solution with horizon angular velocity $\omega_{\rm H} = 1/2$ is also shown

wormholes. Also shown are the respective curves for the Myers–Perry black holes with equal angular momenta, where the black dots mark the respective extremal Myers–Perry black hole.

Comparing Fig. 3.11 with Fig. 3.1 for the symmetric four-dimensional case and with Fig. 3.8 for the nonsymmetric one, we indeed observe the completely analogous features. In particular, all families of rotating wormholes end in an extremal rotating vacuum black hole, and for values of the asymmetry parameter $\gamma < 0$ the rotational velocity of the throat v_e exceeds the velocity of light, when approaching the limiting configuration.

As shown in Fig. 3.12a, the scalar charge D decreases from the respective static value monotonically to zero along these families of solutions, analogously to Fig. 3.9a, and likewise the violation of the NEC decreases and disappears in the limit, when the extremal Myers–Perry black hole is reached. Figure 3.12b illustrates for the metric function f that the metric of the rotating wormholes itself approaches the metric of the respective extremal Myers–Perry black hole.

The geometric properties of these five-dimensional rotating wormholes are also very much akin to those of the four-dimensional ones. As an example, we illustrate in Fig. 3.13a the deformation of the throat with increasing rotational velocity v_e for the same families of solutions. The location of the ergosurface is shown in Fig. 3.13b. As in four dimensions the rotational velocity of the throat has to be sufficiently large in order that the ergosurface extends into the asymptotically flat region with positive radial coordinate η.

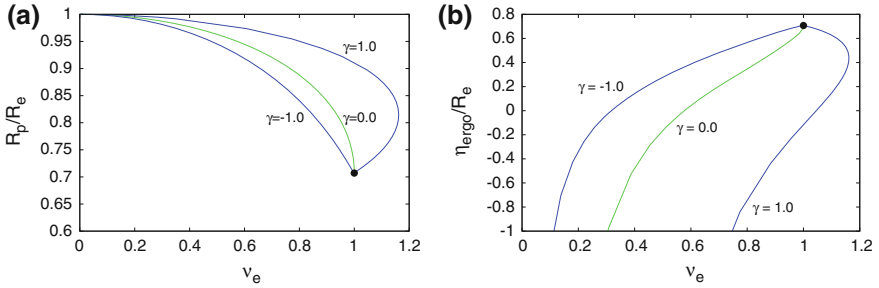

Fig. 3.13 Geometric properties of wormholes at fixed equatorial throat radius R_e: The measure of the deformation of the throat R_p/R_e (**a**) and the location of the ergosurface $\eta_{\rm ergo}/R_e$ (**b**) versus ν_e for symmetric ($\gamma = 0$) and nonsymmetric ($\gamma = \pm 1$) rotating wormholes. The *black dots* mark the respective extremal Myers–Perry values

3.3.3 Stability

Having established that the global charges and geometric properties of rotating wormholes in four and five dimensions are very similar, we now turn to the interesting question of stability. For static Ellis wormholes in four dimensions it has been shown that they are unstable [24–26]. A linear stability analysis, in particular, has revealed the presence of an unstable radial mode. For higher dimensional static Ellis wormholes a linear stability analysis has shown that the radial instability is retained [27]. In the following we investigate the effect of rotation on the radial instability of five dimensional Ellis wormholes.

We introduce the metric Ansatz

$$\begin{aligned} ds^2 = & -e^{2F_0}dt^2 + pe^{-F_0}\left\{e^{F_0-F_2}\left[e^{F_1}d\eta^2 + hd\theta^2\right]\right. \\ & + e^{F_3-F_0}h\left[\sin^2\theta(d\varphi_1 - F_\omega dt)^2 + \cos^2\theta(d\varphi_2 - F_\omega dt)^2\right] \\ & \left. + \left(e^{F_0-F_2} - e^{F_3-F_0}\right)h\sin^2\theta\cos^2\theta(d\varphi_2 - d\varphi_1)^2\right\}\,, \end{aligned} \tag{3.74}$$

where the functions F_0, F_1, F_2, F_3, and F_ω depend on the coordinates η and t. Likewise we assume the Ansatz

$$\Psi = \Psi(\eta, t)\,, \tag{3.75}$$

for the scalar field. Next, we substitute these Ansätze into the Einstein and scalar field equations, imposing perturbations with a harmonic time dependence,

$$\begin{aligned} & F_0 = f + \lambda H_0 e^{i\Omega t}\,, \qquad F_1 = \lambda H_1 e^{i\Omega t}\,, \qquad F_2 = q + \lambda H_2 e^{i\Omega t}\,, \\ & F_3 = q + \lambda H_3 e^{i\Omega t}\,, \qquad F_\omega = \omega + \lambda H_\omega e^{i\Omega t}\,, \qquad \Psi = \psi + \lambda H_\psi e^{i\Omega t}\,, \end{aligned} \tag{3.76}$$

where the functions H_0, H_1, H_2, H_3, H_ω, and H_ψ depend on the radial coordinate η only. Expanding the field equations in the perturbation parameter λ, we obtain the perturbation equations by selecting the terms of first order in λ.

Analyzing the resulting system of equations, we realize that the perturbation function H_ω can be integrated, once the functions $H_0 - H_3$ are known. This follows from the equation $R^{\varphi_1}_\eta = 0$, since

$$H'_\omega = \frac{c_\omega e^{4f-q}}{p^2 h^{5/2}} \left[8H_0 + H_1 + H_2 - 3H_3\right] . \tag{3.77}$$

We next consider the equation for the perturbation function H_ψ of the scalar field, and impose the gauge

$$H_1 = H_3 - H_2 . \tag{3.78}$$

We multiply the ordinary differential equation for H_ψ by H_ψ and obtain after taking into account the gauge choice (3.78)

$$H_\psi \left(p\, h^{3/2} H'_\psi\right)' + \Omega^2 p^2 h^{3/2} e^{-2f-q} H_\psi^2 = 0 . \tag{3.79}$$

Now we integrate this equation and employ integration by parts. This yields

$$\left[p\, h^{3/2} H_\psi H'_\psi\right]_{-\infty}^{\infty} = \int_{-\infty}^{\infty} \left[p\, h^{3/2} (H'_\psi)^2 - \Omega^2 p^2 h^{3/2} e^{-2f-q} H_\psi^2\right] d\eta . \tag{3.80}$$

Since the expression on the left hand side vanishes, the right hand side must vanish as well. For unstable modes the eigenvalue Ω^2 is negative. Consequently, the integrand is nonnegative for unstable modes, and the integral vanishes only if H_ψ is zero everywhere. Thus the scalar perturbation function H_ψ vanishes for unstable modes.

We now reformulate the remaining three equations for the perturbation functions H_2, H_3, and H_0 in terms of the functions G_0, G_1, and G_2, where

$$H_0 = G_2 + G_0 , \qquad H_2 = -G_2 , \quad H_3 = 2G_0 + G_1 .$$

This results in a system of homogeneous ordinary differential equations for the perturbation functions G_i

$$\frac{1}{\xi}(\xi G'_0)' = V_{00} G_0 + V_{01} G_1 + V_{02} G_2 - \Omega^2 (G_0 + G_1)\, e^{-2f-q} p , \tag{3.81}$$

$$\frac{1}{\xi}(\xi G'_1)' = V_{10} G_0 + V_{11} G_1 + V_{12} G_2 - \Omega^2 G_1 e^{-2f-q} p , \tag{3.82}$$

$$\frac{1}{\xi}(\xi G'_2)' = V_{20} G_0 + V_{21} G_1 + V_{22} G_2 - \Omega^2 G_2 e^{-2f-q} p , \tag{3.83}$$

where we have introduced the abbreviation $\xi = p\, h^{3/2}$, and the quantities V_{ij} are functions of the unperturbed solutions (see [29] for the explicit expressions).

Now, we are ready to solve the set of Eqs. (3.81)–(3.83). Starting with the static case, we note that there is a zero mode

$$G_0 = -2G_2\,, \qquad G_1 = 3G_2\,, \qquad G_2 = \text{const.}\,, \tag{3.84}$$

which is clearly not normalizable. This mode is indicated in Fig. 3.14a by the straight lines. To obtain normalizable modes we need to impose an appropriate set of boundary conditions, which we choose to be

$$G_0(-\infty) = G_1(-\infty) = G_2(-\infty) = 0\,, \quad G_0(\infty) = G_1(\infty) = G_2(\infty) = 0\,, \quad G_2(0) = 1\,, \tag{3.85}$$

where we impose the last condition to obtain nontrivial solutions. Since we now have seven boundary conditions instead of the six needed for the system (3.81)–(3.83), we add as an auxilliary first order equation $\Omega^{2\prime} = 0$. The numerical procedure then results in the correct eigenvalues Ω^2.

In the static case the equations yield the known normalizable unstable mode [27] besides the non-normalizable zero mode (3.84). Interestingly, as rotation is turned on, the non-normalizable static zero mode becomes a normalizable unstable mode. Thus after the onset of rotation the wormhole carries two unstable modes. The two modes are illustrated in Fig. 3.14a for a symmetric wormhole with rotational velocity $v_e = 0.216$ of the throat in the equatorial plane.

When the rotational velocity of the throat increases, the eigenvalue of the lower unstable mode increases as well, while the eigenvalue of the higher unstable mode decreases. This is illustrated in Fig. 3.14b, both for symmetric and nonsymmetric wormholes. Here we observe the crucial result, that at a particular value of the

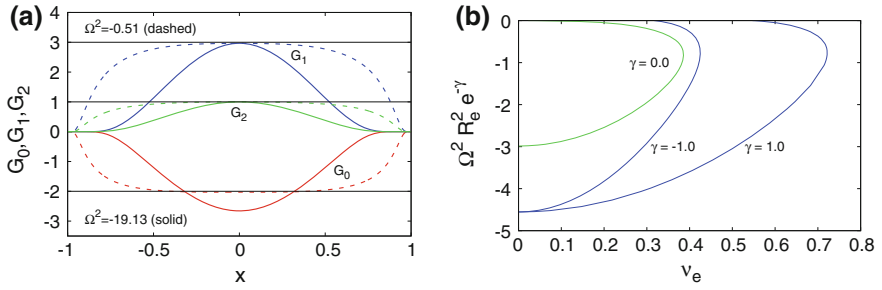

Fig. 3.14 Unstable modes of rotating wormholes: **a** The perturbation functions G_0, G_1, and G_2 versus the compactified coordinate $x = (2/\pi)\arctan(\eta/\eta_0)$ for symmetric wormholes with throat parameter $\eta_0 = 0.5$ for the two unstable modes at $v_e = 0.216$. For comparison the non-normalizable zero mode of the static wormhole is indicated by the *straight lines*. **b** The scaled eigenvalue $\Omega^2 R_e^2 e^{-\gamma}$ versus v_e for symmetric ($\gamma = 0$) and nonsymmetric ($\gamma = \pm 1$) rotating wormholes

rotational velocity, which depends on the asymmetry parameter γ, both unstable modes merge and disappear. Thus beyond a certain magnitude of the rotation, the notoriously unstable mode of the Ellis wormhole is no longer present.

3.4 Conclusions and Outlook

In this chapter we have addressed rotating wormholes in four and five dimensions in General Relativity, where the violation of the null energy condition is provided by a phantom field. Whereas the slowly rotating wormhole solutions are known in closed form, in the general case of arbitrary rotation numerical integration appears to be necessary to obtain the wormhole solutions.

In four dimensions, the inclusion of rotation leads to a set of coupled partial differential equations. In five dimensions, however, we obtain a set of coupled ordinary differential equations, when we choose both angular momenta to be of equal magnitude. This provides a much simpler setting for the study of the wormhole features, and allows for a first step towards determining their stability, a feat, that will be much more difficult for wormholes in four dimensions [38].

Rotating wormholes in four and five dimensions have many important properties in common. These include, in particular, that rotating wormholes:

- satisfy a Smarr-like mass formula akin to the Smarr formula of extremal vacuum black holes;
- approach limiting configurations, which correspond to extremal vacuum black holes;
- possess a rotational velocity of the throat, which tends to the speed of light when the limiting configuration is approached;
- can possess a rotational velocity of the throat which in the nonsymmetric case ($\gamma > 0$) seems to exceed the speed of light for asymptotic observers;
- possess ergoregions in the asymptotically flat (positive η) universe, when their rotational velocity exceeds a certain value.

The similarity of the properties of rotating wormholes in four and five dimensions suggests that they might also have similar properties with respect to stability. For five-dimensional wormholes a stability analysis of the notoriously unstable radial modes has revealed the following intriguing scenario: As rotation is turned on, the eigenvalue of the unstable radial mode of the static black holes increases, while the zero mode of the static black holes becomes normalizable and its eigenvalue decreases. Both unstable eigenmodes then merge and disappear at a critical value of the rotation.

While this analysis indicates, that rotation can stabilize the wormholes, a more complete study will have to be done in five dimensions to investigate, whether this conclusion really holds. Subsequently a stability analysis will also have to be done in the four-dimensional case, since this will be the case of interest for astrophysical applications. Alternatively, rotating wormholes in generalized models of gravity can

be studied, where no exotic matter is necessary to achieve the nontrivial topology, and which may already be stable in the static case.

For such stable or at least long-lived rotating wormholes a general analysis of their geodesics should also be interesting. The restricted analysis of orbits in the equatorial plane has already shown, that there are stable bound orbits for massive particles and unstable bound orbits for light. A general analysis will tell us on the theoretical side, whether the orbits in rotating wormhole spacetimes display chaos, while on the observational side it will, in particular, let us understand how the shadows of these rotating wormholes compare to the shadows of rotating black holes.

Acknowledgements We would like to thank our collaborators Xiao Yan Chew, Vladimir Dzhunushaliev, Vladimir Folomeev and Eugen Radu, and we gratefully acknowledge support by the DFG within the Research Training Group 1620 "Models of Gravity" and by FP7, Marie Curie Actions, People, International Research Staff Exchange Scheme (IRSES-606096).

References

1. Ellis HG. Ether flow through a drainhole - a particle model in general relativity. J Math Phys. 1973;14:104–18.
2. Ellis HG. The evolving, flowless drain hole: a nongravitating particle model in general relativity theory. Gen Rel Grav. 1979;10:105–23.
3. Bronnikov KA. Scalar-tensor theory and scalar charge. Acta Phys Polon B. 1973;4:251–66.
4. Kodama T. General relativistic nonlinear field: a kink solution in a generalized geometry. Phys Rev D. 1978;18:3529–34.
5. Morris MS, Thorne KS. Wormholes in space-time and their use for interstellar travel: a tool for teaching general relativity. Am J Phys. 1988;56:395–412.
6. Morris MS, Thorne KS, Yurtsever U. Wormholes, time machines, and the weak energy condition. Phys Rev Lett. 1988;61:1446.
7. Lobo FSN. Phantom energy traversable wormholes. Phys Rev D. 2005;71:084011.
8. Hochberg D. Lorentzian wormholes in higher order gravity theories. Phys Lett B. 1990;251:349–54.
9. Fukutaka H, Tanaka K, Ghoroku K. Wormhole solutions in higher derivative gravity. Phys Lett B. 1989;222:191–4.
10. Ghoroku K, Soma T. Lorentzian wormholes in higher derivative gravity and the weak energy condition. Phys Rev D. 1992;46:1507–16.
11. Furey N, DeBenedictis A. Wormhole throats in R^m gravity. Class Quant Grav. 2005;22:313–22.
12. Bronnikov KA, Elizalde E. Spherical systems in models of nonlocally corrected gravity. Phys Rev D. 2010;81:044032.
13. Kanti P, Kleihaus B, Kunz J. Wormholes in dilatonic Einstein-Gauss-Bonnet theory. Phys Rev Lett. 2011;107:271101.
14. Kanti P, Kleihaus B, Kunz J. Stable Lorentzian wormholes in dilatonic Einstein-Gauss-Bonnet theory. Phys Rev D. 2012;85:044007.
15. Abe F. Gravitational microlensing by the Ellis wormhole. Astrophys J. 2010;725:787.
16. Toki Y, Kitamura T, Asada H, Abe F. Astrometric image centroid displacements due to gravitational microlensing by the Ellis wormhole. Astrophys J. 2011;740:121.
17. Takahashi R, Asada H. Observational upper bound on the cosmic abundances of negative-mass compact objects and Ellis wormholes from the sloan digital sky survey quasar lens search. Astrophys J. 2013;768:L16.

18. Cramer JG, Forward RL, Morris MS, Visser M, Benford G, Landis GA. Natural wormholes as gravitational lenses. Phys Rev D. 1995;51:3117.
19. Perlick V. On the exact gravitational lens equation in spherically symmetric and static spacetimes. Phys Rev D. 2004;69:064017.
20. Tsukamoto N, Harada T, Yajima K. Can we distinguish between black holes and wormholes by their Einstein ring systems? Phys Rev D. 2012;86:104062.
21. Bambi C. Can the supermassive objects at the centers of galaxies be traversable wormholes? the first test of strong gravity for mm/sub-mm VLBI facilities. Phys Rev D. 2013;87:107501.
22. Nedkova PG, Tinchev VK, Yazadjiev SS. Shadow of a rotating traversable wormhole. Phys Rev D. 2013;88:124019.
23. Zhou M, Cardenas-Avendano A, Bambi C, Kleihaus B, Kunz J. Search for astrophysical rotating Ellis wormholes with X-ray reflection spectroscopy. Phys Rev D. 2016;94:024036.
24. Shinkai H-a, Hayward SA. Fate of the first traversible wormhole: black hole collapse or inflationary expansion. Phys Rev D. 2002;66:044005.
25. Gonzalez JA, Guzman FS, Sarbach O. Instability of wormholes supported by a ghost scalar field I. Linear Class Quant Grav. 2009;26:015010.
26. Gonzalez JA, Guzman FS, Sarbach O. Instability of wormholes supported by a ghost scalar field II. Nonlinear Class Quant Grav. 2009;26:015011.
27. Torii T, Shinkai H-a. Wormholes in higher dimensional space-time: exact solutions and their linear stability analysis. Phys Rev D. 2013;88:064027.
28. Matos T, Nunez D. Rotating scalar field wormhole. Class Quant Grav. 2006;23:4485.
29. Dzhunushaliev V, Folomeev V, Kleihaus B, Kunz J, Radu E. Rotating wormholes in five dimensions. Phys Rev D. 2013;88:124028.
30. Kashargin PE, Sushkov SV. Slowly rotating wormholes: the first order approximation. Grav Cosmol. 2008;14:80.
31. Kashargin PE, Sushkov SV. Slowly rotating scalar field wormholes: the second order approximation. Phys Rev D. 2008;78:064071.
32. Kleihaus B, Kunz J. Rotating Ellis wormholes in four dimensions. Phys Rev D. 2014;90:121503.
33. Chew XY, Kleihaus B, Kunz J. Geometry of spinning Ellis wormholes. Phys Rev D. 2016;94(10):104031.
34. Teo E. Rotating traversable wormholes. Phys Rev D. 1998;58:024014.
35. Smarr L. Mass formula for Kerr black holes. Phys Rev Lett. 1973;30:71 Erratum: [Phys Rev Lett 1973;30:521].
36. Smarr L. Surface geometry of charged rotating black holes. Phys Rev D. 1973;7:289.
37. Hauser O, Ibadov R, Kleihaus B, Kunz J. Hairy wormholes and Bartnik-McKinnon solutions. Phys Rev D. 2014;89:064010.
38. Konoplya RA, Zhidenko A. Wormholes versus black holes: quasinormal ringing at early and late times. JCAP 2016;12:043.

Chapter 4
Astrophysical Signatures of Thin Accretion Disks in Wormhole Spacetimes

Tiberiu Harko, Zoltán Kovács and Francisco S.N. Lobo

4.1 Introduction

One of the most important evidence for the existence of the black holes comes from the electromagnetic radiation emitted by the gaseous matter in orbital motion around them. The radiation is emitted mostly in the X-ray band, but other frequency ranges can also be observed. The radiation originates due to the presence of inward-falling matter, which forms an accretion disk around the central compact general relativistic object. Thus, the astrophysical objects increase their mass through the mechanism of mass accretion. In this context, a large number of astrophysical observations have shown that gas clouds surrounding the central compact object exist around almost all of the known active galactic nuclei (AGN's), or black hole candidates. These clouds, existing in either a molecular or atomic phase, form an associated accretion disk, extending on a variety of scales ranging from a tenth of a parsec to a few hundred parsecs [1] (for an in-depth discussion of accretion disks and their observational properties, we refer the reader to [2–4]). In many astrophysical situations the gas around the black hole forms a geometrically and optically thick torus (or a warped

T. Harko (✉)
Department of Physics, Babes-Bolyai University, Kogălniceanu Street,
400084 Cluj-Napoca, Romania
e-mail: t.harko@ucl.ac.uk

T. Harko
Department of Mathematics, University College London, Gower Street,
London WC1E 6BT, UK

Z. Kovács
Max-Fiedler-Str. 7, 45128 Essen, Germany
e-mail: kovacs.z@protonmail.com

F.S.N. Lobo
Faculdade de Ciências da Universidade de Lisboa, Instituto de Astrofísica
e Ciências do Espaço, Edifício C8, 1749-016 Campo Grande, Lisbon, Portugal
e-mail: fslobo@fc.ul.pt

F.S.N. Lobo (ed.), *Wormholes, Warp Drives and Energy Conditions*,
Fundamental Theories of Physics 189, DOI 10.1007/978-3-319-55182-1_4

disk), which absorbs most of the radiation emitted in the ultraviolet and soft X-rays bands.

From an observational point of view, the most important early evidence for the existence of supermassive black holes outside our galaxy came from the VLBI (Very-Long-Baseline Interferometry) imaging of molecular H_2O masers, which were first studied in the active galaxy NGC 4258 [5]. The VLBI imaging, based on the Doppler shift measurements of the masering source, assumed to be in Keplerian motion around the central object, led to a quite precise estimation of the mass of the black hole, which has been found to be of the order of $3.6 \times 10^7 M_\odot$, i.e., a supermassive dark object, located within 0.13 parsecs. Hence, the observation of the motion of gaseous flows in the gravitational field of black holes or other compact objects can provide relevant astrophysical information on the nature of the astrophysical source.

As seen by an observer located at infinity, the dominant features in the X-ray spectrum of an accretion disk are the iron lines, with broad skewed proles [6]. The energy of the Fe Kα line is of the order of 6.4 keV, with the natural bandwidth of the order of a few eV. Relativistic effects, as well as the extremely high velocity of the matter in the disk cause the deformation of the line [6], and determine the typical observed bandwidth, which is of about 200 eV. On the other hand, the Fe Kα line is not significantly affected by absorption phenomena, and hence the broad red wing of the line can be used as an extremely powerful tool to obtain and analyze the main astrophysical characteristics of the central massive object [7]. Theoretical and numerical models of the relativistic Fe Kα line for a maximally rotating Kerr black hole were developed in [8–10]. These theoretical studies opened the possibility of obtaining some unique information on the dynamics, geometry, and structure of the accretion flows near the central general relativistic object [6, 9].

The study of the mass accretion around rotating black holes was initiated within the framework of a general relativistic approach in [11]. By extending the theory of non-relativistic accretion, as developed in [12], steady-state thin disk models were constructed [11], by using the equatorial approximation to describe the stationary and axisymmetric spacetime of rotating black holes. In these types of models the accreting matter has a Keplerian motion, while the hydrodynamical equilibrium is maintained by the efficient cooling due to radiation transport. The radiation emitted by the disk surface, assumed to be in thermodynamical equilibrium, was considered as being that of a black body. The radiation properties of thin accretion disks were further investigated and analyzed in [13, 14], and the effects of the photon capture by the black hole on the spin evolution were also considered. An important physical quantity, the efficiency with which black holes convert rest mass into outgoing radiation in the accretion process was also introduced, and explicitly computed. The emissivity properties of the accretion disks opened the possibility of providing definite signatures that could distinguish between different classes of exotic central objects, such as non-rotating or rotating quark, boson or fermion stars [15–18]. The radiation power per unit area, the temperature of the disk and the spectrum of the emitted radiation provides the possibility, once they are compared with the radiation properties of a Schwarzschild or Kerr black hole of an equal mass, to make some explicit predictions on the nature of the central object.

In this context, the nature of the supermassive black hole candidates in galactic nuclei can be tested by analyzing the profile of the Kα iron line observed in their X-ray spectrum. The possibility that the spacetime in the immediate vicinity of compact objects may be described by some non-vacuum exact solutions of Einstein's equations resulting as the end-state of gravitational collapse was investigated in [19]. The iron line generated around this class of objects has specific features, which can be used to distinguish such objects from Kerr black holes. One particular signature is that their iron line cannot have the characteristic low-energy tail of the line generated from accretion disks around fast-rotating Kerr black holes. The effect of a massive accretion disk in the measurement of the black hole spin was estimated with a simple analytical model in [20]. For typical accretion disks, the mass of the disk is completely negligible, even for future more accurate measurements. However, for systems with very massive disks the effect may not be ignored. The Polish doughnut model was used in [21] to describe an optically thin and constant angular momentum ion torus in hydrodynamical equilibrium and model the accretion structure around SgrA*. The spectrum as seen by a distant observer in Kerr and non-Kerr spacetimes was computed, and it was studied how an accurate measurement can constrain possible deviations form the Kerr solution. There is a substantial degeneracy between the determination of the spin and of the possible deviations from the Kerr geometry, even when the parameters of the ion torus are fixed.

Hypothetical astrophysical objects with naked singularities, which are characterized by a gravitational singularity without an event horizon, were also analyzed. Note, however, that Penrose has proposed a conjecture according to which there exists a cosmic censor who forbids the occurrence of naked singularities. Distinguishing between astrophysical black holes and naked singularities is a major challenge for present day observational astronomy. A possibility of differentiating naked singularities from black holes is through the comparative study of thin accretion disks properties around rotating naked singularities and Kerr-type black holes, respectively [22]. A first major difference between rotating naked singularities and Kerr black holes is in the frame dragging effect, the angular velocity of a rotating naked singularity being inversely proportional to its spin parameter. Due to the differences in the exterior geometry, the thermodynamic and electromagnetic properties of the disks are different for these two classes of compact objects, consequently giving clear observational signatures that could discriminate between black holes and naked singularities [22]. For specific values of the spin parameter and of the scalar charge, the energy flux from the disk around a rotating naked singularity can exceed by several orders of magnitude the flux from the disk of a Kerr black hole. The conversion efficiency of the accreting mass into radiation by rotating naked singularities is always higher than the conversion efficiency for black holes.

Due to their superfluid properties some compact astrophysical objects, like neutron or quark stars, may contain a significant part of their matter in the form of a Bose–Einstein Condensate. Observationally distinguishing between neutron/quark stars and Bose–Einstein Condensate stars is a major challenge for this latter theoretical model. An observational possibility of indirectly distinguishing Bose–Einstein

Condensate stars from neutron/quark stars is through the study of the thin accretion disks around compact general relativistic objects [23]. A detailed comparative study of the electromagnetic and thermodynamic properties of the thin accretion disks around rapidly rotating Bose–Einstein Condensate stars, neutron stars and quark stars, respectively, was performed in [23]. Due to the differences in the exterior geometry, the thermodynamic and electromagnetic properties of the disks (energy flux, temperature distribution, equilibrium radiation spectrum and efficiency of energy conversion) are different for these classes of compact objects.

The possibility of observationally discriminating between various types of neutron stars, described by different equations of state of the nuclear matter, as well as differentiating neutron stars from other types of exotic objects, like, for example, quark stars, from the study of the emission properties of the accretion disks around them, was investigated in [24]. The energy flux, the temperature distribution and the emission spectrum from the accretion disks around several classes of rapidly rotating neutron stars, described by different equations of state of the neutron matter, and for quark stars, described by the MIT bag model equation of state and in the CFL (Color-Flavor-Locked) phase, respectively, was obtained. Particular signatures appear in the electromagnetic spectrum, thus leading to the possibility of directly testing the equation of state of the dense matter by using astrophysical observations of the emission spectra from accretion disks. The accretion process in an arbitrary static, spherically symmetric spacetime was considered in [25], where a general formalism for the study of accretion was developed, and the temperature, and density profiles were obtained for the case of the polytropic equation of state.

Several astrophysical compact objects have been proposed, in the literature, as alternatives to the standard black hole picture of general relativity, such as gravastars [26]. These consist of a dark energy condensate surrounded by a strongly correlated thin shell of anisotropic matter. In the context of stationary and axially symmetrical geometries, a possibility of distinguishing gravastars from black holes is through the comparative study of thin accretion disks around rotating gravastars and Kerr-type black holes, respectively [27]. Due to the differences in the exterior geometry, the thermodynamic and electromagnetic properties of the disks (energy flux, temperature distribution, and equilibrium radiation spectrum) are different for these two classes of compact objects, consequently giving clear observational signatures that may distinguish them observationally. In fact, it was shown that gravastars provide a less efficient mechanism for converting mass to radiation than black holes [27].

In modified theories of gravity, the physical properties of matter forming a thin accretion disk in the static and spherically symmetric spacetime metric of vacuum $f(R)$ gravity were also analyzed [28], and it was shown that particular signatures can appear in the electromagnetic spectrum, thus leading to the possibility of directly testing modified gravity models by using astrophysical observations of the emission spectra from accretion disks. The energy flux, the emission spectrum and accretion efficiency from the accretion disks around several classes of static and rotating brane world black holes were obtained in [29], and they were compared with the general relativistic case. The general formalism was applied to the study of the accretion properties of several classes of brane-world black holes, and the distribution of the

main physical parameters of the gas was obtained. The astrophysical determination of these physical quantities could discriminate, at least in principle, between the different brane-world models, and place some constraints on the existence of the extra dimensions. The thin accretion disk signatures in dynamical Chern–Simons modified gravity and in Horãva-Lifshitz gravity were obtained in [30, 31], respectively.

In this chapter, we will apply the analysis of the thin accretion disk models in wormholes geometries. This study was initiated in [32, 33], respectively, where the analysis of the properties of the radiation emerging from the surface of the disk around static and rotating axially symmetric wormhole geometries was performed. As a result of these investigations it was shown that specific signatures appear in the electromagnetic spectrum of accretion disks around wormholes made of exotic matter. Hence the observational study of the radiation emitted by accretion disks could lead to the possibility of clearly distinguishing wormhole geometries from the static Schwarzschild or rotating Kerr spacetimes. The expected Kα iron line in some wormhole spacetimes was studied in [34], and it was compared with the line produced around Kerr black holes. The line generated by non-rotating or very slow-rotating wormholes is relatively similar to the one expected around Kerr black holes with mild or high values of the spin parameter. On the other hand for wormholes with spin parameter $a_* \geq 0.02$, the associated Kα iron line is quite different from the one produced around Kerr black holes.

In [35], it was suggested that the nature of supermassive objects at the centers of galaxies—traversable wormholes or black holes—could be tested by using mm/sub-mm VLBI facilities. As shown in [36], in a few years, the VLTI instrument GRAVITY will have the capability to image blobs of plasma orbiting near the innermost stable circular orbit of SgrA*, the supermassive black hole candidate in the Milky Way. Since the secondary image of a hot spot orbiting around a wormhole is substantially different from that of a hot spot around a black hole, astrophysical observations may allow to test if at the center of our Galaxy a black hole or a wormhole is located. High energy collision of two particles in wormhole spacetimes [37] or the study of collisional Penrose process in rotating wormhole spacetimes [38] could also provide important information on the nature of compact astrophysical objects. The iron line profile in the X-ray reflection spectrum of a thin accretion disk around rotating Ellis wormholes also have some specific observational signatures that can be used to distinguish these objects from Kerr black holes [39].

The present chapter is organized as follows. In Sect. 4.2, we review the formalism of the thin disk accretion onto compact objects for static and spherically symmetric spacetimes. In Sect. 4.3, we analyze the basic properties of matter forming a thin accretion disk in static and spherically symmetric wormhole spacetimes, and for rotating wormhole geometries in Sect. 4.4. We discuss and conclude our results in Sect. 4.5. Throughout this work, we use a system of units so that $c = G = \hbar = k_B = 1$, where k_B is Boltzmann's constant.

4.2 Electromagnetic Radiation Properties of Thin Accretion Disks in General Relativistic Spacetimes

Accretion disks are flattened astronomical structures made of rapidly rotating particles (gas) in orbital motion around a massive central gravitating body. The gas slowly spirals inwards towards the central body, while its gravitational energy is transformed into heat. The gravitational and the frictional forces raise the temperature of the disk, such that radiation emission occurs, leading to the eventual cooling down of the disk. The radiation emitted by the disk provides invaluable information on the physics of the accretion disks. The emission of the disk is in the radio, optical, and X-ray energy bands, and from the analysis of the observed electromagnetic spectrum, and of its time variability, important information on the disk and its environment can be obtained. In the following we will restrict our analysis to thin accretion disks, in which most of the matter is located close to the radial plane.

4.2.1 Marginally Stable Orbits

The physical properties of the disk, as well as the characteristics of the electromagnetic radiation emitted by particles moving in circular orbits around general relativistic compact objects are fully determined by the geometry of the spacetime in which the disk is embedded. For a stationary and axially symmetric geometry we adopt for the metric the general form given by

$$ds^2 = g_{tt}\,dt^2 + 2g_{t\phi}\,dtd\phi + g_{rr}\,dr^2 + g_{\theta\theta}\,d\theta^2 + g_{\phi\phi}\,d\phi^2\,. \tag{4.1}$$

Moreover, we also adopt the equatorial approximation, in which the metric functions g_{tt}, $g_{t\phi}$, g_{rr}, $g_{\theta\theta}$ and $g_{\phi\phi}$ only depend on the radial coordinate r, that is, we assume that the condition $|\theta - \pi/2| \ll 1$ is satisfied for all particles in the disk.

From a physical point of view the physical quantities characterizing the particles in the disk moving in circular orbits in a stationary and axially symmetric geometry are the angular velocity Ω, the specific energy $\widetilde{E}$, and the specific angular momentum $\widetilde{L}$, respectively. These quantities can be obtained from the geodesic equations, which take the following form

$$\frac{dt}{d\tau} = \frac{\widetilde{E}g_{\phi\phi} + \widetilde{L}g_{t\phi}}{g_{t\phi}^2 - g_{tt}g_{\phi\phi}}, \qquad \frac{d\phi}{d\tau} = -\frac{\widetilde{E}g_{t\phi} + \widetilde{L}g_{tt}}{g_{t\phi}^2 - g_{tt}g_{\phi\phi}}, \tag{4.2}$$

$$g_{rr}\left(\frac{dr}{d\tau}\right)^2 = -1 + \frac{\widetilde{E}^2 g_{\phi\phi} + 2\widetilde{E}\widetilde{L}g_{t\phi} + \widetilde{L}^2 g_{tt}}{g_{t\phi}^2 - g_{tt}g_{\phi\phi}}. \tag{4.3}$$

With the use of Eq. (4.3) we can introduce an effective potential term $V_{eff}(r)$ defined as

$$V_{eff}(r) = -1 + \frac{\widetilde{E}^2 g_{\phi\phi} + 2\widetilde{E}\widetilde{L} g_{t\phi} + \widetilde{L}^2 g_{tt}}{g_{t\phi}^2 - g_{tt} g_{\phi\phi}}. \tag{4.4}$$

The conditions for the existence of stable circular orbits in the equatorial plane are given by $V_{eff}(r) = 0$ and $V_{eff,\,r}(r) = 0$, respectively, where the comma in the subscript denotes the ordinary derivative with respect to the radial coordinate r. These conditions imposed on the effective potential allow us to obtain Ω, $\widetilde{E}$, and $\widetilde{L}$ for the particles moving in circular orbits around general relativistic compact spheres as

$$\widetilde{E} = -\frac{g_{tt} + g_{t\phi}\Omega}{\sqrt{-g_{tt} - 2g_{t\phi}\Omega - g_{\phi\phi}\Omega^2}}, \qquad \widetilde{L} = \frac{g_{t\phi} + g_{\phi\phi}\Omega}{\sqrt{-g_{tt} - 2g_{t\phi}\Omega - g_{\phi\phi}\Omega^2}}, \tag{4.5}$$

$$\Omega = \frac{d\phi}{dt} = \frac{-g_{t\phi,r} + \sqrt{(g_{t\phi,r})^2 - g_{tt,r} g_{\phi\phi,r}}}{g_{\phi\phi,r}}. \tag{4.6}$$

The radii of the marginally stable orbits around the central compact object are determined by the condition $V_{eff,\,rr}(r) = 0$. By formally representing the effective potential as $V_{eff}(r) \equiv -1 + f/g$, where

$$f \equiv \widetilde{E}^2 g_{\phi\phi} + 2\widetilde{E}\widetilde{L} g_{t\phi} + \widetilde{L}^2 g_{\phi\phi}, \qquad g \equiv g_{t\phi}^2 - g_{tt} g_{\phi\phi}, \qquad g \neq 0,$$

from $V_{eff}(r) = 0$ it follows first that $f = g$. Then from the condition $V_{eff,\,r}(r) = 0$ we find $f_{,r} g - f g_{,r} = 0$. Thus, with the use of these conditions we can write down explicitly the condition $V_{eff,\,rr}(r) = 0$, which reduces to

$$0 = (g_{t\phi}^2 - g_{tt} g_{\phi\phi}) V_{eff,rr} = \widetilde{E}^2 g_{\phi\phi,rr} + 2\widetilde{E}\widetilde{L} g_{t\phi,rr} + \widetilde{L}^2 g_{tt,rr} - (g_{t\phi}^2 - g_{tt} g_{\phi\phi})_{,rr}\,. \tag{4.7}$$

By substituting Eqs. (4.5) and (4.6) into Eq. (4.7) we obtain an equation that can be solved for r. Thus the radii of the marginally stable orbits can be easily obtained, once the metric coefficients g_{tt}, $g_{t\phi}$ and $g_{\phi\phi}$ are given explicitly.

4.2.2 Physical Properties of Thin Accretion Disks

In the following we will restrict our analysis to thin accretion disks, for which the vertical size (defined along the z-axis), given by the disk height H, is always much smaller than the characteristic radius R of the disk, $H \ll R$. R characterizes the horizontal extension of the disk, (defined along the radial direction r), while H can be taken as equal to the maximum half thickness of the disk.

From a physical point of view we assume that the thin disk is in hydrodynamical equilibrium. Moreover, the pressure gradient, as well as the vertical entropy gradient, are both negligibly small in the disk. On the other hand, due to the efficient cooling

mechanisms via the radiation over the entire disk surface, the heat generated by local stresses and dynamical friction cannot be deposited in the disk. Consequently, the hydrodynamic equilibrium forces the disk to mechanically stabilize its thin vertical size. At the marginally stable orbit of the central compact object potential the thin disk has an inner edge, while the accreting matter in higher orbits has a Keplerian motion.

In the most common steady-state accretion disk models, it is assumed that the mass accretion rate $\dot{M}_0$ is a time-independent constant. Hence all the quantities describing the physical properties of the orbiting matter particles are averaged over a characteristic time scale Δt, over the azimuthal angle $\Delta\phi = 2\pi$, and over the height H, respectively [11–13].

As we have already seen in the previous Section, the particles moving in Keplerian orbits around general relativistic compact objects with an angular velocity $\Omega = d\phi/dt$ have a specific energy $\widetilde{E}$, and a specific angular momentum $\tilde{L}$, respectively. In the steady-state thin disk model these quantities depend only on the radii r of their orbits. The disk particles, rotating with the four-velocity u^μ, form a matter disk having a surface density Σ, representing the average of the rest mass density ρ_0 of the disk matter, vertically integrated. We model the matter in the disk by an anisotropic fluid source, characterized from the thermodynamic point of view by the density ρ_0, the energy flow vector q^μ and the stress tensor $t^{\mu\nu}$ (we neglect the specific heat of the disk fluid). All these quantities are measured in the averaged rest-frame. Then, the first quantity describing the disk structure is the surface density $\Sigma(r)$, defined as [11, 13]

$$\Sigma(r) = \int_{-H}^{H} \langle \rho_0 \rangle dz, \tag{4.8}$$

where $\langle \rho_0 \rangle$ is the averaged rest mass density $\langle \rho_0 \rangle$ over a time Δt and the angle 2π. Second, we can introduce the torque

$$W_\phi{}^r = \int_{-H}^{H} \langle t_\phi{}^r \rangle dz, \tag{4.9}$$

where $\langle t^r_\phi \rangle$ is the average of the component t^r_ϕ of the stress tensor over Δt and 2π. The radiation flux $\mathscr{F}(r)$, an important physical quantity describing the disk, is obtained as the time and orbital average of the energy flux vector q^z over the disk surface, so that

$$\mathscr{F}(r) = \langle q^z \rangle. \tag{4.10}$$

For the stress–energy tensor of the matter in the disk we adopt the form

$$T^{\mu\nu} = \rho_0 u^\mu u^\nu + 2u^{(\mu} q^{\nu)} + t^{\mu\nu}, \tag{4.11}$$

where $u_\mu q^\mu = 0$, and $u_\mu t^{\mu\nu} = 0$, respectively. In a local basis the four-vectors of the energy flux and angular momentum flux are defined as $-E^\mu \equiv T^\mu_\nu (\partial/\partial t)^\nu$ and $J^\mu \equiv T^\mu_\nu (\partial/\partial\phi)^\nu$, respectively.

In order to derive the structure equations of the thin disk we integrate the conservation laws of the rest mass, of the energy, and of the angular momentum of the disk matter, respectively [11, 13]. First, from the equation of the rest mass conservation, $\nabla_\mu(\rho_0 u^\mu) = 0$, we obtain the important result that the time averaged rate of the rest mass accretion is independent of the disk radius,

$$\dot{M}_0 \equiv -2\pi r \Sigma u^r = \text{constant}, \tag{4.12}$$

where a dot represents the derivative with respect to the coordinate time t. The law of energy conservation $\nabla_\mu E^\mu = 0$ can be reformulated in an integral form as the integral form

$$[\dot{M}_0 \widetilde{E} - 2\pi r \Omega W_\phi{}^r]_{,r} = 4\pi r \mathscr{F} \widetilde{E}. \tag{4.13}$$

From a physical point of view Eq. (4.13) states that the sum of the energies transported by the rest mass flow, $\dot{M}_0 \widetilde{E}$, and by the dynamical stresses in the disk, $2\pi r \Omega W_\phi{}^r$, respectively, equal the energy emitted in the form of electromagnetic radiation from the surface of the disk, $4\pi r \mathscr{F} \widetilde{E}$. Similarly, from the law of the angular momentum conservation, $\nabla_\mu J^\mu = 0$, we obtain the balance equation of the angular momentum transport,

$$[\dot{M}_0 \widetilde{L} - 2\pi r W_\phi{}^r]_{,r} = 4\pi r \mathscr{F} \widetilde{L}. \tag{4.14}$$

To obtain an expression for the energy flux $\mathscr{F}$ we eliminate first $W_\phi{}^r$ from Eqs. (4.13) and (4.14), respectively. Then, we use the universal energy-angular momentum relation $dE = \Omega dJ$, which for circular geodesic orbits takes the form $\widetilde{E}_{,r} = \Omega \widetilde{L}_{,r}$. Therefore it follows that the flux $\mathscr{F}$ of the radiant energy over the entire surface of the disk can be expressed as a function of the specific energy, angular momentum and of the angular velocity of the disk matter in the form [11, 13],

$$\mathscr{F}(r) = -\frac{\dot{M}_0}{4\pi\sqrt{-g}} \frac{\Omega_{,r}}{(\widetilde{E} - \Omega \widetilde{L})^2} \int_{r_{ms}}^{r} (\widetilde{E} - \Omega \widetilde{L}) \widetilde{L}_{,r} dr. \tag{4.15}$$

The efficiency ε with which the central compact general relativistic object converts the rest mass energy into outgoing electromagnetic radiation is another important characteristic of the mass accretion process in thin accretion disks. The efficiency ε of the disk is defined as the ratio of the rate of the energy of the photons traveling from the disk surface to infinity, and the rate at which mass energy is accreted by the central massive general relativistic object [11, 13]. Both energy rates are measured at infinity If all the photons emitted from the disk surface can escape to infinity, the efficiency of the disk is given as a function of the specific energy measured at the marginally stable orbit r_{ms},

$$\varepsilon = 1 - \widetilde{E}_{ms}. \tag{4.16}$$

The efficiency ε for Schwarzschild black holes is of the order of 6%, no matter if the photon capture by the black hole is considered, or not. For rapidly rotating black holes, by ignoring the capture of radiation by the hole, ε has a value of around 42%, whereas by assuming photon capture in the Kerr potential the efficiency is about 40% [14].

A fundamental assumption on the accreting matter in the steady-state thin disk model is that it is in thermodynamical equilibrium. Therefore, in this approximation, the radiation emitted by the entire disk surface can be described as a perfect black body radiation, with the energy flux given by $\mathscr{F}(r) = \sigma T^4(r)$, where T is the disk temperature, and σ is the Stefan–Boltzmann constant. Then the observed luminosity $L(\nu)$ of the disk can be represented by a redshifted black body spectrum, which in natural units $\hbar = c = 1$ is given by [16],

$$L(\nu) = 4\pi d^2 I(\nu) = 16\pi^2 \cos\gamma \int_{r_{in}}^{r_f} \int_0^{2\pi} \frac{\nu_e^3 r d\phi dr}{\exp(2\pi\nu_e/T) - 1}. \tag{4.17}$$

In Eq. (4.17) d is the distance to the radiation source (the disk), $I(\nu)$ is the Planck distribution function, γ is the disk inclination angle, and r_i and r_f give the positions of the inner and outer edges of the disk, respectively. In the integral over the radial coordinate we assume $r_i = r_{ms}$ and $r_f \to \infty$, respectively, since we expect that for any kind of general relativistic compact object geometry the electromagnetic flux from the disk surface vanishes at infinity, $r \to \infty$. The electromagnetic radiation frequency emitted from the disk is given by $\nu_e = \nu(1 + z)$, with the redshift factor z given by [40, 41] as

$$1 + z = \frac{1 + \Omega r \sin\phi \sin\gamma}{\sqrt{-g_{tt} - 2\Omega g_{t\phi} - \Omega^2 g_{\phi\phi}}}. \tag{4.18}$$

In Eq. (4.18) we have neglected the bending of light.

With respect to the simple scaling transformation of the radial coordinate, given by $r \to \tilde{r} = r/M$, where M is the mass of the central compact general relativistic object, the electromagnetic flux and the emission spectrum of the accretion disks satisfy some simple, but important and very useful scaling relations. Generally, the components of the metric tensor $g_{\mu\nu}$ are invariant with respect of this scaling transformation. On the other hand the specific energy, the angular momentum and the angular velocity transform as $\widetilde{E} \to \widetilde{E}$, $\widetilde{L} \to M\widetilde{L}$ and $\Omega \to \widetilde{\Omega}/M$, respectively. The electromagnetic flux scales as $F(r) \to F(\tilde{r})/M^4$, which gives the transformation law of the temperature as $T(r) \to T(\tilde{r})/M$. A rescaling of the frequency of the radiation emitted by the disk of the form $\nu \to \tilde{\nu} = \nu/M$, rescales the luminosity of the disk as $L(\nu) \to L(\tilde{\nu})/M$. On the other hand, since the energy flux of the disk is proportional to the accretion rate $\dot{M}_0$, an increase in the accretion rate $\dot{M}_0$ results in a linear increase of the radiation flux from the disk.

4.3 Electromagnetic Signatures of Accretion Disks in Static Wormhole Geometries

In the present Section, we will review the thin disk accretion properties in static and spherically symmetric wormhole geometries [32]. After introducing the wormhole geometry, and discuss some of their general properties, we will compare in detail the dynamic and electromagnetic properties of particle forming a thin disk in Schwarzschild and wormhole geometries, respectively.

4.3.1 Static Spherically Symmetric Wormhole Geometries

As a first example of a wormhole geometry that can be tested by using the emission properties of thin accretion disks we consider the Morris–Thorne wormhole [42], which is described by the static and spherically symmetric metric and is given by

$$ds^2 = -e^{2\Phi(r)}\,dt^2 + \frac{dr^2}{1-b(r)/r} + r^2\left(d\theta^2 + \sin^2\theta\,d\phi^2\right). \tag{4.19}$$

This metric describes a wormhole geometry consisting of two identical, asymptotically flat regions, which are joined together at the throat located at $r_0 > 0$. As for the radial coordinate r, it has a range that increases from a minimum value at r_0, representing the wormhole throat, and extends to ∞ (we refer the reader to Chap. 2 for more details).

An important requirement for a wormhole geometry is the avoidance of event horizons, which requires that the redshift function $\Phi(r)$ be finite for the adopted radial coordinate range. On the other hand at the throat r_0, the shape function is given by $b(r_0) = r_0$. A fundamental property of the wormhole geometries is the flaring-out condition, given by $\left[b'(r)r - b(r)\right]/b^2(r) < 0$, which follows from the mathematical properties of the embedding [42].

An interesting possibility that follows from wormhole geometries is that they have a repulsive/attractive character [43]. In order to show this property, consider a static observer, located at constant r, θ, ϕ, whose four-acceleration of the observer is given $a^t = 0$, and $a^r = \Phi_{,r}\ (1 - b/r)$ respectively (we refer the reader to Chap. 2 and [43] for more details). Note that a^r represents the radial component of the proper acceleration required for an observer to remain at rest at a constant location $r,\ \theta,\ \phi$. If $a^r > 0$, the geometry is attractive, that is, the observers must permanently have an outward-directed radial acceleration, in order to keep them from being pulled into the wormhole. On the other hand, if $a^r < 0$, the gravitational field (and the geometry) is repulsive, so that the observers must have an inward-directed radial acceleration in order to avoid being pushed away from the wormhole. Obviously this difference is dictated by the sign of $\Phi_{,r}$. Thus, the convention we will use is that $\Phi_{,r}(r)$ is

positive for an inwardly oriented (attractive) gravitational force, and negative for an outwardly oriented gravitational force (repulsion).

The above results are of particular interest for the observationally important case of particles moving in circular orbits around wormholes. For the specific case of $\Phi_{,r}(r) < 0$, due to the outward gravitational repulsion, the particles in the disk are unstable. Therefore, in the following, we restrict our analysis to the case $\Phi_{,r}(r) > 0$. In particular, as a specific example, we will adopt for $\Phi(r)$ the functional form

$$\Phi(r) = -\frac{r_0}{r}, \tag{4.20}$$

which we will consider in detail in the following analysis.

4.3.2 *Electromagnetic Signatures of Static Spherically Symmetric Wormhole Geometries*

In a static spherically symmetric geometry with metric represented by Eq. (4.19), the effective potential that determines the geodesic motion of the test particles in the equatorial plane, given in its general form by Eq. (4.4), reduces to

$$V_{eff}(r) \equiv e^{2\Phi}\left(1 + \frac{\widetilde{L}^2}{r^2}\right). \tag{4.21}$$

The physical parameters of the particle motion in the disk (effective potential V_{eff}, the angular velocity Ω, the specific energy $\widetilde{E}$ and the specific angular momentum $\widetilde{L}$, respectively) are presented, for the specific case of $\Phi(r) = -r_0/r$, in Fig. 4.1, for a wormhole with a total mass of the order of $M = 0.06776 M_{\odot}$, with the throat located at $r_0 = GM/c^2 = 10^4$cm. The orbiting particles have a specific angular momentum of $\widetilde{L} = 4M$. The corresponding physical parameters in the Schwarzschild geometry, plotted as solid lines, are also presented for comparison.

Since the angular velocity Ω, the specific energy $\widetilde{E}$ and the specific angular momentum $\widetilde{L}$, given generally by Eqs. (4.5) and (4.6), depend only on the metric function $\Phi(r)$, they are identical for all wormhole geometries, and are independent of the choice of the shape function $b(r)$. It is interesting to note here that the only quantity in the flux integral (4.15) that has a dependence on the metric tensor coefficient $b(r)$ is the determinant of the metric tensor $-g$. The invariant volume element of the different types of static wormholes can be obtained as

$$\sqrt{-g} = \frac{r^2 e^{\Phi}}{\sqrt{1 - b(r)/r}}. \tag{4.22}$$

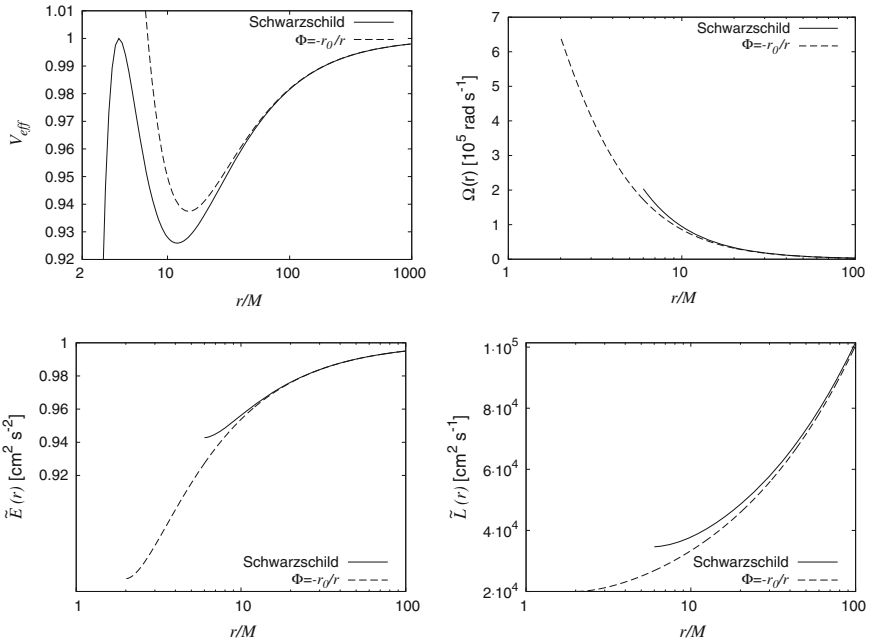

Fig. 4.1 The effective potential $V_{eff}(r)$ (*top left hand*), the angular velocity Ω (*top right hand*), the specific energy $\widetilde{E}$ (*bottom left hand*) and the specific angular momentum $\widetilde{L}$ (*bottom right hand*) of the orbiting particles in a thin accretion disk around a wormhole of a total mass $M = 0.06776 M_{\odot}$ and for the specific angular momentum $\widetilde{L} = 4M$. We have considered the specific case of $\Phi = -r_0/r$, and we have compared it with the Schwarzschild solution, which is depicted as the *solid line*

Therefore different flux values can be obtained when computing Eq. (4.15) for different choices of $b(r)$. As one can see from Fig. 4.1, for the wormhole geometry under study the orbiting particles in the thin accretion disk have a somewhat smaller angular velocity, specific energy, and specific angular momentum, respectively, as compared to the case of the Schwarzschild geometry.

The energy flux, the disk temperature and the emission spectra $\omega L(\omega)$ of the electromagnetic radiation emitted by a thin accretion disk are plotted in Figs. 4.2, 4.3 and 4.4, for a mass accretion rate of $\dot{M}_0 = 10^{-12} M_{\odot}/\text{yr}$, and for various wormhole geometries.

In order to investigate the effects of the geometry on the accretion disk properties, in the left plots of all Figs. 4.2, 4.3 and 4.4 we have chosen the following shape functions,

$$b(r) = r_0\,, \qquad b(r) = \frac{r_0^2}{r}\,, \qquad b(r) = \sqrt{r r_0}\,. \tag{4.23}$$

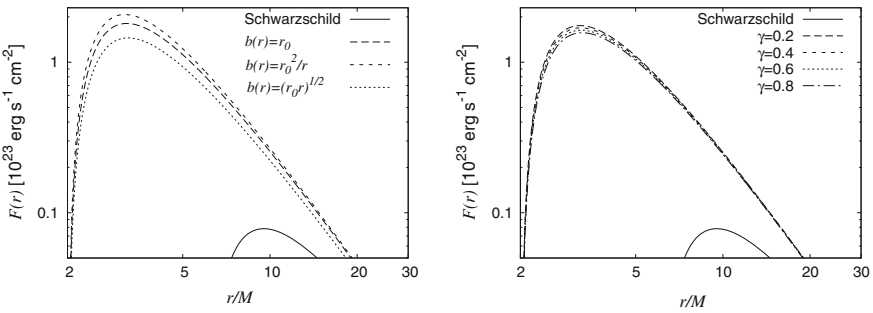

Fig. 4.2 The time averaged flux $\mathscr{F}(r)$ radiated by a thin accretion disk around a wormhole with effective mass $M = 0.06776 M_{\odot}$ and for a mass accretion rate $\dot{M}_0 = 10^{-12} M_{\odot}/\text{yr}$. Different shape functions were used to obtain the fluxes. Thus, in the *left plot* the following cases were considered: $b(r) = r_0$ (the *long dashed line*), $b(r) = r_0^2/r$ (the *short dashed line*) and $b(r) = (r_0 r)^{1/2}$ (the *dotted line*), respectively. The flux emitted by a thin accretion disk around a Schwarzschild black hole is presented as a *solid curve*. The *right plot* shows the case of $b(r) = r_0 + \gamma r_0(1 - r_0/r)$, for different values of γ

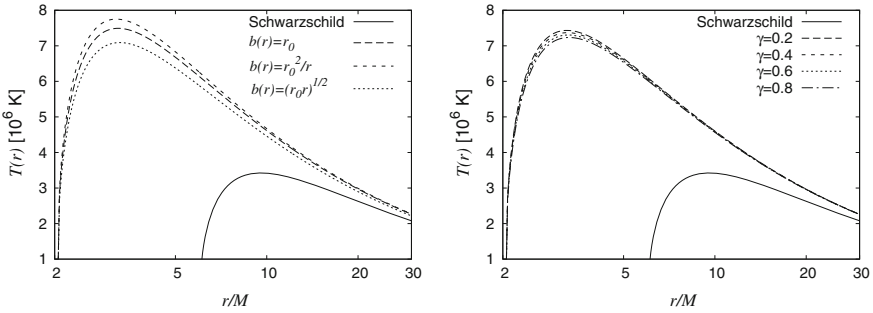

Fig. 4.3 Temperature distribution of the accretion disk around a wormhole with effective mass $M = 0.06776 M_{\odot}$ and for a mass accretion rate $\dot{M}_0 = 10^{-12} M_{\odot}/\text{yr}$. Different shape functions were used to obtain the fluxes. Thus, in the *left plot* the following cases were considered: $b(r) = r_0$ (the *long dashed line*), $b(r) = r_0^2/r$ (the *short dashed line*) and $b(r) = (r_0 r)^{1/2}$ (the *dotted line*), respectively. The flux emitted by a thin accretion disk around a Schwarzschild black hole is presented as a *solid curve*. The *right plot* shows the case of $b(r) = r_0 + \gamma r_0(1 - r_0/r)$, for different values of γ

In the right plots of Figs. 4.2, 4.3 and 4.4 we consider the shape function

$$b(r) = r_0 + \gamma r_0 \left(1 - \frac{r_0}{r}\right), \tag{4.24}$$

where $0 < \gamma < 1$.

Note that not only Ω, $\widetilde{E}$ and $\widetilde{L}$ have smaller values for the wormhole geometries under consideration, as compared to the case of the static Schwarzschild black holes, but the invariant volume element (4.22) also has relatively small values for any choice

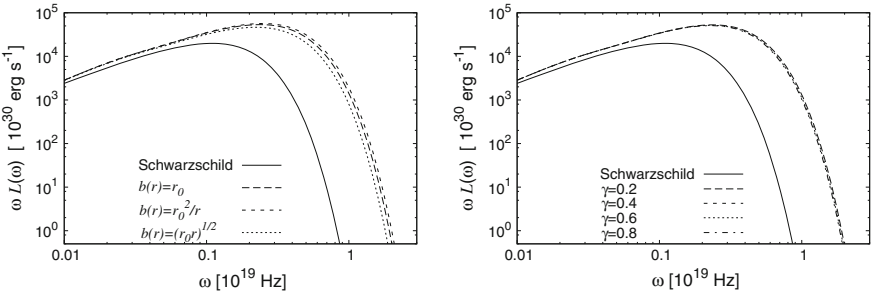

Fig. 4.4 The emission spectra $\omega L(\omega)$ of the accretion disks around a wormhole with effective mass $M = 0.06776 M_{\odot}$ and for a mass accretion rate $\dot{M}_0 = 10^{-12} M_{\odot}/\mathrm{yr}$. Different shape functions were used to obtain the fluxes. Thus, in the *left plot* the following cases were considered: $b(r) = r_0$ (the *long dashed line*), $b(r) = r_0^2/r$ (the *short dashed line*) and $b(r) = (r_0 r)^{1/2}$ (the *dotted line*), respectively. The flux emitted by a thin accretion disk around a Schwarzschild black hole is presented as a *solid curve*. The *right plot* shows the case of $b(r) = r_0 + \gamma r_0(1 - r_0/r)$, for different values of γ

of the function $b(r)$. Consequently, it turns out that more energy is radiated away by the wormhole disk than in the case of the Schwarzschild potential, a result which is clearly shown in Fig. 4.2.

Important observational information can be extracted from the position of the marginally stable orbits, which are located at the radius $2r_0$ for wormholes, while for the Schwarzschild black hole we have $r_{ms} = 6r_0$. Consequently, the inner edge of the accretion disk is closer to the throat of the wormhole than to the event horizon of the black hole, a result valid for any wormhole and black hole with the same geometrical mass r_0. Therefore it follows that the wormhole efficiency ε of the conversion of the accreted mass into radiation is of the order of 0.1422, a value which is much higher than the corresponding value for black holes, $\varepsilon = 0.0572$. Even though an efficiency of 14% is still much lower than the 40% efficiency obtained for Kerr black holes, it still shows that static wormholes may provide a much more efficient accretion mechanism for the conversion of the gravitational energy of the compact object into electromagnetic luminosity, as compared with the mass accretion taking place in a static black hole geometry.

These qualitative features of the disk energy radiation can also be found in the radial profiles of the temperature on the disk surface, which closely follow the flux distributions, and which are shown in Fig. 4.3. The emission spectra $\omega L(\omega)$ of the accretion disks in both static wormhole and Schwarzschild geometry are depicted in Fig. 4.4.

Thus, as a general conclusion of this Section, for the static and spherically symmetric wormhole solutions of general relativity it follows that specific signatures appear in the electromagnetic spectrum of the accretion disks. These particular signatures may lead to the possibility of distinguishing wormhole geometries from the Schwarzschild geometry by using astrophysical observations of the electromagnetic radiation coming from accretion disks built around compact objects.

4.4 Accretion Disk Properties in Rotating Wormhole Geometries

In the present Section, we study the physical properties and the equilibrium thermal radiation emission characteristics of matter forming thin accretion disks in stationary axially symmetric wormhole spacetimes. Several thin disk models are constructed by adopting different numerical values of the wormhole's angular velocity. In each case we obtain the time averaged energy flux, the disk temperature and the emission spectra of the accretion disks. We also compare the mass accretion properties in a rotating wormhole geometry with the same properties of a rotating Kerr black hole.

4.4.1 Stationary Axially Symmetric Wormhole Spacetimes

The standard metric for a stationary, axisymmetric traversable wormhole can be represented as [44]

$$ds^2 = -N^2dt^2 + e^{\mu}\,dr^2 + r^2K^2[d\theta^2 + \sin^2\theta(d\phi - \omega\,dt)^2]\,, \tag{4.25}$$

where N, μ, K and ω are functions of r and θ only. To ensure that the metric is nonsingular on the rotation axis ($\theta = 0, \pi$), we need to impose the regularity conditions on N, μ and K [44], which require that the θ derivatives of the metric tensor coefficients must vanish on the rotation axis.

In the following, for simplicity, we will adopt the following representations for the functions N and e^{μ} [44],

$$N(r,\theta) = e^{\Phi(r,\theta)}\,, \qquad e^{-\mu(r,\theta)} = 1 - \frac{b(r,\theta)}{r}\,, \tag{4.26}$$

which are very useful in describing a traversable wormhole. As usual, $\Phi(r,\theta)$ is the redshift function, satisfying the important requirement of finiteness, which ensures that there are no event horizons or curvature singularities in the wormhole geometry. The shape function $b(r,\theta)$ satisfies the condition $b \leq r$, as well as the flaring-out condition. From a geometric point of view $K(r,\theta)$ determines the proper radial distance, while the function ω determines the angular velocity of the rotating wormhole.

In order to avoid curvature singularities one needs to further impose the conditions $b_{\theta} = 0$ and $b_{\theta\theta} = 0$ at the throat. These two conditions show that the location of the throat is at a constant value of r. (We refer the reader to [44] for more details).

4.4.2 Effective Potential for Rotating Wormhole Geometries

The radial geodesic equation (4.3) for the metric (4.25) follows immediately from Eq. (4.4), and is given by

$$\left(1-\frac{b}{r}\right)^{-1}\left(\frac{dr}{d\tau}\right)^2 = V_{eff}\ . \tag{4.27}$$

By using the important relationship $g_{t\phi}^2 - g_{tt}g_{\phi\phi} = r^2K^2e^{2\Phi}$, the effective potential can be represented as

$$V_{eff}(r) = -1 + \left[\widetilde{E}^2r^2K^2 - 2\widetilde{E}\widetilde{L}r^2K^2\omega - \frac{\widetilde{L}^2\left(e^{2\Phi} - r^2K^2\omega^2\right)}{\left(r^2K^2e^{2\Phi}\right)}\right]. \tag{4.28}$$

Using this relationship, Eq. (4.27) can be reformulated in an alternative form as

$$r^4\left(\frac{dr}{d\tau}\right)^2 = V(r), \tag{4.29}$$

where $V(r)$ given by

$$V(r) = r^4\left(1-\frac{b}{r}\right)V_{eff}(r)\ . \tag{4.30}$$

In the following for the function ω we consider the specific case in which ω is given by

$$\omega = \frac{2J}{r^3}\,, \tag{4.31}$$

with $J = M^2a_*$ representing the total angular momentum of the wormhole. Since in the present investigation we are only interested in the equatorial approximation, with $|\theta - \pi/2| \ll 1$, we also fix K as $K = 1$ throughout our computations.

Moreover, in this section of the disk properties, we consider the case of the redshift function given by Eq. (4.20), while for the shape functions we adopt the choices given by Eqs. (4.23) and (4.24), provided in the previous section.

4.4.3 Electromagnetic Signatures of Thin Accretion Disks in Rotating Wormhole Geometries

In the following, for simplicity, we will adopt the following values for the mass M and the spin parameter a_* of the rotating wormhole,

$$M = 0.06776\, M_{\odot}\ (= 1000\ \text{cm}), \tag{4.32}$$

and

$$a_* = 0.2,\ 0.4,\ 0.6,\ 0.8,\ 1.0\,, \tag{4.33}$$

respectively. Moreover, we fix the mass accretion rate as $\dot{M}_0 = 10^{-12} M_{\odot}/\text{yr}$.

In Figs. 4.5, 4.6, 4.7, 4.8, 4.9 and 4.10 we present the energy flux $F(r)$, the disk temperature $T(r)$ and the electromagnetic emission spectra $\nu L(\nu)$ from an accretion disk for different wormhole geometries. For the shape functions we have adopted the expressions given by Eqs. (4.23) and (4.24), respectively. For the sake of comparison we also present, for each case, the electromagnetic emission properties of the thin disks in the Kerr black hole geometry.

A comparison of the energy fluxes emitted from the thin disk in a stationary rotating wormhole geometry, as shown in Figs. 4.5 and 4.6, with the energy flux emitted by a Kerr black hole for $a_* < 0.8$, immediately leads to the conclusion that the intensity of the energy flux emitted from the disk surface is at least two orders of

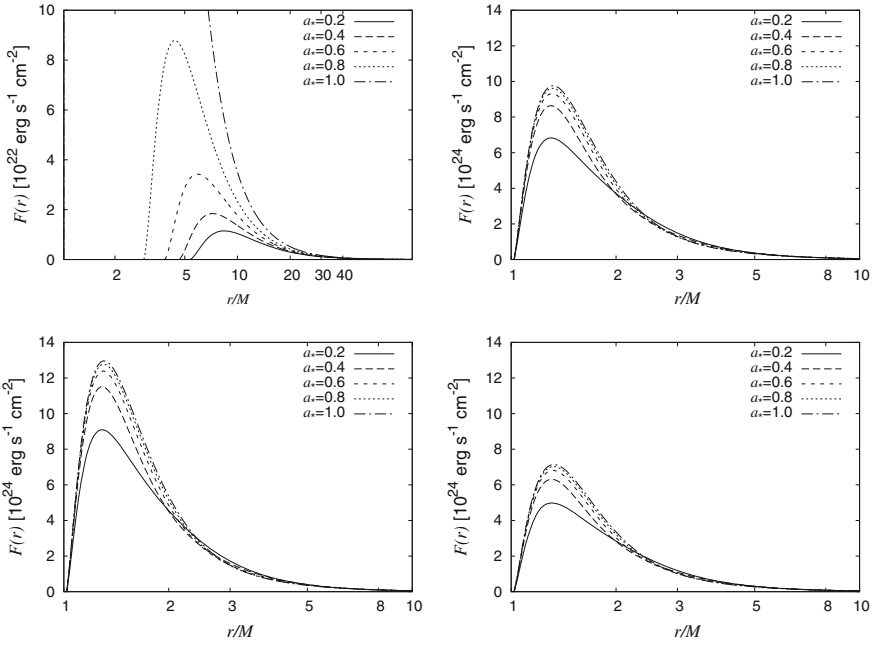

Fig. 4.5 The energy flux $\mathscr{F}(r)$ radiated by an accretion disk in a Kerr black hole geometry (*upper left-hand plot*), and in the stationary axially symmetric wormhole spacetimes for $\Phi = -r_0/r$ and $b = r_0$ (*upper right-hand plot*), $b = r_0^2/r$ (*lower left hand plot*) and $b = (r_0 r)^{1/2}$ (*lower right-hand plot*), respectively. In all plots $r_0 = 1000\,\text{cm}$, and the values of the spin parameter are $a_* = 0.2, 0.4, 0.6, 0.8$ and 1, respectively

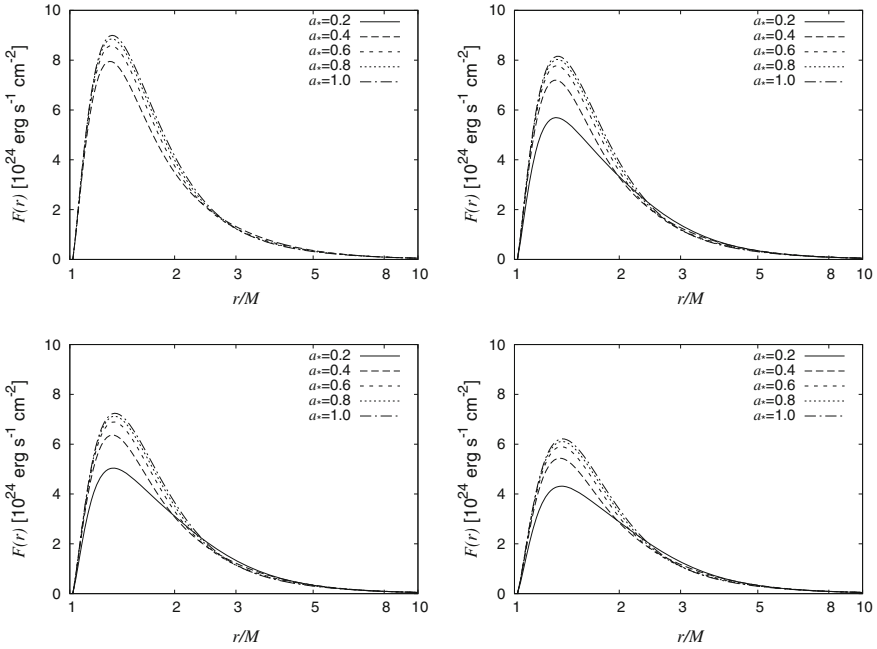

Fig. 4.6 The energy flux $\mathscr{F}(r)$ from an accretion disks in stationary axially symmetric wormhole spacetimes for $\Phi = -r_0/r$, and $b = r_0 + \gamma r_0(1 - r_0/r)$, where $\gamma = 0.2$ (*upper left-hand plot*), 0.4 (*upper right-hand plot*), 0.6 (*lower left-hand plot*) and 0.8 (*lower right-hand plot*), respectively. In all plots $r_0 = 1000\,\mathrm{cm}$, and the values of the spin parameter are $a_* = 0.2, 0.4, 0.6, 0.8$ and 1, respectively

magnitude greater for rotating wormholes than for the rotating Kerr black hole, with both compact objects having the same geometrical mass r_0 and accretion rate $\dot{M}_0$. However, the flux amplitudes indicate a similar dependence on the spin parameter a_* for both types of the rotating central compact objects. As we can see from the plots, with the increase in the values of a_*, the maximal admissible values of $\mathscr{F}(r)$ are also increasing. Once the angular velocity of the central object increases, the maximal flux values are located closer to the black hole. On the other hand, in wormhole spacetimes they are located at somewhat lower disk radii. In the case of wormhole geometries, the left edge of the electromagnetic energy flux profile is always located at r_0, the throat of the wormhole. On the other hand, the inner edge of the electromagnetic energy flux profile is located at different positions of the disk around the rotating Kerr black hole. These results follow from the fact that each value of a_* in the plots is greater than the critical spin parameter.

On the other hand the different shape functions (4.23) and (4.24) adopted to describe the wormhole metric affect only the amplitudes of the flux profiles. It turns out that the wormhole accretion disk with the shape function $b = r_0^2/r$ produces the electromagnetic radiation flux with the highest intensity, while the lowest values

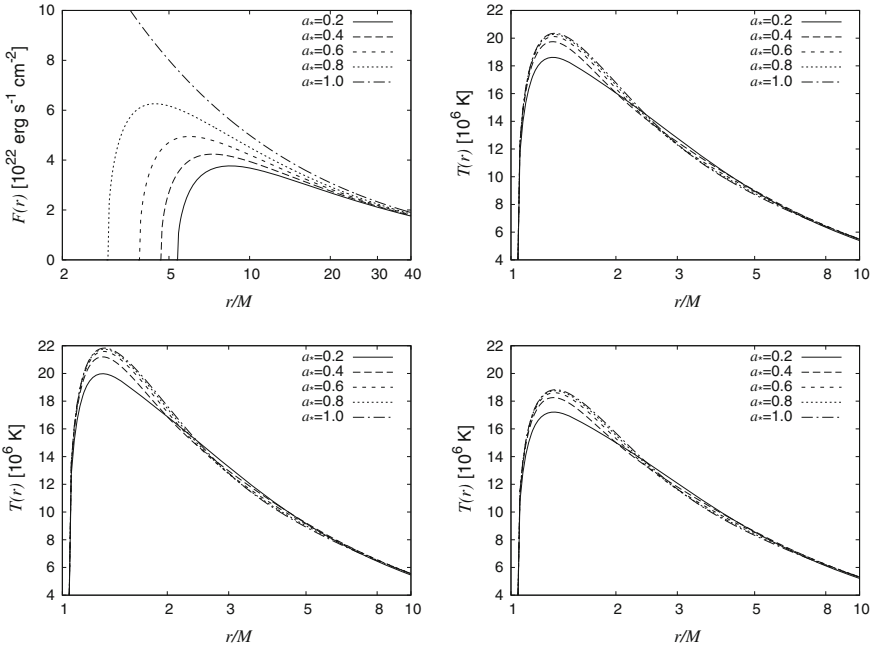

Fig. 4.7 Temperature distribution of the accretion disk in the Kerr spacetime (*upper left-hand plot*), and of the stationary axially symmetric wormhole spacetimes for $\Phi = -r_0/r$, and $b = r_0$ (*upper right-hand plot*), $b = r_0^2/r$ (*lower left-hand plot*), and $b = (r_0 r)^{1/2}$ (*lower right-hand plot*), respectively. In all plots $r_0 = 1000\,\text{cm}$, and the values of the spin parameter are $a_* = 0.2, 0.4, 0.6, 0.8$ and 1, respectively

are obtained for the case $\mathscr{F}(r)$ for $b(r) = (r_0 r)^{1/2}$. Interestingly, by increasing the numerical value of the parameter γ in the shape function $b(r) = r_0 + \gamma r_0(1 - r_0/r)$, it turns out that the intensity of the electromagnetic flux is decreasing, since the $1/r$ term in $b(r)$ is becoming more and more dominant.

All these physical characteristics also appear in the disk temperature profiles, which are presented in Figs. 4.7 and 4.8, respectively. Note that the temperature distribution of the wormhole disks and Kerr black hole disks have the same orders of magnitude only for $a_* \approx 1$. For lower values of the spin parameter a_* the disks in rotating wormhole geometries are much hotter than those located in the geometric frame of the Kerr black holes.

The disk spectra for the rotating wormholes and black holes are displayed in Figs. 4.9 and 4.10, respectively. It turns out that even that there are no significant differences between the spectral amplitudes of the electromagnetic radiation from the disk for the different types of rotating central compact objects, the cut-off frequencies of the spectra significantly depend on the nature and geometry of the central objects, as well as on their rotational velocities. The cut-off frequencies for the radiation from rotating Kerr black holes are lower than those for the radiation coming from disks in

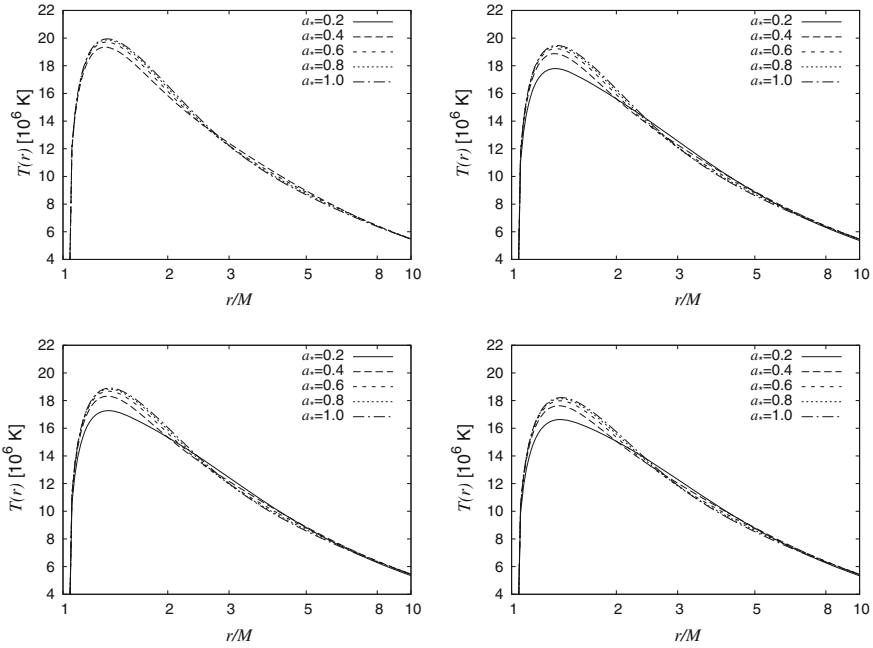

Fig. 4.8 Temperature distribution of the accretion disk in the stationary axially symmetric wormhole spacetime for $\Phi = -r_0/r$, and $b = r_0 + \gamma r_0(1 - r_0/r)$, where $\gamma = 0.2$ (*upper left-hand plot*), 0.4 (*upper right-hand plot*), 0.6 (*lower left-hand plot*) and 0.8 (*lower right-hand plot*), respectively. In all plots $r_0 = 1000$ cm, and the values of the spin parameter are $a_* = 0.2$, 0.4, 0.6, 0.8 and 1, respectively

wormhole geometries. On the other hand, for the wormhole spacetimes, the spectral profiles of the radiation emitted by the accretion disks are relatively similar, no matter which of the shape functions $b(r)$ we use in our analysis. The cut-off frequencies of the spectra have the lowest values for $b(r) = (r_0 r)^{1/2}$, while the highest values are obtained for the case $b(r) = r_0 + \gamma r_0(1 - r_0/r)$. However, these differences are negligible.

On the other hand, the plots in Fig. 4.10 indicate that the spectral features of the disk radiation are also largely insensitive to the changes in the numerical values of the parameter γ in the shape function $b(r) = r_0 + \gamma r_0(1 - r_0/r)$.

In Table 4.1 we present the conversion efficiency ε of the accreting mass into radiation. These values are obtained by ignoring the photon capture by the massive central object. From a physical point of view the numerical value of ε indicates the efficiency of energy conversion and generation mechanism by mass accretion in the corresponding spacetime geometry. The amount of energy emitted by the matter departing from the accretion disk, and falling down into the black hole through its event horizon, or through the throat of the wormhole, is nothing but the binding energy $\widetilde{E}(r)|_{r=r_{in}}$ of the compact object effective potential.

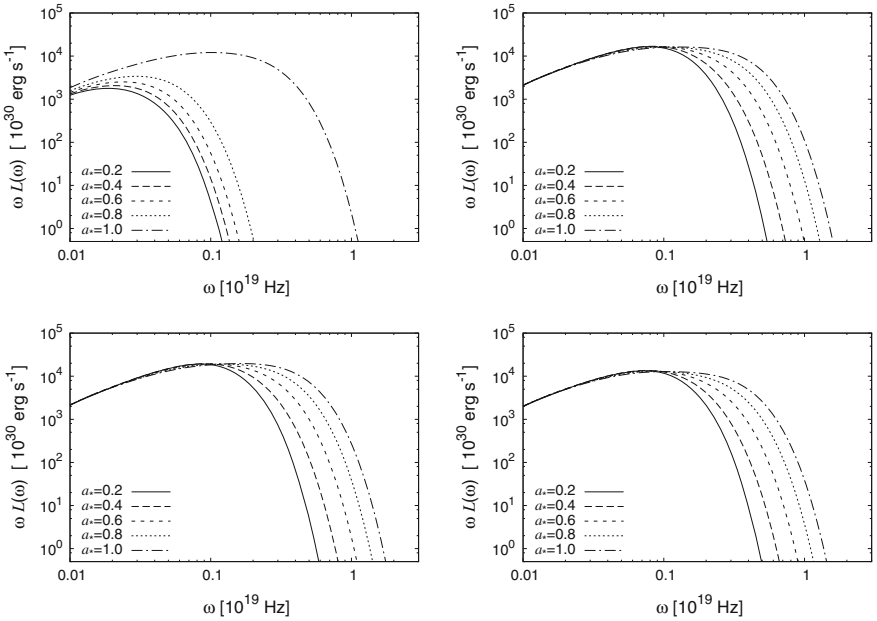

Fig. 4.9 The emission spectra of the accretion disk in the Kerr spacetime (*upper left-hand plot*) and in the stationary axially symmetric wormhole spacetime for $\Phi = -r_0/r$, and $b = r_0$ (*upper right-hand plot*), $b = r_0^2/r$ (*lower left hand plot*), and $b = (r_0 r)^{1/2}$ (*lower right-hand plot*), respectively. In all plots $r_0 = 1000\,\text{cm}$, and the values of the spin parameter are $a_* = 0.2, 0.4, 0.6, 0.8$ and 1, respectively

An important result that can be read from Table 4.1 is that ε is always higher for axially symmetric rotating wormholes as compared to the case of Kerr black holes. Even for a relatively small value of the spin parameter of $a_* = 0.2$, the efficiency of the energy conversion process of the matter in the wormhole geometry is greater than ε obtained for the extreme Kerr black hole geometry with $a_* = 1$. In the case of rapidly rotating wormholes, the efficiency ε is even higher. However, in this case there is an upper limit of ε for high values of the spin parameter: for $a_* \sim 0.6$ we obtain $\varepsilon = 0.508$. For this value of a_* the accretion process is reaching its saturation point, and higher efficiencies cannot be obtained, even if we further increase the spin parameter a_*. However, it is important to note this high efficiency indicate that the rotating wormholes geometries represent a much more efficient astrophysical system for the transformation of the energy of the accreting matter into electromagnetic radiation, as compared to the case of the Kerr black holes.

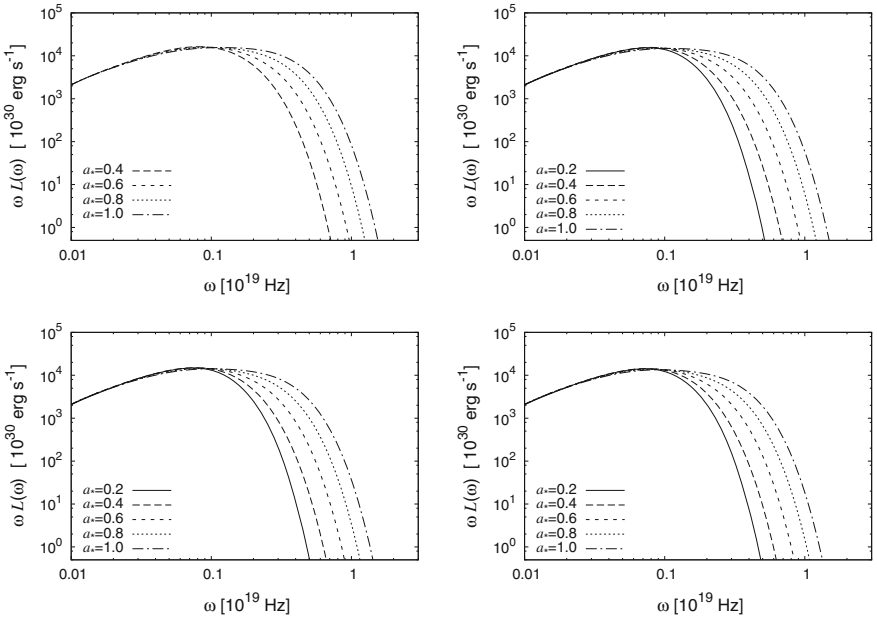

Fig. 4.10 The emission spectra of the accretion disk in the stationary axially symmetric wormhole spacetime for $\Phi = -r_0/r$, and $b = r_0 + \gamma r_0(1 - r_0/r)$, where $\gamma = 0.2$ (*upper left-hand plot*), 0.4 (*upper right-hand plot*), 0.6 (*lower left hand plot*) and 0.8 (*lower right-hand plot*), respectively. In all plots $r_0 = 1000\,\text{cm}$, and the values of the spin parameter are $a_* = 0.2, 0.4, 0.6, 0.8$ and 1, respectively

Table 4.1 The position of the inner edge of the accretion disk, and the efficiency ε for rotating black hole and wormhole geometries

	Kerr black hole		Wormhole	
a_*	r_{in}/r_0	ε	r_{in}/r_0	ε
0.2	5.33	0.065	1.00	0.498
0.4	4.62	0.075	1.00	0.506
0.6	3.83	0.091	1.00	0.507
0.8	2.91	0.122	1.00	0.508
1.0	1.00	0.421	1.00	0.508

4.5 Discussions and Final Remarks

In the present paper, we have studied thin accretion disk models applied to the study of static and spherically symmetric wormhole geometries, and have carried out an analysis of the properties of the radiation emerging from the surface of the disk. In classical general relativity, wormholes are supported by exotic matter, which involves a stress–energy tensor that violates the null energy condition. Thus, it has proved interesting to analyze the properties, namely, the time averaged energy flux, the disk temperature, and the emission spectra of the accretion disks around these

wormholes comprising of exotic matter. For the static and spherically symmetric wormhole geometries under study, we have verified that the potential well is higher than the Schwarzschild potential, and consequently more energy is radiated away. These effects in the disk radiation were also observed in the radial profiles of temperature corresponding to the flux distributions, and in the emission spectrum $\omega L(\omega)$ of the accretion disks. Thus, for these solutions, we conclude that the specific signatures, that appear in the electromagnetic spectrum, lead to the possibility of distinguishing wormhole geometries from the Schwarzschild solution by using astrophysical observations of the emission spectra from accretion disks.

In this context, observations in the near-infrared (NIR) or X-ray bands have provided important information about the spin of the black holes, or the absence of a surface in stellar type black hole candidates. In the case of the source Sgr A*, where the putative thermal emission due to the small accretion rate peaks in the near infrared, the results are particularly robust. However, up to now, these results have confirmed the predictions of general relativity mainly in a qualitative way, and the observational precision achieved cannot distinguish between the different classes of compact/exotic objects that appear in the theoretical framework of general relativity [17]. However, important technological developments may allow to image black holes and other compact objects directly. A background illuminated black hole will appear in a silhouette with radius $\sqrt{27}GM/c^2$, with an angular size of roughly twice that of the horizon, and may be directly observed. With an expected resolution of $20\,\mu$ as, submillimeter very-long baseline interferometry (VLBI) would be able to image the silhouette cast upon the accretion flow of Sgr A*, with an angular size of $\sim 50\,\mu$as, or M87, with an angular size of $\sim 25\,\mu$as. For a black hole embedded in an accretion flow, the silhouette will generally be asymmetric regardless of the spin of the black hole. Even in an optically thin accretion flow an asymmetry will result from special relativistic effects (aberration and Doppler shifting). In principle, detailed measurements of the size and shape of the silhouette could yield information about the mass and spin of the central black hole, and provide invaluable information on the nature of the accretion flows in low luminosity galactic nuclei.

We suggest that by using the same imaging technique, which gives the physical/geometrical properties of the silhouette of the compact object cast upon the accretion flows on the compact objects, would be able to provide clear observational evidence for the existence of wormholes, and differentiate them from other types of compact general relativistic objects. We conclude by pointing out that specific signatures appear in the electromagnetic spectrum of the thin accretion disks around wormholes, thus leading to the possibility of detecting and distinguishing wormhole geometries by using astrophysical observations of the emission spectra from accretion disks.

Acknowledgements TH would like to thank the Yat Sen School of the Sun Yat-Sen University in Guangzhou, P. R. China, for the kind hospitality offered during the preparation of this work. FSNL acknowledges financial support of the Fundação para a Ciência e Tecnologia through an Investigador FCT Research contract, with reference IF/00859/2012, funded by FCT/MCTES (Portugal).

References

1. Urry CM, Padovani P. Unified schemes for radio-loud active galactic nuclei. Publ Astron Soc Pac. 1995;107:803.
2. Abramowicz MA, Björnsson G, Pringle JE. Theory of black hole accretion discs. Cambridge: Cambridge University Press; 1999.
3. Fabrika S. THE jets and supercritical accretion disk in SS433. Cambridge: Cambridge Scientific Publishers; 2004.
4. Fridman AM, Bisikalo DV. The nature of accretion disks of close binary stars: overreflection instability and developed turbulence. PHYS-USP. 2008;51(6):551576.
5. Miyoshi M, Moran J, Herrnstein J, Greenhill L, Nakai N, Diamond P, Inoue M. Evidence for a black hole from high rotation velocities in a sub-parsec region of NGC4258. Nature. 1995;373:127.
6. Fabian AC, Rees MJ, Stella L, White NE. X-ray fluorescence from the inner disc in Cygnus X-1. Mon Not Roy Astron Soc. 1989;238:729.
7. Aldi GF, Bozza V. Relativistic iron lines in accretion disks: the contribution of higher order images in the strong deflection limit. arXiv:1607.05365 [astro-ph.HE].
8. Kojima Y. The effects of black hole rotation on line profiles from accretion discs. Mon Not Roy Astron Soc. 1991;250:629.
9. Laor A. Line profiles from a disk around a rotating black hole. Astrophys J. 1991;376:90.
10. Arnaud KA. PASJ. 1996;41:763.
11. Novikov ID, Thorne KS. In: DeWitt C, DeWitt B, editors. Black Holes. New York: Gordon and Breach; 1973.
12. Shakura NI, Sunyaev RA. Black holes in binary systems. Observational appearance. Astron Astrophys. 1973;24:337.
13. Page DN, Thorne KS. Disk-accretion onto a black hole. Time-averaged structure of accretion disk. Astrophys J. 1974;191:499.
14. Thorne KS. Disk accretion onto a black hole. 2. Evolution of the hole. Astrophys J. 1974;191:507.
15. Bhattacharyya S, Thampan AV, Bombaci I. Temperature profiles of accretion discs around rapidly rotating strange stars in general relativity: a comparison with neutron stars. Astron Astrophys. 2001;372:925.
16. Torres DF. Accretion disc onto a static nonbaryonic compact object. Nucl Phys B. 2002;626:377.
17. Yuan YF, Narayan R, Rees MJ. Constraining alternate models of black holes: type I x-ray bursts on accreting fermion - fermion and boson - fermion stars. Astrophys J. 2004;606:1112.
18. Guzman FS. Accretion disc onto boson stars: a way to supplant black holes. Phys Rev D. 2006;73:021501.
19. Bambi C, Malafarina D. Kα iron line profile from accretion disks around regular and singular exotic compact objects. Phys Rev D. 2013;88:064022.
20. Bambi C, Malafarina D, Tsukamoto N. Note on the effect of a massive accretion disk in the measurements of black hole spins. Phys Rev D. 2014;89:127302.
21. Lin N, Li Z, Arthur J, Asquith R, Bambi C. Testing SgrA* with the spectrum of its accretion structure. JCAP. 2015;1509(09):038.
22. Kovacs Z, Harko T. Can accretion disk properties observationally distinguish black holes from naked singularities? Phys Rev D. 2010;82:124047.
23. Dănilă B, Harko T, Kovcs Z. Thin accretion disks around cold Bose–Einstein condensate stars. Eur Phys J C. 2015;75(5):203.
24. Kovacs Z, Cheng KS, Harko T. Thin accretion disks around neutron and quark stars. Astron Astrophys. 2009;500:621.
25. Harko T. Matter accretion by brane-world black holes. J Korean Phys Soc. 2009;54:2583.
26. Mazur PO, Mottola E. Gravitational vacuum condensate stars. Proc Nat Acad Sci. 2004;101:9545.

27. Harko T, Kovacs Z, Lobo FSN. Can accretion disk properties distinguish gravastars from black holes? Class Quant Grav. 2009;26:215006.
28. Pun CSJ, Kovacs Z, Harko T. Thin accretion disks in f(R) modified gravity models. Phys Rev D. 2008;78:024043.
29. Pun CSJ, Kovacs Z, Harko T. Thin accretion disks onto brane world black holes. Phys Rev D. 2008;78:084015.
30. Harko T, Kovacs Z, Lobo FSN. Thin accretion disk signatures in dynamical Chern–Simons modified gravity. Class Quant Grav. 2010;27:105010.
31. Harko T, Kovacs Z, Lobo FSN. Thin accretion disk signatures of slowly rotating black holes in Hořava gravity. Class Quant Grav. 2011;28:165001.
32. Harko T, Kovács Z, Lobo FSN. Electromagnetic signatures of thin accretion disks in wormhole geometries. Phys Rev D. 2008;78:084005.
33. Harko T, Kovács Z, Lobo FSN. Thin accretion disks in stationary axisymmetric wormhole spacetimes. Phys Rev D. 2009;79:064001.
34. Bambi C. Broad K iron line from accretion disks around traversable wormholes. Phys Rev D. 2013;87:084039.
35. Bambi C. Can the supermassive objects at the centers of galaxies be traversable wormholes? The first test of strong gravity for mm/sub-mm very long baseline interferometry facilities. Phys Rev D. 2013;87:107501.
36. Li Z, Bambi C. Distinguishing black holes and wormholes with orbiting hot spots. Phys Rev D. 2014;90:024071.
37. Tsukamoto N, Bambi C. High energy collision of two particles in wormhole spacetimes. Phys Rev D. 2015;91(8):084013.
38. Tsukamoto N, Bambi C. Collisional Penrose process in a rotating wormhole spacetime. Phys Rev D. 2015;91:104040.
39. Zhou M, Cardenas-Avendano A, Bambi C, Kleihaus B, Kunz J. Search for astrophysical rotating Ellis wormholes with X-ray reflection spectroscopy. Phys Rev D. 2016;94(2):024036.
40. Luminet JP. Image of a spherical black hole with thin accretion disk. Astron Astrophys. 1979;75:228.
41. Bhattacharyya S, Misra R, Thampan AV. General relativistic spectra of accretion disks around rotating neutron stars. Astrophys J. 2001;550:841.
42. Morris MS, Thorne KS. Wormholes in space-time and their use for interstellar travel: a tool for teaching general relativity. Am J Phys. 1988;56:395.
43. Lobo FSN. Van der Waals quintessence stars. Phys Rev D. 2007;75:024023.
44. Teo E. Rotating traversable wormholes. Phys Rev D. 1998;58:024014.

Chapter 5
Horndeski Wormholes

Sergey V. Sushkov

5.1 Introduction

The discovery of the current Universe acceleration [29, 30] requires a theoretical explanation. From the phenomenological viewpoint, a small cosmological term is a very good explanation [33], but it is problematic from the quantum field theory viewpoint, since it is difficult to explain the origin and value of this term [43]. Therefore, alternative dark energy models have been proposed, most of which introduce a scalar field, as in the Brans–Dicke theory, quintessense, k-essence, etc. (see [8, 25] for reviews), while the others, as for example the $F(R)$ gravity [9, 37], although apparently different, are equivalent to a specific scalar–tensor theory.

In view of this interest towards theories with a gravitating scalar field one may ask, what is the most general theory of this type? The answer was obtained already in 1974 by Horndeski [24]—this theory should have at most second order field equations to avoid the Ostrogradsky ghost [44], and it is determined by the following action density (in the parameterization of Ref. [9])

$$L_{\rm H} = \sqrt{-g}\,(\mathscr{L}_2 + \mathscr{L}_3 + \mathscr{L}_4 + \mathscr{L}_5)\,, \tag{5.1}$$

where, with $X \equiv -\frac{1}{2}\nabla_\mu\Phi\nabla^\mu\Phi$, one has

$$\begin{aligned}
\mathscr{L}_2 &= G_2(X,\Phi)\,,\\
\mathscr{L}_3 &= G_3(X,\Phi)\,\Box\Phi\,,\\
\mathscr{L}_4 &= G_4(X,\Phi)\,R + \partial_X G_4(X,\Phi)\,\delta^{\mu\nu}_{\alpha\beta}\,\nabla^\alpha_\mu\Phi\nabla^\beta_\nu\Phi\,,\\
\mathscr{L}_5 &= G_5(X,\Phi)\,G_{\mu\nu}\nabla^{\mu\nu}\Phi - \frac{1}{6}\,\partial_X G_5(X,\Phi)\,\delta^{\mu\nu\rho}_{\alpha\beta\gamma}\,\nabla^\alpha_\mu\Phi\nabla^\beta_\nu\Phi\nabla^\gamma_\rho\Phi\,,
\end{aligned} \tag{5.2}$$

S.V. Sushkov (✉)
Institute of Physics, Kazan Federal University, Kremlevskaya Street 16a,
Kazan 420008, Russia
e-mail: sergey_sushkov@mail.ru

F.S.N. Lobo (ed.), *Wormholes, Warp Drives and Energy Conditions*,
Fundamental Theories of Physics 189, DOI 10.1007/978-3-319-55182-1_5

and $G_k(X, \Phi)$ are arbitrary functions, while $\delta^{\lambda\rho}_{\nu\alpha} = 2!\,\delta^{\lambda}_{[\nu}\delta^{\rho}_{\alpha]}$ and $\delta^{\lambda\rho\sigma}_{\nu\alpha\beta} = 3!\,\delta^{\lambda}_{[\nu}\delta^{\rho}_{\alpha}\delta^{\sigma}_{\beta]}$. This theory contains all previously studied models with a gravity-coupled scalar field. Note also that Horndeski developed his theory on the base of mathematical facts but later the same results were obtained on the basis of more intuitive approach from research in Galileons [10, 11, 28].

The simplest Lagrangian in the Horndeski theory contains a term $G^{\mu\nu}\phi_{,\mu}\phi_{,\nu}$ providing a nonminimal kinetic coupling of a scalar field to the curvature. Cosmological applications of such this have been intensively investigated in [3, 14, 17–23, 32, 34, 36, 38–40]. In particular, as was shown in our works [34, 36, 39], nonminimal kinetic coupling provides essentially a new inflationary mechanism. Less studied is a problem of the black hole and wormhole existence in the theory of gravity with a nonminimal kinetic coupling. Recently, Rinaldi [31] found a class of exact solutions with characteristic features of black holes, particularly, with an event horizon. Soon afterwards, the Rinaldi method was applied in [1, 2, 7, 27] to find new particular solutions with event horizons.

Wormhole solutions in the theory of gravity with nonminimal kinetic coupling was studied in [26, 41]. General solutions describing asymptotically flat traversable wormholes have been obtained by means of numerical methods [26]. Particular exact wormhole solutions in an analytical form have been found by using the Rinaldi method [41]. The throat of such wormholes connects two anti-de Sitter spacetimes.

5.2 Action and Field Equations

Let us consider a gravitational theory with a nonminimal derivative coupling given by the action

$$S = \frac{1}{2}\int dx^4\sqrt{-g}\left\{M_{\rm Pl}^2 R - \left[\varepsilon g_{\mu\nu} + \eta G_{\mu\nu}\right]\nabla^\mu\phi\nabla^\nu\phi - 2V(\phi)\right\}, \tag{5.3}$$

where $M_{\rm Pl} = \sqrt{1/8\pi G}$ is the reduced Planck mass, $g_{\mu\nu}$ is a metric, $g = \det(g_{\mu\nu})$, R is the scalar curvature, $G_{\mu\nu}$ is the Einstein tensor, ϕ is a real massless scalar field, η is a parameter of nonminimal kinetic coupling with the dimension of length-squared. The ε parameter equals ± 1. In the case $\varepsilon = 1$ we have a canonical scalar field with a positive kinetic term; and the case $\varepsilon = -1$ describes a phantom scalar field with negative kinetic term.

Variation of the action (5.3) with respect to the metric $g_{\mu\nu}$ and scalar field ϕ provides the following field equations:

$$M_{\rm Pl}^2 G_{\mu\nu} = \varepsilon T_{\mu\nu} + \eta\Theta_{\mu\nu}, \tag{5.4}$$

$$\nabla_\mu J^\mu = -V_\phi, \tag{5.5}$$

respectively, where

$$J^{\mu} = (\varepsilon g^{\mu\nu} + \eta G^{\mu\nu})\nabla_{\nu}\phi, \tag{5.6}$$

$$T_{\mu\nu} = \nabla_{\mu}\phi\nabla_{\nu}\phi - \tfrac{1}{2}g_{\mu\nu}(\nabla\phi)^2, \tag{5.7}$$

$$\begin{aligned}\Theta_{\mu\nu} = &-\tfrac{1}{2}\nabla_{\mu}\phi\,\nabla_{\nu}\phi\,R + 2\nabla_{\alpha}\phi\,\nabla_{(\mu}\phi R^{\alpha}_{\nu)} + \nabla^{\alpha}\phi\,\nabla^{\beta}\phi\,R_{\mu\alpha\nu\beta}\\ &+ \nabla_{\mu}\nabla^{\alpha}\phi\,\nabla_{\nu}\nabla_{\alpha}\phi - \nabla_{\mu}\nabla_{\nu}\phi\,\Box\phi - \tfrac{1}{2}(\nabla\phi)^2 G_{\mu\nu}\\ &+ g_{\mu\nu}\Big[-\tfrac{1}{2}\nabla^{\alpha}\nabla^{\beta}\phi\,\nabla_{\alpha}\nabla_{\beta}\phi + \tfrac{1}{2}(\Box\phi)^2 - \nabla_{\alpha}\phi\,\nabla_{\beta}\phi\,R^{\alpha\beta}\Big].\end{aligned} \tag{5.8}$$

Due to the Bianchi identity $\nabla^{\mu}G_{\mu\nu} = 0$, Eq. (5.4) leads to a differential consequence given by

$$\nabla^{\mu}\Big[\varepsilon T_{\mu\nu} + \eta\Theta_{\mu\nu}\Big] = 0. \tag{5.9}$$

One can check straightforwardly that the substitution of expressions (5.7) and (5.8) into (5.9) yields Eq. (5.5). In other words, the equation of motion of the scalar field (5.5) is the differential consequence of the system (5.4).

5.3 Static Spherically Symmetric Asymptotically Flat Wormholes

Consider a static spherically symmetric configuration in the theory (5.3). In this case the spacetime metric can be taken as follows:

$$ds^2 = -A(r)dt^2 + A^{-1}(r)du^2 + \rho^2(r)d\Omega^2, \tag{5.10}$$

where $d\Omega^2 = d\theta^2 + \sin^2\theta d\varphi^2$ is the linear element of the unit sphere, and $A(r)$ and $\rho(r)$ are functions of the radial coordinate r. Consider also that the scalar field ϕ depends only on r, so that $\phi = \phi(r)$.

Now the field equations (5.4) and (5.5) yield

$$\begin{aligned}M_{\rm Pl}^2\left[2\frac{\rho''}{\rho} + \frac{A'\rho'}{A\rho} + \frac{\rho'^2}{\rho^2} - \frac{1}{A\rho^2}\right] = &-\frac{1}{2}\varepsilon\phi'^2 - A^{-1}V(\phi) + 2\eta\phi'\phi''\frac{A\rho'}{\rho}\\ &+ \eta\phi'^2\left(\frac{3A'\rho'}{2\rho} + \frac{A\rho'^2}{2\rho^2} + \frac{1}{2\rho^2} + \frac{A\rho''}{\rho}\right),\end{aligned} \tag{5.11}$$

$$\begin{aligned}M_{\rm Pl}^2\left[\frac{A'\rho'}{A\rho} + \frac{\rho'^2}{\rho^2} - \frac{1}{A\rho^2}\right] = &\frac{1}{2}\varepsilon\phi'^2 - A^{-1}V(\phi)\\ &+ \eta\phi'^2\left(\frac{3A\rho'^2}{2\rho^2} + \frac{3A'\rho'}{2\rho} - \frac{1}{2\rho^2}\right),\end{aligned} \tag{5.12}$$

$$M_{\rm Pl}^2\left[\frac{1}{2}\frac{A''}{A}+\frac{\rho''}{\rho}+\frac{A'\rho'}{A\rho}\right]=-\frac{1}{2}\varepsilon\phi'^2-A^{-1}V(\phi)+\eta\phi'\phi''\left(\frac{A\rho'}{\rho}+\frac{1}{2}A'\right)$$
$$+\eta\phi'^2\left(\frac{A'\rho'}{\rho}+\frac{1}{2}\frac{A\rho''}{\rho}+\frac{1}{4}\frac{A'^2}{A}+\frac{1}{4}A''\right), \quad (5.13)$$

$$\varepsilon\phi''+\varepsilon\phi'\left(\frac{A'}{A}+2\frac{\rho'}{\rho}\right)+\eta\phi''\left(\frac{A'\rho'}{\rho}+\frac{A\rho'^2}{\rho^2}-\frac{1}{\rho^2}\right)$$
$$+\eta\phi'\left(\frac{A'\rho''}{\rho}-\frac{A'}{A\rho^2}+3\frac{A'\rho'^2}{\rho^2}+\frac{A'^2\rho'}{A\rho}+2\frac{A\rho'\rho''}{\rho^2}+\frac{A''\rho'}{\rho}\right)=A^{-1}V_\phi, \quad (5.14)$$

respectively, where the prime denotes d/dr, and Eqs. (5.11)–(5.13) are the $\binom{0}{0}$, $\binom{1}{1}$, $\binom{2}{2}$ components of Eq. (5.4), respectively. Equations (5.11)–(5.14) represent a system of four ordinary differential equations of second order for three functions $\rho(r)$, $A(r)$, $\phi(r)$. As was mentioned above, Eq. (5.14) is a differential consequence of Eqs. (5.11)–(5.13). It is also worth noticing that Eqs. (5.11), (5.13) and (5.14) are of second order, while Eq. (5.12) is a first-order differential constraint for $\rho(r)$, $A(r)$, and $\phi(r)$.

Combining the above equations one can easily rewrite them into the more compact form

$$2M_{\rm Pl}^2\frac{\rho''}{\rho}=-\varepsilon\phi'^2+\eta A\left(\phi'^2\frac{\rho'}{\rho}\right)'+\eta\phi'^2\frac{1}{\rho^2}, \quad (5.15)$$

$$M_{\rm Pl}^2(A'\rho^2)'=-2\rho^2V+\frac{1}{2}\eta(AA'\rho^2\phi'^2)'+\eta\phi'^2(AA'\rho\rho'+A^2\rho'^2-A), \quad (5.16)$$

$$M_{\rm Pl}^2\big(A(\rho^2)''-A''\rho^2-2\big)=\frac{1}{2}\eta[\phi'^2(2A^2\rho\rho'-AA'\rho^2)]'+\eta A\phi'^2, \quad (5.17)$$

$$\varepsilon(A\rho^2\phi')'+\eta[\phi'(AA'\rho\rho'+A^2\rho'^2-A)]'=\rho^2V_\phi. \quad (5.18)$$

5.3.1 Wormhole Configuration

In this section, we will focus our attention on wormhole solutions of the field equations (5.11)–(5.14), or equivalently (5.15)–(5.18), obtained in the previous section. Note that Eqs. (5.11)–(5.14) are a rather complicated system of nonlinear ordinary differential equations, and we do not know if it is possible to find any exact analytical solutions to this system. Instead, we will construct wormhole solutions numerically studying previously their asymptotic properties near and far from the wormhole throat.

To describe a traversable wormhole the metric (5.10) should possess a number of specific properties. In particular, (i) the radial coordinate r runs through the domain $(-\infty,+\infty)$; (ii) there exist two asymptotically flat regions $\mathscr{R}_\pm:\ r\to\pm\infty$ connected by the throat; (iii) $\rho(r)$ has a global positive minimum at the wormhole throat

$r = r_{\rm th}$; without a loss of generality one can set $r_{\rm th} = 0$, so that $\rho_0 = \min\{\rho(r)\} = \rho(0)$ is the throat radius; (iv) $A(r)$ is everywhere positive and regular, i.e., there are no event horizons and singularities in the spacetime. Taking into account the necessary conditions for the minimum of function, we obtain also

$$\rho_0' = 0, \quad \rho_0'' > 0, \tag{5.19}$$

where the subscript '0' means that values are calculated at the throat $r = 0$. Concerning wormholes, the above relations are known as the flare-out conditions.

5.3.2 Initial Condition Analysis

Let us consider the field equations at the throat $r = 0$. By assuming $\rho_0' = 0$, Eqs. (5.11) and (5.12) after a little algebra yield

$$\frac{1}{\rho_0^2} = -\frac{\varepsilon A_0 \phi_0'^2 - 2V_0}{2M_{\rm Pl}^2 - \eta A_0 \phi_0'^2}, \tag{5.20}$$

$$\frac{\rho_0''}{\rho_0} = -\frac{\phi_0'^2(\varepsilon M_{\rm Pl}^2 - \eta V_0)}{M_{\rm Pl}^2(2M_{\rm Pl}^2 - \eta A_0 \phi_0'^2)^2}. \tag{5.21}$$

To provide the flare-out conditions (5.19) the right-hand sides of Eq. (5.20), then Eq. (5.21) should be positive. This is possible if $\phi_0'^2 \neq 0$ and the following inequalities take place:

$$\frac{\varepsilon A_0 \phi_0'^2 - 2V_0}{2M_{\rm Pl}^2 - \eta A_0 \phi_0'^2} < 0, \tag{5.22}$$

$$\varepsilon M_{\rm Pl}^2 - \eta V_0 < 0. \tag{5.23}$$

For given ε and η these inequalities provide restrictions for the initial values of $A_0\phi_0'^2$ and $V_0 = V(\phi_0)$ at the throat. Let us consider separately various cases.

1. $\eta = 0$. This is the case of a minimally coupled scalar field. Now (5.23) yields $\varepsilon < 0$, i.e. $\varepsilon = -1$, for any V_0. In turn, if $\varepsilon = -1$ Eq. (5.22) is fulfilled provided $V_0 > -\frac{1}{2}A_0\phi_0'^2$. Thus, we have obtained a well-known result that a solution with the throat in general relativity with a minimally coupled scalar field is permitted only for phantom fields with negative kinetic energy (see, for example, [5]).

Further we will consider cases with nonminimal derivative coupling.

2. $\varepsilon = 1$, $\eta > 0$. The constraints (5.22) and (5.23) give

$$(A) \quad A_0\phi_0'^2 < \frac{M_{\rm Pl}^2}{2\eta}, \quad V_0 > \frac{M_{\rm Pl}^2}{\eta},$$

$$(B) \quad A_0\phi_0'^2 > \frac{M_{\rm Pl}^2}{2\eta}, \quad \frac{M_{\rm Pl}^2}{\eta} < V_0 < \frac{1}{2}A_0\phi_0'^2.$$

Thus, in the case $\eta > 0, \varepsilon = 1$ there are domains of initial values $A_0\phi_0'^2$ and V_0 which provide the flare-out conditions (5.19). We also stress that the initial value V_0 should be necessarily positive at the throat.

3. $\varepsilon = 1, \eta < 0$. It is easy to check that Eqs. (5.22) and (5.23) are inconsistent in this case, and hence the flare-out conditions (5.19) are not fulfilled.

4. $\varepsilon = -1, \eta > 0$. Eqs. (5.22) and (5.23) give

$$A_0\phi_0'^2 < \frac{M_{\rm Pl}^2}{2\eta}, \quad V_0 > -\frac{1}{2}A_0\phi_0'^2. \tag{5.24}$$

5. $\varepsilon = -1, \eta < 0$. Eqs. (5.22) and (5.23) give

$$A_0\phi_0'^2 > 0, \quad -\frac{1}{2}A_0\phi_0'^2 < V_0 < \frac{M_{\rm Pl}^2}{|\eta|}. \tag{5.25}$$

Thus, in case $\varepsilon = -1$ there are domains of initial values $A_0\phi_0'^2$ and V_0 which provide the flare-out conditions (5.19). It is worth noticing that the value $V_0 = 0$ is admissible, and so one may expect to get a wormhole solution without a potential.

In the model with nonminimal derivative coupling there is a nontrivial case $\varepsilon = 0$, when the free kinetic term is absent. Let us consider also this case.

6. $\varepsilon = 0, \eta > 0$. Eqs. (5.22) and (5.23) give

$$A_0\phi_0'^2 < \frac{M_{\rm Pl}^2}{2\eta}, \quad V_0 > 0.$$

Thus, in this case there are domains of initial values $A_0\phi_0'^2$ and V_0 which provide the flare-out conditions. As well as for $\varepsilon = 1$ and $\eta > 0$, the initial value V_0 should be necessarily positive at the throat.

7. $\varepsilon = 0, \eta < 0$. Eqs. (5.22) and (5.23) are inconsistent.

Summarizing, we can conclude that the flare-out conditions (5.19) in the model with nonminimal derivative coupling can be fulfilled for various values of ε and η. Respectively, the flare-out conditions provide an existence of solutions with the throat. It is worth a special notice that the throat in the model with nonminimal derivative coupling can exist not only if $\varepsilon = -1$ (phantom case), but also if $\varepsilon = 1$ (normal case) and $\varepsilon = 0$ (no free kinetic term).

To finish the analysis of the field equations (5.15)–(5.18) at the throat, let us consider the metric function $A(r)$ and its first and second derivatives at $r = 0$. The value A_0 is a free parameter. Though A_0' is also free, we assume, just for simplicity, $A_0' = 0$. Note that in this case $A(r)$ has an extremum at the throat $r = 0$. Using Eq. (5.17), we can find

$$A_0'' = -\frac{2}{\rho_0}\frac{\eta A_0\phi_0'^2 + 2\rho_0^2 V_0}{2M_{\rm Pl}^2 - \eta A_0\phi_0'^2}. \tag{5.26}$$

The sign of A_0'' determines a kind of the extremum of $A(r)$; it is a maximum if $A_0'' < 0$, and a minimum if $A_0'' > 0$. It is worth noticing that, with the physical point of view, the maximum (minimum) of $A(r)$ corresponds to maximum (minimum) of gravitational potential. In turn, the gravitational force equals to zero at extrema of the gravitational potential; moreover, in the vicinity of a maximum (minimum) the gravitational force is repulsive (attractive). As a consequence, the throat is repulsive or attractive depending on the sign of A_0''.

As an example, let us consider the model with $\varepsilon = -1$. By using the relations (5.24) and (5.25), we can see that $A_0'' < 0$ if $\eta > 0$, and $A_0'' > 0$ if $\eta < 0$. Hence, the throat is repulsive in the first case, and attractive in the second one.

5.3.3 Asymptotic Analysis

While the throat is an essential feature of the wormhole geometry, its asymptotic properties could be varied for different models. Traversable wormholes are usually assumed possessing two asymptotically flat regions connected by the throat, and in this paper we will look for wormhole solutions with an appropriate asymptotic behavior.

The spacetime with the metric (5.10) has two asymptotically flat regions $\mathscr{R}_\pm : r \to \pm\infty$ provided $\lim_{r\to\pm\infty}\{\rho(r)/|r|\} = \delta_\pm$ and $\lim_{r\to\pm\infty} A(r) = A_\pm$. Since a flat spacetime is necessarily empty, we have also to suppose that $\lim_{r\to\pm\infty}\phi(r) = \phi_\pm$ and $\lim_{r\to\pm\infty} V(\phi(r)) = V(\phi_\pm) = 0$. Assume the following asymptotics at $|r| \to \infty$:

$$\rho(r) = \delta_\pm |r| \left[1 + \frac{\alpha_\pm}{|r|} + O(r^{-2})\right], \tag{5.27}$$

$$A(r) = A_\pm \left[1 - \frac{\beta_\pm}{|r|} + O(r^{-2})\right], \tag{5.28}$$

$$\phi(r) = \phi_\pm \left[1 - \frac{\gamma_\pm}{|r|} + O(r^{-2})\right], \tag{5.29}$$

$$V(\phi(r)) = O(r^{-5}). \tag{5.30}$$

Substituting the above expressions into Eq. (5.12) and collecting leading terms gives

$$A_\pm = \delta_\pm^{-2}. \tag{5.31}$$

Thus, the asymptotic form of the metric (5.10) is

$$ds^2 = -\delta_\pm^{-2}\left(1 - \frac{\beta_\pm}{|r|}\right)dt^2 + \delta_\pm^2\left(1 - \frac{\beta_\pm}{|r|}\right)^{-1}dr^2 + \delta_\pm^2 r^2\left(1 + \frac{\alpha_\pm}{|r|}\right)^2 d\Omega^2. \tag{5.32}$$

Introducing in the asymptotically flat regions $\mathscr{R}_\pm$ new radial coordinates

$$r_\pm = \delta_\pm |r| \left(1 + \frac{\alpha_\pm}{|r|}\right)$$

and neglecting terms $O(r_\pm^{-2})$, we obtain

$$ds^2 = -\left(1 - \frac{2m_\pm}{r_\pm}\right) dt_\pm^2 + \left(1 - \frac{2m_\pm}{r_\pm}\right)^{-1} dr_\pm^2 + r_\pm^2 d\Omega^2, \tag{5.33}$$

where $2m_\pm = \delta_\pm \beta_\pm$ and $t_\pm = \delta_\pm^{-1} t$. This is nothing but two Schwarzschild asymptotics at $r \to \pm\infty$ with masses $m_\pm$. Taking into account that $\delta_\pm |r| = \lim_{r\to\pm\infty} \rho(r)$ and $\delta_\pm = \pm \lim_{r\to\pm\infty} \rho'(r)$ we can find the following asymptotic formula

$$m_\pm = \lim_{r\to\pm\infty} [\rho(r)(1 - \rho'^2(r) A(r))]. \tag{5.34}$$

5.3.4 Exact Wormhole Solution with $\eta = 0$

Let us discuss the particular case $\eta = 0$ (no nonminimal derivative coupling). In this case, the system of field equations (5.15)–(5.18) reduces to the well-known equations for a minimally coupled scalar field

$$2M_{\rm Pl}^2 \frac{\rho''}{\rho} = -\varepsilon \phi'^2, \tag{5.35}$$

$$M_{\rm Pl}^2 (A' \rho^2)' = -2\rho^2 V, \tag{5.36}$$

$$A(\rho^2)'' - A'' \rho^2 = 2, \tag{5.37}$$

$$\varepsilon (A \rho^2 \phi')' = \rho^2 V_\phi. \tag{5.38}$$

Supposing additionally $\varepsilon = -1$ (phantom scalar) and $V = 0$ (no potential term), one can find an exact wormhole solution to the system (5.35)–(5.38) (see [4, 13]). Adopting the result of [42] we can write down the solution as follows

$$ds^2 = -e^{2\lambda(r)} dt^2 + e^{-2\lambda(r)} \left[dr^2 + (r^2 + r_0^2) d\Omega^2\right], \tag{5.39}$$

$$\phi(r) = \left(\frac{2M_{\rm Pl}^2 (m^2 + r_0^2)}{m^2}\right)^{1/2} \lambda(r), \tag{5.40}$$

where $\lambda(r) = (m/r_0) \arctan(r/r_0)$, and m, r_0 are two free parameters. Taking into account the following asymptotic behavior:

$$e^{2\lambda(r)} = \exp\left(\pm\frac{\pi m}{r_0}\right)\left[1 - \frac{2m}{r}\right] + O(r^{-2}),$$

in the limit $r \to \pm\infty$, we may see that the spacetime with the metric (5.39) possesses by two asymptotically flat regions. These regions are connected by the throat whose radius corresponds to the minimum of the radius of the two-dimensional sphere, $\rho^2(r) = e^{-2\lambda(r)}(r^2 + r_0^2)$. The minimum of $\rho(r)$ is achieved at $r = m$ and equal to

$$\rho_0 = \exp\left(-\frac{m}{r_0}\arctan\frac{m}{r_0}\right)(r^2 + r_0^2)^{1/2}.$$

The asymptotic masses, corresponding to $r \to \pm\infty$, are given by

$$m_\pm = \pm m \exp(\pm\pi m/2r_0).$$

It is worth noticing that the masses $m_\pm$ have both different values and different signs, and so wormholes supported by the minimally coupled scalar field inevitably have a negative mass in one of the asymptotic regions.

Note also that there is a particularly simple case $m = 0$ when the static solution (5.39) and (5.40) reduces to

$$ds^2 = -dt^2 + dr^2 + (r^2 + r_0^2)d\Omega^2, \tag{5.41}$$

$$\phi(r) = \sqrt{2}M_{\rm Pl}\arctan(r/r_0). \tag{5.42}$$

In this case both asymptotic masses are equal to zero, $m_\pm = 0$, and thus the wormhole is massless.

5.3.5 *Numerical Analysis*

In this section, we present the results of a numerical analysis of the field equations (5.11)–(5.14). Note that in order to realize a numerical analysis in practice one needs first to specify a form of the potential $V(\phi)$. The requirement of asymptotic flatness dictates $\lim_{r\to\pm\infty} V(\phi(r)) = V(\phi_\pm) = 0$. The simplest choice obeying this asymptotic behavior corresponds to zero potential, and hereafter we will assume $V(\phi) \equiv 0$. As the initial condition analysis has shown, the flare-out conditions with $V_0 = 0$ are only fulfilled in case $\varepsilon = -1$.

An initial conditions for the system of second-order ordinary differential equations (5.11)–(5.14) read $r = 0$, $\rho(0) = \rho_0$, $\rho'(0) = \rho_0'$, $A(0) = A_0$, $A'(0) = A_0'$, $\phi(0) = \phi_0$, $\phi'(0) = \phi_0'$. Without loss of generality one can set $A_0 = 1$ and $\phi_0 = 0$. Since $r = 0$ is assumed to be a wormhole throat, one gets $\rho_0' = 0$. Now the throat's radius ρ_0 given by Eq. (5.20) can be found as

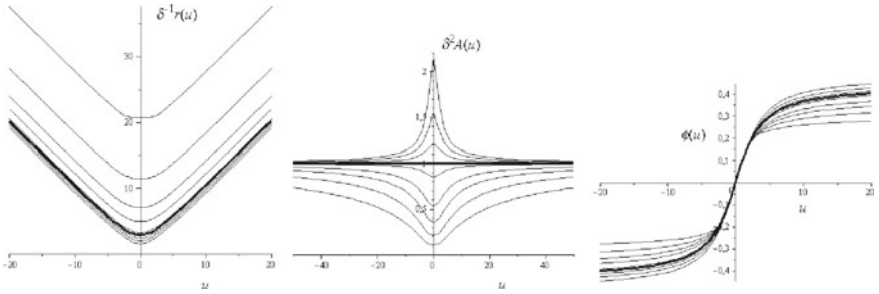

Fig. 5.1 Graphs for $\delta^{-1}\rho(r)$, $\delta^2 A(r)$, and $\phi(r)$ are constructed for the initial values $A'_0 = 0$, $\phi'_0 = 0.1$ and $\eta = -40, -20, -10, -5, -1, 0, 1, 2, 3$ (*up-bottom* for $\rho(r)$, *bottom-up* for $A(r)$, *bottom-up* for the *right* branch of $\phi(r)$); $\delta = \delta_+ = \lim_{r\to\infty}\rho(r)/r$ ($\delta_+ = \delta_-$). The *bold lines* correspond to $\eta = 0$ (no nonminimal derivative coupling)

$$\rho_0 = \sqrt{\frac{2M_{\rm Pl}^2 - \eta\phi_0'^2}{\phi_0'^2}}. \tag{5.43}$$

Then the only two free parameters determining the initial conditions remain: A'_0 and ϕ'_0.

First let us consider the case $A'_0 = 0$. In Fig. 5.1 we represent numerical solutions for $\rho(r)$, $A(r)$, and $\phi(r)$ for various values of η. Note that both $\rho(r)$ and $A(r)$ are even functions possessing an extremum at the throat $r = 0$; $\rho(r)$ has a minimum due to the flare-out conditions, and, as was mentioned above, $A(r)$ has a maximum if $\eta > 0$, and a minimum if $\eta < 0$. In case $\eta = 0$ one get $A(r) = 1$; this coincides with the analytical result (5.41). The function $\phi(r)$ is odd; it smoothly varies between two asymptotic values $-\phi_+$ and ϕ_+, where $\phi_+ = \lim_{r\to\infty}\phi(r)$. The functions $\rho(r)$ and $A(r)$ given in Fig. 5.1 also possess a proper asymptotic behavior: $\lim_{r\to\pm\infty}\rho(r) = \delta_\pm|r|$ and $\lim_{r\to\pm\infty}A(r) = \delta_\pm^{-2}$. In case $A'_0 = 0$ we have $\delta_- = \delta_+ = \delta$ and the value of δ depends generally on η, i.e., $\delta = \delta(\eta)$. The asymptotic Schwarzschild masses $m_\pm$ corresponding to the numerical solutions $\rho(r)$ and $A(r)$ are shown in Fig. 5.3. Because of the symmetry $r \leftrightarrow -r$ we have $m_- = m_+ = m$. Moreover, m is positive if $\eta < 0$, negative if $\eta > 0$, and $m = 0$ for $\eta = 0$. Note also that wormhole solutions exist only for $\eta < \eta_{max}$, and $m \to -\infty$ if $\eta \to \eta_{max}$.

The numerical solutions for $\rho(r)$ and $A(r)$ in the case $A'_0 \neq 0$ are shown in Fig. 5.2. It is worth noticing that in this case both $\rho(r)$ and $A(r)$ have different asymptotics at $r \to \pm\infty$: $\lim_{r\to\pm\infty}\rho(r) = \delta_\pm|r|$ and $\lim_{r\to\pm\infty}A(r) = \delta_\pm^{-2}$, where $\delta_- \neq \delta_+$. As a consequence, we get a wormhole configuration with two different asymptotic masses $m_\pm$. The value of $m_\pm$ depends on η; this dependence is shown in Fig. 5.3. Note that for $\eta < \eta_1$ both m_+ and m_- are positive, for $\eta > \eta_2$ both m_+ and m_- are negative, and for $\eta_1 < \eta < \eta_2$ (in particular, for $\eta = 0$) the asymptotic masses $m_\pm$ have opposite signs. Note also that $\eta < \eta_{max}$, and $m_\pm \to -\infty$ if $\eta \to \eta_{max}$.

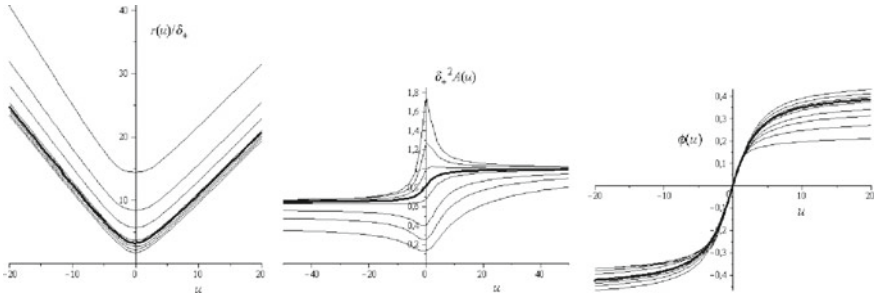

Fig. 5.2 Graphs for $\delta^{-1}\rho(r)$, $\delta^2 A(r)$, and $\phi(r)$ are constructed for the initial values $A'_0 = 0.05$, $\phi'_0 = 0.1$ and $\eta = -40, -20, -10, -5, -1, 0, 1, 2, 3$ (*up-bottom* for $\rho(r)$, *bottom-up* for $A(r)$, *bottom-up* for the *right* branch of $\phi(r)$); $\delta = \delta_+ = \lim_{r\to\infty} \rho(r)/r$ ($\delta_+ \neq \delta_-$). The *bold lines* correspond to $\eta = 0$ (no nonminimal derivative coupling)

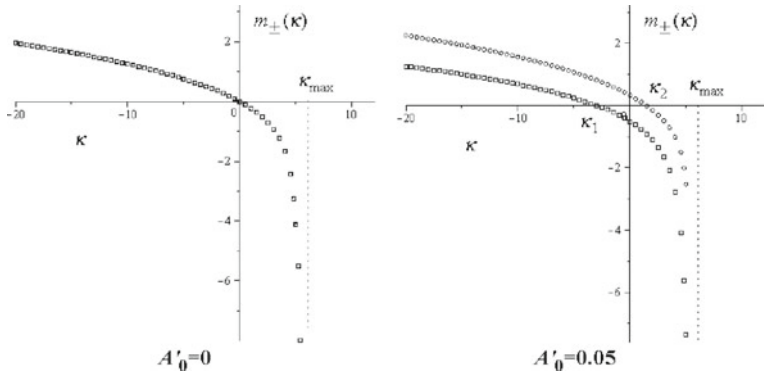

Fig. 5.3 Asymptotic masses $m_\pm$ vs η for $A'_0 = 0$ and $A'_0 = 0, 05$. Note that $m_- = m_+$ if $A'_0 = 0$. In case $A'_0 = 0.05$ the masses m_+ and m_- are represented by *upper* and *lower* graphs, respectively; $m_-(k_1) = m_+(k_2) = 0$

Note that a qualitative behavior of numerical solutions for $\rho(r)$, $A(r)$, and $\phi(r)$ does not depend on the initial value ϕ'_0, and above results were obtained for the specific choice $\phi'_0 = 0.1$.

5.4 Exact Black Hole and Wormhole Solutions in Horndeski Theory

Generally, a static spherically symmetric spacetime metric can be taken as follows

$$ds^2 = -f(r)dt^2 + g(r)dr^2 + \rho^2(r)d\Omega^2, \tag{5.44}$$

where $f(r)$, $g(r)$, $\rho(r)$ are three arbitrary metric functions of the radial coordinate r. Note that a freedom in choosing the radial coordinate allows us to fix the form of one of the metric functions $f(r)$, $g(r)$ or $\rho(r)$, but at this stage we will not do it for the sake of generality. Now, using the above-mentioned metric and assuming that $\phi = \phi(r)$, we can represent the field equations (5.4) and (5.5) in the following form:

$$\frac{\sqrt{fg}}{g}\psi\left[\varepsilon\rho^2+\eta\left(\frac{\rho\rho' f'}{fg}+\frac{\rho'^2}{g}-1\right)\right]=C_0, \tag{5.45}$$

$$\rho\rho'\frac{f'}{f}=\frac{2M_{\rm Pl}^2\, g(g-\rho'^2)-\eta\psi^2(g-3\rho'^2)+\varepsilon\rho^2\psi^2 g}{2M_{\rm Pl}^2\, g-3\eta\psi^2}, \tag{5.46}$$

$$\frac{\rho\rho'}{2}\left(\frac{f'}{f}-\frac{g'}{g}\right)=\frac{2M_{\rm Pl}^2\, g(g-\rho'^2-\rho\rho'')+\eta\psi^2(2\rho'^2+\rho\rho'')+\eta\rho\rho'(\psi^2)'}{2M_{\rm Pl}^2\, g-3\eta\psi^2}, \tag{5.47}$$

where C_0 is an integration constant, and $\psi \equiv \varphi'$. It is worth noting that the Eq. (5.45) is a first integral of the equation of motion (5.5).

Then, following Rinaldi [31], we will search for analytical solutions of the system (5.45)–(5.47) in the particular case supposing that

$$C_0 = 0. \tag{5.48}$$

In this case the Eq. (5.45) yields

$$\rho\rho'\frac{f'}{f}=g-\rho'^2-\frac{\varepsilon\rho^2 g}{\eta}, \tag{5.49}$$

This gives the following expression for the function $f(r)$:

$$f(r)=\frac{C_1}{\rho}\exp\left(-\int\frac{(\varepsilon\rho^2-\eta)g}{\eta\rho\rho'}dr\right), \tag{5.50}$$

where C_1 is an integration constant. From Eq. (5.46), using the relation (5.49), one can derive ψ^2:

$$\psi^2(r)=\frac{\varepsilon\rho^2 g}{8\pi\eta(\varepsilon\rho^2-\eta)}. \tag{5.51}$$

The scalar curvature for the metric (5.44) takes the following form:

$$R=\frac{2}{\rho^2}-\frac{2\rho' f'}{\rho g f}+\frac{2\rho' g'}{\rho g^2}-\frac{2\rho'^2}{\rho^2 g}-\frac{4\rho''}{\rho g}+\frac{f'^2}{2gf^2}-\frac{f''}{gf}+\frac{g' f'}{2g^2 f}. \tag{5.52}$$

By using the relation (5.49), one can eliminate the function $f(r)$ from the expression for R. As a result we find

$$R = \frac{2(\varepsilon\rho^2+\eta)}{\eta\rho^2} - \frac{3\rho'}{2\rho g}\left(\frac{\rho'}{\rho} - \frac{g'}{g}\right) - \frac{3\rho''}{\rho g} - \frac{g}{2\rho^2\rho'^2} - \frac{\varepsilon g(\varepsilon\rho^2-2\eta)}{2\eta^2\rho'^2} + \frac{g'(\varepsilon\rho^2-\eta)}{2\eta\rho\rho' g} - \frac{\rho''(\varepsilon\rho^2-\eta)}{\eta\rho\rho'^2}. \tag{5.53}$$

Formulas (5.50), (5.51) and (5.53) states the functions $f(r)$, $\psi(r)$ and $R(r)$ in terms of $g(r)$. The equation for $g(r)$ can be obtained by eliminating $f(r)$ and $\psi(r)$ from Eq. (5.47) by using the relations (5.49) and (5.51)

$$\rho\rho'(\varepsilon\rho^2-2\eta)\frac{g'}{g} - \left(\tfrac{1}{\eta}\rho^4 - 3\varepsilon\rho^2 + 2\eta\right) g + \rho'^2\left(3\varepsilon\rho^2+2\eta\right) - 2\rho\rho''(\varepsilon\rho^2-2\eta) - \frac{4\rho^4\rho'^2}{\varepsilon\rho^2-\eta} = 0. \tag{5.54}$$

It is worth noting that a general solution of Eq. (5.54) could be obtained analytically for an arbitrary function $\rho(r)$. Depending on the sign of $\varepsilon\eta$ the solution takes the following forms:

A. $\varepsilon\eta > 0$.

$$g(r) = \frac{\rho'^2(\rho^2-2l_\eta^2)^2}{(\rho^2-l_\eta^2)^2 F(r)}, \tag{5.55}$$

$$F(r) = 3 - \frac{8m}{\rho} - \frac{\rho^2}{3l_\eta^2} + \frac{l_\eta}{\rho}\operatorname{arctanh}\frac{\rho}{l_\eta}, \tag{5.56}$$

B. $\varepsilon\eta < 0$.

$$g(r) = \frac{\rho'^2(\rho^2+2l_\eta^2)^2}{(\rho^2+l_\eta^2)^2 F(r)}, \tag{5.57}$$

$$F(r) = 3 - \frac{8m}{\rho} + \frac{\rho^2}{3l_\eta^2} + \frac{l_\eta}{\rho}\arctan\frac{\rho}{l_\eta}, \tag{5.58}$$

Here m is an integration constant and $l_\eta = |\varepsilon\eta|^{1/2}$ is a characteristic scale of non-minimal kinetic coupling.

For the specified function $\rho(r)$ formulas (5.55)–(5.58) together with (5.50) and (5.51) give a solution to the problem of $g(r)$, $f(r)$, and $\psi(r)$ construction. Below we consider two special examples of the function $\rho(r)$.

5.4.1 Schwarzschild Coordinates: $\rho(r) = r$

As was mentioned above, a freedom in choosing the radial coordinate r allows to specify additionally the form of one of the metric functions. Let us make a choice:

$$\rho(r) = r. \tag{5.59}$$

This case corresponds to Schwarzschild coordinates, so that r is the curvature radius of coordinate sphere $r = \text{const} > 0$.

Substituting $\rho(r) = r$ into the formulas (5.50), (5.51), (5.55)–(5.58) and calculating the integral in (5.50), we derive the solutions for $g(r)$, $f(r)$ $\psi(r)$. For the first time the solutions in the case $\rho(r) = r$ were obtained by Rinaldi [31]. Below we briefly discuss these solutions separately depending on a sign of the product $\varepsilon\eta$.

A. $\varepsilon\eta > 0$. In this case the solution reads

$$f(r) = C_1 F(r), \tag{5.60}$$

$$g(r) = \frac{(r^2 - 2l_\eta^2)^2}{(r^2 - l_\eta^2)^2 F(r)}, \tag{5.61}$$

$$\psi^2(r) = \frac{\varepsilon M_{\rm Pl}^2}{l_\eta^2} \frac{r^2(r^2 - 2l_\eta^2)^2}{(r^2 - l_\eta^2)^3 F(r)}, \tag{5.62}$$

where C_1 is an integration constant and

$$F(r) = 3 - \frac{r^2}{3l_\eta^2} - \frac{8m}{r} + \frac{l_\eta}{r}\text{arctanh}\frac{r}{l_\eta}. \tag{5.63}$$

In the limit $r \to 0$ the solution (5.60) for the function $f(r)$ takes the asymptotic form

$$f(r) \approx 4C_1\left(1 - \frac{2m}{r}\right).$$

To compare the derived asymptotic with the Schwarzschild solution it is convenient to set $C_1 = 1/4$.

Note that the expressions (5.60)–(5.62) contain the function $(l_\eta/r)\text{arctanh}r/l_\eta$, which is defined in the domain $r \in (0, l_\eta)$. To continue the solution into the interval $r \in (l_\eta, \infty)$, one should make use of the identity

$$\frac{l_\eta}{r}\text{arctanh}\frac{r}{l_\eta} = \frac{l_\eta}{2r}\ln\frac{l_\eta + r}{l_\eta - r},$$

and then turn to the function $\frac{l_\eta}{2r}\ln\left|\frac{l_\eta+r}{l_\eta-r}\right|$. At $r \to \infty$ the asymptotic of the function $f(r)$ with the domain extended to the interval (l_η, ∞) has a form of the de Sitter solution:

$$f(r) \approx \frac{3}{4} - \frac{r^2}{12l_\eta^2}.$$

Also note that at $r = l_\eta$ the function $\frac{l_\eta}{2r} \ln \left| \frac{l_\eta + r}{l_\eta - r} \right|$ has a logarithmic singularity and that is why its domain consists of two disconnected parts $\mathscr{R}_1 : 0 < r < l_\eta$ and $\mathscr{R}_2 : l_\eta < r < \infty$. This implies that we have two different classes of solutions of the form (5.60)–(5.62) which are defined independently within separate domains $\mathscr{R}_1$ and $\mathscr{R}_2$.

Further let us take into account the fact that we consider the real scalar field, so the value ψ^2 should be nonnegative, i.e., $\psi^2 \geq 0$. In view of this requirement the formula (5.62) imposes additional restrictions on the domain of r. In particular, it should be noted that in each of the intervals $\mathscr{R}_1$ and $\mathscr{R}_2$ at fixed ε a sign of the function $\psi^2(r)$ is defined by a sign of $F(r)$ and reverses where the function $F(r)$ reverses its sign. Hence we can resume that the solution (5.60)–(5.62) cannot be considered as a solution which describes a black hole in the theory of gravity with nonminimal kinetic coupling.

B. $\varepsilon\eta < 0$. In this case the solution reads as follows:

$$f(x) = \frac{1}{4} F(r), \tag{5.64}$$

$$g(x) = \frac{(r^2 + 2l_\eta^2)^2}{(r^2 + l_\eta^2)^2 F(r)}, \tag{5.65}$$

$$\psi^2(r) = -\frac{\varepsilon M_{\rm Pl}^2}{l_\eta^2} \frac{r^2 (r^2 + 2l_\eta^2)^2}{(r^2 + l_\eta^2)^3 F(r)}, \tag{5.66}$$

where

$$F(r) = 3 + \frac{r^2}{3l_\eta^2} - \frac{8m}{r} + \frac{l_\eta}{r} \arctan \frac{r}{l_\eta}. \tag{5.67}$$

Now the solution contains a function $\frac{l_\eta}{r} \arctan \frac{r}{l_\eta}$ and has a domain $r \in (0, \infty)$. In the limit $r \to 0$ the function $f(r)$ yields the Schwarzschild asymptotics: $f(r) \approx 1 - \frac{2m}{r}$, and in the limit $r \to \infty$ – the anti-de Sitter one: $f(r) \approx \frac{3}{4} + \frac{r^2}{12 l_\eta^2}$. However, the obtained solution cannot be considered as an analogue of the Schwarzschild-anti-de Sitter solution, as in the case of $m > 0$ the function $F(r)$ reverses sign at a point r_h inside the interval $r \in (0, \infty)$ and hence the value of ψ^2 becomes negative in one of the intervals $(0, r_h)$ or (r_h, ∞) according to the sign of ε.

From a physical point of view a case $m = 0$ may be of some interest. In this case the function $F(r)$ is everywhere positive and regular. About a zero point the metric functions have asymptotics $f(r) = 1 + O(r^2)$ and $g(r) = 1 + O(r^2)$, as well as $\psi^2(r) = \frac{\varepsilon M_{\rm Pl}^2}{l_\eta^2} \frac{r^2}{l_\eta^2} (1 + O(r^2))$. Thus, at $\varepsilon = +1$ we obtain static spherically symmetric configuration with regular center and the anti-de Sitter structure at infinity.

5.4.2 Wormhole Configuration: $\rho(r) = \sqrt{r^2 + a^2}$

In this section we consider static spherically symmetric configurations with the metric function $\rho(r)$ of the following form:

$$\rho(r) = \sqrt{r^2 + a^2}, \tag{5.68}$$

where $a > 0$ is a parameter. Then the metric (5.44) reads

$$ds^2 = -f(r)dt^2 + g(r)dr^2 + (r^2 + a^2)d\Omega^2. \tag{5.69}$$

If $f(r)$ and $g(r)$ are everywhere positive and regular functions with a domain $r \in (-\infty, \infty)$, then the metric (5.69) describes a wormhole configuration with a throat at $r = 0$; the parameter a is a throat radius.

Substituting $\rho(r) = \sqrt{r^2 + a^2}$ into the formulas (5.51), (5.55)–(5.58), we derive the solutions for $g(r)$, $f(r)$ and $\psi^2(r)$ in an explicit form. Below we consider these solutions for each sign of the product $\varepsilon\eta$.

A. $\varepsilon\eta > \mathbf{0}$. In this case the solution for $g(r)$ is given by the formulas (5.55)–(5.56). The solution contains the function $(l_\eta/\sqrt{r^2 + a^2})\,\mathrm{arctanh}\,(\sqrt{r^2 + a^2}/l_\eta)$ with the domain that could be found from condition $\sqrt{r^2 + a^2}/l_\eta < 1$, i.e., $|r| < r_1 \equiv (l_\eta^2 - a^2)^{1/2}$. At the points $|r| = r_1$ the function $(l_\eta/\sqrt{r^2 + a^2})\,\mathrm{arctanh}\,(\sqrt{r^2 + a^2}/l_\eta)$ logarithmically diverges. Consequently, the metric function $g(r)$ guides the singular behavior near $|r| = r_1$, that makes this solution unphysical.

B. $\varepsilon\eta < \mathbf{0}$. In this case, by substituting $\rho(r) = \sqrt{r^2 + a^2}$ into the formulas (5.57), (5.58) and (5.50), we obtain the following solutions for the metric functions $g(r)$ and $f(r)$ and the function $\psi^2(r)$:

$$f(r) = C_1 F(r), \tag{5.70}$$

$$g(r) = \frac{r^2(r^2 + a^2 + 2l_\eta^2)^2}{(r^2 + a^2)(r^2 + a^2 + l_\eta^2)^2 F(r)}, \tag{5.71}$$

$$\psi^2(r) = -\frac{\varepsilon M_{\mathrm{Pl}}^2}{l_\eta^2}\frac{r^2(r^2 + a^2 + 2l_\eta^2)^2}{(r^2 + a^2)(r^2 + a^2 + l_\eta^2)^3 F(r)}, \tag{5.72}$$

where

$$F(r) = 3 - \frac{8m}{\sqrt{r^2 + a^2}} + \frac{r^2 + a^2}{3l_\eta^2} + \frac{l_\eta}{\sqrt{r^2 + a^2}}\arctan\left(\frac{\sqrt{r^2 + a^2}}{l_\eta}\right), \tag{5.73}$$

and the integration constant $C_1 = 1/F(0)$ in the expression for $f(r)$ is chosen so that $f(0) = 1$. The function $F(r)$ has a minimum at $r = 0$, thus to make it everywhere positive one should demand $F(0) > 0$. Hence one can derive the limitation on the upper value of the parameter m

$$2m < a\left(\frac{3}{4} + \frac{\alpha^2}{12} + \frac{1}{4\alpha}\arctan\alpha\right), \tag{5.74}$$

where $\alpha \equiv a/l_\eta$ is the dimensionless parameter which defines the ratio of two characteristic sizes: the wormhole throat radius a and the scale of the nonminimal kinetic coupling l_η. In the particular case $a \ll l_\eta$ we get $2m < a$. Further, we assume that the value of m satisfies the condition (5.74), and therefore the function $F(r)$ is positively definite, i.e. $F(r) > 0$.

Let us consider the asymptotic properties of the obtained solution. Far from the throat in the limit $|r| \to \infty$ the metric functions $g(r)$ and $f(r)$ have the following asymptotics:

$$g(r) = 3\frac{l_\eta^2}{r^2} + O\left(\frac{1}{r^4}\right), \quad f(r) = A\frac{r^2}{l_\eta^2} + O(r^0), \tag{5.75}$$

where the constant A depends on the parameters a, l_η and m and can be calculated only numerically. Let us note that the derived asymptotics correspond to the geometry of anti-de Sitter space with a constant negative curvature.

In the neighborhood of the throat $r = 0$ we obtain

$$g(r) = B\frac{r^2}{l_\eta^2} + O(r^4), \quad f(r) = 1 + O(r^2), \tag{5.76}$$

where

$$B = \frac{(\alpha^2+2)^2}{\alpha^2(\alpha^2+1)^2\left(3 + \frac{1}{3}\alpha^2 - \frac{8m}{a} + \frac{1}{\alpha}\arctan\alpha\right)}.$$

It is worth noticing that at the throat $r = 0$ the metric function $g(r)$ vanishes, i.e., $g(0) = 0$. This implies that there is a coordinate singularity at $r = 0$. To answer the question whether there is a geometric singularity at this point, one should compute the curvature invariants for the metric (5.44). In this paper we confine ourselves to discussion of the scalar curvature (5.53). By substituting the solution (5.71) into (5.53) one can check that the curvature near the throat is regular: $R(r) = R_0 + O(r^2)$, where the value $R_0 = R(0)$ is cumbersomely expressed in terms of the parameters a, l_η m. Far from the throat in the limit $|r| \to \infty$ the scalar curvature tends asymptotically to a constant negative value, i.e. $R \to R_\infty$, where

$$R_\infty = -\frac{5 + 3l_\eta^2}{2l_\eta^2}. \tag{5.77}$$

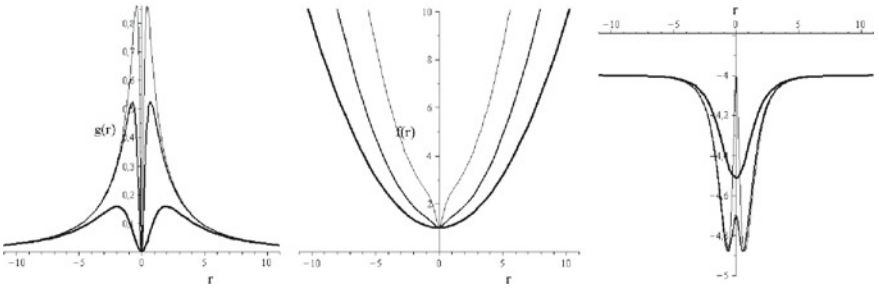

Fig. 5.4 Graphs for the metric functions $g(r)$, $f(r)$ and the scalar curvature $R(r)$ with $l_\eta = 1$, $m = 0.1$. Curves, from *thin* to *thick*, are given for $a = 0.3; 0.5; 1.5$

It is worthwhile to note that the asymptotic value R_∞ is determined only by the characteristic scale of nonminimal kinetic coupling l_η and does not depend on a and m. We also note that $R_\infty \to -\infty$ in the limit $l_\eta \to 0$.

Finally, we discuss briefly the solution (5.72) for $\psi^2(r)$. Since $F(r) > 0$, hence the condition $\psi^2(r) \geq 0$ holds only for $\varepsilon = -1$. Now taking into account that the solutions (5.71), (5.70), and (5.72) was obtained in the case $\varepsilon\eta < 0$, we can conclude that $\eta > 0$.

To illustrate the performed analysis, we show the numerical solutions for $g(r)$, $f(r)$ and the scalar curvature $R(r)$ in Fig. 5.4.

5.5 Summary and Discussion

We have explored static spherically symmetric wormhole solutions in the Horndeski theory of gravity with the simplest lagrangian containing the terms $(\varepsilon g^{\mu\nu} + \eta G^{\mu\nu})\phi_{,\mu}\phi_{,\nu}$ and $V(\phi)$ and representing a particular case of the general Horndeski lagrangian [24], which leads to second-order equations of motion.

Carrying out a local analysis of the flare-out conditions, we have shown that solutions with a throat in the theory (5.3) with a nonzero kinetic coupling parameter $\eta \neq 0$ could exist for all possible values of $\varepsilon = -1, 0, +1$; in the case $\varepsilon = -1$ the value $V_0 = 0$ is admissible, while in the case $\varepsilon = +1$ and $\varepsilon = 0$ the initial value V_0 should be necessarily positive at the throat. For comparison, it is worth noticing that solutions with a throat in the minimally coupling model with $\eta = 0$ are forbidden for an ordinary scalar field with $\varepsilon = +1$ [5].

Note that the flare-out condition does not guaranty by itself the existence of asymptotic regions and so it is a necessary but not sufficient condition for a wormhole solution to exist. Assuming additionally an asymptotic flatness, we have found numerical solutions describing traversable (Lorentzian) wormholes in the particular case $V(\phi) \equiv 0$ (no potential) and $\varepsilon = -1$.

The wormhole solutions constructed numerically could be classified by their asymptotic behavior which, in turn, is determined by asymptotics of the metric functions $\rho(r)$ and $A(r)$ at $r \to \pm\infty$. If $A'_0 = 0$, then both $\rho(r)$ and $A(r)$ are even, and so a wormhole configuration is symmetrical relative to the throat $r = 0$. In this case both asymptotic masses $m_\pm$ are equal, i.e., $m_- = m_+ = m$, and one has the following cases: (i) $m > 0$ if $\kappa < 0$; (ii) $m = 0$ if $\kappa = 0$; (iii) $m < 0$ if $\kappa > 0$. In case $A'_0 \neq 0$ a wormhole configuration has no symmetry relative to the throat, hence the asymptotic masses $m_\pm$ are different, i.e., $m_- \neq m_+$, and one gets (i) $m_- > 0$, $m_+ > 0$ if $\eta < \eta_1 < 0$; (ii) $m_- \leq 0$, $m_+ > 0$ if $\eta_1 < \eta < \eta_2$; (iii) $m_- < 0$, $m_+ \leq 0$ if $\eta > \eta_2 > 0$. Thus, depending on η, a wormhole could possess positive and/or negative asymptotic Schwarzschild masses. It is worth emphasizing that both masses are positive only provided $\eta < \eta_1$ (for a symmetrical wormhole configuration one has $\eta_1 = \eta_2 = 0$), otherwise one or both wormhole masses are negative. For example, let us consider the case $\eta = 0$, when the scalar field is minimally coupled to the curvature. In this case well-known wormhole solutions have been analytically obtained by Ellis [13] and Bronnikov [4]. Such wormholes inevitably possess a negative Schwarzschild mass in one of the asymptotic regions, or, in the particular case of a symmetric wormhole configuration, both asymptotic masses are equal to zero. (Note that our numerical calculations given in Figs. 5.1, 5.2 and 5.3 completely reproduce this particular analytical result.)

The stability of wormhole configurations is an important test of their possible viability. The stability of wormholes supported by phantom scalar fields was intensively investigated in the literature [6, 16, 35, 42], and the final resolution states that both static and non-static (see Ref. [42]) scalar wormholes are unstable. Though this result is technically complicated, there is a simple qualitative explanation of this instability. Actually, as was mentioned above, a scalar wormhole inevitably possesses a negative Schwarzschild mass in one of the asymptotic regions; for example, let it be $\mathscr{R}_- : r \to -\infty$. This means that the gravitational potential is *decreasing* and the gravitational force is *repulsive* far from the throat. Consider now a small scalar perturbation of the wormhole geometry localized near the throat. Such a perturbation shall play a role of a small bunch of energy density and, because of the repulsive character of the gravitational field, it shall be pushed to the infinity $\mathscr{R}_-$. Similarly, any scalar perturbations will propagate from the throat vicinity to infinity, and this indicates an instability of the throat.

In comparison with wormholes supported by a phantom scalar field minimally coupled to the curvature, the scalar wormholes with nonminimal derivative coupling described in this chapter have a more general asymptotic behavior. Namely, depending on a value of the nonminimal derivative coupling parameter η one of the following qualitatively different cases is realized: (i) one of the asymptotic wormhole masses or both of them are negative; (ii) both asymptotic masses are positive. Taking into account the previous qualitative consideration, one can expect that a wormhole configuration will be unstable in the first case and stable in the second one. Actually, if both asymptotic masses are positive, then the gravitational potential is *increasing* and the gravitational field is *attractive* on both sides of the wormhole throat. In this

case all scalar perturbations should be localized in the vicinity of the throat, and this would provide a stability.[1]

Previously, Rinaldi [31] found a class of exact solutions with nonminimal kinetic coupling with characteristic features of black holes, particularly, with event horizon. In this work, using the Rinaldi approach, we have found and examined analytical solutions describing wormholes. A detailed analysis revealed a number of characteristic features of the obtained solutions. In particular, it turned out that the wormhole solution exists only if $\varepsilon = -1$ (phantom case) and $\eta > 0$. The wormhole metric has a specific coordinate singularity at the wormhole throat, namely, the metric component g_{rr} is vanished at $r = 0$. However, there is no curvature singularity at the throat, since all the curvature invariants stay regular. Also it was shown that the wormhole throat connects two asymptotic regions with anti-de Sitter geometry of spacetime.

Acknowledgements The work was supported by the Russian Government Program of Competitive Growth of Kazan Federal University.

References

1. Anabalon A, Cisterna A, Oliva J. Asymptotically locally AdS and flat black holes in Horndeski theory. Phys Rev D. 2014;89:084050.
2. Babichev E, Charmousis C. Dressing a black hole with a time-dependent Galileon. JHEP. 2014;1408:106.
3. Banijamali A, Fazlpour B. Crossing of $\omega = -1$ with Tachyon and non-minimal derivative coupling. Phys Lett B. 2011;703:366.
4. Bronnikov KA. Scalar-tensor theory and scalar charge. Acta Phys Pol B. 1973;4:251.
5. Bronnikov KA. Spherically symmetric false vacuum: no-go theorems and global structure. Phys Rev D. 2001;64:064013.
6. Bronnikov KA, Fabris JC, Zhidenko A. On the stability of scalar-vacuum space-times. Eur Phys J C. 2011;71:1791.
7. Cisterna A, Erices C. Asymptotically locally AdS and flat black holes in the presence of an electric field in the Horndeski scenario. Phys Rev D. 2014;89:084038.
8. Copeland EJ, Sami M, Tsujikawa S. Dynamics of dark energy. Int J Mod Phys D. 2006;15:1753.
9. De Felice A, Tsujikawa S. $f(R)$ theories. Living Rev Rel. 2010;13:3.
10. Deffayet C, Esposito-Farese G, Vikman A. Covariant Galileon. Phys Rev D. 2009;79:084003.
11. Deffayet C, Deser S, Esposito-Farese G. Generalized Galileons: all scalar models whose curved background extensions maintain second-order field equations and stress tensors. Phys Rev D. 2009;80:064015.
12. Eiroa EF. Stability of thin-shell wormholes with spherical symmetry. Phys Rev D. 2008;78:024018.
13. Ellis HG. Ether flow through a drainhole: a particle model in general relativity. J Math Phys. 1973;14:104.
14. Gao C. When scalar field is kinetically coupled to the Einstein tensor. JCAP. 2010;06:023.
15. Garcia NM, Lobo FSN, Visser M. Generic spherically symmetric dynamic thin-shell traversable wormholes in standard general relativity. Phys Rev D. 2012;86:044026.

[1] Note that wormhole solutions with positive asymptotic masses are known in the literature. In particular, various thin-shell configurations represent wormholes with positive asymptotic masses; it is worth noticing that thin-shell wormholes could be stable (see, for example, Refs. [12, 15] and references therein).

16. Gonzalez JA, Guzman FS, Sarbach O. Instability of wormholes supported by a ghost scalar field. I. Linear stability analysis. Class Quantum Grav. 2009;26:015010.
17. Granda LN. Non-minimal kinetic coupling and the phenomenology of dark energy. Class Quantum Grav. 2011;28:025006.
18. Granda LN. Inflation driven by scalar field with non-minimal kinetic coupling with Higgs and quadratic potentials. JCAP. 2011;1104:016.
19. Granda LN. Late time cosmological scenarios from scalar field with Gauss Bonnet and non-minimal kinetic couplings. Int J Theor Phys. 2012;51:2813–29 arXiv:1109.1371.
20. Granda LN. Dark energy from scalar field with Gauss Bonnet and non-minimal kinetic coupling. Mod Phys Lett A. 2012;27:1250018.
21. Granda LN, Cardona W. General non-minimal kinetic coupling to gravity. JCAP. 2010;1007:021.
22. Granda LN, Torrente-Lujan E, Fernandez-Melgarejo JJ. Non-minimal kinetic coupling and Chaplygin gas cosmology. Eur Phys J C. 2011;71:1704.
23. Gubitosi G, Linder EV. Purely kinetic coupled gravity. Phys Lett B. 2011;703:113.
24. Horndeski GW. Second-order scalar-tensor field equations in a four-dimensional space. Int J Theor Phys. 1974;10:363.
25. Joyce A, Jain B, Khoury J, Trodden M. Beyond the cosmological standard model. Phys Rept. 2015;568:1.
26. Korolev RV, Sushkov SV. Exact wormhole solutions with nonminimal kinetic coupling. Phys Rev D. 2014;90:124025.
27. Minamitsuji M. Solutions in the scalar-tensor theory with nonminimal derivative coupling. Phys Rev D. 2014;89:064017.
28. Nicolis A, Rattazzi R, Trincherini E. The Galileon as a local modification of gravity. Phys Rev D. 2009;79:064036.
29. Perlmutter S, et al. Measurements of omega and lambda from 42 high-redshift supernovae. Astrophys J. 1999;517:565.
30. Riess A, et al. Observational evidence from supernovae for an accelerating universe and a cosmological constant. Astron J. 1998;116:1009.
31. Rinaldi M. Black holes with non-minimal derivative coupling. Phys Rev D. 2012;86:084048.
32. Sadjadi HM. Super-acceleration in non-minimal derivative coupling model. Phys Rev D. 2011;83:107301.
33. Sahni V, Starobinsky AA. The case for a positive cosmological lambda-term. Int J Mod Phys D. 2000;9:373.
34. Saridakis EN, Sushkov SV. Quintessence and phantom cosmology with non-minimal derivative coupling. Phys Rev D. 2010;81:083510.
35. Shinkai H-a, Hayward SA. Fate of the first traversible wormhole: black-hole collapse or inflationary expansion. Phys Rev D. 2002;66:044005.
36. Skugoreva MA, Sushkov SV, Toporensky AV. Cosmology with nonminimal kinetic coupling and a power-law potential. Phys Rev D. 2013;88:083539.
37. Sotiriou TP, Faraoni V. $f(R)$ theories of gravity. Rev Mod Phys. 2010;82:451.
38. Starobinsky AA, Sushkov SV, Volkov MS. The screening Horndeski cosmologies. JCAP. 2016;1606(06):007.
39. Sushkov SV. Exact cosmological solutions with nonminimal derivative coupling. Phys Rev D. 2009;80:103505.
40. Sushkov S. Realistic cosmological scenario with non-minimal kinetic coupling. Phys Rev D. 2012;85:123520.
41. Sushkov SV, Korolev R. Scalar wormholes with nonminimal derivative coupling. Class Quant Grav. 2012;29(8):085008.
42. Sushkov SV, Zhang Y-Z. Scalar wormholes in cosmological setting and their instability. Phys Rev D. 2008;77:024042.
43. Weinberg S. The cosmological constant problem. Rev Mod Phys. 1989;61:1.
44. Woodard RP. Ostrogradsky's theorem on Hamiltonian instability. Scholarpedia. 2015;10:32243.

Chapter 6
Self-Sustained Traversable Wormholes

Remo Garattini and Francisco S.N. Lobo

6.1 Introduction

A wormhole can be represented by two asymptotically flat regions joined by a bridge, and are solutions to the Einstein field equations, and is given by the following line element [1–3]

$$ds^2 = -\exp\left(-2\Phi\left(r\right)\right)dt^2 + \frac{dr^2}{1-b(r)/r} + r^2\left(d\theta^2 + \sin^2\theta d\varphi^2\right), \qquad (6.1)$$

where $\Phi\left(r\right)$ is called the redshift function, while $b\left(r\right)$ is called the shape function. A proper radial distance can be related to the shape function by $l\left(r\right) = \pm\int_{r_0}^{r} d\bar{r}/\sqrt{1-b_{\pm}(\bar{r})/\bar{r}}$, where the plus (minus) sign is related to the upper (lower) part of the wormhole or universe. Two coordinate patches are required, each one covering the range $[r_0, +\infty)$. Each patch covers one universe, and the two patches join at r_0, the throat of the wormhole defined by $r_0 = \min\{r\left(l\right)\}$. One of the prerogatives of a wormhole is its ability to connect two distant points in space–time. In this amazing perspective, it is immediate to recognize the possibility of traveling crossing wormholes as a shortcut in space and time.

R. Garattini (✉)
Dipartimento di Ingegneria e scienze applicate, Università degli Studi di Bergamo,
Viale Marconi, 5, 24044 Dalmine (Bergamo), Italy
e-mail: remo.garattini@unibg.it

R. Garattini
I.N.F.N. - sezione di Milano, Milan, Italy

F.S.N. Lobo
Faculdade de Ciências, Instituto de Astrofísica e Ciências do Espaço,
Universidade de Lisboa, Campo Grande, 1749-016 Lisboa, Portugal
e-mail: fslobo@fc.ul.pt

F.S.N. Lobo (ed.), *Wormholes, Warp Drives and Energy Conditions*,
Fundamental Theories of Physics 189, DOI 10.1007/978-3-319-55182-1_6

The Einstein field equation provides the following relationships

$$p_r' = \frac{2}{r}\left(p_t - p_r\right) - \left(\rho + p_r\right)\Phi', \tag{6.2}$$

$$b' = 8\pi G\rho\left(r\right)r^2, \tag{6.3}$$

$$\Phi' = \frac{b + 8\pi G p_r r^3}{2r^2\left(1 - b\left(r\right)/r\right)}, \tag{6.4}$$

where the prime denotes a derivative with respective to the radial coordinate. The quantity $\rho\left(r\right)$ is the energy density, $p_r\left(r\right)$ is the radial pressure, and $p_t\left(r\right)$ is the lateral pressure. However, these solutions are accompanied by unavoidable violations of null energy conditions, namely, the matter threading the wormhole's throat has to be *exotic*. Classical matter satisfies the usual energy conditions, therefore, it is likely that wormholes must belong to the realm of semiclassical or perhaps a possible quantum theory of the gravitational field.

Since a complete theory of quantum gravity has yet to be devised, it is important to approach this problem with another strategy. On this ground, in a series of papers [4, 5], the idea of *self-sustained* traversable wormhole was introduced. A traversable wormhole is said to be *self-sustained* if it is totally supported by its own quantum fluctuations. This is quite similar to compute the Casimir energy on a fixed background, where it is known that for different physical systems, the Casimir energy is negative. This is exactly the feature that exotic matter should possess. Usually, the Casimir energy is related to the Zero Point Energy (ZPE) and usually is Ultraviolet (UV) divergent.[1] To this purpose, in this contribution, two methods to keep under control the UV divergences will be discussed: (1) a standard regularization/renormalization process; (2) the distortion of gravity at the Planck scale.

We will discuss specific wormhole models such as: (i) the Ellis wormhole [8, 9]; (ii) a wormhole geometry supported by an equation of state (EoS)[2] givenby $p_r = \omega\rho$; (iii) and a geometry supported by an EoS given by $p_r = \omega(r)\rho$, where the parameter is now dependent on the radial coordinate; (iv) and finally, a traversable wormhole induced by a noncommutative geometry. Of course, this selection does not exhaust the list of interesting profiles, but it is large enough to show the whole procedure of a self-sustained traversable wormhole. Although the semiclassical approach can be judged suspicious because of the suspected validity of semiclassical methods[3] at the Planck scale [16], one can consider that the whole calculational approach is sufficiently robust to be adopted.

The rest of the paper is structured as follows: In Sect. 6.2 we define the effective Einstein equations, and we provide some of the basic rules to perform the functional

[1] See for example Refs. [6, 7] to see how the Casimir procedure comes into play for ZPE calculations.

[2] See also Refs. [10–13], where the authors search for classical traversable wormholes supported by phantom energy.

[3] To this purpose, see also paper of Hochberg, Popov, and Sushkov [14], and the paper of Khusnutdinov and Sushkov [15].

integration. In Sect. 6.3, we define the Hamiltonian approximated up to second order, while in Sect. 6.4, we study the spectrum of the spin-two operator acting on transverse traceless tensors. In Sect. 6.5, we regularize and renormalize the one loop energy contribution and we speculate about the self-consistency of the result. In Sect. 6.6, we distort gravity to regularize and renormalize the one loop energy contribution. We summarize and conclude in Sect. 6.7.

6.2 Effective Einstein Equations and the Hamiltonian

6.2.1 Einstein Equations and the Hamiltonian

Let us consider the Einstein equations

$$G_{\mu\nu} = R_{\mu\nu} - \frac{1}{2} g_{\mu\nu} R = \kappa T_{\mu\nu}. \tag{6.5}$$

where $G_{\mu\nu}$ is the Einstein tensor, $R_{\mu\nu}$ is the Ricci tensor and R is the scalar curvature, $T_{\mu\nu}$ is the stress–energy tensor and $\kappa = 8\pi G$. If u^μ is a time-like unit vector such that $g_{\mu\nu} u^\mu u^\nu = -1$, then the contraction $G_{\mu\nu} u^\mu u^\nu$ yields

$$G_{\mu\nu} u^\mu u^\nu = R_{\mu\nu} u^\mu u^\nu - \frac{1}{2} g_{\mu\nu} u^\mu u^\nu R = R_{\mu\nu} u^\mu u^\nu + \frac{1}{2} R. \tag{6.6}$$

By means of the Gauss–Codazzi equations [17],

$$R = R^{(3)} \pm 2 R_{\mu\nu} u^\mu u^\nu \mp K^2 \pm K_{\mu\nu} K^{\mu\nu}, \tag{6.7}$$

where $K_{\mu\nu}$ is the extrinsic curvature and $R^{(3)}$ is the three-dimensional scalar curvature. For a time-like vector, we take the lower sign and Eq. (6.6) becomes

$$G_{\mu\nu} u^\mu u^\nu = \frac{1}{2} \left(R^{(3)} + K^2 - K_{\mu\nu} K^{\mu\nu} \right). \tag{6.8}$$

If the conjugate momentum is defined by

$$\pi^{\mu\nu} = \frac{\sqrt{{}^{(3)}g}}{2\kappa} \left(K g^{\mu\nu} - K^{\mu\nu} \right), \tag{6.9}$$

then

$$K^2 - K_{\mu\nu} K^{\mu\nu} = \left(\frac{2\kappa}{\sqrt{{}^{(3)}g}} \right)^2 \left(\frac{\pi^2}{2} - \pi^{\mu\nu} \pi_{\mu\nu} \right) \tag{6.10}$$

and finally

$$\frac{\sqrt{^{(3)}g}}{2\kappa}G_{\mu\nu}u^{\mu}u^{\nu}=\frac{\sqrt{^{(3)}g}}{2\kappa}R^{(3)}+\frac{2\kappa}{\sqrt{^{(3)}g}}\left(\frac{\pi^2}{2}-\pi^{\mu\nu}\pi_{\mu\nu}\right)=-\mathscr{H}^{(0)}\,. \tag{6.11}$$

6.2.2 The Effective Einstein Equations

Consider, a separation of the metric into a background part, $\bar{g}_{\mu\nu}$, and a perturbation, $h_{\mu\nu}$,

$$g_{\mu\nu}=\bar{g}_{\mu\nu}+h_{\mu\nu}. \tag{6.12}$$

The Einstein tensor $G_{\mu\nu}$ can also be divided into a part describing the curvature due to the background geometry and that due to the perturbation,

$$G_{\mu\nu}\left(g_{\alpha\beta}\right)=G_{\mu\nu}\left(\bar{g}_{\alpha\beta}\right)+\Delta G_{\mu\nu}\left(\bar{g}_{\alpha\beta},h_{\alpha\beta}\right), \tag{6.13}$$

where, in principle $\Delta G_{\mu\nu}\left(\bar{g}_{\alpha\beta},h_{\alpha\beta}\right)$ is a perturbation series in terms of $h_{\mu\nu}$.

In the context of semiclassical gravity, Eq. (6.5) becomes

$$G_{\mu\nu}=\kappa\left\langle T_{\mu\nu}\right\rangle^{\text{ren}}, \tag{6.14}$$

where $\left\langle T_{\mu\nu}\right\rangle^{\text{ren}}$ is the renormalized expectation value of the stress–energy tensor operator of the quantized field. If the matter field source is absent, nothing prevents us from defining an effective stress–energy tensor for the fluctuations as[4]

$$\left\langle T_{\mu\nu}\right\rangle^{\text{ren}}=-\frac{1}{\kappa}\left\langle\Delta G_{\mu\nu}\left(\bar{g}_{\alpha\beta},h_{\alpha\beta}\right)\right\rangle^{\text{ren}}. \tag{6.15}$$

From this point of view, the equation governing quantum fluctuations behaves as a backreaction equation. If we fix our attention to the energy component of the Einstein field equations, we need to introduce a time-like unit vector u^{μ} such that $g_{\mu\nu}u^{\mu}u^{\nu}=-1$. Then the semiclassical Einstein's equations (6.14) projected on the constant time hypersurface Σ become

$$G_{\mu\nu}\left(\bar{g}_{\alpha\beta}\right)u^{\mu}u^{\nu}=\kappa\left\langle T_{\mu\nu}u^{\mu}u^{\nu}\right\rangle^{\text{ren}}=-\left\langle\Delta G_{\mu\nu}\left(\bar{g}_{\alpha\beta},h_{\alpha\beta}\right)u^{\mu}u^{\nu}\right\rangle^{\text{ren}}. \tag{6.16}$$

[4]Note that our approach is very close to the gravitational *geon* considered by Anderson and Brill [18]. The relevant difference is in the averaging procedure.

To proceed further, it is convenient to consider the associated tensor density and integrate over Σ. This leads to[5]

$$\begin{aligned}\frac{1}{2\kappa}\int_{\Sigma} d^3x\sqrt{g}G_{\mu\nu}\left(\bar{g}_{\alpha\beta}\right)u^{\mu}u^{\nu} &= -\int_{\Sigma} d^3x\mathscr{H}^{(0)} \\ &= -\frac{1}{2\kappa}\int_{\Sigma} d^3x\sqrt{g}\left\langle\Delta G_{\mu\nu}\left(\bar{g}_{\alpha\beta},h_{\alpha\beta}\right)u^{\mu}u^{\nu}\right\rangle^{\text{ren}},\end{aligned} \tag{6.17}$$

where $\sqrt{g}$ is the spatial part of the determinant of the metric tensor on the traversable wormhole fixed background and

$$\mathscr{H}^{(0)} = (2\kappa)\,G_{ijkl}\pi^{ij}\pi^{kl} - \frac{1}{2\kappa}\sqrt{^3\bar{g}}R, \tag{6.18}$$

is the background field super-hamiltonian. R is the three-dimensional scalar curvature and G_{ijkl} is the DeWitt super metric defined as

$$G_{ijkl} = \frac{1}{2\sqrt{g}}\left(g_{ik}g_{jl} + g_{il}g_{jk} - g_{ij}g_{kl}\right). \tag{6.19}$$

Thus, the fluctuations in the Einstein tensor are, in this context, the fluctuations of the hamiltonian. To compute the expectation value of the perturbed Einstein tensor, we will use a variational procedure. In practice, the right-hand side of Eq. (6.17) will be obtained by expanding

$$E_{\text{wormhole}} = \frac{\langle\Psi\,|H_{\Sigma}|\,\Psi\rangle}{\langle\Psi|\Psi\rangle} = \frac{\left\langle\Psi\left|H_{\Sigma}^{(0)} + H_{\Sigma}^{(1)} + H_{\Sigma}^{(2)} + \ldots\right|\Psi\right\rangle}{\langle\Psi|\Psi\rangle}, \tag{6.20}$$

and retaining only quantum fluctuations contributing to the effective stress energy tensor. $H_{\Sigma}^{(i)}$ represents the hamiltonian approximated to the i^{th} order in h_{ij} and Ψ is a *trial wave functional* of the gaussian form. Then Eq. (6.17) becomes

$$H_{\Sigma}^{(0)} = \int_{\Sigma} d^3x\mathscr{H}^{(0)} = -\frac{\left\langle\Psi\left|H_{\Sigma}^{(1)} + H_{\Sigma}^{(2)} + \ldots\right|\Psi\right\rangle}{\langle\Psi|\Psi\rangle}. \tag{6.21}$$

[5]Details on sign conventions and decomposition of the Einstein tensor can be found in Sect. 6.2.1.

6.3 Energy Density Calculation in Schrödinger Representation

In order to compute the quantity

$$-\int_{\Sigma} d^3x\sqrt{g}\left\langle \Delta G_{\mu\nu}\left(\bar{g}_{\alpha\beta}, h_{\alpha\beta}\right) u^{\mu}u^{\nu}\right\rangle^{\text{ren}}, \tag{6.22}$$

we consider the right hand side of Eq. (6.21). Since $H_{\Sigma}^{(1)}$ is linear in h_{ij} and h, the corresponding gaussian integral disappears and since

$$\frac{\sqrt{g}}{\kappa}G_{\mu\nu}\left(g_{\alpha\beta}\right)u^{\mu}u^{\nu} = -\mathscr{H}, \tag{6.23}$$

it is clear that the hamiltonian expansion in Eq. (6.21) does not coincide with the averaged expanded Einstein tensor of Eq. (6.22) because Eq. (6.23) involves a tensor density. Therefore, the correct setting is

$$\int_{\Sigma} d^3x\sqrt{g}\left\langle \Delta G_{\mu\nu}\left(\bar{g}_{\alpha\beta}, h_{\alpha\beta}\right) u^{\mu}u^{\nu}\right\rangle^{\text{ren}} = \int_{\Sigma} d^3x\sqrt{g}\frac{\left\langle \Psi\left|\mathscr{H}^{(2)} - \sqrt{g^{(2)}}\mathscr{H}^{(0)}\right|\Psi\right\rangle}{\langle\Psi|\Psi\rangle}, \tag{6.24}$$

where $\sqrt{g^{(2)}}$ is the second-order expanded tensor density weight. Following the same procedure of Refs. [4, 5], the potential part of the right-hand side of Eq. (6.24) becomes

$$\int_{\Sigma} d^3x\sqrt{\bar{g}}\left[-\frac{1}{4}h\triangle h + \frac{1}{4}h^{li}\triangle h_{li} - \frac{1}{2}h^{ij}\nabla_l\nabla_i h^l_j + \frac{1}{2}h\nabla_l\nabla_i h^{li}\right.$$
$$\left. + \frac{1}{2}hR_{ij}h^{ij} + \frac{1}{4}Rh^{ij}h_{ij} - \frac{1}{4}hRh - \frac{1}{2}h^{ij}R_{ia}h^a_j\right]. \tag{6.25}$$

The term

$$\int_{\Sigma} d^3x\sqrt{\bar{g}}\left[\frac{1}{4}Rh^{ij}h_{ij} - \frac{1}{4}hRh\right], \tag{6.26}$$

makes the difference between the hamiltonian expansion and the Einstein tensor expansion. To explicitly make calculations, we need an orthogonal decomposition for both π_{ij} and h_{ij} to disentangle gauge modes from physical deformations. We define the inner product

$$\langle h, k\rangle := \int_{\Sigma}\sqrt{g}G^{ijkl}h_{ij}(x)\,k_{kl}(x)\,d^3x, \tag{6.27}$$

by means of the inverse WDW metric G_{ijkl}, to have a metric on the space of deformations, i.e., a quadratic form on the tangent space at h, with

$$G^{ijkl} = g^{ik}g^{jl} + g^{il}g^{jk} - 2g^{ij}g^{kl}. \tag{6.28}$$

The inverse metric is defined on co-tangent space and it assumes the form

$$\langle p, q\rangle := \int_{\Sigma} \sqrt{g} G_{ijkl}\, p^{ij}(x)\, q^{kl}(x)\, d^3x, \tag{6.29}$$

so that

$$G^{ijnm} G_{nmkl} = \frac{1}{2}\left(\delta^i_k \delta^j_l + \delta^i_l \delta^j_k\right). \tag{6.30}$$

Note that in this scheme the "inverse metric" is actually the WDW metric defined on phase space. The desired decomposition on the tangent space of 3-metric deformations [19–21] is:

$$h_{ij} = \frac{1}{3}(\sigma + 2\nabla\cdot\xi)\, g_{ij} + (L\xi)_{ij} + h^{\perp}_{ij}, \tag{6.31}$$

where the operator L maps ξ_i into symmetric tracefree tensors

$$(L\xi)_{ij} = \nabla_i\xi_j + \nabla_j\xi_i - \frac{2}{3} g_{ij}(\nabla\cdot\xi), \tag{6.32}$$

$h^{\perp}_{ij}$ is the traceless-transverse component of the perturbation (TT), namely

$$g^{ij}h^{\perp}_{ij} = 0, \qquad \nabla^i h^{\perp}_{ij} = 0, \tag{6.33}$$

and h is the trace of h_{ij}.

It is immediate to recognize that the trace element $\sigma = h - 2(\nabla\cdot\xi)$ is gauge invariant. Thus the inner product between three-geometries becomes

$$\begin{aligned}\langle h, h\rangle :&= \int_{\Sigma} \sqrt{g} G^{ijkl} h_{ij}(x)\, h_{kl}(x)\, d^3x \\ &= \int_{\Sigma} \sqrt{g}\left[-\frac{2}{3}h^2 + (L\xi)^{ij}(L\xi)_{ij} + h^{ij\perp}h^{\perp}_{ij}\right].\end{aligned} \tag{6.34}$$

With the orthogonal decomposition in hand we can define the trial wave functional[6]

[6] See also Refs. [22, 23] for further details on the decomposition of the perturbation at the quantum level.

$$\Psi\left\{h_{ij}\left(\overrightarrow{x}\right)\right\}=\mathscr{N}\exp\left\{-\frac{1}{4}\left[\left\langle hK^{-1}h\right\rangle_{x,y}^{\perp}+\left\langle (L\xi)\,K^{-1}\,(L\xi)\right\rangle_{x,y}^{\parallel}+\left\langle hK^{-1}h\right\rangle_{x,y}^{Trace}\right]\right\}, \tag{6.35}$$

where $\mathscr{N}$ is a normalization factor. We are interested in perturbations of the physical degrees of freedom. Thus we fix our attention only to the TT tensor sector reducing therefore the previous form into

$$\Psi\left\{h_{ij}\left(\overrightarrow{x}\right)\right\}=\mathscr{N}\exp\left\{-\frac{1}{4}\left\langle hK^{-1}h\right\rangle_{x,y}^{\perp}\right\}. \tag{6.36}$$

Therefore to calculate the energy density, we need to know the action of some basic operators on $\Psi\left[h_{ij}\right]$. The action of the operator h_{ij} on $|\Psi\rangle=\Psi\left[h_{ij}\right]$ is realized by

$$h_{ij}\left(x\right)|\Psi\rangle=h_{ij}\left(\overrightarrow{x}\right)\Psi\left\{h_{ij}\right\}, \tag{6.37}$$

and the action of the operator π_{ij} on $|\Psi\rangle$, in general, is

$$\pi_{ij}\left(x\right)|\Psi\rangle=-i\frac{\delta}{\delta h_{ij}\left(\overrightarrow{x}\right)}\Psi\left\{h_{ij}\right\}. \tag{6.38}$$

The inner product is defined by the functional integration:

$$\langle\Psi_1\mid\Psi_2\rangle=\int\left[\mathscr{D}h_{ij}\right]\Psi_1^{*}\left\{h_{ij}\right\}\Psi_2\left\{h_{kl}\right\}, \tag{6.39}$$

and by applying previous functional integration rules, we obtain the expression of the one loop-like Hamiltonian form for TT (traceless and transverse) deformations

$$H_{\Sigma}^{\perp}=\frac{1}{4}\int_{\Sigma}d^{3}x\sqrt{g}G^{ijkl}\left[(16\pi G)\,K^{-1\perp}\left(x,x\right)_{ijkl}+\frac{1}{(16\pi G)}\left(\hat{\triangle}_{L}\right)_{j}^{a}K^{\perp}\left(x,x\right)_{iakl}\right]. \tag{6.40}$$

The propagator $K^{\perp}\left(x,x\right)_{iakl}$ comes from a functional integration and it can be represented as

$$K^{\perp}\left(\overrightarrow{x},\overrightarrow{y}\right)_{iakl}:=\sum_{\tau}\frac{h_{ia}^{(\tau)\perp}\left(\overrightarrow{x}\right)h_{kl}^{(\tau)\perp}\left(\overrightarrow{y}\right)}{2\lambda\left(\tau\right)}, \tag{6.41}$$

where $h_{ia}^{(\tau)\perp}\left(\overrightarrow{x}\right)$ are the eigenfunctions of $\hat{\triangle}_{L}$, whose eigenvalues will be denoted with $\omega^{2}\left(\tau\right)$. τ denotes a complete set of indices and $\lambda\left(\tau\right)$ are a set of variational parameters to be determined by the minimization of Eq. (6.40). The expectation value of $H^{\perp}$ is easily obtained by inserting the form of the propagator into Eq. (6.40)

$$E\left(\lambda_i\right)=\frac{1}{4}\sum_{\tau}\sum_{i=1}^{2}\left[\left(16\pi G\right)\lambda_i\left(\tau\right)+\frac{\omega_i^2\left(\tau\right)}{\left(16\pi G\right)\lambda_i\left(\tau\right)}\right]. \tag{6.42}$$

By minimizing with respect to the variational function $\lambda_i\left(\tau\right)$, we obtain the total one loop energy for TT tensors

$$E^{TT}=\frac{1}{4}\sum_{\tau}\left[\sqrt{\omega_1^2\left(\tau\right)}+\sqrt{\omega_2^2\left(\tau\right)}\right]. \tag{6.43}$$

The above expression makes sense only for $\omega_i^2\left(\tau\right)>0$, $i=1,2$ (The meaning of ω_i^2 will be clarified in the next section) and

$$E^{(0)}=-E^{TT}, \tag{6.44}$$

where $E^{(0)}$ is the classical energy and E^{TT} is the total regularized graviton one loop energy.

6.4 The Transverse Traceless (TT) Spin 2 Operator for the Traversable Wormhole and the W.K.B. Approximation

In this section, we evaluate the one loop energy expressed by Eq. (6.43). To this purpose, we begin with the operator describing gravitons propagating on the background (6.1). The Lichnerowicz operator in this particular metric is defined by

$$\left(\hat{\triangle}_L h^{\perp}\right)_{ij}=\left(\triangle_L h^{\perp}\right)_{ij}-4R_i^k h_{kj}^{\perp}, \tag{6.45}$$

acting on traceless-transverse tensors of the perturbation and where $\triangle_L$ is the standard Lichnerowicz operator defined by

$$\left(\triangle_L h\right)_{ij}=\triangle h_{ij}-2R_{ikjl}\,h^{kl}+R_{ik}\,h_j^k+R_{jk}\,h_i^k, \tag{6.46}$$

where $\triangle=-\nabla^a\nabla_a$ is the scalar curved Laplacian, whose form is

$$\triangle_S=\left(1-\frac{b\left(r\right)}{r}\right)\frac{d^2}{dr^2}+\left(\frac{4r-b'\left(r\right)r-3b\left(r\right)}{2r^2}\right)\frac{d}{dr}-\frac{L^2}{r^2}, \tag{6.47}$$

and R_j^a is the mixed Ricci tensor whose components are (we have considered that the redshift function is zero, $\Phi(r)=0$, for simplicity):

$$R_i^a = \left\{ \frac{b'(r)}{r^2} - \frac{b(r)}{r^3}, \frac{b'(r)}{2r^2} + \frac{b(r)}{2r^3}, \frac{b'(r)}{2r^2} + \frac{b(r)}{2r^3} \right\}. \tag{6.48}$$

The scalar curvature is

$$R = R_i^j \delta_j^i = 2\frac{b'(r)}{r^2}. \tag{6.49}$$

We are therefore led to study the following eigenvalue equation

$$\left(\triangle_2 h^{TT}\right)_i^j = E^2 h_i^j, \tag{6.50}$$

where E is the eigenvalue of the corresponding equation. In order to use the WKB approximation, one can define two r-dependent radial wave numbers

$$k_i^2(r, l, E_{nl}) = E_{nl}^2 - \frac{l(l+1)}{r^2} - m_i^2(r), \qquad (i = 1, 2), \tag{6.51}$$

where[7]

$$\begin{cases} m_1^2(r) = \frac{6}{r^2}\left(1 - \frac{b(r)}{r}\right) - \frac{1}{2r^2}b'(r) - \frac{3}{2r^3}b(r) \\ \\ m_2^2(r) = \frac{6}{r^2}\left(1 - \frac{b(r)}{r}\right) - \frac{3}{2r^2}b'(r) + \frac{3}{2r^3}b(r) \end{cases} \tag{6.53}$$

are two r-dependent effective masses $m_1^2(r)$ and $m_2^2(r)$. The number of modes with frequency less than E, is given approximately by

$$g_i(E) = \int \nu_i(l, E)(2l+1)\, dl, \qquad i = 1, 2 \tag{6.54}$$

where $\nu_i(l, E)$ $(i = 1, 2)$ is the number of nodes in the mode with (l, E_i), such that

$$\nu_i(l, E) = \frac{1}{\pi}\int_{-\infty}^{+\infty} dx \sqrt{k_i^2(x, l, E)}. \tag{6.55}$$

Here, it is understood that the integration with respect to x and l is taken over those values which satisfy $k_i^2(x, l, E_i) \geq 0$, $i = 1, 2$. Thus, the total one loop energy for TT tensors is given by

[7]Note that sometimes the effective masses are related to the three-dimensional Lichnerowicz operator defined in [24], whose form is

$$\begin{cases} m_1^2(r) = \frac{6}{r^2}\left(1 - \frac{b(r)}{r}\right) + \frac{3}{2r^2}b'(r) - \frac{3}{2r^3}b(r) \\ \\ m_2^2(r) = \frac{6}{r^2}\left(1 - \frac{b(r)}{r}\right) + \frac{1}{2r^2}b'(r) + \frac{3}{2r^3}b(r). \end{cases} \tag{6.52}$$

$$E^{TT} = \frac{1}{4}\sum_{i=1}^{2}\int_0^{+\infty} E dg_i(E)\,. \tag{6.56}$$

The related energy density is composed by the following integrals

$$\begin{cases} \rho_1 = \frac{1}{4\pi^2}\int_{\sqrt{U_1(x)}}^{+\infty} E^2\sqrt{E^2 - U_1(x)}dE \\ \rho_2 = \frac{1}{4\pi^2}\int_{\sqrt{U_2(x)}}^{+\infty} E^2\sqrt{E^2 - U_2(x)}dE \end{cases}. \tag{6.57}$$

Usually ρ_1 and ρ_2 are ultraviolet divergent, so that it is therefore necessary to introduce some regularization procedure.

In this contribution, as mentioned in the Introduction, we will discuss two different methods to keep under control the UV divergence: (i) a standard regularization and renormalization procedure; (ii) the distortion of the gravitational field at Planckian scale. We begin to consider a standard regularization and renormalization procedure to evaluate Eq. (6.56).

6.5 One Loop Energy Regularization and Renormalization

In this section, we proceed to evaluate the one loop energy described by (6.56). The method is equivalent to the scattering phase shift method and to the same method used to compute the entropy in the brick wall model. We use the zeta function regularization method to compute the energy densities ρ_1 and ρ_2. Note that this procedure is also equivalent to the subtraction procedure of the Casimir energy computation, where ZPE in different backgrounds with the same asymptotic properties is involved. To this purpose, we introduce the additional mass parameter μ in order to restore the correct dimension for the regularized quantities. Such an arbitrary mass scale emerges unavoidably in any regularization scheme. Then, we have

$$\rho_i(\varepsilon) = \frac{1}{4\pi^2}\mu^{2\varepsilon}\int_{\sqrt{U_i(x)}}^{+\infty}\frac{E^2 dE}{\left(E^2 - U_i(x)\right)^{\varepsilon-\frac{1}{2}}}\,. \tag{6.58}$$

If one of the functions $U_i(x)$ is negative, then the integration has to be meant in the range where $E^2 + U_i(x) \geq 0$. In both cases the result of the integration is

$$\rho_i(\varepsilon) = -\frac{U_i^2(x)}{64\pi^2}\left[\frac{1}{\varepsilon} + \ln\left(\frac{4\mu^2}{\sqrt{e}U_i(x)}\right)\right]. \tag{6.59}$$

Therefore the self-sustained Eq. (6.44) becomes

$$\frac{b'(r)}{2Gr^2} = -2\left[\rho_1(\varepsilon,\mu) + \rho_2(\varepsilon,\mu)\right], \tag{6.60}$$

where we have considered the energy density instead of the energy. Separating the divergent contribution from the finite one, we can write

$$\frac{b'(r)}{2Gr^2} = \frac{1}{32\pi^2\varepsilon}\left[U_1^2(r)+U_2^2(r)\right] + \frac{1}{32\pi^2}\left[U_1^2(r)\ln\left(\left|\frac{4\mu^2}{U_1(r)\sqrt{e}}\right|\right)+U_2^2(r)\ln\left(\left|\frac{4\mu^2}{U_2(r)\sqrt{e}}\right|\right)\right]. \quad (6.61)$$

It is essential to renormalize the divergent energy by absorbing the singularity in the classical quantity. For example, by redefining the bare classical constant G as

$$\frac{1}{G} \to \frac{1}{G_0} + \frac{\left[U_1^2(r)+U_2^2(r)\right]}{16\pi^2 b'(r)\varepsilon} r^2 , \quad (6.62)$$

the UV divergence is removed. Using this, Eq. (6.61) takes the form

$$\frac{b'(r)}{2G_0 r^2} = \frac{1}{32\pi^2}\left[U_1^2(r)\ln\left(\left|\frac{4\mu^2}{U_1(r)\sqrt{e}}\right|\right)+U_2^2\ln\left(\left|\frac{4\mu^2}{U_2(r)\sqrt{e}}\right|\right)\right]. \quad (6.63)$$

Note that this quantity depends on an arbitrary mass scale. Thus, using the renormalization group equation to eliminate this dependence, we impose that

$$\mu\frac{d}{d\mu}\left[\frac{b'(r)}{G_0 r^2}\right] = \frac{\mu}{16\pi^2}\frac{d}{d\mu}\left[U_1^2(r)\ln\left(\left|\frac{4\mu^2}{U_1(r)\sqrt{e}}\right|\right)+U_2^2\ln\left(\left|\frac{4\mu^2}{U_2(r)\sqrt{e}}\right|\right)\right], \quad (6.64)$$

which reduces to

$$\frac{b'(r)}{r^2}\mu\frac{\partial G_0^{-1}(\mu)}{\partial\mu} = \frac{1}{8\pi^2}\left[U_1^2(r)+U_2^2(r)\right]. \quad (6.65)$$

The renormalized constant G_0 is treated as a running constant, in the sense that it varies provided that the scale μ is varying, so that one may consider the following definition

$$\frac{1}{G_0(\mu)} = \frac{1}{G_0(\mu_0)} + \frac{r^2}{8\pi^2 b'(r)}\left[U_1^2(r)+U_2^2(r)\right]\ln\left(\frac{\mu}{\mu_0}\right). \quad (6.66)$$

Thus, Eq. (6.61) finally provides us with

$$\frac{b'(r)}{G_0(\mu_0)r^2} = \frac{1}{16\pi^2}\left[U_1^2(r)\ln\left(\left|\frac{4\mu_0^2}{U_1(r)\sqrt{e}}\right|\right)+U_2^2(r)\ln\left(\left|\frac{4\mu_0^2}{U_2(r)\sqrt{e}}\right|\right)\right]. \quad (6.67)$$

Note that this result is independent on the choice of the shape function $b(r)$. One possibility is to integrate over the whole space, namely in the range $[r_0, +\infty)$.

6.5.1 Specific Case: Ellis Wormhole

The final result has been shown in Ref. [5], for the special case in which

$$b(r) = \frac{r_0^2}{r}, \tag{6.68}$$

representing the Ellis wormhole. For this special case, the line element (6.1) simply becomes

$$ds^2 = -dt^2 + \frac{dr^2}{1 - r_0^2/r^2} + r^2\left(d\theta^2 + \sin^2\theta d\varphi^2\right), \tag{6.69}$$

while the proper radial distance simplifies into

$$l(r) = \pm\int_{r_0}^{r} \frac{d\bar{r}}{\sqrt{1 - r_0^2/\bar{r}^2}} = \pm\sqrt{r^2 - r_0^2} \quad \Longrightarrow \quad r^2 = l^2 + r_0^2. \tag{6.70}$$

To obtain a wormhole radius, a further minimization procedure has been used. One obtains:

(a) $\bar{r}_0 = 1.16 l_p \quad \Longrightarrow \quad \mu_0 = 0.39 m_p$, where we have identified $G_0(\mu_0)$ with the squared Planck length;
(b) $\bar{r}_0 = .45 l_p \quad \Longrightarrow \quad \sqrt{G_0(\mu_0)} = 0.39 l_p$, where we have identified μ_0 with the Planck scale.

6.5.2 Specific Case: $p_r = \omega\rho$

On this ground one can also impose an equation of state (EoS) of the form $p_r = \omega\rho$, and with the help of Eqs. (6.3) and (6.4), we obtain

$$b(r) = r_0\left(\frac{r_0}{r}\right)^{\frac{1}{\omega}}. \tag{6.71}$$

In this case, the line element (6.1) becomes

$$ds^2 = -Adt^2 + \frac{dr^2}{1 - (r_0/r)^{1+\frac{1}{\omega}}} + r^2\left(d\theta^2 + \sin^2\theta d\varphi^2\right), \tag{6.72}$$

where A is a constant which can be absorbed in a redefinition of the time coordinate. The constant result is obtained by imposing $\Phi' = 0$, so that Eq. (6.4) implies

$$b(r) + \omega b'(r) r = 0. \tag{6.73}$$

The parameter ω is restricted by the following conditions $b'(r_0) < 1$, which follows from the flaring-out condition at the throat; $b(r)/r \to 0$ as $r \to +\infty$, which is necessary to have asymptotic flatness, and $\omega > 0$ or $\omega < -1$.

The proper radial distance is related to the shape function by

$$l(r) = \pm \frac{r_0 2\omega}{\omega+1} \sqrt{\rho^{\left(1+\frac{1}{\omega}\right)} - 1}\ {}_2F_1\left(\frac{1}{2}, \frac{1-\omega}{2\omega+2}; \frac{3}{2}; 1-\rho^{\left(1+\frac{1}{\omega}\right)}\right), \tag{6.74}$$

where the plus (minus) sign is related to the upper (lower) part of the wormhole or universe and where ${}_2F_1\ (a, b; c; x)$ is a hypergeometric function. When $\omega = 1$, we recover the shape function (6.68). We refer to Ref. [4] for the details.

Here, we report only the case in which $G_0(\mu_0)$ is identified with the squared Planck length. Then, the wormhole radius can be approximated by

$$\bar{r}_0 \simeq \begin{cases} \left[\frac{\sqrt{105}}{5\sqrt{\pi}}\left(1+\frac{1}{\omega}\left(\frac{449}{420}-2\ln(2)\right)+O\left(\omega^{-2}\right)\right)\right] l_p & \omega \to +\infty \\ \left[\frac{\sqrt{30}}{12\sqrt{\pi}\sqrt{\omega}}+O\left(\omega^{1/2}\right)\right] l_p & \omega \to 0 \end{cases}. \tag{6.75}$$

As we can see, from the expression (6.75), the radius is divergent when $\omega \to 0$. At this stage, we cannot establish if this is a physical result or a failure of the scheme. When $\omega \to \pm\infty$, $\bar{r}_t$ approaches the value $1.16 l_p$, while for $\omega = 1$, we obtained $\bar{r}_t = 1.16 l_p$. It is interesting to note that when $\omega \to +\infty$, the shape function $b(r)$ in Eq. (6.71) approaches the Schwarzschild value, when we identify $\bar{r}_0$ with $2MG$. It is interesting to note that outside the phantom range we have wormhole solutions. This is not unexpected since the graviton quantum fluctuations play the role of the exotic matter. The positive ω sector seems to corroborate the Casimir process of the quantum fluctuations supporting the opening of the wormhole. Even in this region, we do not know what happens approaching directly the point $\omega = 0$, because it seems that this approach is ill defined.

6.5.3 Specific Case: $p_r = \omega(r)\rho$

If we generalize the EoS $p_r = \omega\rho$ to include a dependence on the radius r, namely $p_r = \omega(r)\rho$, the shape function becomes

$$b(r) = r_0 \exp\left[-\int_{r_0}^{r} \frac{d\bar{r}}{\omega(\bar{r})\bar{r}}\right], \tag{6.76}$$

and solutions for the self-sustained wormhole can be found as shown in Ref. [25], without fixing a specific form for $\omega(r)$. The analysis around the wormhole throat shows in a rather speculative scenario, that the accretion of phantom energy by the wormhole gradually increases the wormhole throat to macroscopic size, much in the

spirit of Refs. [26–30]. It is of course immediate to generalize the inhomogeneous EoS to a polytropic EoS of the form $p_r = \omega\rho^{\gamma}$.

One gets from Eq. (6.4) that it is always possible to impose that $\Phi(r) = C$. This means that

$$b(r) = \left[r_0^{\frac{\gamma-1}{\gamma}} + \gamma \frac{(8\pi G)^{\frac{\gamma-1}{\gamma}}}{\omega^{\frac{1}{\gamma}}} \left(r^3 - r_0^3\right) \right]^{\frac{\gamma}{\gamma-1}}, \tag{6.77}$$

where the throat condition $b(r_0) = r_0$ has been imposed. However, it is straightforward to see that the solution is not asymptotically flat. Indeed $b(r) \simeq r^3$, for $r \to \infty$, $\forall\gamma$, and therefore this case will be discarded.[8]

6.5.4 *Specific Case: Wormhole Geometry Induced by Noncommutative Geometry*

Finally, to conclude the application of the regularization/renormalization procedure to determine the existence of self-sustained traversable wormholes, one can note that this method has been applied also to wormhole geometries induced by noncommutative geometry. With noncommutative wormholes we mean that the energy density is represented by a Gaussian distribution of minimal length $\sqrt{\alpha}$. In particular, in Ref. [32], the energy density of a static and spherically symmetric, smeared, and particle-like gravitational source has been considered in the following form

$$\rho_{\alpha}(r) = \frac{M}{(4\pi\alpha)^{3/2}} \exp\left(-\frac{r^2}{4\alpha}\right), \tag{6.78}$$

where the mass M is diffused throughout a region of linear dimension $\sqrt{\alpha}$. Thus, Eq. (6.3) can be immediately integrated, and provides the following solution

$$b(r) = C + \frac{8\pi G M}{(4\pi\alpha)^{3/2}} \int_{r_0}^{r} \bar{r}^2 \exp\left(-\frac{\bar{r}^2}{4\alpha}\right) d\bar{r}, \tag{6.79}$$

where C is a constant of integration. To be a wormhole solution we need $b(r_0) = r_0$ at the throat which imposes the condition $C = r_0$.

However, in the context of noncommutative geometry, without a significant loss of generality, the above solution may be expressed mathematically in terms of the incomplete lower gamma functions in the following form

$$b(r) = C - \frac{2r_S}{\sqrt{\pi}}\gamma\left(\frac{3}{2}, \frac{r_0^2}{4\alpha}\right) + \frac{2r_S}{\sqrt{\pi}}\gamma\left(\frac{3}{2}, \frac{r^2}{4\alpha}\right). \tag{6.80}$$

[8] It is interesting to note that the inhomogeneous case, namely $p_r = \omega(r)\rho^{\gamma}$ potentially can produce results [31].

In order to create a correspondence between the spacetime metric (6.1) and the spacetime metric of Ref. [32], we impose that

$$b(r) = \frac{2r_S}{\sqrt{\pi}}\gamma\left(\frac{3}{2}, \frac{r^2}{4\alpha}\right), \tag{6.81}$$

where

$$C = \frac{2r_S}{\sqrt{\pi}}\gamma\left(\frac{3}{2}, \frac{r_0^2}{4\alpha}\right). \tag{6.82}$$

The shape function expressed in this form is particularly simplified, as one may now use the properties of the lower incomplete gamma function, and compare the results directly with the solution in Ref. [32]. However, in this form we have to see if a solution of the condition $b(r_0) = r_0$ exists. If we define

$$x_0 = \frac{r_0}{2\sqrt{\alpha}} \qquad \text{and} \qquad a = \frac{\sqrt{\alpha\pi}}{r_S}, \tag{6.83}$$

then the throat condition becomes

$$\frac{1}{a}\gamma\left(\frac{3}{2}, x_0^2\right) = x_0. \tag{6.84}$$

In order to have one and only one solution we search for extrema of

$$\frac{1}{x_0}\gamma\left(\frac{3}{2}, x_0^2\right) = a, \tag{6.85}$$

which provides

$$\bar{x}_0 = 1.5112 = \frac{\bar{r}_0}{2\sqrt{\alpha}}, \quad \text{and} \quad \frac{1}{\bar{x}_0}\gamma\left(\frac{3}{2}, \bar{x}_0^2\right) = 0.4654. \tag{6.86}$$

From these relationships we deduce that

$$\frac{\sqrt{\alpha\pi}}{r_S} = 0.4654 = a, \tag{6.87}$$

or

$$3.81\sqrt{\alpha} = r_\alpha = r_S, \tag{6.88}$$

which finally provides a relationship between r_0 and r_S given by

$$r_S = \bar{r}_0\frac{\sqrt{\pi}}{2\bar{x}_0 a} = 1.2599\bar{r}_0. \tag{6.89}$$

Only the case in which $r_\alpha < r_S$ produces solutions: we have two roots denoting an inner throat r_- and an outer throat r_+ with $r_+ > r_-$. Note that we necessarily have $r_+ > \bar{r}_0 \simeq 3\sqrt{\alpha}$. Since the throat location depends on the value of a, we can set without a loss of generality $r_+ = k\sqrt{\alpha}$ with $k > 3$. Therefore

$$b\left(r_+\right) = r_+ = k\sqrt{\alpha} = \frac{2r_S}{\sqrt{\pi}}\gamma\left(\frac{3}{2}, \frac{k^2}{4}\right). \tag{6.90}$$

To avoid the region $r_- \leq r \leq r_+$ in which $(1 - b(r)/r) < 0$, we define the range of r to be $r_+ \leq r < \infty$.

In the analysis below, we require the form of $b'(r_+)$ and $b''(r_+)$. Thus, we define

$$x = \frac{r_+}{2\sqrt{\alpha}}. \tag{6.91}$$

The application of the regularization/renormalization procedure, reduces Eq. (6.67) to

$$\ln\left(\frac{3\sqrt{e}}{8\mu_0^2 r_+^2}\right) = \frac{8\alpha}{r_+^2}\ln\left(\frac{3e}{8\mu_0^2 r_+^2}\right), \tag{6.92}$$

which in turn may be reorganized to yield the following useful relationship

$$\left(1 - \frac{8}{k^2}\right)\ln\left(\frac{3e}{8\mu_0^2\alpha k^2}\right) = \frac{1}{2}, \tag{6.93}$$

where we have set, as defined in Eq. (6.90), $r_+ = k\sqrt{\alpha}$, with $k > 4$. Isolating the k-dependent term provides the expression

$$\frac{8\mu_0^2\alpha}{3\sqrt{e}} = k^{-2}\exp\left(-\frac{4}{k^2 - 8}\right). \tag{6.94}$$

It is interesting to note that the right-hand side has two extrema for positive k: $k_1 = 2$ and $k_2 = 4$. In terms of the wormhole throat the first value becomes $r_1 = 2\sqrt{\alpha}$, which will be discarded because its location is below the extreme radius, as emphasized in Sect. 3 of Ref. [33]. Relative to the second extrema k_2, i.e., $r_2 = 4\sqrt{\alpha}$, despite the fact that k_2 is larger than the extreme value ($k = 3$), it does not fall into the range of the approximation of $b'\left(r_+\right) \ll 1$. Thus, it may also be discarded.

Following Ref. [33], we fix $k \geq 6$. To this purpose, we build the following table

Values of k	$\mu_0\sqrt{\alpha}$
6	0.12202
7	0.10698
8	0.09484

. (6.95)

Plugging the expression of $\mu_0\sqrt{\alpha}$, i.e., Eq. (6.94), into Eq. (6.67), we get

$$\frac{9}{2\pi^2 k^5\left(k^2-8\right)}\gamma\left(\frac{3}{2},\frac{k^2}{4}\right)\exp\left(\frac{k^2}{4}\right)=\frac{\alpha}{G_0(\mu_0)}. \tag{6.96}$$

The following table illustrates the behavior of $\sqrt{G_0(\mu_0)/\alpha}$, and therefore of $r_+/\sqrt{G_0(\mu_0)}$

Values of k	$\sqrt{\alpha/G_0\,(\mu_0)}$	$r_+/\sqrt{G_0\,(\mu_0)}$
6	0.12260	0.74
7	0.35006	2. 5
$\bar{k}=7.77770$	1	7.77770
8	1.39883	11
9	7.64175	69.
10	56.23620	5.6×10^2

. (6.97)

Note that in table (6.95), as k increases then $\mu_0\sqrt{\alpha}$ decreases. This means that we are approaching the classical value where the noncommutative parameter $\alpha\to 0$. It appears also that there exists a critical value of k where $\alpha=G_0\,(\mu_0)$. To fix ideas, suppose we fix $G_0\,(\mu_0)$ at the Planck scale, then below $\bar{k}$, the noncommutative parameter becomes more fundamental than $G_0\,(\mu_0)$. This could be a signal of another scale appearing, maybe connected with string theory. On the other hand above $\bar{k}$, we have the reverse. However, the increasing values in the table is far to be encouraging because the non-commutative approach breaks down when k is very large. Nevertheless, note the existence of interesting solutions in the neighborhood of the value $\bar{k}=7.7$. In this section, we have considered a self-sustained wormhole and we have evaluated the one loop contribution with the help of a regularization/renormalization procedure.

In the next section, we will consider the same traversable wormholes solutions, but the UV divergences will be kept under control distorting the gravitational field.

6.6 Distorting Gravity

Distorting gravity means that one adopts a procedure to modify the gravitational field at very high energies, actually at the Planckian scale, in such a way to keep under control the UV divergences. This method is completely different to the one discussed in Sect. 6.5. To this purpose, we have considered two possibilities: (a) Gravity's Rainbow, and (b) Noncommutative geometries.

6.6.1 Gravity's Rainbow

Gravity's Rainbow is a distortion of the spacetime metric at energies comparable to the Planck scale. A general formalism for a curved spacetime was introduced in [34], where two unknown functions $g_1(E/E_P)$ and $g_2(E/E_P)$, denoted as the *Rainbow's functions* modify the basic line element (6.1). They have the following property

$$\lim_{E/E_P\to 0} g_1\left(E/E_P\right) = 1 \qquad \text{and} \qquad \lim_{E/E_P\to 0} g_2\left(E/E_P\right) = 1\,, \tag{6.98}$$

and the line element (6.1) becomes[9]

$$ds^2 = -\frac{N^2\left(r\right)}{g_1^2\left(E/E_P\right)}dt^2 + \frac{dr^2}{\left(1-b\left(r\right)/r\right)g_2^2\left(E/E_P\right)} + \frac{r^2}{g_2^2\left(E/E_P\right)}\left(d\theta^2+\sin^2\theta d\phi^2\right). \tag{6.100}$$

(Note that here $N^2(r) = \exp[2\Phi(r)]$). The distorted wormhole background (6.100) comes into play at the classical level and for the graviton one loop. For the classical energy of the wormhole, one gets [35]

$$\begin{aligned} H_\Sigma^{(0)} = \int_\Sigma d^3x\,\mathscr{H}^{(0)} &= -\frac{1}{16\pi G}\int_\Sigma d^3x\,\sqrt{g}\,R \\ &= -\frac{1}{2G}\int_{r_0}^{\infty}\frac{dr\,r^2}{\sqrt{1-b(r)/r}}\,\frac{b'(r)}{r^2 g_2\left(E/E_P\right)}\,, \end{aligned} \tag{6.101}$$

while the one loop energy is given by

$$E^{TT} = -\frac{1}{\pi}\sum_{i=1}^{2}\int_0^{+\infty} E\,\frac{g_1\left(E/E_P\right)}{g_2^2\left(E/E_P\right)}\,\frac{d\tilde{g}_i\left(E\right)}{dE}dE\,, \tag{6.102}$$

---

[9] Of course, one could also consider a generalized uncertainty principle (GUP) to obtain finite results. However, it is easy to see that if one postulates the validity of Gravity's Rainbow, to obtain modified dispersion relations one necessarily has to impose

$$\begin{aligned} dx^\mu p_\mu &= dx^0 p_0 + dx^i p_i \\ &= g^{00}dx_0 p_0 + g^{ij}dx_i p_j\,, \end{aligned} \tag{6.99}$$

namely plane wave solutions which remain plane, even if the metric is described by Eq. (6.100); only in this way can one argue that the modified dispersion relations are a consequence of gravity's rainbow. However, if we relax the condition of imposing plane wave solutions even at the Planck scale, the distorted metric, Eq. (6.100), leads to a GUP which differs from the Heisenberg uncertainty principle, by terms linear and quadratic in particle momenta. The GUP-induced terms become relevant near the Planck scale and lead to the existence of a minimum measurable length. This could be interpreted as the breakdown of the validity of continuum space–time at very small scales.

where

$$\tilde{g}_i\left(E\right)=\int_0^{l_{\max}}\nu_i\left(l,E\right)\left(2l+1\right)dl\,, \tag{6.103}$$

is the number of modes with frequency less than E and

$$\nu_i\left(l,E\right)=\frac{1}{\pi}\int_{-\infty}^{+\infty}dx\sqrt{k_i^2\left(r,l,E\right)}\,, \tag{6.104}$$

is the number of nodes with (l,E_i), such that $(r\equiv r\left(x\right))\,k_i^2\left(r,l,E\right)\geq 0.\,k_i^2\left(r,l,E\right)$ are the distorted version of the two r-dependent radial wave numbers defined in Eq. (6.51). They are obtained by the distorted Lichnerowicz eigenvalue equation

$$\left(\hat{\triangle}_L^m h^{\perp}\right)_{ij}=\frac{E^2}{g_2^2\left(E/E_P\right)}h_{ij}^{\perp}\,, \tag{6.105}$$

and assume the following expression

$$k_i^2\left(r,l,E_{nl}\right)=\frac{E_{nl}^2}{g_2^2\left(E/E_P\right)}-\frac{l\left(l+1\right)}{r^2}-m_i^2\left(r\right)\,,\qquad\left(i=1,2\right). \tag{6.106}$$

Finally, the self-sustained equation, in terms of energy density becomes

$$\frac{1}{2G}\,\frac{b'(r)}{r^2 g_2\left(E/E_P\right)}=\frac{2}{3\pi^2}\left(I_1+I_2\right)\,. \tag{6.107}$$

The integrals I_1 and I_2 are defined as

$$I_1=\int_{E^*}^{\infty}E\frac{g_1\left(E/E_P\right)}{g_2^2\left(E/E_P\right)}\frac{d}{dE}\left(\frac{E^2}{g_2^2\left(E/E_P\right)}-m_1^2\left(r\right)\right)^{\frac{3}{2}}dE\,, \tag{6.108}$$

and

$$I_2=\int_{E^*}^{\infty}E\frac{g_1\left(E/E_P\right)}{g_2^2\left(E/E_P\right)}\frac{d}{dE}\left(\frac{E^2}{g_2^2\left(E/E_P\right)}-m_2^2\left(r\right)\right)^{\frac{3}{2}}dE\,, \tag{6.109}$$

respectively. E^* is the value which annihilates the argument of the root. In I_1 and I_2 we have included an additional 4π factor coming from the angular integration and we have assumed that the effective mass does not depend on the energy E. It is important to observe that I_1 and I_2 are finite only for some appropriate choices of $g_1\left(E/E_P\right)$ and $g_2\left(E/E_P\right)$. Indeed, a pure polynomial cannot be used without the reintroduction of a regularization and a renormalization process. It is immediate to see that integrals I_1 and I_2 can be easily solved when $g_2(E/E_P)=g_1(E/E_P)$. However, the classical term keeps a dependence on the function $g_2(E/E_P)$ that

cannot be eliminated except for the simple case of $g_2(E/E_P) = 1$. For instance, if we assume that the shape function is represented by Eq. (6.68) and

$$g_1\left(E/E_P\right) = \exp\left(-\alpha E^2/E_P^2\right), \qquad g_2\left(E/E_P\right) = 1, \tag{6.110}$$

with $\alpha \in \mathbb{R}$, the classical term is not distorted. Then Eq. (6.107) has the following solution at

$$r_0 E_P = 2.97\sqrt{\alpha}, \tag{6.111}$$

with $\alpha \simeq 0.242$. This means that $r_0 E_P = 1.46$, to be compared with the roots given in Sect. 6.5.1. One can also adopt a *relaxed* form for the Rainbow's functions described by

$$g_1\left(E/E_P\right) = 1, \qquad g_2\left(E/E_P\right) = \begin{cases} 1 & \text{when} \quad E < E_P \\ \\ E/E_P & \text{when} \quad E > E_P \end{cases}, \tag{6.112}$$

to obtain the following result $r_0 E_P = 4.12$. On the other hand, if we take into account an EoS, the shape function (6.71) can give interesting results only in the range

$$-1 \geq \omega \geq -4.5, \qquad 2.038 \geq r_0 E_P \geq 1.083. \tag{6.113}$$

It is interesting to note that Eq. (6.73) works also for an inhomogeneous EoS. Indeed, the presence of the rainbow's function does not affect the form of (6.73) except for an explicit dependence on r of the ω parameter, so that $b(r) + \omega(r) b'(r) r = 0$ leads to the following general form of the shape function

$$b(r) = r_0 \exp\left[-\int_{r_0}^{r} \frac{d\bar{r}}{\omega(\bar{r})\bar{r}}\right]. \tag{6.114}$$

The situation appears completely different when a polytropic with an inhomogeneous parameter ω is considered. Indeed, when the polytropic EoS, i.e., $p_r = \omega(r)\rho^{\gamma}$, is plugged into Eq. (6.4), one arrives

$$\begin{aligned} \Phi' &= \frac{b + 8\pi G p_r r^3/g_2^2\left(E/E_P\right)}{2r^2\left(1 - b(r)/r\right)} = \frac{b + 8\pi G\left(\omega(r)\rho^{\gamma}\right) r^3/g_2^2\left(E/E_P\right)}{2r^2\left(1 - b(r)/r\right)} \\ &= \frac{b + (8\pi G)^{1-\gamma}\,\omega(r)\left(b(r)'\right)^{\gamma} r^{3-2\gamma} g_2^{2(\gamma-1)}\left(E/E_P\right)}{2r^2\left(1 - b(r)/r\right)}. \end{aligned} \tag{6.115}$$

We can always impose that $\Phi(r) = C$, but this means that

$$b + (8\pi G)^{1-\gamma}\,\omega(r)\left(b(r)'\right)^{\gamma} r^{3-2\gamma} g_2^{2(\gamma-1)}\left(E/E_P\right) = 0 \tag{6.116}$$

and a dependence on $g_2\left(E/E_P\right)$ appears. For this reason this case will be discarded.

6.6.2 Noncommutative Geometries

In Sect. 6.5, we have introduced an example of a noncommutative spacetime. Actually, we have considered a smeared energy density of a static and spherically symmetric particle-like gravitational source described by (6.78) acting on the configuration space. However, if we adopt a noncommutative scheme acting in phase space, the distorted Liouville measure [36]

$$dn_i = \frac{d^3\mathbf{x}d^3\mathbf{k}}{(2\pi)^3}\exp\left[-\frac{\alpha}{4}\left(\omega_{i,nl}^2 - m_i^2(r)\right)\right], \qquad i = 1, 2, \tag{6.117}$$

allows the computation of the graviton to one loop. This is possible because the distortion induced by the noncommutative space–time allows the counting of states to be finite. This deformation corresponds to an effective cutoff on the background geometry (6.1). The UV cutoff is triggered only by higher momenta modes $\gtrsim 1/\sqrt{\theta}$ which propagate over the background geometry. In this framework, the wormhole radius can be found to be

$$r_0 = 0.28 l_P, \tag{6.118}$$

with θ fixed at the value

$$\theta = \frac{2.20 l_P^2}{3\pi^2} = 7.43 \times 10^{-2} l_P^2. \tag{6.119}$$

It is immediate to recognize that this procedure seems to produce results close to the results obtained in Sect. 6.5.

6.7 Summary and Conclusions

In this contribution, we have presented the possible existence of a self-consistent solution of the semiclassical Einstein's equations in a traversable wormhole background. In particular, we have fixed our attention to the graviton quantum fluctuations around such a background. The fluctuations, contained in the perturbed Einstein tensor, play the role of the *exotic matter* considered in Ref. [15]. A variational approach with the help of gaussian trial wave functionals has been used to compute the one loop term. To handle the divergences appearing in such a calculation we have used two different procedures: (a) a standard regularization/renormalization process, and (b) the distortion of gravity at the Planck scale.

For the standard regularization/renormalization process, a zeta function calculation has been used. This procedure is formally equivalent to a Casimir energy subtraction procedure. The renormalization is performed promoting Newton's constant G as a bare coupling constant to absorb the UV divergences. To avoid dependences on the renormalization scale a renormalization group equation has been introduced. While

the renormalization process is not new in the context of the semiclassical Einstein field equations, to our knowledge it is the use of the renormalization group equation that seems to be unknown, especially concerning self-consistent solutions. The procedure has been tested on the prototype of traversable wormholes, namely, the Ellis wormhole with $b(r) = r_0^2/r$. The result shows that the obtained "*traversability*" has to be regarded as in "*principle*" rather than in "*practice*" because the size of the wormhole radius is of the Planckian order.

On the other hand if we adopt to distort gravity, the result is slightly improved. The introduction of an EoS with $\omega \in \mathbb{R}$ shows that the *phantom* energy range is forbidden. Indeed phantom energy works in the range $\omega < -1$. However, the classical term is well defined in the range $-1 < \omega < +\infty$ and the interval $-1 < \omega < 0$ is connected to a "*dark*" energy sector. Nevertheless, the "*dark*" energy domain lies outside the asymptotically flatness property. So, unless one is interested in wormholes that are not asymptotically flat, i.e., asymptotically de Sitter or asymptotically anti-de Sitter, we also have to reject this possibility. Therefore, the final stage of computation has been restricted only to positive values of the parameter ω. On the other hand, the positive ω sector seems to corroborate the Casimir process of the quantum fluctuations supporting the opening of the wormhole. Even in this region, we do not know what happens approaching directly the point $\omega = 0$, because it seems that this approach is ill defined, even if the wormhole radius becomes much larger than the Planckian size. Note that the situation is always slightly better when we use *Distorted Gravity* as a regulator procedure.

Regarding Gravity's Rainbow the good news is that every shape function analyzed is traversable. The bad news is that the traversability is always in *principle* but not in *practice* as the wormhole radius in of the Planckian size, even if the radii are greater that the radius discovered in Ref. [5]. One way to obtain a larger radius is to reinterpret the self-sustained equation as an ignition equation. Indeed, one possibility is to use the self-sustained equation in the following manner

$$\frac{1}{2G}\frac{\left(b'(r)\right)^{(n)}}{r^2} = \frac{2}{3\pi^2}\left[I_1\left(b^{(n-1)}(r)\right) + I_2\left(b^{(n-1)}(r)\right)\right], \tag{6.120}$$

where n is the order of the approximation. In this way, if we discover that fixing the radius to some value of a fixed background of the right-hand side, and we discover on the left-hand side a different radius, we could conclude that if the radius is larger that the original, the wormhole is growing, otherwise it is collapsing. Note that in Ref. [37], Eq. (6.120) has been used to show that a traversable wormhole can be generated with a topology change starting from a Minkowski spacetime. This is because we are probing a region, where the gravitational field develops quantum fluctuations so violent to be able to suggest a topology change [37].

To conclude, in this contribution we have shown that a self-sustained wormhole exists in *principle*. The next step will be about the possibility to have a traversable wormhole also in *practice*. A serious analysis of Eq. (6.120) could be a beginning, but also the addition of rotations could be an interesting improvement.

References

1. Morris MS, Thorne KS. Wormholes in spacetime and their use for interstellar travel: a tool for teaching General Relativity. Am J Phys. 1988;56:395.
2. Morris MS, Thorne KS, Yurtsever U. Wormholes, time machines, and the weak energy condition. Phys Rev Lett. 1988;61:1446.
3. Visser M. Lorentzian wormholes. New York: AIP Press; 1995.
4. Garattini R. Self sustained traversable wormholes and the equation of state. Class Quantum Gravity. 2007;24:1189.
5. Garattini R. Self sustained traversable wormholes? Class Quantum Gravity. 2005;22:1105.
6. Garattini R. Casimir energy and black hole pair creation in Schwarzschild-de Sitter spacetime. Class Quantum Gravity. 2001;18:571.
7. Garattini R. Casimir energy and variational methods in AdS spacetime. Class Quantum Gravity. 2000;17:3335.
8. Ellis H. Ether flow through a drainhole – a particle model in general relativity. J Math Phys. 1973;14:104.
9. Bronnikov KA. Scalar-tensor theory and scalar charge. Acta Phys Pol B. 1973;4:251.
10. Lobo FSN. Phantom energy traversable wormholes. Phys Rev D. 2005;71:084011.
11. Lobo FSN. Stability of phantom wormholes. Phys Rev D. 2005;71:124022.
12. Kuhfittig PKF. Seeking exactly solvable models of traversable wormholes supported by phantom energy. Class Quantum Gravity. 2006;23:5853.
13. Sushkov S. Wormholes supported by a phantom energy. Phys Rev D. 2005;71:043520.
14. Hochberg D, Popov A, Sushkov SV. Self-consistent wormhole solutions of semiclassical gravity. Phys Rev Lett. 1997;78:2050.
15. Khusnutdinov NR, Sushkov SV. Ground state energy in a wormhole space-time. Phys Rev D. 2002;65:084028.
16. Fewster CJ, Olum KD, Pfenning MJ. Averaged null energy condition in spacetimes with boundaries. Phys Rev D. 2007;75:025007.
17. Hawking SW, Ellis GFR. The large scale structure of spacetime. Cambridge: Cambridge University Press; 1973.
18. Anderson PR, Brill DR. Gravitational geons revisited. Phys Rev D. 1997;56:4824.
19. Berger M, Ebin D. Some decompositions of the space of symmetric tensors on a Riemannian manifold. J Differ Geom. 1969;3:379.
20. York JW Jr. Conformally invariant orthogonal decomposition of symmetric tensors on Riemannian manifolds and the initialvalue problem of general relativity. J Math Phys. 1973;14:4.
21. York JW Jr. Covariant decompositions of symmetric tensors in the theory of gravitation. Ann Inst Henri Poincaré A. 1974;21:319.
22. Garattini R. The Cosmological constant and the Wheeler-DeWitt Equation. PoS CLAQG08, vol. 012. 2011.
23. Garattini R. Wormholes or Gravastars? JHEP. 2013;1309:052.
24. Garattini R, Mandanici G. Modified dispersion relations lead to a finite zero point gravitational energy. Phys Rev D. 2011;83:084021.
25. Garattini R, Lobo FSN. Self sustained phantom wormholes in semi-classical gravity. Class Quantum Gravity. 2007;24:2401.
26. González-Díaz PF. Wormholes and ringholes in a dark-energy universe. Phys Rev D. 2003;68:084016.
27. González-Díaz PF. Achronal cosmic future. Phys Rev Lett. 2004;93:071301.
28. González-Díaz PF, Jimenez-Madrid JA. Phantom inflation and the 'Big Trip'. Phys Lett B. 2004;596:16.
29. González-Díaz PF. On the accretion of phantom energy onto wormholes. Phys Lett B. 2006;632:159.
30. González-Díaz PF. Some notes on the Big Trip. Phys Lett B. 2006;635:1.
31. In preparation.

32. Nicolini P, Smailagic A, Spallucci E. Noncommutative geometry inspired Schwarzschild black hole. Phys Lett B. 2006;632:547.
33. Garattini R, Lobo FSN. Self-sustained traversable wormholes in noncommutative geometry. Phys Lett B. 2009;671:146.
34. Magueijo J, Smolin L. Class Quantum Gravity. 2004;21:1725.
35. Garattini R, Lobo FSN. Self-sustained wormholes in modified dispersion relations. Phys Rev D. 2012;85:024043.
36. Garattini R, Nicolini P. A noncommutative approach to the cosmological constant problem. Phys Rev D. 2011;83:064021.
37. Garattini R, Lobo FSN. Gravity's Rainbow induces topology change. Eur Phys J C. 2014;74:2884.

Chapter 7
Trapped Ghosts as Sources for Wormholes and Regular Black Holes. The Stability Problem

Kirill A. Bronnikov

7.1 Introduction

Very soon after Einstein presented his general relativity (GR) theory that identified gravity with spacetime curvature, researchers realized that if spacetime is curved, it can be very strongly curved. The best-known examples of strong distinctions from flat Minkowskian geometry are what we now call black holes and wormholes. However, as early as in 1916, Schwarzschild found his famous solution [1] describing, in modern terms, the simplest black hole. Somewhat less well known is the paper by Ludwig Flamm [2], also dated 1916, where he noticed that the spatial part of the Schwarzschild metric describes something like a bridge or shortcut between two worlds or two parts of the same world, i.e., in modern terminology, a wormhole.

It is now clear that the Schwarzschild spacetime as a whole, though it really has spatial sections with a wormhole geometry, represents a black hole while its wormhole sections are not traversable since their different static regions are connected only by spacelike paths.

The Schwarzschild spacetime is vacuum, whereas it has been shown that the existence of traversable Lorentzian wormholes as solutions to the Einstein equations requires some kind of so-called "exotic matter", i.e., matter that violates the null energy condition (NEC) [3, 4], which is in turn a part of the weak energy condition

K.A. Bronnikov (✉)
Center of Gravitation and Fundamental Metrology, VNIIMS, Ozyornaya St. 46,
Moscow 119361, Russia
e-mail: kb20@yandex.ru

K.A. Bronnikov
Institute of Gravitation and Cosmology, PFUR, Miklukho-Maklaya St. 6,
Moscow 117198, Russia

K.A. Bronnikov
National Research Nuclear University MEPhI (Moscow Engineering Physics Institute),
Kashirskoe Highway 31, Moscow 115409, Russia

F.S.N. Lobo (ed.), *Wormholes, Warp Drives and Energy Conditions*,
Fundamental Theories of Physics 189, DOI 10.1007/978-3-319-55182-1_7

(WEC) whose physical meaning is that the energy density is nonnegative in any reference frame.

In particular, for static, spherically symmetric configurations in which the source of gravity is a minimally coupled scalar field, wormhole solutions are only possible, and are really obtained, if the scalar field is phantom (or ghost), i.e., has a wrong sign of the kinetic energy [5–8]. It is also known that in alternative theories of gravity, such as scalar-tensor, multidimensional and curvature-nonlinear theories, wormhole solutions can also be obtained only if some of the degrees of freedom are of phantom nature [5, 9–11] (see also the reviews [12, 13] and references therein). This concerns both continuous sources of gravity and thin shells [9]. In some cases, it is 4D gravity itself that becomes phantom in a certain region of space [5, 9, 14], in others this role is played by different geometric quantities such as torsion [15, 16] or higher dimensional or higher derivative metric variables [17–19] or unusual matter field couplings [20].

There is nevertheless a good reason to adhere to GR and macroscopic matter and fields if our interest is in obtaining (potentially) realistic and manageable wormholes since it is this theory that is quite well verified by experiment at the macroscopic level and even serves as a tool in a number of engineering applications such as, for instance, GPS navigation.

Meanwhile, macroscopic phantom matter has never been observed, and this casts doubt on whether it can exist in principle and whether it is possible to obtain realistic wormholes, suitable, for example, for interstellar travel, even in a remote future and even by a highly advanced civilization.

An interesting opportunity to circumvent these problems and to obtain wormhole configurations in GR is to find such a kind of matter that possesses phantom properties only in a restricted region of space, somewhere close to the throat, whereas far away from it all standard energy conditions are observed [21]. As an example of such matter, we can consider a minimally coupled scalar field with the Lagrangian

$$L_s = h(\phi) g^{\mu\nu} \partial_\mu \phi \partial_\nu \phi - V(\phi), \tag{7.1}$$

as a source of gravity in static, spherically symmetric configurations, with arbitrary functions $h(\phi)$ and $V(\phi)$. If $h(\phi)$ has a variable sign, it cannot be absorbed by a redefinition of ϕ in its whole range. A case of interest is that $h > 0$ (that is, the scalar field is canonical, with positive kinetic energy) in a weak field region and $h < 0$ (the scalar field is of phantom, or ghost nature) in some restricted region where a wormhole throat can be expected. In this sense it can be said that the ghost is trapped. A possible transition between $h > 0$ and $h < 0$ in cosmology was considered in [22].

Phantom fields are known to produce not only wormhole configurations but also different kinds of regular black holes, see, e.g., [23–25]. Of particular interest among such models are those which combine black hole physics with nonsingular cosmology, they have been termed *black universes* [23, 24]. These objects look like "conventional" black holes (spherically symmetric ones in the known examples) on one side, where they can be asymptotically flat, but a possible explorer, after crossing the event horizon, gets, instead of a singularity, to an expanding universe. Thus, such

hypothetic configurations combine the properties of a wormhole (absence of a center, a regular minimum of the area function $r^2(x)$), a black hole (a Killing horizon separating static (R-) and nonstatic (T-) regions), and a nonsingular cosmological model. Moreover, the Kantowski-Sachs cosmology that emerges in the T-region, is asymptotically isotropic and approaches a de Sitter mode of expansion, which makes such models potentially viable as a description of a pre-inflationary epoch.

The trapped ghost concept can certainly be applied to such models as well [26, 27]: in such cases, as in wormhole models, the scalar field is phantom in a neighborhood of the minimum of $r^2(x)$ (which in general does not coincide with the horizon) and is canonical in the weak field region, both on the static and cosmological sides.

In this paper, we will briefly review both wormhole and black-universe solutions with a trapped-ghost scalar field and discuss the stability problem. The stability properties are of importance for any static model since unstable configurations cannot survive in the real Universe (at least for a long time). It has been shown that many of wormhole and black-universe models are unstable under radial perturbations [28–35]. It will be shown here that the same problem for trapped-ghost configuration has its distinctive features leading to a somewhat unexpected conclusion that transition surfaces between phantom and canonical scalar fields play a stabilizing role.

The paper is organized as follows. Section 7.2 presents the basic equations and shows why the "trapped-ghost" strategy cannot be realized for a massless scalar field ($V(\phi) \equiv 0$). Section 7.3 describes some general properties of the system and presents some explicit examples of "trapped-ghost" wormhole and black-universe solutions obtained using the inverse-problem method. Section 7.4 discusses the stability problem for spherically symmetric scalar field configurations in GR and its particular features which emerge when we consider "trapped-ghost" scalars. Section 7.5 is a conclusion.

7.2 Basic Equations. NEC Violation and the Necessity of a Nonzero Potential

7.2.1 General Relations

Let us begin with the general static, spherically symmetric metric which can be written in the form[1]

$$ds^2 = \mathrm{e}^{2\gamma(u)}dt^2 - \mathrm{e}^{2\alpha(u)}du^2 - \mathrm{e}^{2\beta(u)}d\Omega^2, \tag{7.2}$$

[1] Our conventions are: the metric signature $(+\ -\ -\ -)$, the curvature tensor $R^\sigma{}_{\mu\rho\nu} = \partial_\nu \Gamma^\sigma_{\mu\rho} - \ldots$, $R_{\mu\nu} = R^\sigma{}_{\mu\sigma\nu}$, so that the Ricci scalar $R > 0$ for de Sitter spacetime and the matter-dominated cosmological epoch; the sign of T^ν_μ such that T^0_0 is the energy density, and the system of units $8\pi G = c = 1$.

where u is an arbitrary radial coordinate and $d\Omega^2 = d\theta^2 + \sin^2\theta d\varphi^2$ is the linear element on a unit sphere.[2]

Then the Ricci tensor has the following nonzero components:

$$R^t_t = -\mathrm{e}^{-2\alpha}[\gamma'' + \gamma'(\gamma' - \alpha' + 2\beta')], \tag{7.3}$$

$$R^u_u = -\mathrm{e}^{-2\alpha}[\gamma'' + 2\beta'' + \gamma'^2 + 2\beta'^2 - \alpha'(\gamma' + 2\beta')], \tag{7.4}$$

$$R^\theta_\theta = \mathrm{e}^{-2\beta} - \mathrm{e}^{-2\alpha}[\beta'' + \beta'(\gamma' - \alpha' + 2\beta')] = R^\varphi_\varphi, \tag{7.5}$$

where the prime stands for d/du. The Einstein equations can be written in two equivalent forms

$$G^\nu_\mu \equiv R^\nu_\mu - \tfrac{1}{2}\delta^\nu_\mu R = -T^\nu_\mu, \qquad \text{or} \qquad R^\nu_\mu = -(T^\nu_\mu - \tfrac{1}{2}\delta^\nu_\mu T^\alpha_\alpha), \tag{7.6}$$

where T^ν_μ is the stress-energy tensor (SET) of matter. The most general SET compatible with the geometry (7.2) has the form

$$T^\nu_\mu = \mathrm{diag}(\rho,\ -p_r,\ -p_\perp,\ -p_\perp), \tag{7.7}$$

where ρ is the energy density, p_r is the radial pressure, and $p_\perp$ is the tangential pressure.

Let us illustrate the necessity of exotic matter for wormhole existence using static, spherically symmetric spacetimes as an example [3, 13]. Choosing the so-called quasiglobal coordinate $u = x$ under the condition $\alpha + \gamma = 0$ and denoting $\mathrm{e}^{2\gamma} = \mathrm{e}^{-2\alpha} = A$, $\mathrm{e}^\beta = r$, we rewrite the metric as

$$ds^2 = A(x)dt^2 - \frac{dx^2}{A(x)} - r^2(x)d\Omega^2. \tag{7.8}$$

A (traversable) wormhole geometry implies, by definition, that the function $r(x)$ has a regular minimum (say, at $x = x_0$), called a throat, and reaches values much larger than $r(x_0)$ on both sides of the throat, while $A(x) > 0$ in the whole range of x. The latter requirement excludes horizons, which characterize black holes rather than wormhole geometries.

Then the difference of the $\binom{t}{t}$ and $\binom{x}{x}$ components of the Einstein equations reads

$$2A\,r''/r = -(T^t_t - T^x_x) \equiv -(\rho + p_r). \tag{7.9}$$

---

[2] In what follows we will use different radial coordinates, to be denoted by different letters:
u — a general notation,
x — quasiglobal, such that $\alpha = -\gamma$,
y — harmonic, such that $\alpha = 2\beta + \gamma$,
z — "tortoise," such that $\alpha = \gamma$.

On the other hand, at a throat as a minimum of $r(x)$ one should have

$$r = r_0 > 0, \qquad r' = 0, \qquad r'' > 0. \tag{7.10}$$

(In special cases where $r'' = 0$ at the minimum, it inevitably happens that $r'' > 0$ in its neighborhood.) Then from (7.9) it immediately follows $\rho + p_r < 0$. This inequality really looks exotic, but to see an exact result, let us recall that the NEC requires $T_\mu^\nu k^\mu k_\nu \geq 0$, where k^μ is any null vector, $k^\mu k_\mu = 0$. Choosing $k^\mu = (1/\sqrt{A}, \sqrt{A}, 0, 0)$, we see that $T_\mu^\nu k^\mu k_\nu = \rho + p_r$. Thus the inequality $\rho + p_r < 0$ does indeed violate the NEC.

Considering a black-universe spacetime, this also means that $r(x)$ reaches large values at the ends of the x range, hence it again has a minimum at some $x = x_0$, but now $A(x)$ changes its sign at some (in general) other $x = x_h$ (a horizon), say, $A > 0$ at larger x and $A < 0$ at smaller x. It can happen that the minimum of r occurs in a T-region ($A < 0$), where x is a temporal coordinate, and it is appropriate to rewrite the metric (7.8) as

$$ds^2 = \frac{dx^2}{|A(x)|} - |A(x)|dt^2 - r^2(x)d\Omega^2. \tag{7.11}$$

A minimum of $r(x)$ is then not a throat but a bounce in the time evolution of one of the scale factors in a Kantowski–Sachs homogeneous anisotropic cosmology (the other scale factor is $|A(x)|^{1/2}$, and the proper time element is $d\tau = |A(x)|^{-1/2}dx$). The coordinate t is spatial in (7.11), the quantity $-T_t^t = p_t$ is the pressure along the t direction, while the density is $\rho = T_x^x$; however, the condition $r'' > 0$ in Eq. (7.9) (which is the same for any sign of A) leads to $\rho + p_t < 0$, again violating the NEC. In the intermediate case of $A = 0$ (a horizon) at a minimum of $r(x)$, the condition $r'' > 0$ should hold in its vicinity, with all its consequences. Thus a minimum of r always implies a NEC (and hence WEC) violation.

7.2.2 Solutions with a Massless Scalar

Consider now a scalar field $\phi(u)$ with the Lagrangian (7.1) in a spacetime with the metric (7.2). Its SET has the form

$$T_\mu^\nu = h(\phi)\, \mathrm{e}^{-2\alpha}\phi'(u)^2\, \mathrm{diag}(1,\ -1,\ 1,\ 1) + \delta_\mu^\nu V(u). \tag{7.12}$$

The kinetic energy density is positive if $h(\phi) > 0$ and negative if $h(\phi) < 0$, and we also have $\rho + p_r = 2h(\phi)\, \mathrm{e}^{-2\alpha}\phi'(u)^2$. Thus wormhole or black-universe solutions require $h < 0$ close to the minimum of $r(u) = \mathrm{e}^\beta$, but we can have $h > 0$ at larger values of $r(u)$. One can show, however, that this goal cannot be achieved with a massless field ($V(\phi) \equiv 0$).

Indeed, in the massless case, the SET (7.12) has the same structure as for a usual massless scalar field with $h = \pm 1$. Therefore, the metric has the same form as in this simple case and should reduce to the Fisher metric [36] if $h > 0$ and to the corresponding solution for a phantom scalar, first found by Bergmann and Leipnik [37] (and sometimes called "anti-Fisher") if $h(\phi) < 0$. Let us reproduce this solution for our scalar (7.1) in the simplest joint form, following [5].

Two combinations of the Einstein equations for the metric (7.2) and the SET (7.12) with $V \equiv 0$ read $R^t_t = 0$ and $R^t_t + R^\theta_\theta = 0$. We can easily solve these equations, choosing the harmonic radial coordinate $u = y$, such that $\alpha(y) = 2\beta(y) + \gamma(y)$. Indeed, the first of them reads simply $\gamma'' = 0$, while the second one has the Liouville form $\beta'' + \gamma'' = \mathrm{e}^{2(\beta+\gamma)}$ (the prime here stands for d/dy). Their solution is

$$\begin{aligned} &\gamma = -my, \\ &\mathrm{e}^{-\beta-\gamma} = s(k, y) := \begin{cases} k^{-1} \sinh ky, & k > 0, \\ y, & k = 0, \\ k^{-1} \sin ky, & k < 0, \end{cases} \end{aligned} \tag{7.13}$$

where k and m are integration constants; two more integration constants have been suppressed by choosing the zero point of y and the scale along the t axis. As a result, the metric has the form [5]

$$ds^2 = \mathrm{e}^{-2my} dt^2 - \frac{\mathrm{e}^{2my}}{s^2(k, y)} \left[\frac{dy^2}{s^2(k, y)} + d\Omega^2 \right], \tag{7.14}$$

(note that spatial infinity here corresponds to $y = 0$ and m has the meaning of the Schwarzschild mass). Moreover, with these metric functions, the $\binom{1}{1}$ component of the Einstein equations (7.6) leads to

$$k^2 \operatorname{sign} k = m^2 + h(\phi)\phi'^2. \tag{7.15}$$

It means that $h(\phi)\phi'^2 = \text{const}$, hence $h(\phi)$ cannot change its sign within a particular solution which is characterized by certain fixed values of the constants m and k.[3]

The situation remains the same if, instead of a single scalar field, there is a nonlinear sigma model with multiple scalar fields ϕ^a and the Lagrangian

$$L_\sigma = -h_{ab} g^{\mu\nu} \partial_\mu \phi^a \partial_\nu \phi^b, \tag{7.16}$$

[3] For a detailed description of the properties of Fisher and anti-Fisher solutions see [8, 13, 38, 39] and references therein. Let us here only mention that the metric (7.14) describes wormholes [5, 6] if $k < 0$, which is only possible with negative h; one flat spatial infinity then corresponds to $y = 0$, the other one to $y = \pi/|k|$.

where h_{ab} are functions of ϕ^a: the metric then has the same form (7.14), and a relation similar to (7.15) reads [39]

$$k^2 \operatorname{sign} k = m^2 + h_{ab}(\phi^a)'(\phi^b)'.$$

Therefore, the quantity that determines the canonical or phantom nature of the scalars, $h_{ab}(\phi^a)'(\phi^b)'$, is constant. If the matrix h_{ab} is positive-definite, we are dealing with a set of canonical fields, then $k > 0$, and (7.14) is the Fisher metric with a naked singularity. If h_{ab} is negative-definite, there is a set of phantom fields, hence there is a family of solutions with $k < 0$ describing wormholes, and there is also a subset of $k > 0$ solutions with horizons of infinite area which have received the name of "cold black holes" [38] since they have zero Hawking temperature. If h_{ab} is neither positive- nor negative-definite, then some special solutions can be of wormhole nature while others correspond to a canonical scalar and have a Fisher central singularity [39], but there are no solutions of trapped-ghost character. More complicated examples appear only with nonzero potentials, such as the one with an "invisible ghost" [40]: this expression means that one of the two scalar fields is phantom, and it rapidly decays at large r, while the other is canonical and decays comparatively slowly.

7.2.3 *Equations with an Arbitrary Potential*

Returning to our system with the Lagrangian (7.1), we can assert that trapped-ghost configurations can only exist with a nonzero potential $V(\phi)$. To find such solutions, it is helpful to use again the quasiglobal gauge $\alpha + \gamma = 0$ and the metric (7.8). Then the Einstein-scalar equations can be written as follows:

$$2(Ar^2 h\phi')' - Ar^2 h'\phi' = r^2 dV/d\phi, \tag{7.17}$$

$$(A'r^2)' = -2r^2 V, \tag{7.18}$$

$$r''/r = -h(\phi)\phi'^2, \tag{7.19}$$

$$A(r^2)'' - r^2 A'' = 2, \tag{7.20}$$

$$-1 + A'rr' + Ar'^2 = r^2(hA\phi'^2 - V), \tag{7.21}$$

where the prime again denotes d/dx. Equation (7.17) is the scalar field equation, (7.18) is the component $R_t^t = \ldots$, (7.19) and (7.20) are the combinations $R_t^t - R_x^x = \ldots$ and $R_t^t - R_\theta^\theta = \ldots$, respectively, and (7.21) is the constraint equation $G_x^x = \ldots$, free from second-order derivatives. It is easy to verify that Eqs. (7.17) and (7.21) follow from (7.18)–(7.20), which, given the potential $V(\phi)$ and the kinetic function $h(\phi)$, form a determined set of equations for the unknowns $r(x)$, $A(x)$, $\phi(x)$. Moreover, Eq. (7.20) can be integrated giving

$$B'(x) \equiv (A/r^2)' = 2(3m - x)/r^4, \tag{7.22}$$

where $B(x) \equiv A/r^2$ and m is an integration constant equal to the Schwarzschild mass if the metric (7.2) is asymptotically flat as $x \to \infty$ ($r \approx x$, $A = 1 - 2m/x + o(1/x)$). If there is a flat asymptotic as $x \to -\infty$, the Schwarzschild mass there is equal to $-m$ ($r \approx |x|$, $A = 1 + 2m/|x| + o(1/x)$).

Thus, we have a general result for *any* solution with two flat asymptotic regions in the presence of *any* potential $V(\phi)$ compatible with such behavior (such solutions can represent wormholes or regular black holes): we inevitably have masses of opposite signs, just as is the case in the well-known special solution — the anti-Fisher wormhole [6, 8, 38] whose metric in the gauge (7.8) reads

$$ds^2 = -\,\mathrm{e}^{-2my} dt^2 + \mathrm{e}^{2my}[dx^2 + (k^2 + x^2) d\Omega^2],$$

with $k < 0$ and $y = |k|^{-1} \cot^{-1}(x/|k|)$. (The constants m and k have here the same meaning as in (7.13)–(7.15), and y is the harmonic coordinate used in Sect. 7.2.2.)

It is also clear that $m = 0$ in all symmetric solutions to Eqs. (7.17)–(7.21), such that $r(x)$ and $A(x)$ are even functions. Indeed, in this case $B'(x)$ is odd, hence $m = 0$ in (7.22).

7.3 Models with a Trapped Ghost

If one specifies the functions $V(\phi)$ and $h(\phi)$ in the Lagrangian (7.1), it is, in general, hard to solve the above equations. Alternatively, to find examples of solutions possessing some particular properties, one may employ the inverse-problem method, choosing some of the functions $r(x)$, $A(x)$ or $\phi(x)$ and then reconstructing the form of $V(\phi)$ and/or $h(\phi)$. We will do so, choosing a function $r(x)$ suitable for both wormhole and black-universe models. Then $A(x)$ is found from (7.22) and $V(x)$ from (7.18). The function $\phi(x)$ is found from (7.19) provided $h(\phi)$ is known; alternatively, using the scalar field parametrization freedom, we can, vice versa, choose a monotonic function $\phi(x)$ (which will yield an unambiguous function $V(\phi)$) and find $h(x)$ from Eq. (7.19).

Let us discuss which kind of function $r(x)$ should be chosen for our purposes.

1. In both wormhole and black universe solutions there must be a minimum of $r(x)$ ($x = 0$ without loss of generality), so that

$$r(0) = a, \qquad r'(0) = 0, \qquad r''(0) > 0, \qquad a = \mathrm{const} > 0. \tag{7.23}$$

2. In a trapped-ghost configuration, by definition, the kinetic coupling function $h(\phi)$ is negative near the minimum of r and positive far from it. According to (7.19), this means that r'' is positive at small $|x|$ and negative at sufficiently large $|x|$.
3. If our model is asymptotically flat or asymptotically (anti-) de Sitter at large $|x|$, we should have

$$r(x) \approx |x| \qquad \text{as} \qquad x \to \pm\infty.$$

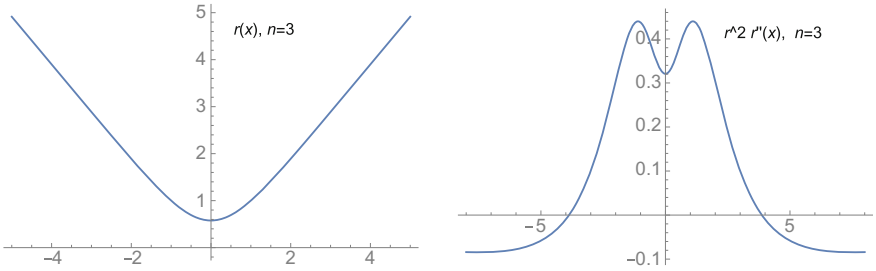

Fig. 7.1 Plots of $r(x)$ and $r^2 r''$ for $n = 3$

A simple example of the function $r(x)$ satisfying the requirements 1–3 is [27] (see Fig. 7.1)

$$r(x) = a\frac{(x/a)^2 + 1}{\sqrt{(x/a)^2 + n}}, \qquad n = \text{const} > 2, \tag{7.24}$$

where a is an arbitrary constant that has the meaning of the throat radius and can be used as the length scale. It differs from the function $r(x)$ used in [21, 26] and leads to slightly simpler resulting expressions.

In what follows, we put $a = 1$, which actually means that the length scale is arbitrary but the quantities r and m (the Schwarzschild mass in our geometrized units) etc., with the dimension of length, are expressed in units of a, the quantities B, V and others with the dimension $(\text{length})^{-2}$ in units of a^{-2}, etc.; the quantities A, ϕ, h are dimensionless. Since

$$r''(x) = \frac{1}{a}\frac{x^2(2-n) + n(2n-1)}{(x^2+n)^{5/2}}, \tag{7.25}$$

we have $r'' > 0$ at $x^2 < n(2n-1)/(n-2)$ and $r'' < 0$ at larger $|x|$, as required; it is also clear that $r \approx |x|$ at large $|x|$. It guarantees $h < 0$ at small $|x|$ and $h > 0$ at large $|x|$ (see Fig. 7.1, right panel).

Further integration can be performed analytically but leads to rather cumbersome expressions for $B(x)$ and other quantities, therefore, we will restrict ourselves to the choice $n = 3$. An inspection shows that a particular choice of the parameter $n > 2$ does not change the qualitative features of the solutions though certainly affects their numerical characteristics.

Integrating (7.26) for $n = 3$, we obtain

$$B = B_0 + \frac{26 + 24x^2 + 6x^4 + 3mx(69 + 100x^2 + 39x^4)}{6(1+x^2)^3} + \frac{39m}{2}\arctan x, \tag{7.26}$$

where B_0 is an integration constant.

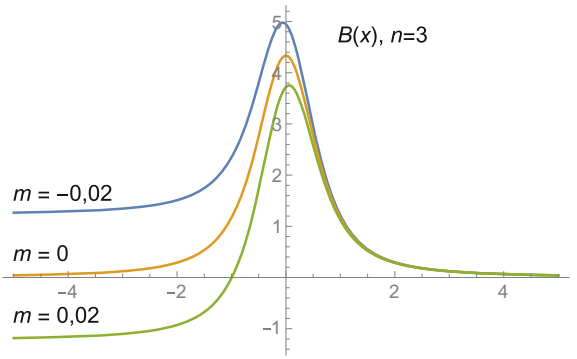

Fig. 7.2 Plots of $B(x)$ for different values of m. With $m < 0$ we obtain an asymmetric M-AdS wormhole, with $m = 0$ a symmetric M-M wormhole, and with $m > 0$ a black universe with a dS behavior as $x \to -\infty$

Now suppose that our system is asymptotically flat at large positive x. Since $B = A/r^2$ and $A \to 1$ at infinity, we require $B \to 0$ as $x \to \infty$ and thus fix B_0 as

$$B_0 = -\frac{39\pi m}{4}. \tag{7.27}$$

The form of $B(x)$ (and consequently $A(x) = Br^2$) now depends on the mass m, see Fig. 7.2. We see that with a negative mass we obtain $B(x)$ tending to a positive constant as $x \to -\infty$, hence $A \sim r^2$, and we obtain a wormhole with an anti-de Sitter (AdS) asymptotic behavior at the "far end" (an M-AdS wormhole for short, where M stands for Minkowski). With zero mass there is a twice asymptotically flat (M-M) wormhole, and lastly in the case $m > 0$, $B(x)$ changes its sign and tends to a negative constant: we thus obtain a black universe with a de Sitter asymptotic at large negative x.

Now we know the metric completely, and the remaining quantities $\phi(x)$ and $V(\phi(x))$ can be easily found from Eqs. (7.18) and (7.19), respectively. To construct V as an unambiguous function of ϕ and to find $h(\phi)$, it makes sense to choose a monotonic function $\phi(u)$. It is convenient to assume

$$\phi(x) = \frac{1}{\sqrt{3}} \arctan \frac{x}{\sqrt{3}}, \tag{7.28}$$

so that ϕ has a finite range: $\phi \in (-\phi_0, \phi_0)$, $\phi_0 = \pi/(2\sqrt{3})$, which is common to kink configurations. Thus we have $x = \sqrt{3}\tan(\sqrt{3}\phi)$, whose substitution into the expression for $V(x)$, found from (7.18), gives $V(\phi)$ defined in this finite range.

The expression for the kinetic coupling function $h(\phi)$ is then found from (7.19) as follows:

$$h(\phi) = \frac{x^2 - 15}{x^2 + 1} = \frac{3\tan^2(\sqrt{3}\phi) - 15}{3\tan^2(\sqrt{3}\phi) + 1}. \tag{7.29}$$

The function $h(\phi)$ given by Eq. (7.29) is also defined in the interval $(-\phi_0, \phi_0)$ and can be extended to $\mathbb{R}$ by supposing $h(\phi) \equiv 1$ at $|\phi| \geq \phi_0$. Evidently, the NEC is violated where and only where $h(\phi) < 0$.

For $V(x)$ we obtain [27]

$$V(x) = -\frac{1}{12(1+x^2)^2(3+x^2)^3}\Big\{32(-6+x^2+3x^4) + 6mx(2655+6930x^2+5420x^4+1326x^6+117x^8) + 117m(1+x^2)^2(15+89x^2+29x^4+3x^6)(-\pi+2\arctan x)\Big\}. \quad (7.30)$$

The function $V(\phi)$ can also be extended to the whole real axis, $\phi \in \mathbb{R}$, by supposing $V(\phi) \equiv 0$ at $\phi \geq \phi_0$ (since $V(x = +\infty) = 0$) and $V(\phi) = V(-\phi_0) > 0$ at $\phi < -\phi_0$.

It is easy to verify that the asymptotic values of the function $B(x)$ as $x \to -\infty$ are directly related to those of the potential V which in this case plays the role of an effective cosmological constant:

$$V(-\infty) = 117m\pi/2 = -3B(-\infty), \quad (7.31)$$

and thus, as already mentioned, a negative $B(-\infty)$, corresponding to $m > 0$, leads to a dS asymptotic, with $m = 0$ and $B(-\infty) = 0$ it is flat, and with $B(-\infty) > 0$ ($m < 0$) it is AdS (Fig. 7.3).

More complicated models with various global structures emerge if, in addition to a scalar field, there is an electromagnetic field. Examples of such solutions, which include M–M and M-AdS wormholes and regular black holes with up to three horizons, are presented in [27]; the structures obtained are similar to those found earlier with a scalar field which is everywhere phantom [25].

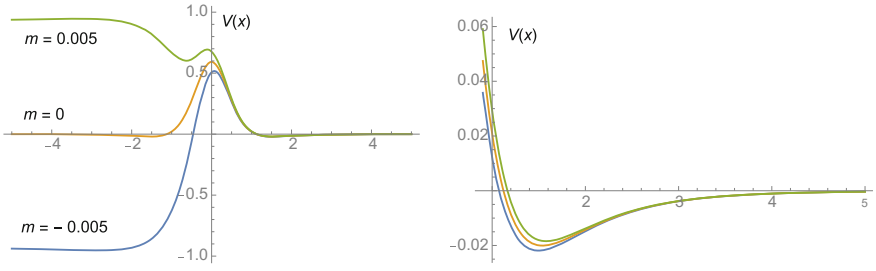

Fig. 7.3 Plots of the potential $V(x)$ for different values of m; the *right panel* shows the behavior of V at larger x, where the curves almost merge

7.4 Spherically Symmetric Perturbations

7.4.1 Perturbation Equations

The stability problem is of great importance while considering any equilibrium configurations since only those ones can exist for a sufficiently long time which are either stable or decay very slowly. On the other hand, the evolution of unstable systems can lead to many phenomena of interest, from structure formation in the Universe to Supernova explosions.

Let us discuss the stability problem for the scalar-vacuum configurations like those described in the previous section. The problem is whether or not an initially arbitrarily small time-dependent perturbation will grow in the future thus destroying the system. So we will study the perturbations in a linear approximation, neglecting their quadratic and higher order combinations. Moreover, we will only consider perturbations preserving spherical symmetry (they are also called radial, or monopole perturbations) which are, on one hand, the simplest, and, on the other, the most "dangerous" ones, which lead to instabilities in many configurations with self-gravitating scalar fields [28–35]. Other kinds of perturbations usually do not develop instabilities, see, e.g., [35, 41]. We do not restrict ourselves to the particular solutions presented above but suppose that a certain static solution is known and study its time-dependent perturbations.

Let us follow the lines of [13, 34, 40] and consider the same field system as previously, so the total action is

$$\mathcal{S} = \frac{1}{16\pi} \int \sqrt{-g} d^4x \Big[R + 2h(\phi) g^{\alpha\beta} \phi_{;\alpha} \phi_{;\beta} - 2V(\phi) \Big], \tag{7.32}$$

which leads to the scalar field equation

$$2h \nabla^\mu \nabla_\mu \phi + (dh/d\phi) \phi^{;\mu} \phi_{;\mu} + dV/d\phi = 0, \tag{7.33}$$

and the Einstein equations (7.6) with the scalar field SET:

$$T_\mu^\nu[\phi] = h(\phi)[2\phi_\mu \phi^\nu - \delta_\mu^\nu \phi^\alpha \phi_\alpha] + \delta_\mu^\nu V(\phi), \tag{7.34}$$

The general spherically symmetric metric is chosen in the form (7.2), that is,

$$ds^2 = \mathrm{e}^{2\gamma} dt^2 - \mathrm{e}^{2\alpha} du^2 - \mathrm{e}^{2\beta} d\Omega^2, \tag{7.35}$$

where γ, α, and β are now functions of both the radial coordinate u and time t. We also use the notation $r(u) \equiv \mathrm{e}^\beta$. There remains a coordinate freedom of choosing u.

Consider linear spherically symmetric perturbations of static solutions to the field equations due to (7.32). Thus for the scalar field and the metric functions we write now

$$\phi(u,t) = \phi(u) + \delta\phi(u,t), \qquad \gamma(u,t) = \gamma(u) + \delta\gamma(u,t) \tag{7.36}$$

and similarly for other quantities, with small "deltas" (perturbations).

Preserving only linear terms with respect to time derivatives, we can write all nonzero components of the Ricci tensor as

$$R^t_t = \mathrm{e}^{-2\gamma}(\ddot{\alpha} + 2\ddot{\beta}) - \mathrm{e}^{-2\alpha}[\gamma'' + \gamma'(\gamma' - \alpha' + 2\beta')], \tag{7.37}$$

$$R^u_u = \mathrm{e}^{-2\gamma}\ddot{\alpha} - \mathrm{e}^{-2\alpha}[\gamma'' + 2\beta'' + \gamma'^2 + 2\beta'^2 - \alpha'(\gamma' + 2\beta')], \tag{7.38}$$

$$R^\theta_\theta = R^\varphi_\varphi = \mathrm{e}^{-2\beta} + \mathrm{e}^{-2\gamma}\ddot{\beta} - \mathrm{e}^{-2\alpha}[\beta'' + \beta'(\gamma' - \alpha' + 2\beta')], \tag{7.39}$$

$$R_{tu} = 2[\dot{\beta}' + \dot{\beta}\beta' - \dot{\alpha}\beta' - \dot{\beta}\gamma'], \tag{7.40}$$

where dots and primes denote $\partial/\partial t$ and $\partial/\partial u$, respectively.

Accordingly, the zero-order (static) scalar equation and the $\binom{t}{t}$, $\binom{u}{u}$, and $\binom{\theta}{\theta}$ components of the Einstein equations (7.6) read

$$2h[\phi'' + \phi'(\gamma' + 2\beta' - \alpha')] + h'\phi' = \mathrm{e}^{2\alpha} dV/d\phi, \tag{7.41}$$

$$\gamma'' + \gamma'(\gamma' + 2\beta' - \alpha') = -\mathrm{e}^{2\alpha} V, \tag{7.42}$$

$$\gamma'' + 2\beta'' + \gamma'^2 + 2\beta'^2 - \alpha'(\gamma' + 2\beta') = -2h\phi'^2 - \mathrm{e}^{2\alpha} V, \tag{7.43}$$

$$-\mathrm{e}^{2\alpha-2\beta} + \beta'' + \beta'(\gamma' + 2\beta' - \alpha') = -V\,\mathrm{e}^{2\alpha}. \tag{7.44}$$

The first-order perturbed equations (scalar, $R_{ut} = \ldots$, and $R^\theta_\theta = \ldots$) have the form

$$\begin{aligned} &2\,\mathrm{e}^{2\alpha-2\gamma} h\delta\ddot{\phi} - 2h[\delta\phi'' + \delta\phi'(\gamma' + 2\beta' - \alpha') + \phi'(\delta\gamma' + 2\delta\beta' - \delta\alpha')] \\ &\quad - 2\delta h[\phi'' + \phi'(2\beta' + \gamma' - \alpha')] - h'\delta\phi' - \phi'\delta h' + \delta(\mathrm{e}^{2\alpha} V_\phi) = 0, \end{aligned} \tag{7.45}$$

$$\delta\dot{\beta}' + \beta'\delta\dot{\beta} - \beta'\delta\dot{\alpha} - \gamma'\delta\dot{\beta} = -h\phi'\delta\dot{\phi}, \tag{7.46}$$

$$\begin{aligned} \delta(\mathrm{e}^{2\alpha-2\beta}) + \mathrm{e}^{2\alpha-2\gamma}\delta\ddot{\beta} - \delta\beta'' - \delta\beta'(\gamma' + 2\beta' - \alpha') \\ - \beta'(\delta\gamma' + 2\delta\beta' - \delta\alpha') = \delta(\mathrm{e}^{2\alpha} V), \end{aligned} \tag{7.47}$$

Equation (7.46) may be integrated in t; we are interested in time-dependent perturbations and thus omit the appearing arbitrary function of u since it describes static perturbations, obtaining

$$\delta\beta' + \delta\beta(\beta' - \gamma') - \beta'\delta\alpha = -h\phi'\delta\phi. \tag{7.48}$$

In this problem, we have two independent forms of arbitrariness: one consists in the freedom of choosing a *radial coordinate* u in the static configuration, the other is a *perturbation gauge*, connected with the freedom to choose a reference frame in the perturbed spacetime. This can be expressed in imposing a certain relation for $\delta\alpha$, $\delta\beta$, etc. In what follows we will employ both kinds of freedom. All the above equations have been written in the most universal form, without fixing the u coordinate or the perturbation gauge.

Let us now choose the so-called "tortoise" coordinate $u = z$, corresponding to the condition $\alpha = \gamma$ (which is the best for considering wave equations), and the perturbation gauge $\delta\beta \equiv 0$ that substantially simplifies the equations. Then Eq. (7.48) expresses $\delta\alpha$ in terms of $\delta\phi$ (the prime now means d/dz):

$$\beta'\delta\alpha = h(\phi)\phi'\delta\phi. \tag{7.49}$$

Equation (7.47) expresses $\delta\gamma' - \delta\alpha'$ in terms of $\delta\alpha$ and $\delta\phi$:

$$\beta'(\delta\gamma' - \delta\alpha') = 2\,\mathrm{e}^{2\alpha-2\beta}\delta\alpha - \delta(\,\mathrm{e}^{2\alpha}V). \tag{7.50}$$

Substituting all this into (7.45), we obtain the following wave equation:

$$\delta\ddot{\phi} - \delta\phi'' - \delta\phi'(2\beta' + h'/h) + U\delta\phi = 0, \tag{7.51}$$

$$U \equiv \mathrm{e}^{2\alpha}\left[\frac{2h\phi'^2}{\beta'^2}(V - \mathrm{e}^{-2\beta}) + \frac{2\phi'}{\beta'}V_\phi + \frac{V_{\phi\phi}}{2h}\right] - \frac{h'' + h_\phi\phi''}{2h} - \frac{2\beta'h'}{h}, \tag{7.52}$$

where the index ϕ denotes $d/d\phi$. This expression for U directly generalizes the one obtained in [34] for scalar-vacuum configurations for the case $h = \varepsilon = \pm 1$.

Next, we can get rid of the first-order derivative of $\delta\phi$ in (7.51) by substituting

$$\delta\phi = \psi(z,t)\,\mathrm{e}^{-\eta}, \qquad \eta' = \beta' + \frac{h'}{2h}, \tag{7.53}$$

and reduce the wave equation to its canonical form

$$\ddot{\psi} - \psi'' + V_{\mathrm{eff}}(z)\psi = 0, \tag{7.54}$$

with the effective potential

$$V_{\mathrm{eff}}(z) = U + \eta'' + \eta'^2$$

$$= \mathrm{e}^{2\alpha}\left[\frac{2h\phi'^2}{\beta'^2}(V - \mathrm{e}^{-2\beta}) + \frac{2\phi'}{\beta'}V_\phi - \frac{h_\phi}{4h^2}V_\phi + \frac{V_{\phi\phi}}{2h}\right] + \beta'' + \beta'^2. \tag{7.55}$$

A further substitution, possible since the background is static,

$$\psi(x,t) = Y(x)\,\mathrm{e}^{i\omega t}, \qquad \omega = \mathrm{const}, \tag{7.56}$$

leads to the Schrödinger-like equation

$$Y'' + [\omega^2 - V_{\mathrm{eff}}(x)]Y = 0. \tag{7.57}$$

Now, if there is a nontrivial solution to (7.57) with $\mathrm{Im}\,\omega < 0$ satisfying some physically reasonable conditions at the ends of the range of z (in particular, the absence of ingoing waves), then the static system is unstable since $\delta\phi$ can exponentially grow with t. Otherwise our static system is stable in the linear approximation. Thus, as usual in such studies, the stability problem is reduced to a boundary-value problem for Eq. (7.57) — see, e.g., [13, 28–30, 32, 34, 35, 41, 42].

The gauge $\delta\beta = 0$ is technically the simplest one, but apparently causes some problems when applied to wormholes and other configurations with throats. The reason is that the assumption $\delta\beta = 0$ leaves invariable the throat radius, while perturbations must in general admit its time dependence [13, 32, 42]. It may even seem that the emergence of a pole in V_{eff} due to $\delta\beta$ in the denominator in (7.52) is an artifact of the gauge. It can be shown, however, by analogy with [13, 32, 34], that Eq. (7.57) is in fact gauge-invariant, while $\delta\phi$ is a representation of a gauge-invariant quantity in the gauge $\delta\beta = 0$. In the next subsection we will discuss this issue in some detail.

7.4.2 Gauge-Invariant Perturbations

As in all numerous problems with perturbation dynamics in gravitation theory, it is necessary to make sure that we are dealing with real perturbations rather than pure coordinate effects, therefore it is necessary to construct gauge-invariant quantities from perturbations.

Consider the general metric (7.35) and small coordinate transformations $x^a \mapsto x^a + \xi^a$ in the (t, u) subspace:

$$t = \bar{t} + \Delta t(t, u), \qquad u = \bar{u} + \Delta u(t, u), \tag{7.58}$$

where Δt and Δu are supposed to be small. This transformation adds an increment to any scalar with respect to transitions to new coordinates in the (t, u) subspace (2-scalar, for short), such as, e.g., $\phi(t, u)$ and $r(t, u)$:

$$\Delta\phi = \dot{\phi}\Delta t + \phi'\Delta u \approx \phi'\Delta u, \tag{7.59}$$

in the linear approximation since both $\dot{\phi}$ and Δt are small and similarly for $r(t, u)$ and other 2-scalars, if any. If there are perturbations $\delta\phi$ and δr, the transformation (7.58) changes them as follows:

$$\begin{aligned} \delta\phi \;&\mapsto\; \overline{\delta\phi} = \delta\phi + \Delta\phi = \delta\phi + \phi'\Delta u, \\ \delta r \;&\mapsto\; \overline{\delta r} = \delta r + \Delta r = \delta r + r'\Delta u, \end{aligned} \tag{7.60}$$

since in our static background solution $\dot{\phi} = \dot{r} = 0$. It then follows that the combination

$$\Psi \equiv r'\delta\phi - \phi'\delta r, \tag{7.61}$$

does not change under the transformation (7.58), or — in other words — is gauge-invariant. Note that the prime here denotes d/du in the background static configuration, and u is an arbitrary admissible radial coordinate, in particular, it may be thought of as our "tortoise" coordinate z used to formulate the boundary-value problem for perturbation modes.

One can notice that combinations constructed like (7.61) from *any* 2-scalars (for example, such as e^{ϕ} and $\beta = \ln r$, or two different linear combinations of ϕ and r) are also gauge-invariant. Moreover, gauge-invariant is Ψ multiplied by any 2-scalar or any combination of background quantities which are known and fixed functions of u and are certainly also gauge-independent.

The physical properties of perturbations must not depend on which gauge-invariant quantity Ψ is chosen to describe them. Meanwhile, with different Ψ, the effective potentials can, in general, also be different. However, given a specific background configuration, in order that the theory be consistent, these different potentials should lead to the same perturbation spectrum.

Due to gauge invariance of Ψ, equations that govern it may be written in any admissible gauge, in particular, $\delta\beta = 0$, and Eq. (7.54) for ψ then may be considered as a result of substituting $\psi = (r/r')\Psi = r\delta\phi$ in a manifestly correct equation for $\Psi = r'\delta\phi$.

We conclude that Eqs. (7.54) and (7.57) are themselves gauge-invariant since their unknown functions are gauge invariants (though written down in a particular gauge) while other functions involved are taken from the background solution.

A similar problem for cosmological perturbations is discussed, e.g., in the review [43].

7.5 Throats, Trapped Ghosts and Stability

7.5.1 Perturbations Near a Throat

We have verified that Eq. (7.57) is gauge-invariant, and it really makes sense to pose boundary-value problems to find out whether or not there are unstable perturbation modes. However, the stability problem is complicated by the singular nature of the effective potential V_{eff}. There are two kinds of singularities: one is related to throats, if any, since there are terms proportional to $1/\beta'^2$ and $1/\beta'$ in V_{eff} (and $\beta' = 0$ on a throat); the other exists at transitions from canonical to phantom scalar since V_{eff} contains terms with h^{-2} and h^{-1} while $h = 0$ at such a transition. In this subsection we discuss singularities on a throat, partly following [32, 34].

Suppose that a throat occurs at $z = 0$ (without loss of generality) and that the spherical radius $r(z) = \mathrm{e}^{\beta}$ has a generic minimum at $z = 0$, so that we have a Taylor expansion of the form, $r(z) = r_0 + \frac{1}{2} r_2 z^2 + o(z^2)$ with $r_0 > 0$, $r_2 > 0$. Also, without loss of generality, in a certain neighborhood of the throat we can put $h(\phi) = -1$ since Eq. (7.19) definitely requires $h < 0$, and $h(\phi) = -1$ can be achieved by a regular redefinition of ϕ. Then, using the zero-order (background) equations, it is not difficult to show that near the throat

$$V_{\mathrm{eff}}(\phi) = 2/z^2 + O(1), \tag{7.62}$$

and there is no $O(z^{-1})$ contribution. We see that there is an infinitely high potential wall separating perturbations on the left of the throat ($z < 0$) from those on the right ($z > 0$) because a natural boundary condition at $z = 0$ is $\psi(0) = 0$. It immediately implies that perturbations of all other quantities vanish at $z = 0$. We are thus unable to consider a mode of obvious physical significance, the one corresponding to dynamic changes of the throat radius.

This difficulty can be overcome using the so-called S-deformation method applied to the potential V_{eff}. It has been used in [44, 45] for transforming a partly negative potential to a positive-definite one for perturbations of higher-dimensional black holes. Later, with its aid, Gonzalez et al. [32] transformed a singular potential to a nonsingular one for perturbations of the anti-Fisher wormholes and found that an exponentially growing mode, making such wormholes unstable, is just the one connected with an evolving throat radius. The same scheme in a more general formulation was used in [34, 35] for revealing instabilities in other solutions with throats, including some black universe models. Let us briefly describe the method.

Consider a wave equation of the type (7.54)

$$\ddot{\psi} - \psi'' + W(z)\psi = 0, \tag{7.63}$$

with an arbitrary potential $W(z)$ (whose specific example is the above potential V_{eff}). Let us present $W(z)$ in the form

$$W(z) = S^2(z) + S', \tag{7.64}$$

which is actually a Riccati equation with respect to $S(z)$, so such a function can in general be found. Then Eq. (7.63) can be rewritten as

$$\ddot{\psi} + (\partial_z + S)(-\partial_z + S)\psi = 0. \tag{7.65}$$

Now, if we introduce the new function

$$\chi = (-\partial_z + S)\psi, \tag{7.66}$$

then, applying the operator $-\partial_z + S$ to the left-hand side of Eq. (7.65), we obtain the following wave equation for χ:

$$\ddot{\chi} - \chi'' + W_{\rm reg}(z)\chi = 0, \tag{7.67}$$

with the new effective potential

$$W_{\rm reg}(x) = -S' + S^2 = -W(z) + 2S^2. \tag{7.68}$$

If a static solution $\psi_s(z)$ of Eq. (7.63) is known, so that $\psi_s'' = W(z)\psi_s$, then we can choose

$$S(z) = \psi_s'/\psi_s, \tag{7.69}$$

to carry out the above transformation. Furthermore, if we assume that $W(x) \approx az^{-n}$ at small z, then, requiring that $W_{\rm reg}$ should be finite at $z = 0$ and using (7.68), we easily find that necessary conditions for such a singularity in $W(z)$ to be removable by the above transformation is $n = 1,\ a = 2$, that is, $W \approx 2/z^2$. Fortunately, by Eq. (7.62), the potential $V_{\rm eff}$ behaves precisely in this way. A point of interest is that such a removal is only possible for $W \to +\infty$ as $z \to 0$, so that a potential wall in $W(z)$ can be removed but a potential well cannot.

From (7.68) with finite $W_{\rm reg}$ it also follows that at small z

$$S \approx -1/z \quad \Rightarrow \quad \psi_s \propto 1/z. \tag{7.70}$$

To summarize, we have seen that singularities of the effective potential $V_{\rm eff}$ existing at a throat can be regularized in the generic case [32, 34]. What is of equal importance, it has also been shown that regular solutions to the regularized wave equation describe regular perturbations of both the scalar field and the metric. It was this procedure that made it possible to prove the instability of anti-Fisher (Ellis type [5, 6]) wormholes [32] and other scalar field configurations in GR [34, 35].

7.5.2 *Perturbations Near the Surface $h = 0$*

The effective potential $V_{\rm eff}$ also possesses singularities at the values of the radial coordinate where $h = 0$, which exist in cases where the function $h(\phi)$ in (7.32) changes its sign. This happens in the framework of the trapped ghost concept. Such singularities are quite different in nature than those occurring on a throat: they are rather similar to those found at transition surfaces in systems with conformal continuations [14, 29, 30]. The latter phenomenon is observed, for instance, in scalar-tensor theories of gravity where it sometimes happens that the whole manifold in the Einstein frame maps to only a part of the Jordan frame manifold (or vice versa). It was found that if such configurations are static and spherically symmetric, then their monopole perturbations are described by wave equations like (7.54) with effective potentials that have a singularity of the form

$$V_{\text{eff}} \approx -1/(4z^2) \quad \text{as} \quad z \to 0, \tag{7.71}$$

if $z = 0$ is the transition surface where the Einstein frame metric has a singularity while the Jordan frame metric is regular [29].

Indeed, let us assume that near the value of z where $h = 0$ (let it be $z = 0$) the metric functions $\alpha = \gamma$ (our gauge) and β as well as the ϕ field are regular, so that the following Taylor expansions are valid:

$$\begin{aligned} &\alpha = \alpha_0 + \alpha_1 z + \ldots, \quad \beta = \beta_0 + \beta_1 z + \ldots, \quad \phi = \phi_0 + \phi_1 z + \tfrac{1}{2}\phi_2 + \ldots, \\ &h(z) = h_1 z + \tfrac{1}{2} h_2 z^2 + \ldots, \qquad \phi_1 \neq 0, \quad h_1 \neq 0. \end{aligned} \tag{7.72}$$

It can be shown that in this generic situation the effective potential (7.55) is represented near $z = 0$ by the Laurent series expansion

$$V_{\text{eff}}(z) = -\frac{1}{4z^2} + \frac{1}{z}\left[\frac{h_2}{h_1} + 2\left(\beta_1 - \alpha_1 + \frac{\phi_2}{\phi_1}\right)\right] + O(1). \tag{7.73}$$

Thus, the surface where $h = 0$ creates an infinitely deep potential well for perturbations. In quantum mechanics such a potential in the stationary Schrödinger equation would mean that there are negative energy levels of unlimited depth. Returning to a stability study, it is tempting to conclude that there are perturbation modes with $\omega^2 < 0$ and an arbitrarily large $|\omega|$, and the corresponding growth ($\delta\phi \sim e^{|\omega| t}$) of the perturbations then immediately leads them out of the linear regime and necessitates a nonlinear or nonperturbative analysis.

However, the stability study implies other physical requirements on ψ in Eq. (7.54) or Y in (7.57): $\delta\phi$ should be finite in the whole space and should vanish at infinities or horizons, whereas quantum mechanics only requires quadratic integrability of ψ.

With the potential (7.73), the general solution of (7.57) at small z has, independently of ω, the leading terms

$$Y(z) = \sqrt{|z|}(C_1 + C_2 \ln|z|) + O(z^{3/2}), \qquad C_1,\ C_2 = \text{const}. \tag{7.74}$$

On the other hand, according to (7.53), $\delta\phi \sim Y/\sqrt{h} \sim Y/\sqrt{|z|}$, therefore,

$$\delta\phi \sim C_1 + C_2 \ln|z| + O(z), \tag{7.75}$$

and for physically meaningful perturbations we must require $C_2 = 0$. Thus, the negative pole of the potential (7.73) leads to a constraint which should be added to the ordinary boundary conditions which, combined with the equation itself, in more conventional cases completely determine the solution to a boundary-value problem. Due to this constraint it may happen that the boundary-value problem with Eq. (7.57) has no discrete spectrum. Indeed, suppose we have a background configuration with a surface $z = 0$ where $h = 0$, and there is a solution to (7.57) satisfying the boundary conditions at infinities and/or a horizon; then there is in general zero probability that

this solution will be finite at $z = 0$. There could be an exception if the background were $\mathbb{Z}_2$-symmetric relative to the surface $z = 0$, but here it is manifestly not the case because $h > 0$ on one side of $z = 0$ and $h < 0$ on the other. A similar situation was discussed in [46] concerning the stability of black holes with a conformal scalar field [47, 48], and after all, with some more reasoning, it was stated that such black holes are stable under monopole perturbations.

(Let us note that, contrary to this situation, the quantum-mechanical requirement of quadratic integrability of $Y(z)$ does hold since the integral $\int z^n \ln^2 z\, dz$ converges at $z = 0$ for any $n \geq 0$. The quantum particle in a field with such a potential well, as is sometimes said, "falls onto the center" [49] because the wave function, as one descends to deeper and deeper negative energy levels, more and more concentrates near $z = 0$.)

We conclude that a transition from a canonical scalar to a phantom one plays a strong stabilizing role in all configurations with such self-gravitating scalar fields. One cannot, however, say whether or not a particular trapped-ghost solution is stable or not without its investigation because this evidently depends on the details of each model.

7.6 Conclusion

It has been shown [21, 22, 26, 27] that scalar fields may change their nature from canonical to ghost in a smooth way without creating any spacetime singularities. This feature significantly widens the opportunities of scalar field dynamics and the possible choice of scalar-tensor theories of gravity, although here we have only considered minimally coupled scalars.

More specifically, trapped ghosts make possible spherically symmetric wormhole and regular black hole models where the ghost is present in some restricted strong-field region whereas in the weak-field region, where observers can live, the scalar has usual canonical properties. It can be speculated that if such ghosts do exist in Nature, they are all confined to strong-field regions ("all genies are sitting in their bottles"), but just one of them, having been released, has occupied the whole Universe and plays the part of dark energy (if dark energy is really phantom, which is more or less likely but not certain).

For static, spherically symmetric models in the Einstein-scalar field system under consideration, in addition to examples of exact solutions, some general properties have been found:

(i) Trapped-ghost solutions to the field equations are only possible with nonzero potentials $V(\phi)$.
(ii) If a solution to the Einstein-scalar equations (be it of trapped-ghost nature or not) is twice asymptotically flat, and the Schwarzschild mass is equal to m at one of the infinities, it is equal to $-m$ at the other. Hence, mirror ($\mathbb{Z}_2$) symmetry with respect to a certain value of the radial coordinate is only possible if $m = 0$.

(iii) The transition surfaces from canonical to phantom behavior of the scalar field create a potential well for spherically symmetric perturbations, and the generic shape of this well (see Eq. (7.73)) does not depend on details of the model. Moreover, the natural requirement that perturbations must be finite, leads to a constraint which, being added to the boundary conditions, substantially restricts the set of possible solutions and thus plays a stabilizing role.

The latter result is somewhat unexpected and, in my view, can raise an interest in trapped-ghost models. This opportunity can probably be used in attempts to solve various problems of gravitational physics and cosmology. Stability studies for specific trapped-ghost configurations like those described here make one of evident tasks for the near future.

Acknowledgements This work was supported in part by the Russian Foundation for Basic Research grant 16-02-00602.

References

1. Schwarzschild K. Uber das Gravitationsfeld eines Massenpunktes nach der Einsteinschen Theorie. Sitzungsberichte der Königlich Preussischen Akademie der Wissenschaften. 1916;1:189–96.
2. Flamm L. Beiträge zur Einsteinschen Gravitationstheorie. Phys Z. 1916;17:48.
3. Morris MS, Thorne KS. Wormholes in spacetime and their use for interstellar travel: a tool for teaching general relativity. Am J Phys. 1988;56:395.
4. Hochberg D, Visser M. Geometric structure of the generic static traversable wormhole throat. Phys Rev D. 1997;56:4745.
5. Bronnikov KA. Scalar-tensor theory and scalar charge. Acta Phys Pol B. 1973;4:251.
6. Ellis H. Ether flow through a drainhole – a particle model in general relativity. J Math Phys. 1973;14:104.
7. Bronnikov KA. Spherically symmetric false vacuum: no-go theorems and global structure. Phys Rev D. 2001;64:064013.
8. Sushkov SV, Zhang Y-Z. Scalar wormholes in cosmological setting and their instability. Phys Rev D. 2008;77:024042.
9. Bronnikov KA, Starobinsky AA. No realistic wormholes from ghost-free scalar-tensor phantom dark energy. JETP Lett. 2007;85:1.
10. Bronnikov KA, Starobinsky AA. Once again on thin-shell wormholes in scalar-tensor gravity. Mod Phys Lett A. 2009;24:1559.
11. Bronnikov KA, Skvortsova MV, Starobinsky AA. Notes on wormhole existence in scalar-tensor and F(R) gravity. Grav Cosmol. 2010;16:216.
12. Lobo FSN. Exotic solutions in general relativity: traversable wormholes and warp drive spacetimes. In: Classical and Quantum Gravity Research. Nova Sci. Pub.; 2008. pp. 1–78
13. Bronnikov KA, Rubin SG. Black holes, cosmology, and extra dimensions. World Scientific; 2012.
14. Bronnikov KA. Scalar-tensor gravity and conformal continuations. J Math Phys. 2002;43:6096–115.
15. Bronnikov KA, Galiakhmetov AM. Wormholes without exotic matter in Einstein-Cartan theory. Grav Cosmol. 2015;21:283.
16. Bronnikov KA, Galiakhmetov AM. Wormholes and black universes without phantom fields in Einstein-Cartan theory. Phys Rev D. 2016;94:124006.

17. Dotti Gustavo, Oliva Julio, Troncoso Ricardo. Static wormhole solution for higher-dimensional gravity in vacuum. Phys Rev D. 2007;75:024002.
18. Harko T, Lobo FSN, Mak MK, Sushkov SV. Gravitationally modified wormholes without exotic matter.
19. Bronnikov KA, Kim S-W. Possible wormholes in a brane world. Phys Rev D. 2003;67:064027.
20. Korolev RV, Sushkov SV. Exact wormhole solutions with nonminimal kinetic coupling. arXiv: 1408.1235.
21. Bronnikov KA, Sushkov SV. Trapped ghosts: a new class of wormholes. Quantum Grav. 2010;27:095022.
22. Kroger H, Melkonian G, Rubin SG. Cosmological dynamics of scalar field with non-minimal kinetic term. Gen Rel Grav. 2004;36:1649.
23. Bronnikov KA, Fabris JC. Regular phantom black holes. Phys Rev Lett. 2006;96:251101.
24. Bronnikov KA, Melnikov VN, Dehnen H. Regular black holes and black universes. Gen Rel Grav. 2007;39:973.
25. Bolokhov SV, Bronnikov KA, Skvortsova MV. Magnetic black universes and wormholes with a phantom scalar. Class Quantum Grav. 2012;29:245006.
26. Bronnikov KA, Donskoy EV. Black universes with trapped ghosts. Grav Cosmol. 2011;17:176–80.
27. Bronnikov KA, Donskoy EV, Korolyov P. Magnetic wormholes and black universes with trapped ghosts. Vestnik RUDN No. 2013;2:139–49.
28. Bronnikov KA, Khodunov AV. Scalar field and gravitational instability. Gen Rel Grav. 1979;11:13.
29. Bronnikov KA, Grinyok SV. Instability of wormholes with a nonminimally coupled scalar field. Grav Cosmol. 2001;7:297.
30. Bronnikov KA, Grinyok SV. Conformal continuations and wormhole instability in scalar-tensor gravity. Grav Cosmol. 2004;10:237.
31. Shinkai Hisa-aki, Hayward Sean A. Fate of the first traversible wormhole: black-hole collapse or inflationary expansion. Phys Rev D. 2002;66:044005.
32. Gonzalez JA, Guzman FS, Sarbach O. Instability of wormholes supported by a ghost scalar field. I. Linear stability analysis. Class Quantum Grav. 2009;26:015010.
33. Gonzalez JA, Guzman FS, Sarbach O. On the instability of charged wormholes supported by a ghost scalar field. Phys Rev D. 2009;80:024023.
34. Bronnikov KA, Fabris JC, Zhidenko A. On the stability of scalar-vacuum space-times. Eur Phys J C. 2011;71(11):1791.
35. Bronnikov KA, Konoplya RA, Zhidenko A. Instabilities of wormholes and regular black holes supported by a phantom scalar field. Phys Rev D. 2012;86:024028.
36. Fisher IZ. Scalar mesostatic field with regard for gravitational effects. Zh Eksp Teor Fiz. 1948;18:636.
37. Bergmann O, Leipnik R. Space-time structure of a static spherically symmetric scalar field. Phys Rev. 1957;107:1157.
38. Bronnikov KA, Chernakova MS, Fabris JC, Pinto-Neto N, Rodrigues ME. Cold black holes and conformal continuations. Int J Mod Phys D. 2008;17:25–42.
39. Bronnikov KA, Chervon SV, Sushkov SV. Wormholes supported by chiral fields. Grav Cosmol. 2009;15:241.
40. Bronnikov KA, Korolyov PA. Magnetic wormholes and black universes with invisible ghosts. Grav Cosmol. 2015;21:157–65.
41. Bronnikov KA, Lipatova LN, Novikov ID, Shatskiy AA. Example of a stable wormhole in general relativity. Grav Cosmol. 2013;19:269.
42. Bronnikov KA, Clément G, Constantinidis CP, Fabris JC. Cold scalar-tensor black holes: causal structure, geodesics, stability. Grav Cosmol. 1998;4:128.
43. Brandenberger RH, Feldman HA, Mukhanov VF. Theory of cosmological perturbations. Part 1. Classical perturbations. Part 2. Quantum theory of perturbations. Part 3. Extensions. Phys Rep. 1992;215:203.

44. Ishibashi A, Kodama H. Stability of higher-dimensional Schwarzschild black holes. Prog Theor Phys. 2003;110:901.
45. Ishibashi A, Kodama H. Perturbations and stability of static black holes in higher dimensions. Prog Theor Phys Suppl. 2011;189:165.
46. McFadden Paul L, Turok Neil G. Effective theory approach to brane world black holes. Phys Rev D. 2005;71:086004.
47. Bocharova N, Bronnikov K, Melnikov V. On an exact solution of the Einstein-scalar field equations. Vestn Mosk Univ Fiz Astron. 1970;6:706.
48. Bekenstein JD. Exact solutions of Einstein–conformal scalar equations. Ann Phys (NY). 1974;82:535.
49. Landau LD, Lifshits EM. Quantum mechanics. non-relativistic theory. 3rd ed. Oxford: Pergamon; 1991.

Chapter 8
Geons in Palatini Theories of Gravity

Gonzalo J. Olmo and Diego Rubiera-Garcia

8.1 Introduction

Einstein's deep insight on the nature of gravitation had a crucial impact on our understanding of the universe. In order to make gravitation compatible with his new principle of relativity, the rigid Minkowskian spacetime had to be extended to a locally deformable dynamical structure using the language of differential geometry. The description of spacetime as a field theory of a metric tensor in interaction with the matter led to a number of important predictions, some of which were observationally verified shortly after the publication of the theory. Among those, of particular relevance are the orbital properties of point-like particles around a central object (see [1, 2] for some recent reviews on the current experimental status of General Relativity).

Though the notion of point particles was very successful for the development and observational verification of the theory, their presence in a field theory of the metric leads to severe conceptual problems and technical inconsistencies. In particular, massive point particles should be seen as black holes or naked singularities, implying an ill definition of the metric at their location and an inherent difficulty in the use of perturbative methods for their description. In order to overcome this situation, Wheeler

G.J. Olmo (✉)
Departamento de Física Teórica and IFIC, Centro Mixto Universidad de Valencia - CSIC.
Universidad de Valencia, 46100 Burjassot, Valencia, Spain
e-mail: gonzalo.olmo@csic.es

G.J. Olmo
Departamento de Física, Universidade Federal da Paraíba,
João Pessoa, Paraíba 58051-900, Brazil

D. Rubiera-Garcia
Instituto de Astrofísica e Ciências do Espaço, Faculdade de Ciências, Universidade de Lisboa,
Campo Grande, 1749-016 Lisboa, Portugal
e-mail: drgarcia@fc.ul.pt

F.S.N. Lobo (ed.), *Wormholes, Warp Drives and Energy Conditions*,
Fundamental Theories of Physics 189, DOI 10.1007/978-3-319-55182-1_8

[3] addressed the notion of point particle from a field theory perspective introducing the concept of *geon*, abbreviation for "gravitational-electromagnetic entity," in an attempt to describe extended bodies as long-lived excitations of self-gravitating fields.

The first examples of geons that Wheeler considered were toroidal distributions of electromagnetic waves and spherical balls of light [3]. The combination of these ideas with the fact that Einstein's gravity only determines the local aspects of the gravitational field (the geometry) but does not restrict in any way its global properties (topology) soon led to the consideration of wormholes as mathematically admissible entities which could play a relevant role in combining gravitation with other branches of Physics (for a detailed account on the nature and properties of wormholes see [4]). In fact, Misner and Wheeler found [5] that free (sourceless) electric fields flowing through holes in the spacetime topology could engender pairs of massive particles with opposite charges. Those charges would be similar in all respects to elementary point particles, satisfying their own conservation laws, but without being associated to any mass or charge density. This is known as the *mass-without mass* and *charge-without charge* mechanisms.

Though within the framework of general relativity (GR) the electrically charged geons with wormhole structure envisioned by Misner and Wheeler are not possible [6, 7], they turn out to be rather common solutions in certain extensions of the theory. The main purpose of this chapter is thus to provide an overview of the results obtained in this context over the last 5 years or so.

Our starting point will be the consideration of gravitation as a geometric phenomenon, and geometry as something else than a mere theory of metrics. By working in a metric-affine geometric scenario, i.e., recognizing that metric and connection are logically and mathematically independent entities (see [8, 9] for some introductory material regarding metric-affine geometries), we will see that free electric fields (as well as other sources with similar algebraic properties) naturally engender wormholes. Given that these solutions represent self-gravitating fields, they can be naturally seen as geons in Wheeler's sense. In order to understand why and how metric-affine geometry is related with the emergence of wormholes, it will be very useful to have a brief look at the modern description of defects in ordered structures in condensed matter physics. This will also allow us to motivate the use of these geometries in gravitational scenarios.

The emergence of wormholes in self-gravitating electrovacuum configurations has a deep impact on the properties of the resulting spacetimes. In the models to be studied here, the central region of black holes and naked singularities is typically replaced by a wormhole. An immediate consequence of this is that geodesics become complete, thus implying that the resulting spacetime is nonsingular. As we will see, the completeness of geodesics is not necessarily tied to the absence of curvature divergences. Though this aspect is well known in applications such as those involving thin-shell wormholes [10, 11], it seems to have been overlooked in discussions about the problem of singularities in black hole scenarios. Part of our discussion will thus be aimed at clarifying the implications of this important point.

The content of this chapter is organized as follows: In Sect. 8.2 we introduce a treatment of metric-affine spaces in the context of ordered structures with defects in solid state physics, where it is shown that spaces with nonmetricity (associated to point defects) and torsion (associated to dislocations) are needed in order to describe properly such structures. This provides an empirical rather than purely theoretical motivation for the consideration of metric-affine geometries. Section 8.3 contains the bulk of our results, where we discuss the cases of $f(R)$ models, quadratic gravity, Born–Infeld gravity and higher dimensional generalizations. When such extensions of GR are considered in combination with electric fields, one finds a number of wormhole solutions, whose properties are discussed in detail. The main lesson of this section is that wormhole solutions are a generic feature of metric-affine geometries, that no violation of the energy conditions is needed, and that metric-affine geometries may provide valuable insights to go beyond GR. A summary of our results and some conclusions are presented in Sect. 8.4.

8.2 Microstructures, Holes, Metric-Affine Geometry, and Wormholes

An important result of Misner and Wheeler is the fact that charge and mass need not be idealized as properties of point particles, but rather can be seen as aspects of the interplay between the geometrical and topological structure of spacetime. This idea has strongly influenced current views on how the microcosmos could behave. Indeed, at the shortest scales, quantum effects could make spacetime fluctuate wildly in all manners of nontrivial topologies, yielding a dynamical microstructure able to engender pairs of virtual particles and other complex entities connected by wormholes. This microstructure is known as *spacetime foam*.

Though a system of the type suggested by the *spacetime foam* idea raises many questions, it is a useful exercise to focus attention on how a smooth, continuum spacetime may arise out of an underlying microstructure. In this respect, ordered structures such as Bravais crystals or graphene may provide useful information [12]. These systems possess a microscopic (discrete) structure which admits a continuum limit when the interatomic spacing is much smaller than the scale of the probe. The discreteness of the lattice and the existence of certain preferred (crystallographic) directions allow to introduce notions of distance and parallel transport in a straightforward manner. In the simplest scenarios (monatomic lattices with equal spacings between nearby atoms), distances can be measured by step counting, while parallel transport is defined by moving along the crystallographic directions. This provides intuitive notions of metric and connection at the level of the microstructure. It turns out that when the lattice contains defects, the resulting continuum description requires the use of independent metric and affine structures [13, 14]. This is so because dislocations (a type of one-dimensional defect) represent the discrete version of torsion [15–17], while interstitials and vacancies (types of point defects) break the

step-counting prescription for determining distances, thus involving some kind of nonmetricity [18]. The bottom line of this analysis is that the existence of a microstructure may require going beyond Riemannian geometry, where torsion and nonmetricity are frozen a priori by convention.

The existence of point defects in crystals generates local stresses due to the deformations of the lattice induced by missing atoms (vacancies) and/or interstitials. This type of defects may arise by thermal excitation or by the collision of neutrons with atoms in the lattice, see for instance [19]. The geometric description of the crystal in the continuum limit is carried out by considering a reference undefected configuration, $q_{\mu\nu}$, that is mapped into the physical one, $g_{\mu\nu}$, via mappings that specify the type and distribution of defects, $D_\mu{}^\nu$, or, in other words, $g_{\mu\nu} = D_\mu{}^\alpha q_{\alpha}$. The reference configuration is typically Euclidean or Riemannian with a well-defined parallel transport, $\nabla^\Gamma_\alpha q_{\mu\nu} = 0$, whereas the defected one involves independent metric and connection with a nonmetricity tensor, $Q_{\alpha\mu\nu} \equiv \nabla^\Gamma_\alpha g_{\mu\nu} \neq 0$.

It has been shown recently that extensions of general relativity in metric-affine spaces have an intimate correspondence with the kinematic description of crystals with point defects [20, 21]. It turns out that the role played by the density of point defects in crystals is analogous to that played by the energy–momentum tensor of the matter fields in the gravitational context. Both generate the nonmetricity tensor and define the deformation that relates the physical and reference (or auxiliary/undefected) metric.

This analogy or correspondence allows to interpret the emergence of wormholes in gravitational scenarios in a very natural way. On the one hand, the energy–momentum tensor of the matter fields generates gravitational attraction. On the other, the presence of a vacancy in a lattice induces a local deformation that brings nearby atoms around the hole closer to one another, which can be seen as an *attraction* effect. Now, in regions of very high stress-energy density, our analogy suggests that it should correspond to a high density of vacancies. Obviously, the maximum density of vacancies is achieved when many holes get together to form a large hole. But a large hole represents a region where the effective geometry is not defined, where no collective motion of the lattice atoms can occur. As we will see, this is analogous to what happens in the central regions of black holes and naked objects. Where the stress-energy density reaches its maximum values, a spherical portion of spacetime is missing. A wormhole has effectively been formed. Note that this kind of procedures has also been considered to construct wormholes in graphene layers described by gauge fields [22].

8.3 Analytical Models with Nonmetricity

In our presentation, we will focus on the effects of nonmetricity only, leaving aside the role of torsion. Nevertheless, our derivation of the field equations will be carried out allowing torsion to exist in the theory, even if we end up setting it to zero. This can be justified on simplicity grounds but also from a physical perspective. Following

our condensed matter analogy, we find that defects in crystals have dynamics and interactions. In fact, many point defects (associated to nonmetricity) may generate dislocations (torsion), and dislocations can disappear by the addition of interstitial atoms or the removal of more atoms. This means that a complete theory should consider the combined existence of both torsion and nonmetricity. If we focus on low-energy phenomena, one expects dislocations to arise as a result of the existence of many point defects (we do not consider the possibility of generating dislocations by other means such as traction or the application of external forces). Therefore, in a first approximation one can neglect the presence of torsion and just focus on nonmetricity as the simplest departure from a Riemannian structure.

8.3.1 *f(R) Theories with Nonlinear Electromagnetic Fields and Anisotropic Fluids*

For pedagogical convenience, we shall begin our discussion with perhaps the simplest extension of GR via modifications in the Lagrangian of the theory. This is described by an action of the form

$$S = \frac{1}{2\kappa^2}\int d^4x\sqrt{-g}f(R) + S_M(g_{\mu\nu}, \psi_m), \tag{8.1}$$

where $f(R)$ is a given function (unspecified at this stage) of the curvature scalar, $R \equiv g_{\mu\nu}R^{\mu\nu}$ (thus, GR would correspond simply to the choice $f(R) = R$). For the rest of the paper, the following definitions apply: κ^2 is Newton's gravitational constant in suitable units (in GR, $\kappa^2 = 8\pi G/c^3$), g is the determinant of the spacetime metric $g_{\mu\nu}$, which is a priori independent of the affine connection $\Gamma \equiv \Gamma^{\rho}_{\mu\nu}$ (Palatini approach), while $R_{\mu\nu} \equiv R^{\alpha}_{\mu\alpha\nu}$ is the Ricci tensor, which is constructed entirely out of the independent connection Γ, since it is defined from the Riemann tensor

$$R^{\alpha}{}_{\beta\mu\nu} = \partial_\mu\Gamma^{\alpha}_{\nu\beta} - \partial_\nu\Gamma^{\alpha}_{\mu\beta} + \Gamma^{\alpha}_{\mu\lambda}\Gamma^{\lambda}_{\nu\beta} - \Gamma^{\alpha}_{\nu\lambda}\Gamma^{\lambda}_{\mu\beta}\,, \tag{8.2}$$

without any need of lowering indexes with a metric. Finally, the matter sector, S_M, is assumed to depend on the metric [but not on the connection, for simplicity] and the matter fields are collective labeled by ψ_m.

The theory described by the action (8.1) has been extensively studied in the metric approach [23–26]. However, in order to implement the analogy between point defects and metric-affine geometries, here we perform independent variations of the action (8.1) with respect to metric and connection. This yields two systems of equations, namely

$$f_R R_{\mu\nu}(\Gamma) - \frac{f}{2}g_{\mu\nu} = \kappa^2 T_{\mu\nu}\,, \tag{8.3}$$

$$\nabla_\alpha\left[\sqrt{-g}f_R g^{\mu\nu}\right] = 0\,, \tag{8.4}$$

with the notation $f_R \equiv df/dR$, while $T_{\mu\nu} = \frac{2}{\sqrt{-g}}\frac{\delta S_M}{\delta g^{\mu\nu}}$ is the energy–momentum tensor of the matter. Let us point out that in this derivation one may assume vanishing torsion, $\Gamma^{\rho}_{[\mu\nu]} = 0$, and a symmetric Ricci tensor, $R_{[\mu\nu]} = 0$, though the result is independent of those assumptions due to the projective invariance of the theory [9]. To solve these equations the first point to be noted is that tracing with the metric $g^{\mu\nu}$ over the Eq. (8.3) one obtains

$$Rf_R - 2f = \kappa^2 T \ . \tag{8.5}$$

where $T \equiv g^{\mu\nu}T_{\mu\nu}$ is the trace of the energy–momentum tensor. This is not a differential equation, but just an algebraic one whose solution, $R = R(T)$, generalizes the linear relation $R = -\kappa^2 T$ of GR to $f(R)$ models. This relation implies that the curvature scalar can always be eliminated in favor of the matter sources and, consequently, that the connection Eq. (8.4) can be seen as algebraic and linear in the connection Γ. This means that one can rewrite (8.4) as

$$\nabla_\alpha \left[\sqrt{-h}h^{\mu\nu}\right] = 0 \ , \tag{8.6}$$

where the rank-two tensor $h_{\mu\nu}$ is defined as

$$h_{\mu\nu} \equiv f_R g_{\mu\nu} \ , \qquad h^{\mu\nu} \equiv \frac{1}{f_R} g^{\mu\nu} \ . \tag{8.7}$$

Equation (8.4) can be easily shown to be equivalent to $\nabla_\alpha h_{\mu\nu} = 0$, whose well-known solution is given by

$$\Gamma^{\lambda}_{\mu\nu} = \frac{h^{\lambda\alpha}}{2}\left(\partial_\mu h_{\alpha\nu} + \partial_\nu h_{\alpha\mu} - \partial_\alpha h_{\mu\nu}\right) \ . \tag{8.8}$$

which is nothing but the Christoffel symbols of the auxiliary metric $h_{\mu\nu}$. This is in agreement with the fact that nonmetricity, $Q_{\alpha\mu\nu} \equiv \nabla_\alpha g_{\mu\nu} = g_{\mu\nu}\nabla_\alpha \ln f_R(T) \neq 0$, is present in metric-affine spaces, which in turn is consistent with the discussion on defected ordered structures presented in Sect. 8.2 above. Moreover, this puts forward that the stress-energy density of the matter fields is the cause for nonvanishing nonmetricity, in analogy with the relation between nonmetricity and density of defects in crystals.

The introduction of the auxiliary metric $h_{\mu\nu}$ provides a natural strategy to solve the metric field equations. Contracting Eq. (8.3) with $h^{\mu\alpha}$ and using the transformations (8.7), one can write the field equations as

$$R^{\mu}{}_{\nu}(h) = \frac{1}{f_R^2}\left(\frac{f}{2}\delta^{\mu}{}_{\nu} + \kappa^2 T^{\mu}{}_{\nu}\right) \ , \tag{8.9}$$

where $R^{\mu}{}_{\nu}(h) = h^{\mu\alpha}R_{\alpha\nu}(\Gamma)$. Note that all the R-dependences on the right-hand side of the field equations (8.9) can be traded by T-dependences, i.e., the right-hand side

is entirely determined by the matter sources. These equations are manifestly second-order and, since the physical metric $g_{\mu\nu}$ is obtained through the set of algebraic transformations (8.7), which depend only on the matter [again because $f(R) \equiv f(R(T))$], the field equations for $g_{\mu\nu}$ are second-order as well. This way, once an $f(R)$ gravity is given, and a matter source S_M is specified, one can solve the field equations (8.9) for $h_{\mu\nu}$, and then transform it back to the metric $g_{\mu\nu}$ using (8.7).

This strategy proves itself adequate provided that one can find closed expressions for $f(R) \equiv f(R(T))$, which might not be straightforward. Otherwise, it is better to write the field equations directly for $g_{\mu\nu}$, which replaces (8.9) by

$$G_{\mu\nu}(g) = \frac{\kappa^2}{f_R} T_{\mu\nu} - \frac{Rf_R - f}{2f_R} g_{\mu\nu} - \frac{3}{2f_R^2}\left[\partial_\mu f_R \partial_\nu f_R - \frac{1}{2} g_{\mu\nu} (\partial f_R)^2\right] + \frac{1}{f_R}\left[\nabla_\mu \nabla_\nu f_R - g_{\mu\nu} \Box f_R\right] . \tag{8.10}$$

The advantage of this formulation of the field equations lies on the fact that they can be read off as GR-like field equations with a modified energy-matter source on the right-hand side [27]. In this formulation, it is also immediately seen that in vacuum, corresponding to $T^\mu{}_\nu = 0$, the field equations become

$$G_{\mu\nu}(g) = -\Lambda_{\mathit{eff}}\, g_{\mu\nu} , \tag{8.11}$$

which is nothing but GR with $\Lambda_{\mathit{eff}} \equiv (R_0 f_{R_0} - f_0)/2f_{R_0}$ (with $R_0 \equiv R(T = 0)$) playing the role of an effective cosmological constant [this same result could have been obtained from the field equations (8.9) as well]. This result highlights that only when a matter-energy source with a non-traceless energy–momentum tensor is considered, do modifications with respect to GR occur. This makes it pointless obtaining solutions sourced by standard electromagnetic (Maxwell) fields ("Reissner–Nordström-like"), as they would take exactly the same form as in the GR case. Nonetheless, we point out that nonlinear models of the electromagnetic field have been used for decades, in particular as a way to remove the divergence of the electron self-energy within classical electrodynamics through the Born–Infeld model [28], or as resulting from computing effective corrections from quantum electrodynamics upon Coulomb's field when the field intensity grows beyond a critical threshold [29]. In the context of GR, such nonlinear electrodynamics models have been widely used, both in order to modify the innermost and horizon structure of the Reissner–Nordström black hole [30–35], and to obtain singularity-free solutions [36–42].

The matter action of the nonlinear electrodynamics (NED) sector is written as

$$S_M = \frac{1}{8\pi} \int d^4x \sqrt{-g}\, \varphi(X, Y) , \tag{8.12}$$

where $\varphi(X, Y)$ is a given function of $X = -(1/2)F_{\mu\nu}F^{\mu\nu}$ and $Y = -(1/2)F_{\mu\nu}F^{*\mu\nu}$, which are the two field invariants that can be constructed out of the field strength

tensor, $F_{\mu\nu} = \partial_\mu A_\nu - \partial_\nu A_\mu$, and its dual, $F^{*\mu\nu} = \frac{1}{2}\varepsilon^{\mu\nu\alpha\beta}F_{\alpha\beta}$. The electromagnetic field equations follow from variation of the action (8.12) with respect to the vector potential A_μ, and are written as

$$\nabla_\mu \left(\varphi_X F^{\mu\nu} + \varphi_Y F^{*\mu\nu}\right) = 0 \,. \tag{8.13}$$

Restricting ourselves to electrostatic configurations, and assuming spherical symmetry, the only nonvanishing component of the field strength tensor is $F^{tr} \equiv E(r)$, and the field invariants satisfy

$$\varphi_X^2 X = \frac{q^2}{r^4} \,, \qquad Y = 0 \,, \tag{8.14}$$

where q is an integration constant that can be identified as an electric charge. This expression is particularly useful, because the NED energy–momentum tensor, which is obtained as

$$T^\mu{}_\nu = -\frac{1}{4\pi}\left[\varphi_X F^{\mu\alpha}F_{\alpha\nu} - \frac{\varphi}{2}\delta^\mu{}_\nu\right] \,, \tag{8.15}$$

becomes simply

$$T^\mu{}_\nu = \frac{1}{4\pi}\begin{pmatrix} \left(\frac{\varphi}{2} - X\varphi_X\right)\hat{I} & \hat{0} \\ \hat{0} & \frac{\varphi}{2}\hat{I} \end{pmatrix} \,, \tag{8.16}$$

where $\hat{I}$ and $\hat{0}$ represent the 2×2 identity matrix and zero matrix, respectively. Two aspects follow immediately from this expression. First, the trace of the energy–momentum reads

$$T = \frac{1}{2\pi}\left[\varphi - X\varphi_X\right] \,, \tag{8.17}$$

which vanishes for Maxwell electrodynamics, $\varphi(X) = X$. Second, the weak energy condition is fulfilled if the inequality

$$\rho = T^t{}_t = \frac{1}{8\pi}\left(2\varphi_X E^2 - \varphi(X, Y=0)\right) \geq 0 \,, \tag{8.18}$$

is satisfied.

The above discussion completes the formalism of metric-affine $f(R)$ gravity coupled to nonlinear electrodynamics. To proceed further and obtain solutions we have to choose a particular $\varphi(X, Y)$ function. In this sense, Born–Infeld electrodynamics is a natural and well-motivated candidate due to the fact that (i) it yields a finite energy for a point-like charge in flat spacetime, (ii) it is free of birefringence phenomena [43, 44] [indeed, together with Maxwell, it is the only electrodynamics with such a property] and (iii) arises in the low-energy limit of string/D-brane physics [45–49]. Born–Infeld electrodynamics is given by the action

$$\varphi_{BI}(X) = 2\beta^2 \left(1 - \sqrt{1 - \frac{X}{\beta^2} - \frac{Y^2}{4\beta^4}}\right) , \tag{8.19}$$

where β is the so-called Born–Infeld parameter, which controls the deviation with respect to Maxwell electrodynamics, namely, $\lim_{\beta\to\infty} \varphi_{BI} \simeq X$. For this theory, the field invariant X reads as $X = \frac{q^2\beta^2}{q^2+r^4\beta^2}$, and thus Maxwell electrodynamics is also recovered for far distances, $r \gg 0$.

Let us consider a simple $f(R)$ model given by $f(R) = R - \gamma R^2$, where γ is a constant. For this model, the trace equation (8.5) yields $R = -\kappa^2 T$, which is the same result as in GR. Now, inserting (8.16) with the definition (8.19) into the field equations (8.9), a straightforward but lengthly calculation, which involves using the conformal transformations (8.7), yields the static, spherically symmetric spacetime (full details of this calculation can be found in Ref. [50]):

$$ds^2 = -A(x)dt^2 + \frac{1}{A(x)f_R^2}dx^2 + z^2(x)d\Omega^2 , \tag{8.20}$$

where the function $A(x)$ satisfies

$$A(x) = \frac{1}{f_R}\left(1 - \frac{1 + \delta_1 G(z)}{\delta_2 z f_R^{1/2}}\right) , \tag{8.21}$$

and we have introduced the dimensionless radial function $z = r/r_c$, with $r_c \equiv (4\pi)^{1/4}\sqrt{r_q l_\beta}$, while $r_q^2 = \kappa^2 q^2/(4\pi)$ is the charge radius and $l_\beta^2 = 1/(\kappa^2\beta^2)$ the Born–Infeld length. The constants δ_1 and δ_2 characterizing the solutions are given by

$$\delta_1 = 2(4\pi)^{3/4}\frac{r_q}{r_S}\sqrt{\frac{r_q}{l_\beta}} \ , \ \delta_2 = \frac{r_c}{r_S} , \tag{8.22}$$

while the function $G(z)$ in (8.21) satisfies

$$\frac{dG}{dz} = \frac{z^2}{4f_R^{3/2}}\left(\tilde{f} + \frac{\tilde{\varphi}}{4\pi}\right)\left(f_R + \frac{z}{2}f_{R,z}\right) , \tag{8.23}$$

with the following definitions and expressions

$$\tilde{f} \equiv l_\beta^2 f = \frac{\eta(z)}{2\pi}\left(1 - \frac{\alpha}{2}\eta(z)\right) , \tag{8.24}$$

$$f_R = 1 - \alpha\eta(z) , \tag{8.25}$$

$$\tilde{\varphi}(z) = 2\left(1 - \frac{1}{\sqrt{1 + 1/z^4}}\right) , \tag{8.26}$$

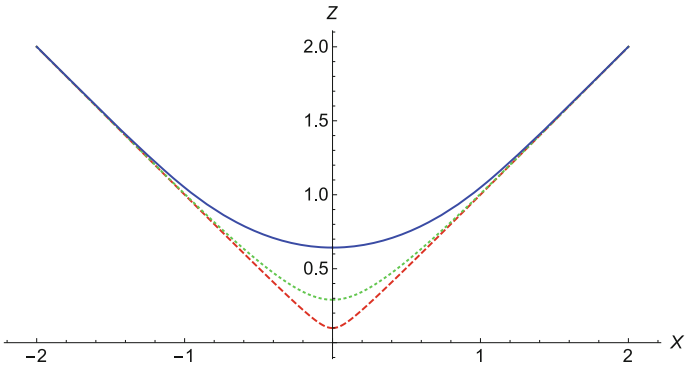

Fig. 8.1 Behavior of the radial function $z(x)$ for $\alpha = 10^{-2}$ (*dashed red*), $\alpha = 10^{-1}$ (*green dotted*) and $\alpha = 1$ (*solid blue*), with the two asymptotically flat regions, $z \simeq |x|$, and the wormhole throat, $z = z_c$ ($x = 0$). When $\alpha = 0$ the wormhole throat closes and the GR point-like singularity is recovered

$$\eta(z) = \frac{\left(z^2 - \sqrt{1+z^4}\right)^2}{z^2\sqrt{1+z^4}}\,, \tag{8.27}$$

with $\alpha \equiv \gamma/(2\pi l_\beta^2)$. The spacetime described by the line element (8.20) with the definitions above corresponds to a modification of the Reissner–Nordström solution of the Einstein–Maxwell field equations, to which the metric reduces for far distances, $r \gg r_c$. However, as the region $r = r_c$ is approached a number of relevant modifications occur. The most important one comes from the behavior of the radial function, which is implicitly defined as $x^2 = z^2 f_R$. This expression can be numerically inverted and the result is plotted in Fig. 8.1, where we see the distinctive features of a wormhole geometry, namely, the existence of two asymptotically flat regions (where $z^2 \simeq x^2$ approaches the GR behavior) and the attainment of a minimum for the radial function given by

$$z_c(\alpha) = \frac{1 + 2\alpha - \sqrt{1+4\alpha}}{2\sqrt{1+4\alpha}}\,, \tag{8.28}$$

at which $z(x)$ bounces off to a different region of spacetime.

The spherical surface of area $S(z_c) = 4\pi z_c^2(\alpha)$ represents the throat of the wormhole, where the Kretchsman curvature invariant behaves as

$$K \sim \frac{1}{(z - z_c)^2}\,. \tag{8.29}$$

Despite the divergence of this scalar at the wormhole throat [we point out that such divergences are much milder than in the RN case, $\sim 1/r^8$, and that in Born–Infeld electrodynamics in the context of GR, $\sim 1/z^4$] we want to investigate the implications

of such divergences on the regularity of the geometry. In this sense, we note that in the formulation of the singularity theorems no reference to curvature divergences is made but, instead, use is made of the concept of geodesic completeness, namely, whether any geodesic curve can be extended to arbitrary large values of the affine parameter or not [51–53]. This is physically relevant because time-like geodesics are associated to idealized observers, while null geodesics are associated to light rays and the transmission of information [we leave aside from this discussion space-like geodesics, because no object in Nature is known to move on such geodesics]. Since it seems reasonable to impose the principle that in Nature *nothing can suddenly cease to exist* and that *nothing can emerge from nowhere*, thus a consistent description of spacetime should meet the completeness of all null and time-like geodesics.

A geodesic curve $\gamma^\mu = x^\mu(\lambda)$, where λ is the affine parameter, satisfies the equation (see, e.g., [54] for a detailed account on this topic)

$$\frac{d^2x^\mu}{d\lambda^2} + \Gamma^\mu_{\alpha\beta}\frac{dx^\alpha}{d\lambda}\frac{dx^\beta}{d\lambda} = 0\,. \tag{8.30}$$

For the analysis of the geodesic equation we recall that in the action (8.1) the matter does not couple to the connection, which implies the conservation of the energy–momentum tensor with respect to the covariant derivative defined with the Christoffel symbols of the metric (the Levi-Civita connection), namely $\nabla^g_\mu T^{\mu\nu} = 0$. The physical interpretation of this statement is that, following Einstein's equivalence principle, test particles should move on geodesics of the metric $g_{\mu\nu}$ and, for that reason, we shall consider the connection compatible with it (i.e., the Levi-Civita connection of $g_{\mu\nu}$).

For our purposes, it is better to rewrite the geodesic equation (8.30) in terms of the unit vector $u^\mu = dx^\mu/d\lambda$ [which satisfies $u_\mu u^\mu = -k$, where $k = 0, 1, -1$ for null, time-like, and space-like geodesics, respectively], which reads

$$\frac{du^\mu}{d\lambda} + \Gamma^\mu_{\nu\sigma}u^\nu u^\sigma = 0\,. \tag{8.31}$$

Taking advantage of the spherical symmetry of our problem, without loss of generality we can rotate the coordinate system to make it coincide with the plane $\theta = \pi/2$, which greatly simplifies the problem. In addition, we can identify two conserved quantities, namely, $E = A^{-1}dt/d\lambda$ and $L = r^2 d\varphi/dr$ (see [55] for a Hamiltonian derivation of this result). For time-like geodesics these quantities carry the meaning of the total energy per unit mass and angular momentum per unit mass around an axis normal to the plane $\theta = \pi/2$, respectively. This interpretation is not possible for null geodesics but, following [54], we can see E/L as an apparent impact parameter as seen from an observer at asymptotic infinity.

Under these conditions, the geodesic equation (8.31) for the line element (8.20) becomes [we point out that this formula is valid for any $f(R)$ gravity model under the assumptions of spherical symmetry and source symmetry $T^t{}_t = T^r{}_r$]

$$\frac{d\tilde{\lambda}}{dz} = \pm \frac{f_R^{1/2}\left(1+\frac{zf_{R,z}}{2f_R}\right)}{\sqrt{E^2 f_R^2 - A(z) f_R\left(k+\frac{L^2}{r_c^2 z^2}\right)}}\,, \tag{8.32}$$

where we have redefined $\tilde{\lambda} \equiv \lambda/r_c$, by convenience. Using the explicit expressions for the metric functions defined in (8.20) one can numerically integrate the geodesic equation on each case. Far from the center, $r \gg r_c$, one obtains the same behavior as in GR, $\tilde{\lambda} \approx z$, which is consistent with the recovery of the Reissner–Nordström solution at far distances. Deviations will arise around the wormhole throat, $z = z_c(\alpha)$, where expansions of the metric for radial null geodesics ($k = L = 0$) allow to integrate the geodesic equation as

$$E\tilde{\lambda}(z) \simeq \mp \frac{2z_c}{a^{1/2}(z-z_c)^{1/2}}. \tag{8.33}$$

It is immediately seen that the affine parameter can be indefinitely extended in the wormhole throat region, which means that these geodesics are complete [see Fig. 8.2]. This is in sharp contrast with the GR result, where radial null geodesics get to $r = 0$ in finite affine time, hence they are incomplete. A similar analysis for radial geodesics with angular momentum ($k = 0, L \neq 0$), for time-like geodesics, $k = 1$, and space-like geodesics, $k = -1$, would show that these geodesics are complete as well. This implies that these wormhole geometries are null, time-like and space-like geodesically complete, no matter the behavior of the curvature scalars at the wormhole throat. It is worth pointing out that null geodesics would take an infinite affine time to reach the wormhole, which means that the latter lies in the future (or past) boundary of the spacetime.

We point out that the completeness of geodesics in this model is an effect entirely due to the gravitational sector, and not stick to the particularly nice properties of Born–Infeld electrodynamics. To check this, let us consider the case of an anisotropic fluid of the form

$$T^{\mu}{}_{\nu} = \text{diag}[-\rho, P_r, P_\theta, P_\varphi] = \text{diag}[-\rho, -\rho, \alpha\rho, \alpha\rho]\,, \tag{8.34}$$

where α is a constant, constrained as $0 \leq \alpha \leq 1$ in order for the energy conditions to be satisfied [note that for $\alpha = 1$, then Eq. (8.34) has the same structure as that of a Maxwell field], and the conservation equation of the fluid in a spherically symmetric spacetime implies that $\rho(x) = C/r(x)^{2+2\alpha}$, where C is a constant with dimensions. Using the same model $f(R) = R - \gamma R^2$ one can solve the combined system of gravitational field and anisotropic fluid, and after some algebra obtain the solution [56]

$$ds^2 = \frac{1}{f_R}\left(-B(x)dt^2 + \frac{1}{B(x)}dx^2\right) + r^2(x)d\Omega^2\,, \tag{8.35}$$

$$B(z) = 1 - \frac{1+\delta_1 G(z)}{\delta_2 z f_R^{1/2}}\,, \tag{8.36}$$

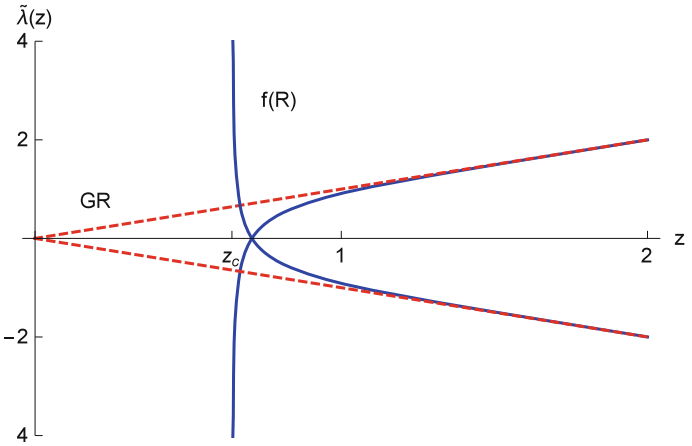

Fig. 8.2 The affine parameter $\lambda(x)$ as a function of the radial coordinate x for ingoing and outgoing radial null geodesics (*solid blue lines*) of the model $f(R) = R - \gamma R^2$ coupled to Born–Infeld electrodynamics. Note the completeness of these geodesics, as opposed to the GR case (*dashed red lines*)

$$G_z = \frac{\left(1 + \frac{\alpha}{z^{2+2\alpha}}\right)}{z^{2\alpha} f_R^{3/2}} \left[\frac{1}{1-\alpha} - \frac{1}{2z^{2+2\alpha}}\right], \tag{8.37}$$

with the definitions $r = r_c z$ and $r_c^{2+2\alpha} \equiv (4\gamma)\kappa^2(1-\alpha)C$. At far distances one recovers the GR solution, namely, $G_\alpha^{GR}(z) = \frac{z^{1-2\alpha}}{(1-\alpha)(1-2\alpha)}$. Like in the case of nonlinear electrodynamics above, the presence of a wormhole structure follows from the relation $x^2 = r(x)^2 f_R$, which implies the existence of a bounce for any value of α, which is similar to that found in Fig. 8.1. In addition, an analysis of geodesics in these spacetimes yields a very similar representation of radial null geodesics as that depicted in Fig. 8.2, as well as the completeness of all null and time-like geodesics.

In this section, we have considered the case of $f(R)$ theories for their conceptual and mathematical simplicity, and have verified with two different matter sources that wormholes may arise and yield geodesically complete spacetimes. Nonetheless, a more detailed analysis is needed to extend the framework to more general cases and to get further into the properties of these wormholes.

8.3.2 *Quadratic Gravity with Maxwell and Born–Infeld Electrodynamics*

The quantization of fields in curved spacetimes states that a high-energy completion of GR would involve higher order powers in the curvature scalars, where each contribution would be suppressed by some fundamental length scale [57, 58]. This is in

agreement with the description made by some fundamental approaches to quantum gravity in their low-energy regime [59] and with the effective lagrangians picture in gravitational physics [60]. In this section, we shall stick ourselves to quadratic Lagrangians and, in particular, to those constructed as general functions $f(R, Q)$ of the curvature scalars $R \equiv g_{\mu\nu}R^{\mu\nu}$ and $Q \equiv g_{\mu\alpha}g_{\nu\beta}R^{\alpha\beta}R^{\mu\nu}$. Note that there is no need to include the Kretchsmann scalar, $K = R^{\alpha}{}_{\beta\gamma\delta}R_{\alpha}{}^{\beta\gamma\delta}$, since it can be always rewritten in terms of the other two invariants using the Gauss–Bonnet term, which becomes a topological invariant in four spacetime dimensions and thus it does not contribute to the field equations [61]. These quadratic models represent a natural generalization of the $f(R)$ theories considered in previous section.

The action is thus given by

$$S[g, \Gamma, \psi_m] = \frac{1}{2\kappa^2}\int d^4x\sqrt{-g}f(R, Q) + S_M[g, \psi_m]\,, \tag{8.38}$$

with the same definitions and notation as in the previous section. Performing independent variations of the action (8.38) with respect to metric and connection yields the result[1]

$$f_R R_{\mu\nu} - \frac{f}{2}g_{\mu\nu} + 2f_Q R_{\mu\alpha}R^{\alpha}{}_{\nu} = \kappa^2 T_{\mu\nu}\,, \tag{8.39}$$

$$\nabla_\beta\left[\sqrt{-g}\left(f_R g^{\mu\nu} + 2f_Q R^{\mu\nu}\right)\right] = 0\,, \tag{8.40}$$

where $f_X \equiv df/dX$. Now, defining a matrix $P_{\mu}{}^{\nu} \equiv R_{\mu\alpha}g^{\alpha\nu}$ we can express (8.39) as

$$2f_Q\hat{P}^2 + f_R\hat{P} - \frac{f}{2}\hat{I} = \kappa^2\hat{T}\,, \tag{8.41}$$

where a hat denotes a matrix. Like in the $f(R)$ case, Eq. (8.41) represents an algebraic equation whose solution, $\hat{P} = \hat{P}(\hat{T})$ allows us to express $\hat{P}$ as a function of the matter. From the fact that R and Q are given by the trace of $\hat{P}$ and $\hat{P}^2$, respectively, this means that the function $f(R, Q)$ can be explicitly eliminated in favor of the matter sources as well. Proceeding further, we introduce a new rank-two tensor $h_{\mu\nu}$ satisfying the equation $\nabla_\beta\left[\sqrt{-h}h^{\mu\nu}\right] = 0$ [note that this strategy is exactly the same as in $f(R)$ theories above], so identifying it with Eq. (8.40) and using a bit of algebra we obtain the result

$$\hat{h}^{-1} = \frac{\hat{g}^{-1}\hat{\Sigma}}{\sqrt{\det\hat{\Sigma}}}\,, \qquad \hat{h} = \left(\sqrt{\det\hat{\Sigma}}\right)\hat{\Sigma}^{-1}\hat{g}\,, \tag{8.42}$$

[1] We point out that, like in the $f(R)$ case above, these equations are derived assuming a symmetric connection and Ricci tensor. For full details on the derivation of the field equations when such constraints are removed, see [62].

where we have introduced the matrix $\hat{\Sigma} = \left(f_R \hat{I} + 2 f_Q \hat{P}\right)$. Finally, we write (8.39) in terms of P as $\hat{P}\hat{\Sigma} = \frac{f}{2}\hat{I} + \kappa^2 \hat{T}$, and considering the object $P_\mu{}^\alpha \Sigma_\alpha{}^\nu = R_{\mu\alpha} h^{\alpha\nu} \sqrt{\det \hat{\Sigma}}$ [where we have used relations (8.42)], one finds that the metric field equations (8.39) can be written as

$$R^\mu{}_\nu(h) = \frac{1}{\sqrt{\det \hat{\Sigma}}} \left(\frac{f}{2} \delta^\mu{}_\nu + \kappa^2 T^\mu{}_\nu \right) , \tag{8.43}$$

where $T^\mu{}_\nu \equiv T_{\mu\alpha} g^{\alpha\nu}$. Several considerations are in order. First, such as in the $f(R)$ case, (8.43) represents a set of second-order equations for the metric $h_{\mu\nu}$ where all the objects on the right-hand side are purely functions of the matter sources. As the metric $g_{\mu\nu}$ follows from the algebraic relations (8.42), which only depend on the matter fields, the field equations for $g_{\mu\nu}$ will be second-order as well. Second, in vacuum, $T^\mu{}_\nu = 0$, one has $h_{\mu\nu} = g_{\mu\nu}$ [modulo a constant reescaling factor] and the field equations (8.43) boil down to those of GR with possibly a cosmological constant term, depending on the Lagrangian $f(R, Q)$ chosen. Finally, we point out that, as opposed to the $f(R)$ case, where only the trace of the energy–momentum tensor played a role, now the consideration of traceless energy-matter sources do excite the modified gravitational dynamics present in the theory.

The last statement allows us to use in this case a standard (Maxwell) electromagnetic field. This will provide a natural generalization of the Reissner–Nordström spacetime of GR. Thus, the energy–momentum tensor follows from Eq. (8.16) as

$$T^\mu{}_\nu = \frac{q^2}{8\pi r^4} \begin{pmatrix} -\hat{I} & \hat{0} \\ \hat{0} & \hat{I} \end{pmatrix} . \tag{8.44}$$

Next, we need to specify a $f(R, Q)$ Lagrangian. For simplicity we consider a quadratic Lagrangian of the form

$$f(R, Q) = R + l_\varepsilon^2 (a R^2 + Q) , \tag{8.45}$$

where l_ε is some length scale encoding the deviations from GR and a is a dimensionless constant. This choice has the advantage that the traces of $\hat{P}$ and $\hat{P}^2$ in Eq. (8.41) yield $R = -\kappa^2 T$ [which is the same result as in GR] and $Q = \tilde{\kappa}^4 q^4 / r^8$, where $\tilde{\kappa}^2 \equiv \kappa^2/(4\pi)$. For the theory (8.45), a bit of algebra allows to cast the field equations (8.43) for this matter source as

$$R^\mu{}_\nu(h) = \frac{\tilde{\kappa}^2 q^2}{2 r^4} \begin{pmatrix} -\frac{1}{\sigma_+} \hat{I} & \hat{0} \\ \hat{0} & \frac{1}{\sigma_-} \hat{I} \end{pmatrix} , \tag{8.46}$$

where we have introduced the important objects

$$\sigma_\pm = 1 \pm \frac{\tilde{\kappa}^2 q^2 l_\varepsilon^2}{r^4} \,. \tag{8.47}$$

To solve the field equations (8.43) we proceed as follows. Two line elements are introduced with the assumptions of staticity and spherical symmetry, one for $h_{\mu\nu}$

$$d\tilde{s}^2 = -C(x)e^{2\psi(x)}dt^2 + \frac{1}{C(x)}dx^2 + x^2 d\Omega^2 \,. \tag{8.48}$$

and another for $g_{\mu\nu}$

$$ds^2 = -A(x)e^{2\Psi(x)}dt^2 + \frac{1}{A(x)}dx^2 + r^2(x)d\Omega^2 \,. \tag{8.49}$$

Because of the structure of the energy–momentum tensor, $T_x{}^x = T_t{}^t$, which follows from the energy–momentum tensor (8.44), one can set $\psi(x) = 0$ without loss of generality. The remaining function, $C(x)$, in (8.48), follows from the resolution of Eq. (8.46), and transforming the result back to the metric $g_{\mu\nu}$ using the set of relations (8.42) (we refer the reader to Refs. [63–65] for full details of this derivation), we obtain the geometry [in Eddington–Filkenstein coordinates]

$$ds^2 = -A(x)dv^2 + \frac{2}{\sigma_+}dvdx + r^2(x)d\Omega^2 \,, \tag{8.50}$$

where the metric functions are given by the expressions

$$A(x) = \frac{1}{\sigma_+}\left[1 - \frac{r_S}{r}\frac{(1+\delta_1 G(r))}{\sigma_-^{1/2}}\right] \,, \tag{8.51}$$

$$\delta_1 = \frac{1}{2r_S}\sqrt{\frac{r_q^3}{l_\varepsilon}} \,, \tag{8.52}$$

$$\sigma_\pm = 1 \pm \frac{r_c^4}{r^4(x)} \,, \tag{8.53}$$

$$\left(\frac{dr}{dx}\right)^2 = \frac{\sigma_-}{\sigma_+^2} \,, \tag{8.54}$$

with the following definitions: $r_c = \sqrt{l_\varepsilon r_q}$ is a constant determining the size of the corrections, which are controlled both by the charge radius $r_q^2 = 2G_N q^2$ and the length scale l_ε appearing in the Lagrangian (8.45), and $M_0 = r_S/2$ is Schwarzschild mass. The function $G(z)$, which comes from integration of the field equations as $G_z = \frac{\sigma_+}{z^2\sigma_-^{1/2}}$, can be integrated and expressed as an infinite power series expansion of the form

$$G(z) = -\frac{1}{\delta_c} + \frac{1}{2}\sqrt{z^4 - 1}\left[f_{3/4}(z) + f_{7/4}(z)\right] \,, \tag{8.55}$$

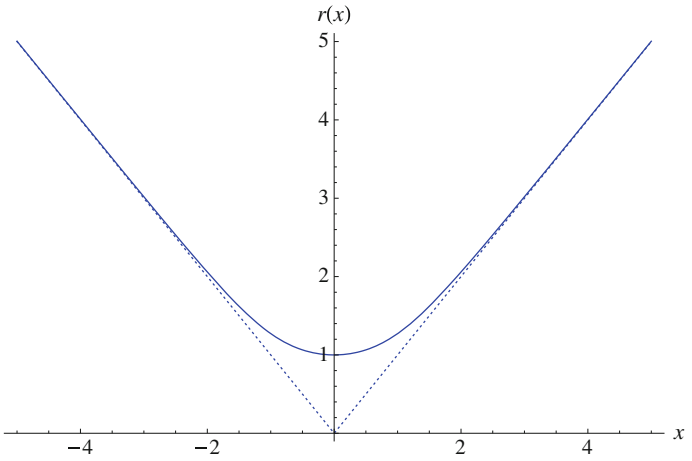

Fig. 8.3 Behavior of the radial function $r(x)$ in Eq. (8.57) (*solid line*) in units of r_c, as compared to the GR result, $r(x) \simeq |x|$ (*dashed*), with the bounce at $r = r_c = 1$, where the wormhole throat is located

where $f_\lambda(z) = {}_2F_1[\frac{1}{2}, \lambda, \frac{3}{2}, 1 - z^4]$ is a hypergeometric function, and $\delta_c \approx 0.572069$ is a constant. Expanding the metric $A(z(x))$ in series of $z \gg 1$, where $G(z) \approx -1/z$ [and $\sigma_\pm \approx 1$, $r^2(x) \approx x^2$], yields the result

$$A(x) \approx 1 - \frac{r_S}{r} + \frac{r_q^2}{2r^2} \,, \tag{8.56}$$

which is nothing but the standard Reissner–Nordström solution of GR. This way, we obtain a spacetime that far from the center looks like the GR counterpart [similarly as in the $f(R)$ with nonlinear electrodynamics above], but as we approach the region $z = 1$, large deviations occur. This follows from the fact that the radial function $r(x)$ in Eq. (8.54) can be explicitly written as

$$r(x)^2 = \frac{x^2 + \sqrt{x^4 + 4r_c^4}}{2} \,. \tag{8.57}$$

and it is plotted in Fig. 8.3. As can be seen there, the behavior of the radial function is distinctive of a wormhole geometry, with a bounce occurring at $r = r_c$, where the radial function reaches a minimum and re-expands.

The geometry behaves around the wormhole throat $r = r_c$ as

$$\lim_{r \to r_c} A(x) \approx \frac{N_q}{4N_c} \frac{(\delta_1 - \delta_c)}{\delta_1 \delta_c} \sqrt{\frac{r_c}{r - r_c}} + \frac{N_c - N_q}{2N_c} + O\left(\sqrt{r - r_c}\right) \,, \tag{8.58}$$

where $N_q = q/e$ is the number of charges and $N_c \equiv \sqrt{2/\alpha_{em}} \simeq 16.55$ (where α_{em} is the fine structure constant) is the critical number of charges (see below for its role). It is clear that the behavior in this region is governed by the charge-to-mass ratio, δ_1, as compared to the critical value, δ_c. Indeed, this ratio governs the horizon structure as well, according to the following characterization [63]:

- If $\delta_1 > \delta_c$ the solutions may have two, one (degenerate) or no horizons, depending on the number of charges N_q. This resembles the standard structure of the Reissner–Nordström solution of GR.
- If $\delta_1 < \delta_c$ a single horizon exist on each side of the wormhole for any value of N_q, which makes this case similar to the Schwarzschild solution of GR.
- If $\delta_1 = \delta_c$ we find a single horizon for $N_q > N_c$, which disappears when $N_q < N_c$.

It should be noted that the above description takes place on one of the sides of the wormhole throat. Nonetheless, a similar description takes place on the other side of the wormhole, due to the symmetry of our scenario.

It is instructive to investigate what is the behavior of the curvature at the wormhole throat itself. Focusing only on the Kretchsman scalar, $K \equiv R^{\alpha}{}_{\beta\mu\nu} R_{\alpha}{}^{\beta\mu\nu}$, one gets the result

$$\begin{aligned} r_c^4 K \approx & \left(16 + \frac{88\delta_1^2}{9\delta_2^2} - \frac{64\delta_1}{3\delta_2}\right) + O(z-1) + \ldots \\ & + \left(1 - \frac{\delta_1^*}{\delta_1}\right)\left[\frac{2(2\delta_1 - 3\delta_2)}{3\delta_2^2 (z-1)^{3/2}} + O\left(\frac{1}{\sqrt{z-1}}\right)\right] \\ & + \left(1 - \frac{\delta_1^*}{\delta_1}\right)^2 \left[\frac{1}{4\delta_2^2 (z-1)^3} + O\left(\frac{1}{(z-1)^2}\right)\right], \end{aligned} \tag{8.59}$$

which is divergent if $\delta_1 \neq \delta_c$ and finite otherwise [similar results are obtained from computation of other curvature scalars]. One thus would be tempted to regard the former case as singular, and the latter as regular. As we already know from the discussion of the $f(R)$ case above, this is not necessarily true.

Before going that way we note that the wormhole picture can be made very robust by investigating other of its properties. First, one can wonder what is the nature of the sources that generate the charge q and the mass M_0 in the geometry. In the case of GR, the assumption that a point-like particle located at the center of the solution is generating the charge and mass of the whole geometry proves mathematically impossible. Indeed, there is no well-defined source able to generate the Reissner–Nordström solution while satisfying the Einstein equations everywhere, a well-known problem in the context of GR [66] due to the fact that such sources would be concentrated in a point of zero volume (the singularity). Nonetheless, following Misner and Wheeler's reasoning, the existence of a finite-size wormhole offers other possibilities. Indeed, a computation of the electric flux flowing through an S^2 surface enclosing one of the wormhole mouths yields the result

$$\Phi = \frac{1}{4\pi}\int_{\mathscr{S}} *F = q\ , \tag{8.60}$$

where $*F$ is the two-form dual to Faraday's tensor. Note that a similar computation on the other side of the wormhole throat would yield the result $-q$ due to the opposite orientation of the normal on that side. This implies that the wormhole is able to generate an electric charge from a sourceless electromagnetic field despite the fact that no point-like charges are present in the system (which is consistent with the fact that they are not explicitly included in the matter sector of the action defining our model). This result, which is a particular realization of Wheeler's charge-without-charge mechanism, is a very primitive concept arising from purely topological considerations and, as such, is not affected by the existence of large metric fluctuations or curvature divergences. Moreover, this flux satisfies the striking property that the density of lines of force crossing the spherical wormhole throat, which is given by

$$\frac{\Phi}{4\pi r_c^2} = \frac{q}{r_c^2} = \sqrt{2\frac{c^7}{(\hbar G)^2}}\ , \tag{8.61}$$

turns out to be a universal constant, not depending on the amounts of mass and charge present in the system, but just on fundamental constants. This implies that local disturbances in the metric will not affect this density, which is a purely topological effect.

To investigate the origin of mass in these solutions we make use of the fact that the coordinate x covers the entire geometry on both sides of the wormhole throat, so we compute the total gravitational + electromagnetic mass of the solutions as

$$\begin{aligned} S &= \frac{1}{2\kappa^2}\int d^4x\sqrt{-g}(R - \frac{l_\varepsilon^2}{2}R^2 + l_\varepsilon^2 Q) + \frac{1}{8\pi}\int d^4x\sqrt{-g}\varphi \\ &= -\int d^4x\sqrt{-g}T_t^t\sigma_+\ , \end{aligned} \tag{8.62}$$

and performing the integration in terms of the coordinate $dx^2 = dz^2/\sigma_-$, a little bit of algebra yields the result

$$S = 2Mc^2\frac{\delta_1}{\delta_c}\int dt\ , \tag{8.63}$$

which is nothing but the action of a point-like particle at rest with mass $M_0\delta_1/\delta_c$! As we see, the charge-to-mass ratio influences the total mass of the spacetime, but not its origin, in a explicit realization of Wheeler's mass-without-mass mechanism. This way, a sourceless electromagnetic field is able, via a nontrivial topological structure, to give both charge and mass to the spacetime.

Having implemented the charge-without-charge and mass-without-mass mechanisms, we turn now to the question of what is the meaning of curvature divergences in our models, since neither the wormhole structure nor its associated properties

feel any qualitative difference between those cases showing curvature divergences ($\delta_1 \neq \delta_c$) and those where such divergences are removed ($\delta_1 = \delta_c$). As discussed in the previous section, the most generally accepted criterion to determine when a spacetime is singular or not is given by geodesic completeness. Proceeding like in the $f(R)$ case, we consider the geodesic equation (8.30) written in terms of the geodesic vector as in Eq. (8.30), and replace there the line element (8.50), which yields the result

$$\frac{1}{\sigma_+^2}\left(\frac{dx}{d\lambda}\right)^2 = E^2 - A\left(\kappa + \frac{L^2}{r^2(x)}\right) , \tag{8.64}$$

with the same notations, but with the new radial function $r(x)$ defined as in Eq. (8.54). Rescaling the radial coordinate as $dy = dx/\sigma_+$, Eq. (8.64) can be seen as a single differential equation akin to that of a particle moving in a potential of the form

$$V(x) = A\left(\kappa + \frac{L^2}{r^2(x)}\right) . \tag{8.65}$$

For null $k = 0$, radial, $L = 0$, geodesics, Eq. (8.64) admits an analytic integration of the form

$$\pm E \cdot \lambda(x) = \begin{cases} {}_2F_1[-\frac{1}{4}, \frac{1}{2}, \frac{3}{4}; \frac{r_c^4}{r^4}]r & \text{if } x \geq 0 \\ \\ 2x_0 - {}_2F_1[-\frac{1}{4}, \frac{1}{2}, \frac{3}{4}; \frac{r_c^4}{r^4}]r & \text{if } x \leq 0 \end{cases} , \tag{8.66}$$

where ${}_2F_1[a, b, c; y]$ is a hypergeometric function, and we have introduced the constant $x_0 = {}_2F_1[-\frac{1}{4}, \frac{1}{2}, \frac{3}{4}; 1] \simeq 0.59907$. The behavior of these geodesics is plotted in Fig. 8.4. There we see that null geodesics extend through the wormhole throat, where the geometry is significantly modified as compared to GR, and can be extended to arbitrary large values of the affine parameter. In GR, these geodesics reach the point $r = 0$, and cannot be further extended because $r > 0$, hence, they are incomplete. In our case, radial geodesics with nonvanishing angular momentum, $k = 0, L \neq 0$ and time-like geodesics for Reissner–Nordström-like configurations ($\delta_1 > \delta_c$) are prevented from reaching the wormhole due to fact that they find an infinite potential wall, similarly as what happens in the standard Reissner–Nordström solution of GR. But in those solutions with $\delta_1 < \delta_c$ (which always have a single horizon), both null and time-like geodesics may reach the wormhole and cross it, similarly as in the case of $\delta_1 = \delta_c$, where geodesics with enough energy can go through the wormhole.

Therefore, we have arrived to the conclusion that these spacetimes are null and time-like geodesically complete, no matter the behavior of curvature scalars at the wormhole throat. Nonetheless, the fact that such divergences may imply the existence of infinitely large tidal forces acting upon physical (extended) objects crossing the wormhole throat, requires a separate analysis. In this sense, one can make use of the methods developed by Tipler [67, 68], Krolak [69, 70] and Nolan [71], among others, which are based on the modelization of physical observers in terms of a congruence of geodesics. At a given point, an invariant volume can be attributed

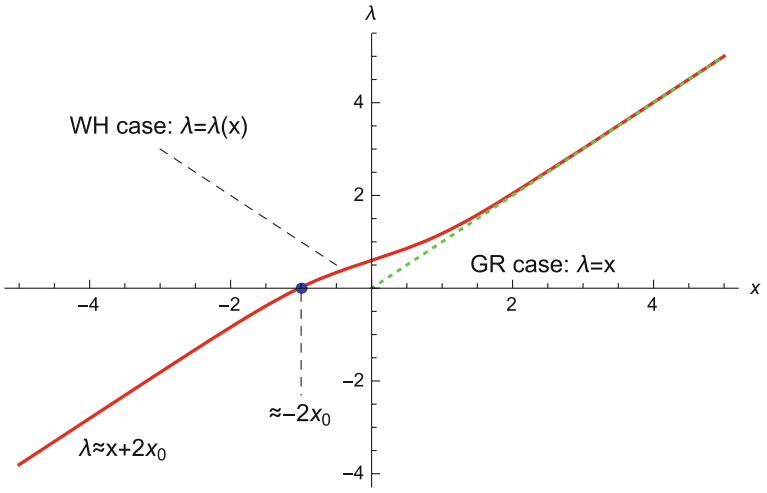

Fig. 8.4 Behavior of the affine parameter $\lambda(x)$ (*solid red curve*) for radial null ($k = L = 0$) geodesics as compared to GR (*dashed green*). Note that in our case $\lambda(x)$ can be arbitrarily extended due to the presence of the wormhole, while in GR these geodesics finish at $r = 0$ due to the fact that $r > 0$. In this plot $E = 1$

to the congruence, and following its evolution as the divergent region is crossed one can determine the existence of a physical singularity if this volume vanishes, that would be interpreted as the extended observer being crushed to zero volume, hence, the singularity would be "strong", otherwise "weak." In our case, a similar analysis reveals [72] that despite the fact that physical observers may experience a *"spaghettization"* process in which the volume diverges as the wormhole throat is crossed (though this process is reversed as soon as the wormhole throat is crossed), no loss of causal contact occurs upon the constituents making up the observer. The latter statement implies that the internal forces among the constituents making up the body could be able to sustain it at all times. This is consistent with the fact that scattering of scalar waves off the wormhole is well posed [73]. Therefore, the presence of curvature divergences seem to have absolutely no destructive effect upon physical observers.

We conclude that the spacetimes described by the line element (8.50) represent sourceless, regular, self-consistent gravitating solutions where Wheeler's charge-without-charge and mass-without-mass mechanism is naturally implemented through the emergence of wormhole structures. Thus, they represent truly genuine geons.

The metric described by (8.50), which arises from a quadratic gravity model in combination with an electromagnetic field, can be further refined. This is due to the fact that in the innermost region of these solutions, the electromagnetic field is expected to get additional corrections due to quantum effects. Taking into account such effects proves a difficult task, due to the inherent complexity of the

perturbative series of quantum electrodynamics. Nonetheless, as was shown in a number of works, these effects can be incorporated, under certain circumstances, in terms of nonlinear electrodynamics [74–76]. Indeed, finding a solution to the coupled system of quadratic gravity (8.45), with Born–Infeld electrodynamics (8.12) is possible, and yields the metric [77]

$$ds^2 = -\frac{A(z)}{\sigma_+(z)}dt^2 + \frac{\sigma_-(z)}{\sigma_+(z)A(z)}\left(1+\frac{z\sigma_{-,z}}{2\sigma_-(z)}\right)^2 dz^2 + z^2(x)d\Omega^2 \,, \tag{8.67}$$

where

$$\delta_1 = \frac{1}{2r_S}\sqrt{\frac{r_q^3}{l_\beta}} \,, \qquad \delta_2 = \frac{\sqrt{r_q l_\beta}}{r_S} \,, \tag{8.68}$$

$$\sigma_\pm = 1 \pm \frac{1}{z^4} \,, \tag{8.69}$$

$$A(z) = 1 - \frac{1+\delta_1 G(z)}{\delta_2 z\sigma_-(z)^{1/2}} \,, \tag{8.70}$$

$$G_z = \frac{z^2\sigma_-^{1/2}}{\sigma_+}\left(1+\frac{z\sigma_{-,z}}{2\sigma_-}\right)\left(l_\beta^2 f + \tilde{\varphi}\right) \,, \tag{8.71}$$

with the definitions of the charge radius, $r_q^2 \equiv \kappa^2 q^2/4\pi$, Born–Infeld scale $l_\beta^2 = (\kappa^2\beta^2/4\pi)^{-1}$ and the radial function $z^4 = r^4/(r_q^2 l_\beta^2)$ satisfies $dx = \pm dz/\sigma_-^{1/2}$, whose integration yields the typical behavior of a wormhole structure [i.e., two asymptotically flat regions and a bounce in between], with $z = 1$ ($x = 0$) setting the location of the wormhole throat. Moreover, the implementation of the charge-without-charge and mass-without-mass mechanisms of the previous section works exactly in the same way in the present case. The most relevant difference is the change in the density of lines of force flowing through the wormhole throat, which now becomes

$$\frac{\Phi}{4\pi r_c^2 z_c^2} = \left(\frac{4\sigma}{1+4\sigma}\right)^{1/2}\sqrt{\frac{c^7}{2(\hbar G)^2}} \,. \tag{8.72}$$

Here $\sigma = l_\varepsilon^2/l_\beta^2$ contains contributions of the modifications of both the gravitational and electromagnetic fields. The second difference lies in the computation of the total mass contained in the spacetime, which takes the same form as in Eq. (8.63), but in the present case the mass, M^{BI}, of those solutions takes the form

$$M^{BI} = \left(\frac{4\sigma}{1+4\sigma}\right)^{1/4} M^M \,, \tag{8.73}$$

where M^M is the mass in Maxwell's case. This way, as one departs from the Maxwell case (corresponding to $\sigma \to \infty$), the mass of the Born–Infeld objects is decreased. In

particular, for $\beta \simeq 10^{18}$ the mass can be lowered down to the order 10^2 GeV, which would put these geonic objects within the reach of current particle accelerators.

8.3.3 Born–Infeld Gravity with Electromagnetic Fields

In this section, we are going to consider a different type of gravitational action, dubbed Born–Infeld gravity [78, 79], which is formally similar in some aspects to Eddington's purely affine theory [80]. This theory is described by the action

$$S = \frac{1}{\kappa^2 \varepsilon} \int d^4x \left[\sqrt{-|g_{\mu\nu} + \varepsilon R_{\mu\nu}(\Gamma)|} - \lambda \sqrt{-g} \right] + S_m \, . \tag{8.74}$$

Oddly enough, this is nothing but the gravitational counterpart of Born–Infeld electrodynamics (written in determinantal form), where the field strength tensor $F_{\mu\nu}$ is replaced by the Ricci tensor $R_{\mu\nu}$. Alternatively, (8.74) can be seen as the comparison of volume elements between the metrics $q_{\mu\nu} \equiv g_{\mu\nu} + \varepsilon R_{\mu\nu}$ and $g_{\mu\nu}$. The meaning of the parameter λ in the action (8.74) is obtained from the expansion in series of the new scale $\varepsilon \ll 1$, which yields the result

$$\begin{aligned} \lim_{\varepsilon \to 0} S = & \frac{1}{2\kappa^2} \int d^4x \sqrt{-g} \left[R - 2\Lambda_{\mathit{eff}} \right] \\ & - \frac{1}{2\kappa^2} \int d^4x \sqrt{-g} \frac{\varepsilon}{2} \left(\frac{-R^2}{2} + Q \right) + S_m \, . \end{aligned} \tag{8.75}$$

The zeroth-order term of this expansion represents GR plus an effective cosmological term $\Lambda_{\mathit{eff}} = \frac{\lambda - 1}{\varepsilon}$, supplemented with higher order terms in the curvature scalars R and Q, and suppressed by inverse powers of the parameter ε which, consistently, has dimensions of length squared [we shall denote, by convenience, $\varepsilon = -2l_\varepsilon^2$].

When formulated in the Palatini approach, the field equations from (8.74) follow as

$$\frac{\sqrt{|q|}}{\sqrt{|g|}} q^{\mu\nu} - \lambda g^{\mu\nu} = -\kappa^2 \varepsilon T^{\mu\nu} \, , \tag{8.76}$$

$$\nabla_\alpha \left(\sqrt{q} q^{\mu\nu} \right) = 0 \, , \tag{8.77}$$

and the usual manipulations of Palatini theories of gravity used in the previous sections apply here as well. In particular, the relation between the metric $q_{\mu\nu}$ and $g_{\mu\nu}$ [for which $\nabla_\alpha \left(\sqrt{g} g^{\mu\nu} \right) \neq 0$] becomes

$$\hat{q} = \sqrt{|\hat{\Sigma}|} \hat{\Sigma}^{-1} \hat{g} \, , \; \hat{q}^{-1} = \frac{\hat{g}^{-1} \hat{\Sigma}}{\sqrt{|\hat{\Sigma}|}} \, , \tag{8.78}$$

where $\hat{\Sigma} = \lambda\hat{I} - \varepsilon\kappa^2\hat{T}$, and the field equations for $q_{\mu\nu}$ read now

$$R^{\mu}{}_{\nu}(q) = \frac{\kappa^2}{|\hat{\Sigma}|^{1/2}}\left[L_G\delta^{\mu}{}_{\nu} + T^{\mu}{}_{\nu}\right], \tag{8.79}$$

where $L_G \equiv (|\hat{\Sigma}|^{1/2} - \lambda)/(\kappa^2\varepsilon)$. It is worth mentioning that, like in the $f(R)$ and $f(R, Q)$ cases above, all the contributions on the right-hand side of the field equations (8.79) only depend on the matter sources (and possibly the metric $g_{\mu\nu}$). Besides, the recovery of the GR equations plus a cosmological constant in vacuum, and the second-order and ghost-free character of the field equations, hold as well.

One could go forward and proceed to obtain the electrostatic, spherically symmetric solutions for this theory. At this point, one finds the surprising result that for either linear or nonlinear electromagnetic fields, which always satisfy $T^t{}_t = T^r{}_r$, the field equations for Born–Infeld gravity (8.74) with $\varepsilon = -2l_\varepsilon^2$ and $a = 1$ *exactly* coincide with those of quadratic gravity (8.45), and not only at the perturbative level given by Eq. (8.75). This is due to the fact that all higher order corrections beyond linear order in ε exactly cancel out due to the above-mentioned symmetry of the energy–momentum tensor associated to electromagnetic fields. Consequently, the discussion of the previous section for both Maxwell and Born–Infeld electrodynamics, and all the found geonic properties also appear in the case of Born–Infeld gravity exactly under the same form.

8.3.4 Higher Dimensional Generalizations

Many generalizations can now be found. In particular, one could explore the dynamics of these theories in the context of higher dimensions. This could be particularly important within the context of the AdS/CFT correspondence [81–84], where exact solutions in the gravitational side may provide interesting tools on the condensed matter side. This is due to the fact that the field equations for higher dimensional $f(R)$ [85], $f(R, Q)$ and Born–Infeld gravity [86] formulated in the Palatini approach are always second-order, as opposed to the fourth-order equations found in the standard metric formulation of these theories (the exception to this rule being the Lovelock family of Lagrangians [61]). In the case of Born–Infeld gravity, Eq. (8.78) gets modified as

$$q_{\mu\nu} = |\hat{\Upsilon}|^{\frac{1}{d-2}}(\Upsilon^{-1})_{\mu}{}^{\alpha}g_{\alpha\nu}\,, \qquad q^{\mu\nu} = \frac{1}{|\hat{\Upsilon}|^{\frac{1}{d-2}}}g^{\mu\alpha}\Upsilon_{\alpha}{}^{\nu}\,, \tag{8.80}$$

where we have defined $\hat{\Upsilon} \equiv |\hat{\Omega}|^{1/2}\hat{\Omega}^{-1} \equiv \lambda\hat{I} - \varepsilon\kappa^2\hat{T}$ and d is the number of spacetime dimensions, while Eq. (8.79) becomes

$$R^{\mu}{}_{\nu}(q) = \frac{\kappa^2}{|\hat{\Upsilon}|^{\frac{1}{d-2}}}\left[L_{BI}\delta^{\mu}{}_{\nu} + T^{\mu}{}_{\nu}\right], \tag{8.81}$$

where the gravitational Lagrangian density is written now as

$$L_{BI} = \frac{|\hat{\Upsilon}|^{\frac{1}{d-2}} - \lambda}{\kappa^2 \varepsilon} \,. \tag{8.82}$$

We point out that the second-order, ghost-free character of the field equations is preserved, while Minkowski spacetime is still recovered in vacuum, $T^{\mu}{}_{\nu} = 0$. Like in the previous cases we couple Born–Infeld gravity in d dimensions to an electrostatic spherically symmetric Maxwell field, and proceeding in the same way, we arrive at the result [with $\tilde{X} \equiv \frac{\varepsilon \kappa^2 q^2}{8\pi r(x)^{2(d-2)}}$]

$$ds^2 = -\frac{A}{\Omega_+} dt^2 + \left(\frac{\Omega_+}{A}\right)\left(\frac{dx}{\Omega_+}\right)^2 + z^2(x) d\Omega^2 \,, \tag{8.83}$$

where

$$\Omega_- = (\lambda + \tilde{X})^{\frac{2}{d-2}} \,, \qquad \Omega_+ = \frac{(\lambda - \tilde{X})}{(\lambda + \tilde{X})^{\frac{d-4}{d-2}}} \,, \tag{8.84}$$

$$A(z) = 1 - \left(\frac{1 + \delta_1 G(z)}{\delta_2 \Omega_-^{\frac{d-3}{2}} z^{d-3}}\right) \,, \tag{8.85}$$

$$G_z = -z^{d-2}\left(\frac{\Omega_- - 1}{\Omega_-^{1/2}}\right)\left(\lambda + \frac{1}{z^{2(d-2)}}\right) \,, \tag{8.86}$$

$$\delta_1 \equiv \frac{(d-3) r_c^{d-1}}{2 M_0 l_\varepsilon^2} \,, \qquad \delta_2 \equiv \frac{(d-3) r_c^{d-3}}{2 M_0} \,. \tag{8.87}$$

Again, the presence of a wormhole structure can be inferred from the behavior of the radial function, now determined by the equation $x^2 = r^2 \Omega_-$, which can be analytically inverted as (see Fig. 8.5 for its graphic representation)

$$r^{d-2} = \frac{|x|^{d-2} + \sqrt{|x|^{2(d-2)} + 4 r_c^{2(d-2)}}}{2} \,. \tag{8.88}$$

In Fig. 8.5 we see the same features as in the previous models, namely, the recovery of the GR behavior, $r^2 \simeq x^2$ at large distances, and the bounce at $z = 1$ ($x = 0$). It should be noted that the transition from the GR-like behavior to the wormhole structure occurs suddenly as the number of dimensions is increased. Properties associated to the wormholes, like the generation of the charge via topological considerations, and the computation of the total mass of the spacetime yielding the action of a point-like particle, also hold in this case. On the other hand, an analysis of the metric and the curvature invariants reveals that only in the case $d = 4$ may curvature scalars become finite around the wormhole throat for some special choice of δ_1 (similarly as

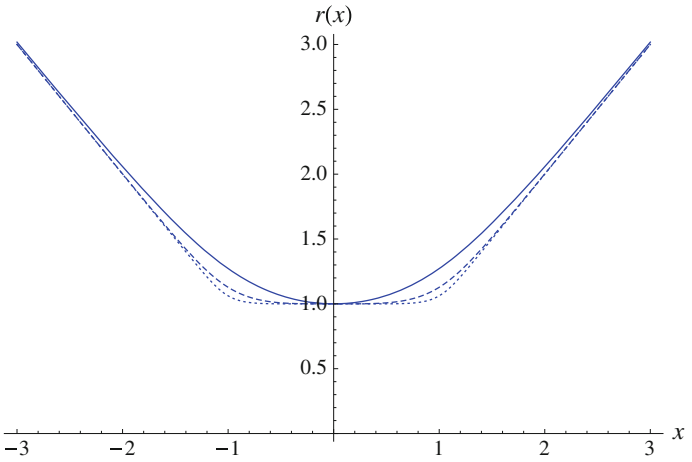

Fig. 8.5 The radial function (8.88) for $d = 4$ (*solid*), $d = 6$ (*dashed*) and $d = 10$ (*dotted*)

in the four-dimensional case). Nonetheless, the corresponding study of the geodesic behavior in these spacetimes reveals the completeness of all null, time-like, and space-like geodesics, for all values of mass and charge, and in any dimension. Therefore, they represent genuine geonic solutions, on equal footing to their four-dimensional counterparts.

8.4 Conclusions

In this chapter we have shown that, contrary to general wisdom, gravity theories with nonlinear curvature terms may yield second-order field equations if formulated à la Palatini. Relaxing the compatibility condition on the connection allows the field equations to modify the dynamics in a way that avoids higher order derivatives (which complicate the analytical treatment), and ghost-like instabilities (which spoil the good perspectives originally posited on such theories as quantum improvements of GR). The second-order character of the equations allows to find analytical solutions using strategies borrowed from GR and adapted to a situation in which two geometries are related by a matter deformation. The examples presented in this work illustrate this procedure with several models which admit exact analytical solutions.

Our analysis of spherically symmetric solutions puts forward that self-gravitating free electric fields are possible and naturally lead to the notion of the geon originally introduced by Wheeler. These geons arise thanks to the nontrivial topology of the solutions, which turn out to be wormholes. Interestingly, these wormholes arise naturally out of the matter plus gravity field equations, i.e., they are not designed a priori as in the usual approach to wormholes, where one hopes that some exotic matter source may be able to thread the previously designed geometry.

We have seen that the resulting wormhole structure has a dramatic impact as far as singularities are concerned. Given that the spacetime is now geodesically complete, one can conclude that such geometries are nonsingular. This is so even though curvature divergences typically arise at the wormhole throat. In the case of $f(R)$ theories, this divergence lies at the asymptotic boundary of the spacetime, requiring an infinite affine time to reach it. As a result, physical observers cannot interact with it and one can readily conclude that they are not observable. In the case of quadratic gravity and the Born–Infeld gravity model, there are situations in which physical observers can go through the wormhole and, therefore, interact with the divergent region. In such cases, it has been found that extended objects do not undergo any pathological effects as the throat is approached or crossed [73]. In the case of naked configurations, the scattering of scalar waves off the divergence has also been investigated finding that the propagation is smooth. In fact, transmission and reflection coefficients can be computed numerically which are in excellent agreement with analytical approximations.

The bottom line is that Palatini theories of gravity seem very well suited to address different aspects of the expected phenomenology of quantum gravity, making black holes, geons, and wormholes to arise all together in the same simple and clean scenarios. Indeed, such objects arise directly from well-motivated actions and by integration of the field equations in analytic form, which is in sharp contrast with the reversed method frequently employed in the context of wormhole physics where a suitable metric is defined first and then the Einstein equations are driven back to find the matter source threading the geometry. Because of this strategy, we have been able to define a well-behaved matter, and let the virtues of the Palatini approach to flow. The fact that the resulting geometries obtained in this approach are nonsingular, and that matter waves can propagate smoothly on those backgrounds may lead to interesting results in the quantum regime. Such aspects will be explored elsewhere.

Acknowledgements G.J.O. is supported by a Ramon y Cajal contract and the Spanish grant FIS2014-57387-C3-1-P from MINECO. D.R.G. is funded by the Fundação para a Ciência e a Tecnologia (FCT, Portugal) postdoctoral fellowship No. SFRH/BPD/102958/2014 and the FCT research grant UID/FIS/04434/2013. Support from the Consolider Program CPANPHY-1205388, the Severo Ochoa grant SEV-2014-0398 (Spain), and the CNPq (Brazilian agency) project No.301137/2014-5 is also acknowledged. This chapter is based upon work from COST Action CA15117, supported by COST (European Cooperation in Science and Technology).

References

1. Will CM. The confrontation between general relativity and experiment. Living Rev Rel. 2014;17:4.
2. Berti E, et al. Testing general relativity with present and future astrophysical observations. Class Quant Grav. 2015;32:243001.
3. Wheeler JA. Geons. Phys Rev D. 1955;97:511.
4. Visser M. Lorentzian wormholes. New York: Springer; 1995.
5. Misner CW, Wheeler JA. Geometrodynamics. Ann Phys. 1957;2:525.

6. Arellano AVB, Lobo FSN. Non-existence of static, spherically symmetric and stationary, axisymmetric traversable wormholes coupled to nonlinear electrodynamics. Class Quant Grav. 2006;23:7229.
7. Arellano AVB, Lobo FSN. Evolving wormhole geometries within nonlinear electrodynamics. Class Quant Grav. 2006;23:5811.
8. Zanelli J. in Lecture notes on Chern-Simons (super-)gravities. 2nd ed. (February 2008). arXiv:hep-th/0502193.
9. Olmo GJ. Palatini approach to modified gravity: $f(R)$ theories and beyond. Int J Mod Phys D. 2011;20:413.
10. Eiroa EF, Romero GE. Linearized stability of charged thin shell wormholes. Gen Rel Grav. 2004;36:651.
11. Dias GAS, Lemos JPS. Thin-shell wormholes in d-dimensional general relativity: solutions, properties, and stability. Phys Rev D. 2010;82:084023.
12. Kittel C. Introduction to solid state physics. 8th ed. New York: Wiley; 2005.
13. Kröner E. The continuized crystal - a bridge between micro and macromechanics? Z angew Math Mech. 1986;66:5.
14. Kröner E. The differential geometry of elementary point and line defects in Bravais crystals. Int J Theor Phys. 1990;29:1219–37.
15. Kröner E. On gauge theory in defect mechanics. Trends in applications of pure mathematics to mechanics, vol. 249. Lecture Notes in Physics, 1986. p. 281–94.
16. Kondo K. On the geometrical and physical foundation of the theory of yielding. In: Proceedings 2nd Japan Kat. Congr. of Appl. at Max-Planek-lnstitut fur Mctallforschung, Postfach 800665, D-7000 Stuttgart 80, BRD. Mechanics; 1952. pp. 41–7.
17. Bilby BA, Bullough R, Smith E. Continuous distributions of dislocations: a new application of the methods of non-Riemannian geometry. Proc Roy Soc London, Ser A. 1955;231:263.
18. Falk F. Theory of elasticity of coherent inclusions by means of non-metric geometry. J Elast. 1981;11(359):359.
19. Clayton JD. Nonlinear mechanics of crystals. Berlin: Springer; 2011.
20. Lobo FSN, Olmo GJ, Rubiera-Garcia D. Crystal clear lessons on the microstructure of space-time and modified gravity. Phys Rev D. 2015;91:124001.
21. Olmo GJ, Rubiera-Garcia D. The quantum, the geon, and the crystal. Int J Mod Phys D. 2015;24:1542013.
22. González J, Herrero J. Graphene wormholes: a Condensed matter illustration of Dirac fermions in curved space. Nucl Phys B. 2010;825:426.
23. De Felice A, Tsujikawa S. $f(R)$ theories. Liv Rev Rel. 2010;13:3.
24. Capozziello S, De Laurentis M. Extended theories of gravity. Phys Rep. 2011;509:167.
25. Nojiri S, Odintsov SD. Unified cosmic history in modified gravity: from $F(R)$ theory to Lorentz non-invariant models. Phys Rep. 2011;505:59.
26. de la Cruz-Dombriz A, Saez-Gomez D. Black holes, cosmological solutions, future singularities, and their thermodynamical properties in modified gravity theories. Entropy. 2012;14:1717.
27. Bejarano C, Lobo FSN, Olmo GJ, Rubiera-Garcia D. Palatini wormholes and energy conditions from the prism of General Relativity. arXiv:1607.01259 [gr-qc].
28. Born M, Infeld L. Proc Roy Soc London A. 1934;144:425.
29. Heisenberg W, Euler H. Consequences of Dirac Theory of the Positron. Z Phys. 1936;120:714. arXiv:physics/0605038.
30. Garcia A, Salazar H, Plebanski JF. Type-D solutions of the Einstein and Born-Infeld nonlinear-electrodynamics equations. Nuovo Cim. 1984;84:65.
31. Demianski M. Static electromagnetic geon. Found Phys. 1986;16:187.
32. Gibbons GW, Rasheed DA. Electric - magnetic duality rotations in nonlinear electrodynamics. Nucl Phys B. 1995;454:185.
33. Breton N. Born-Infeld black hole in the isolated horizon framework. Phys Rev D. 2003;67:124004.
34. Diaz-Alonso J, Rubiera-Garcia D. Electrostatic spherically symmetric configurations in gravitating nonlinear electrodynamics. Phys Rev D. 2010;81:064021.

35. Diaz-Alonso J, Rubiera-Garcia D. Asymptotically anomalous black hole configurations in gravitating nonlinear electrodynamics. Phys Rev D. 2010;82:085024.
36. Bardeen J. Non-singular general-relativistic gravitational collapse. In: Proceedings of GR 5 (Tbilisi, USSR); 1968.
37. Ayón-Beato E, García A. Regular black hole in general relativity coupled to nonlinear electrodynamics. Phys Rev Lett. 1998;80:5056.
38. Ayón-Beato E, García A. Nonsingular charged black hole solution for nonlinear source. Gen Rel Grav. 1999;31:629.
39. Bronnikov KA. Regular magnetic black holes and monopoles from nonlinear electrodynamics. Phys Rev D. 2001;63:044005.
40. Burinskii A, Hildebrandt SR. New type of regular black holes and particle - like solutions from NED. Phys Rev D. 2002;65:104017.
41. Lemos JPS, Zanchin VT. Regular black holes: electrically charged solutions, Reissner-Nordström outside a de Sitter core. Phys Rev D. 2011;83:124005.
42. Dymnikova I. Regular electrically charged structures in nonlinear electrodynamics coupled to general relativity. Class Quant Grav. 2004;21:4417–29.
43. Boillat G. Nonlinear electrodynamics: Lagrangians and equations of motion. J Math Phys. 1970;11:941–51.
44. Boillat G. Simple waves in N-dimensional propagation. J Math Phys. 1970;11:1482–3.
45. Fradkin ES, Tseytlin AA. Nonlinear electrodynamics from quantized strings. Phys Lett B. 1985;163:123–30.
46. Leigh RG. Dirac-Born-Infeld action from dirichlet sigma model. Mod Phys Lett A. 1989;4:2767.
47. Witten E. Bound states of strings and p-branes. Nucl Phys B. 1996;460:335–50.
48. Tseytlin AA. On nonAbelian generalization of Born-Infeld action in string theory. Nucl Phys B. 1997;501:41–52.
49. Perry M, Schwarz JH. Interacting chiral gauge fields in six-dimensions and Born-Infeld theory. Nucl Phys B. 1997;489:47–64.
50. Olmo GJ, Rubiera-Garcia D. Palatini $f(R)$ black holes in nonlinear electrodynamics. Phys Rev D. 2011;84:124059.
51. Penrose R. Gravitational collapse and space-time singularities. Phys Rev Lett. 1965;14:57–9.
52. Penrose R. Gravitational collapse: the role of general relativity. Riv Nuovo Cim. 1969;1:252–76. Gen Rel Grav. 2002;34:1141–65.
53. Hawking SW. Singularities in the universe. Phys Rev Lett. 1966;17:444–5.
54. Chandrasekhar S. The mathematical theory of black holes. Oxford: Oxford University Press; 1983.
55. Olmo GJ. Nonsingular Black Holes in palatini extensions of general relativity. Springer Proc Phys. 2016;176:183.
56. Bejarano C, Olmo GJ, Rubiera-Garcia D. What is a singular black hole beyond General Relativity? Phys Rev D. 2017;95:064043.
57. Parker L, Toms DJ. Quantum field theory in curved spacetime: quantized fields and gravity. Cambridge: Cambridge University Press; 2009.
58. Birrell ND, Davies PCW. Quantum fields in curved space. Cambridge: Cambridge University Press; 1982.
59. Green M, Schwarz J, Witten E. Superstring theory. Cambridge: Cambridge University Press; 1987.
60. Cembranos JAR. Dark matter from R2-gravity. Phys Rev Lett. 2009;102:141301.
61. Charmousis C. Higher order gravity theories and their black hole solutions. Lec Notes Phys. 2008;769:299.
62. Olmo GJ, Rubiera-Garcia D. Importance of torsion and invariant volumes in Palatini theories of gravity. Phys Rev D. 2013;88:084030.
63. Olmo GJ, Rubiera-Garcia D. Reissner-Nordström black holes in extended Palatini theories. Phys Rev D. 2012;86:044014.

64. Olmo GJ, Rubiera-Garcia D. Nonsingular black holes in quadratic Palatini gravity. Eur Phys J C. 2012;72:2098.
65. Olmo GJ, Rubiera-Garcia D. Nonsingular charged black holes à la Palatini. Int J Mod Phys D. 2012;21:1250067.
66. Ortin T. Gravity and strings. U.K.: Cambridge University Press; 2004.
67. Tipler FJ. On the nature of singularities in general relativity. Phys Rev D. 1977;15:942–5.
68. Tipler FJ, Clarke CJS, Ellis GFR. General relativity and gravitation. New York: Plenum; 1980.
69. Krolak A. Towards the proof of the cosmic censorship hypothesis. Class Quant Grav. 1986;3:267–80.
70. Clarke CJS, Krolak A. Conditions for the occurrence of strong curvature singularities. J Geom Phys. 1985;2:127–43.
71. Nolan BC. Strengths of singularities in spherical symmetry. Phys Rev D. 1999;60:024014.
72. Olmo GJ, Rubiera-Garcia D, Sanchez-Puente A. Impact of curvature divergences on physical observers in a wormhole space-time with horizons. 2016;33:115007.
73. Olmo GJ, Rubiera-Garcia D, Sanchez-Puente A. Classical resolution of black hole singularities via wormholes. Eur Phys J C. 2016;76:143.
74. Schwinger J. On Gauge invariance and vacuum polarization. Phys Rev. 1951;82:664.
75. Bialynicka-Birula Z, Bialynicki-Birula I. Nonlinear effects in quantum electrodynamics. photon propagation and photon splitting in an external field. Phys Rev D. 1970;2:2341.
76. Dobado A, Gómez-Nicola A, Maroto AL, Peláez JR. Effective Lagrangians for the standard model. Berlin: Springer; 1997.
77. Olmo GJ, Rubiera-Garcia D. Semiclassical geons at particle accelerators. JCAP. 2014;1402:010.
78. Deser S, Gibbons GW. Born-Infeld-Einstein actions? Class Quant Grav. 1998;15:L35–9.
79. Bañados M, Ferreira PG. Eddington's theory of gravity and its progeny. Phys Rev Lett. 2010;105:011101.
80. Eddington AS. The mathematical theory of relativity. Cambridge: Cambridge University Press; 1924.
81. Maldacena J. The large N limit of superconformal field theories and supergravity. Adv Theor Math Phys. 1998;2:231–52.
82. Maldacena J. The large-N limit of superconformal field theories and supergravity. Int J Theor Phys. 1999;38:1113.
83. Witten E. Anti de sitter space and holography. Adv Theor Math Phys. 1998;2:253–91.
84. Gubser SS, Klebanov IR, Polyakov AM. Gauge theory correlators from non-critical string theory. Phys Lett B. 1999;428:105–14.
85. Bazeia D, Losano L, Olmo GJ, Rubiera-Garcia D. Black holes in five-dimensional Palatini f(R) gravity and implications for the AdS/CFT correspondence. Phys Rev D. 2014;90:044011.
86. Bazeia D, Losano L, Olmo GJ, Rubiera-Garcia D, Sanchez-Puente A. Classical resolution of black hole singularities in arbitrary dimension. Phys Rev D. 2015;92:044018.

Part II
Energy Conditions

Chapter 9
Classical and Semi-classical Energy Conditions

Prado Martín–Moruno and Matt Visser

9.1 Introduction

The energy conditions, be they classical, semi-classical, or "fully quantum" are at heart purely phenomenological approaches to deciding what form of stress–energy is to be considered "physically reasonable". As Einstein put it, the LHS of his field equations $G_{ab} = 8\pi G_N T_{ab}$ represents the "purity and nobility" of geometry, while the RHS represents "dross and uncouth" matter. If one then makes no assumptions regarding the stress–energy tensor, then the Einstein field equations are simply an empty tautology. It is only once one makes *some* assumptions regarding the stress–energy tensor, (zero for vacuum, "positive" in the presence of matter), that solving the Einstein equations becomes closely correlated with empirical reality. The energy conditions are simply various ways in which one can try to implement the idea that the stress–energy tensor be "positive" in the presence of matter, and that gravity always attracts. In this chapter, we shall first discuss the standard point-wise energy conditions, and then move on to their generalizations obtained by averaging along causal curves, and some nonlinear variants thereof, and finally discuss semi-classical variants.

9.2 Standard Energy Conditions

General relativity, as well as other metric theories of gravity, proposes a way in which the matter content affects the curvature of the spacetime. The theory of gravity itself, however, does not per se tell us anything specific about the kind of matter content

P. Martín–Moruno
Departamento de Física Teórica I, Ciudad Universitaria,
Universidad Complutense de Madrid, 28040 Madrid, Spain
e-mail: pradomm@ucm.es

M. Visser (✉)
School of Mathematics and Statistics, Victoria University of Wellington,
PO Box 600, Wellington 6140, New Zealand
e-mail: matt.visser@sms.vuw.ac.nz

F.S.N. Lobo (ed.), *Wormholes, Warp Drives and Energy Conditions*,
Fundamental Theories of Physics 189, DOI 10.1007/978-3-319-55182-1_9

that we should consider. If we are interested in extracting general features about the spacetime, independently of the form of the stress–energy tensor of matter fields, we have to consider purely geometric expressions such as the Raychaudhuri equation. This equation describes the focussing of a congruence of timelike curves in a given geometry. Particularized to geodesic motion it can be expressed as [1]

$$\frac{\mathrm{d}\theta}{\mathrm{d}s} = \omega_{ab}\omega^{ab} - \sigma_{ab}\sigma^{ab} - \frac{1}{3}\theta^2 - R_{ab}V^aV^b, \tag{9.1}$$

where ω_{ab} is the vorticity, σ_{ab} is the shear, θ is the expansion, and V^a is the time-like unit vector tangent to the congruence. Note that for a congruence of time-like geodesics with zero vorticity, for which $V_a \propto \nabla_a \Phi(x)$ with $\Phi(x)$ a scalar field [2], the only term on the RHS of Eq. (9.1) that can be positive is the last term. Hence, if $R_{ab}V^aV^b \geq 0$, then the expansion decreases and, as free-falling observers follow geodesics, observers that only feel the gravitational interaction get closer to each other. This fact allows one to formulate the following geometric condition:

Time-like convergence condition (TCC): Gravity is always attractive provided

$$R_{ab}V^aV^b \geq 0 \quad \text{for any timelike vector } V^a. \tag{9.2}$$

Note that although the TCC ensures focussing of timelike geodesics the contrary statement is not necessarily true, that is $R_{ab}V^aV^b < 0$ does not automatically imply geodesics defocusing [3]. As R_{ab} depends on the stress–energy tensor through the equations of the dynamics, the TCC imposes restrictions on the material content that depends on the specific theory of gravity.

Analogously, one can take the equation for the focussing of a congruence of null geodesics with vanishing vorticity, and formulate the null convergence condition[1] (NCC). This is a particular limit of the TCC and requires that $R_{ab}k^ak^b \geq 0$ for any null-vector k^a. It should be noted that hypothetical astronomical objects like wormholes would necessarily violate the NCC [8–10]. Furthermore, this condition might also be violated during the early universe if one wishes to avoid the big bang singularity [3, 11, 12].

Following a different spirit, one could consider imposing an assumption on the form of the stress–energy tensor based on our daily experience through some energy condition. This can be done restricting attention to a given theory of gravity. Such is the case for the strong energy condition which is formulated as:

[1] There have been interesting attempts to derive the NCC from an underlying fundamental framework [4–7].

Strong energy condition (SEC): Gravity is always attractive in GR.

$$\left(T_{ab} - \frac{1}{2} T g_{ab}\right) V^a V^b \geq 0 \quad \text{for any timelike vector } V. \tag{9.3}$$

This SEC takes into account both the TCC *and the Einstein equations* in its mathematical formulation. Hence, properly speaking, it only makes sense to refer to the SEC in a general relativistic framework.

More generally, by looking at the world around us we can also assert certain properties that any "reasonable" material content should satisfy *independently of the theory of gravity* describing the curvature of spacetime. These energy conditions can be used later to study the geometry once the theory of gravity is fixed. The energy conditions commonly considered in the literature are [1, 13]:

Dominant energy condition (DEC): The energy density measured by any observer is non-negative and propagates in a causal way.

$$T^a{}_b \, V_a \, V^b \geq 0, \qquad F^a F_a \leq 0. \tag{9.4}$$

Here, we have defined the flux 4-vector as $F^a = -T^a{}_b V^b$, and it is understood that the inequalities contained in expression (9.4) have to be satisfied for any timelike vector.

Weak energy condition (WEC): The energy density measured by any observer has to be non-negative.

$$T^a{}_b \, V_a \, V^b \geq 0. \tag{9.5}$$

Therefore, if the WEC is not satisfied, then the DEC has to be violated. However, the WEC and the SEC are, in principle, completely independent.

Null energy condition (NEC): The SEC and the WEC are satisfied in the limit of null observers.

$$T^a{}_b \, k_a \, k^b \geq 0 \quad \text{for any null vector } k^a. \tag{9.6}$$

It should be noted that the NCC is completely equivalent to the NEC within the framework of GR. By its very definition if the NEC is violated, then the SEC, on one hand, and the WEC and DEC, on the other hand, cannot be satisfied.

Historically, there was also a trace energy condition (TEC), the assertion that the trace of the stress-energy tensor should (in $-+++$ signature) be non-positive. While for several decades in the 50s and 60s this was believed to be a physically reasonable condition, opinion has now shifted, (specifically with the discovery of stiff equations of state for neutron star matter), and the TEC has now largely been abandoned [13]. (See also Ref. [14] for uses of the less known subdominant trace energy condition, and Ref. [15] for the practically unnoticed quasilocal energy conditions.) This cautionary tale indicates that one should perhaps take the energy conditions as provisional, they are good ways of qualitatively and quantitatively characterizing the level of weirdness one is dealing with, but they may not actually be fundamental physics.

9.2.1 The Hawking–Ellis Type I — Type IV Classification

The Hawking–Ellis classification, (more properly called the Segre classification), of stress–energy tensors is based on the extent to which the orthonormal components of the stress-energy can be diagonalized by local Lorentz transformations:

$$T^{ab} = (\text{canonical type})^{cd}\; L_c{}^a\; L_d{}^b. \tag{9.7}$$

Equivalently, one is looking at the Lorentz invariant eigenvalue problem

$$\det\left(T^{ab} - \lambda\eta^{ab}\right) = 0, \quad \text{that is,} \qquad \det\left(T^a{}_b - \lambda\delta^a{}_b\right) = 0. \tag{9.8}$$

Here as usual $\eta^{ab} = \text{diag}(-1,\ 1,\ 1,\ 1)$. In Lorentzian signature $T^a{}_b$ is not symmetric, so diagonalization is trickier than one might naively expect. Even the usual Jordan decomposition is not particularly useful, (since for physical reasons one is interested in partial diagonalization using Lorentz transformations, rather than the more general similarity transformations which could lead to non-diagonal unphysical T^{ab}), and so it is more traditional to classify stress-energy tensors in terms of the space-like/light-like/time-like nature of the eigenvectors.

Based on (a minor variant of) the discussion of Hawking and Ellis the four types (when expressed in an orthonormal basis) are:

- Type I:

$$T^{ab} \sim \left[\begin{array}{c|ccc} \rho & 0 & 0 & 0 \\ \hline 0 & p_1 & 0 & 0 \\ 0 & 0 & p_2 & 0 \\ 0 & 0 & 0 & p_3 \end{array}\right]. \tag{9.9}$$

This is the generic case, there is one timelike, and three space-like eigenvectors.

$$T^{ab} = \rho\; u^a u^b + p_1\; n_1^a n_1^b + p_2\; n_2^a n_2^b + p_3\; n_3^a n_3^b, \tag{9.10}$$

where $u^a = (-1;\ 0;\ 0;\ 0)$, $n_1^a = (0;\ 1;\ 0;\ 0)$, $n_2^a = (0;\ 0;\ 1;\ 0)$, and $n_3^a = (0;\ 0;\ 0;\ 1)$.
The Lorentz invariant eigenvalues of $T^a{}_b$ are $\{-\rho,\ p_1,\ p_2,\ p_3\}$. Many classical stress–energy tensors, (for instance, perfect fluids, massive scalar fields, non-null electromagnetic fields), are of this type I form. Similarly many semi-classical stress–energy tensors are of this type I form.
For a type I stress tensor the classical energy conditions can be summarized (in terms of necessary and sufficient constraints) as:

NEC	$\rho + p_i \geq 0$	—
WEC	$\rho + p_i \geq 0$	$\rho \geq 0$
SEC	$\rho + p_i \geq 0$	$\rho + \sum p_i \geq 0$
DEC	$\lvert p_i \rvert \leq \rho$	$\rho \geq 0$

- Type II:

$$T^{ab} \sim \left[\begin{array}{cc|cc} \mu + f & f & 0 & 0 \\ f & -\mu + f & 0 & 0 \\ \hline 0 & 0 & p_2 & 0 \\ 0 & 0 & 0 & p_3 \end{array}\right]. \tag{9.11}$$

This corresponds to one double-null eigenvector $k^a = (1;\ 1;\ 0;\ 0)$, so that:

$$T^{ab} = +f\ k^a k^b - \mu\ \eta_2^{ab} + p_2\ n_2^a n_2^b + p_3\ n_3^a n_3^b, \tag{9.12}$$

with $\eta_2^{ab} = \mathrm{diag}(-1,\ 1,\ 0,\ 0)$.[2] The Lorentz invariant eigenvalues of $T^a{}_b$ are now $\{-\mu, -\mu,\ p_2,\ p_3\}$. Classically, the chief physically significant observed occurrence of type II stress–energy is when $\mu = p_i = 0$, in which case one has

$$T^{ab} = f\ k^a\ k^b. \tag{9.13}$$

This corresponds to classical radiation or null dust.

One could also set $p_i = -\mu$ in which case

$$T^{ab} = -\mu\eta^{ab} + f\ k^a\ k^b. \tag{9.14}$$

This corresponds to a superposition of cosmological constant and classical radiation or null dust. Finally, if one sets $p_i = +\mu$ then one has

[2] For type II Hawking and Ellis choose to set $f \to \pm 1$, which we find unhelpful.

$$T^{ab} \sim \left[\begin{array}{cc|cc} \mu & 0 & 0 & 0 \\ 0 & -\mu & 0 & 0 \\ \hline 0 & 0 & \mu & 0 \\ 0 & 0 & 0 & \mu \end{array}\right] + f\, k^a\, k^b. \tag{9.15}$$

This corresponds to a classical electric (or magnetic) field of energy density μ aligned with classical radiation or null dust.

For a type II stress tensor the classical energy conditions can be summarized as:

NEC	$f > 0$	$\mu + p_i \geq 0$	—
WEC	$f > 0$	$\mu + p_i \geq 0$	$\mu \geq 0$
SEC	$f > 0$	$\mu + p_i \geq 0$	$\sum p_i \geq 0$
DEC	$f > 0$	$\lvert p_i \rvert \leq \mu$	$\mu \geq 0$

- Type III:

$$T^{ab} \sim \left[\begin{array}{ccc|c} \rho & 0 & f & 0 \\ 0 & -\rho & f & 0 \\ f & f & -\rho & 0 \\ \hline 0 & 0 & 0 & p \end{array}\right]. \tag{9.16}$$

This corresponds to one triple-null eigenvector $k^a = (1;\ 1;\ 0;\ 0)$.

$$T^{ab} = -\rho\ \eta_3^{ab} + f\ (n_2^a k^b + k^a n_2^b) + p\ n_3^a n_3^b, \tag{9.17}$$

with $\eta_3^{ab} = \text{diag}(-1,\ 1,\ 1,\ 0)$.[3] The Lorentz invariant eigenvalues of $T^a{}_b$ are now $\{-\rho, -\rho, -\rho,\ p\}$. Classically, type III does not seem to occur in nature — the reason for which becomes "obvious" once we look at the standard energy conditions. Even semi-classically this type III form is forbidden (for instance) by either spherical symmetry or planar symmetry — we know of no physical situation where type III stress–energy tensors arise.

For a type III stress tensor the NEC cannot be satisfied for $f \neq 0$, and so the only way that any of the standard energy conditions can be satisfied for a type III stress–energy tensor is if $f = 0$, in which case it reduces to type I. So if one ever encounters a nontrivial type III stress–energy tensor, one immediately knows that all of the standard energy conditions are violated.

(This of course implies that any classical type III stress tensor, since it would have to violate all the energy conditions, would likely be grossly unphysical — so it is

[3] For type III Hawking and Ellis choose to set $f \to 1$, which we find unhelpful.

not too surprising that no classical examples of type III stress–energy have been encountered.)

- Type IV:

$$T^{ab} \sim \left[\begin{array}{cc|cc} \rho & f & 0 & 0 \\ f & -\rho & 0 & 0 \\ \hline 0 & 0 & p_1 & 0 \\ 0 & 0 & 0 & p_2 \end{array}\right]. \tag{9.18}$$

This corresponds to no timelike or null eigenvectors. The Lorentz invariant eigenvalues of $T^a{}_b$ are now $\{-\rho + if, -\rho - if, p_1, p_2\}$.[4]

Classically, type IV does not seem to occur in nature. Again, a necessary condition for the NEC to be satisfied for a type IV stress tensor is $f = 0$. The only way that any of the standard energy conditions can be satisfied for a type IV stress–energy tensor is if $f = 0$, in which case it reduces to type I. So whenever one encounters a nontrivial type IV stress-energy tensor, one immediately knows that all of the standard energy conditions are violated. (Again, this of course implies that any classical type IV stress tensor, since it would have to violate all the energy conditions, would likely be grossly unphysical — so it is not too surprising that no classical examples of type IV stress–energy have been encountered.)

Semi-classically, however, vacuum polarization effects do often generate type IV stress energy [16]. The renormalized stress–energy tensor surrounding an evaporating (Unruh vacuum) black hole will be type IV in the asymptotic region [17], (with spherical symmetry enforcing $p_1 = p_2$). As it will be type I close to the horizon, there will be a finite radius at which it will be type II.

- Euclidean signature:

Since we have seen this point causes some confusion, it is worth pointing out that when working in Euclidean signature (in an orthonormal basis) the eigenvalue problem simplifies to the standard case

$$\det\left(T^{ab} - \lambda\delta^{ab}\right) = 0. \tag{9.20}$$

Since T^{ab} is symmetric it can be diagonalized by ordinary orthogonal 4-matrices. The symmetry group is now $O(4)$, not $O(3,1)$. So in Euclidean signature *all* stress-energy tensors are of type I.

[4] For type IV Hawking and Ellis choose

$$T^{ab} \sim \left[\begin{array}{cc|cc} 0 & f & 0 & 0 \\ f & -\mu & 0 & 0 \\ \hline 0 & 0 & p_1 & 0 \\ 0 & 0 & 0 & p_2 \end{array}\right] \qquad (\mu^2 < 4f^2). \tag{9.19}$$

We have found the version presented in the text to be more useful.

The other thing that happens in Euclidean signature is that, because one no longer has the time-like/light-like/space-like distinction, both the NEC and DEC simply cannot be formulated. In fact it is best to abandon even the WEC, and concentrate attention on a Euclidean variant of the SEC:

- Euclidean Ricci convergence condition: $R_{ab}V^aV^b \geq 0$ for all vectors.
- Euclidean SEC: $(T_{ab} - \frac{1}{2}\,T\,\eta^{ab})V^aV^b \geq 0$ for all vectors.

- Classifying the Ricci and Einstein tensors:

  Instead of applying the Hawking–Ellis type I — type IV classification to the stress–energy tensor, one could choose to apply these ideas directly to the Ricci tensor (or Einstein tensor). The type I — type IV classification would now become statements regarding the number of space-like/null/eigenvectors of the Ricci/Einstein tensor, and the associated eigenvalues would have a direct interpretation in terms of curvature, (rather than densities, fluxes, and stresses). Formulated in this way, this directly geometrical approach would then lead to constraints on spacetime curvature that would be independent of the specific gravity theory one works with.

9.2.2 Alternative Canonical Form

Sometimes it is useful to side-step the Hawking–Ellis classification and, using only rotations, reduce an arbitrary stress–energy tensor to the alternative canonical form

$$T^{ab} \sim \left[\begin{array}{c|ccc} \rho & f_1 & f_2 & f_3 \\ \hline f_1 & p_1 & 0 & 0 \\ f_2 & 0 & p_2 & 0 \\ f_3 & 0 & 0 & p_3 \end{array}\right]. \tag{9.21}$$

The advantage of this alternative canonical form is that it covers all of the Hawking–Ellis types simultaneously. The disadvantage is that it easily provides us with necessary conditions, but does not easily provide us with sufficient conditions for generic stress tensors. For example, enforcing the NEC requires

$$\rho \pm 2\sum_i \beta_i f_i + \sum_i \beta_i^2 p_i \geq 0, \quad \text{with} \quad \sum_i \beta_i^2 = 1. \tag{9.22}$$

By summing over $\pm\beta$ one obtains

$$\rho + \sum_i \beta_i^2 p_i \geq 0, \quad \text{with} \quad \sum_i \beta_i^2 = 1, \tag{9.23}$$

which in turn implies

$$\text{NEC:} \qquad \left|\sum_i \beta_i f_i\right| \leq \frac{1}{2}\left(\rho + \sum_i \beta_i^2 p_i\right) \geq 0, \quad \text{with} \quad \sum_i \beta_i^2 = 1. \tag{9.24}$$

These are necessary and sufficient conditions for the NEC to hold — the quadratic occurrence of the β_i makes it difficult to simplify these further. Similarly for the WEC one finds

$$\text{WEC:} \qquad \left|\sum_i \beta_i f_i\right| \leq \frac{1}{2}\left(\rho + \sum_i \beta_i^2 p_i\right) \geq 0, \quad \text{with} \quad \sum_i \beta_i^2 \leq 1. \tag{9.25}$$

For the SEC one obtains

$$\text{SEC:} \qquad \left|\sum_i \beta_i f_i\right| \leq \frac{1}{4}\left(\left(\rho + \sum_i p_i\right) + \sum_i \beta_i^2 \left(\rho + p_i - \sum_{j\neq i} p_j\right)\right) \geq 0, \tag{9.26}$$

again with $\sum_i \beta_i^2 \leq 1$. Finally, the DEC is somewhat messier. The DEC amounts to the WEC *plus* the relatively complicated constraint

$$\left(\rho + \sum_i \beta_i f_i\right)^2 - \sum_i (f_i + \beta_i p_i)^2 \geq 0, \quad \text{with} \quad \sum_i \beta_i^2 \leq 1. \tag{9.27}$$

This can be slightly massaged to yield

$$\left|\sum_i \beta_i f_i (\rho - p_i)\right| \leq \frac{1}{2}\left(\rho^2 + \left(\sum_i \beta_i f_i\right)^2 - \sum_i (f_i^2 + \beta_i^2 p_i^2)\right) \geq 0, \tag{9.28}$$

again with $\sum_i \beta_i^2 \leq 1$. Unfortunately this seems to be the best that can generically be done for the DEC in this alternative canonical form.

9.2.3 Limitations of the Standard Energy Conditions

For practical computations the energy conditions are most often rephrased in terms of the parameters appearing in the type I — type IV classification, as presented in Sect. 9.2.1, with type I stress–energy being the most prominent. (The other types are often quietly neglected.) When expressed in this form, the standard energy conditions can easily be compared with both classical and with published semi-classical estimates of the renormalized expectation value of the quantum stress–energy tensor.

Beyond the strong physical intuition in which the energy conditions are based, there are deep theoretical reasons why one should wish the energy conditions to be satisfied. It is known that violations of the NEC, which is the weakest energy condition we have presented for the moment, may signal the presence of instabilities and superluminal propagation[5] [21–24]. Moreover, stress–energy tensors violating the NEC can support hypothetical configurations as wormholes [9] and warp drives [25] in the framework of general relativity,[6] which may lead to pathological situations. In addition, the energy conditions are central to proving the positivity of mass [49] and the singularity theorems [1, 3]. In this context, although one might think that violations of the NEC might always allow us to get rid of uncomfortable singularities, this is not the case [50, 51], and they can instead introduce new kinds of cosmic singularities instead [52–56]. Nevertheless, it is already well-known that the energy conditions are violated in realistic situations, where violations of these energy conditions in the presence of semi-classical effects being very common. Among many situations where one or more of the energy conditions are violated we mention:

- SEC has to be violated in cosmological scenarios during the early phase of inflationary expansion and at the present time [57–61].
- It is easy to find violations of the SEC associated even with quite normal matter [62, 63].
- Non-minimally coupled scalar fields can easily violate all the energy conditions even classically [64].
  (However, those fields may be more naturally interpreted as modifications of general relativity in some cases.)
- The Casimir vacuum violates all the mentioned energy conditions [16].
- Numerically estimated renormalized vacuum expectation values of test-field quantum stress tensors surrounding Schwarzschild and other black holes [65].
  (EC violations occur, to one extent or another, for all of the standard quantum vacuum states: Boulware [66], Hartle–Hawking [67], and Unruh [68].)
- Explicitly calculable renormalized vacuum expectation values of test-field quantum stress tensors in 1+1 dimensional QFTs [69].
  (Again, energy condition violations occur to one extent or another, for all of the standard quantum vacuum states: Boulware, Hartle–Hawking, and Unruh.)

Finally, it should be emphasized that the DEC, WEC, and NEC impose restrictions on the form of the stress–energy tensor of the matter fields independently of the theory of gravity. However, when these conditions are used to extract general features of the spacetime, (such as, for example the occurrence of singularities), one considers a particular theory of gravitation. Therefore, although the existence of wormholes and bouncing cosmologies required violations of the NEC in general relativity, in modified gravity theories the NCC could be violated by material content satisfying the NEC. In that case, it is possible to define an effective stress–energy tensor putting

[5] Note that stable violations of the NEC are now known to be possible when the field has a non-canonical kinetic term [18–20].

[6] See Refs. [26–48] for interesting research along those lines.

together the modifications with respect to general relativity that violates the NEC [64, 70–74]. As this effective tensor is not associated with matter, there is no reason to require that it had some *a priori* characteristics. Hence, one may obtain wormhole solutions supported by matter with "positive" energy [75–77], as in some of the examples reviewed in the first part of this book.

9.3 Averaged Energy Conditions

The key to the averaged energy conditions is simply to integrate the Raychaudhuri equation along a timelike geodesic

$$\theta_f - \theta_i = \int_i^f \left\{ \omega_{ab}\omega^{ab} - \sigma_{ab}\sigma^{ab} - \frac{1}{3}\theta^2 - R_{ab}V^aV^b \right\} ds. \tag{9.29}$$

Assuming zero vorticity, and noting that both $\sigma_{ab}\sigma^{ab} \geq 0$ and $\theta^2 \geq 0$ we have

$$\theta_f \leq \theta_i - \int_i^f R_{ab}V^aV^b ds. \tag{9.30}$$

That is, a constraint on the *integrated* timelike convergence condition, $\int R_{ab}V^aV^b ds$, is sufficient to control the convergence of timelike geodesics. In applications, the integral generally runs from some base point along a timelike geodesic into the infinite future. We formulate the ATCC (averaged timelike convergence condition):

Averaged time-like convergence condition (ATCC): Gravity attracts provided

$$\int_0^\infty R_{ab}V^aV^b ds \geq 0 \quad \text{along any timelike geodesic.} \tag{9.31}$$

In standard general relativity the Einstein equations allow one to reformulate this as

Averaged strong condition (ASEC): Gravity in GR attracts on average.

$$\int_0^\infty \left(T_{ab} - \frac{1}{2}T g_{ab} \right) V^aV^b ds \geq 0 \quad \text{along any timelike geodesic.} \tag{9.32}$$

Similar logic can be applied to null geodesic congruences and the Raychaudhuri equation along null geodesics to deduce

Averaged null convergence condition (ANCC): Gravity attracts provided

$$\int_0^\infty R_{ab}k^a k^b d\lambda \geq 0 \quad \text{along any null geodesic.} \tag{9.33}$$

In standard general relativity the Einstein equations allow one to reformulate this as

Averaged null energy condition (ANEC): A necessary requirement for gravity to attract in GR on average is

$$\int_0^\infty T_{ab}\, k^a k^b\, d\lambda \geq 0 \quad \text{along any null geodesic.} \tag{9.34}$$

Note that the integral must be performed using an affine parameter — with arbitrary parameterization these conditions would be vacuous. This ANEC has attracted considerable attention over the years[7] to prove singularity theorems [85, 86] and is for instance the basis of the *topological censorship theorem* [87, 88] forbidding a large class of traversable wormholes. However, note that even the ANEC can be violated by conformal anomalies [89], so to have any hope of a truly general derivation of the ANEC from more fundamental principles, one would need to enforce some form of conformal anomaly cancellation.

9.4 Nonlinear Energy Conditions

The idea behind nonlinear energy conditions is inspired to some extent by the qualitative difference between the NEC/WEC/SEC and the DEC. The NEC/WEC/SEC are strictly linear — any sum of stress–energy tensors satisfying these conditions will also satisfy the same condition. This linearity fails however for the DEC, which can be rephrased as the two conditions

$$T_{ab}\, V^a V^b \geq 0; \qquad (-T_{ac}\eta^{cd}T_{db})V^a V^b \geq 0; \qquad \forall \quad \text{timelike} \quad V. \tag{9.35}$$

The second quadratic condition is imply the statement that the flux F be non spacelike. We can further combine these into one quadratic condition

$$(-[T_{ac} - \varepsilon\eta_{ac}]\eta^{cd}[T_{db} - \varepsilon\eta_{db}])V^a V^b \geq \varepsilon^2; \quad \forall\varepsilon > 0; \quad \forall \quad \text{timelike} \quad V. \tag{9.36}$$

[7] Interesting studies include (but are not limited to) Refs. [78–84].

That is, the DEC (suitably rephrased) is a nonlinear quadratic constraint on the stress–energy, and it is this version of the DEC that can naturally be integrated along timelike geodesics to develop an ADEC. Furthermore this observation opens up the possibility that other nonlinear constraints on the stress–energy might be physically interesting. Among such possibilities, we mention the flux energy condition [90, 91], determinant energy condition, and trace-of-square energy condition [17].

Flux energy condition (FEC): The energy density measured by any observer propagates in a causal way.

$$F^a F_a \leq 0. \tag{9.37}$$

It has to be emphasized that the FEC does not assume anything about the *sign* of the energy density. Moreover, by its very definition the DEC is just the combination of the WEC and the FEC. For the different types of stress-energy tensor we have

Type I	$\rho^2 \geq p_i^2$	—
Type II	$\mu^2 \geq p_i^2$	$\mu f \geq 0$

The FEC cannot be satisfied for genuine (that is $f \neq 0$) types III and IV. The FEC is a weakening of the DEC, and is equivalent to the single quadratic constraint

$$(T_{ac}\eta^{cd}T_{db})V^a V^b \leq 0; \qquad \forall \quad \text{timelike} \quad V. \tag{9.38}$$

Once phrased in this way, it becomes clear how to formulate an averaged version of the FEC.

Averaged flux energy condition (AFEC):

$$\int_0^\infty (T_{ac}\eta^{cd}T_{db})V^a V^b ds \leq 0; \quad \text{along all timelike geodesics.} \tag{9.39}$$

On the other hand, among other nonlinear combinations of the stress–energy tensor, we might consider the following energy conditions:

Determinant energy condition (DETEC): The determinant of the stress–energy tensor is nonnegative.

$$\det\left(T^{ab}\right) \geq 0. \tag{9.40}$$

In terms of the type decomposition we have

Type I	$\rho p_1 p_2 p_3 \geq 0$
Type II	$-\mu^2 p_1 p_2 \geq 0$
Type III	$\rho^3 p \geq 0$
Type IV	$-\left(\rho^2 + f^2\right) p_1 p_2 \geq 0$
Alternative	$\rho p_1 p_2 p_3 - f_1^2 p_2 p_3 - f_2^2 p_3 p_1 - f_3^2 p_2 p_2 \geq 0$

Trace-of-square energy condition (TOSEC): The trace of the squared stress–energy tensor is nonnegative.

$$T^{ab} T_{ab} \geq 0. \tag{9.41}$$

In terms of the type decomposition we have

Type I	$\rho^2 + \sum p_i^2 \geq 0$
Type II	$2\mu^2 + \sum p_i^2 \geq 0$
Type III	$3\rho^2 + p^2 \geq 0$
Type IV	$2\left(\rho^2 - f^2\right) + \sum p_i^2 \geq 0$
Alternative	$\sum f_i^2 \leq \frac{1}{2}(\rho^2 + \sum_i p_i^2)$

Since the TOSEC is basically a sum of squares, it is only in Lorentzian signature that it can possibly be nontrivial — and even in Lorentzian signature only a type IV stress–energy tensor can violate the TOSEC.

Some comments about the fulfilment of these conditions are in order [17]:

- DETEC is violated in cosmological scenarios during the early inflationary phase and at the present time in the framework of GR.
- FEC is violated by the Casimir vacuum, but it can be satisfied by the renormalized stress–energy tensor of the Boulware vacuum of a Schwarzschild spacetime.
- TOSEC can be violated by the Unruh vacuum of a Schwarzschild spacetime.

9.5 Semi-classical Energy Conditions

We now note that when considering semi-classical effects the ECs may be violated, although the relevant inequalities are typically not satisfied only by a *small amount*. This fact led us to formulate the semi-classical energy conditions in a preliminary

and somewhat vague way, to allow them to quantify the violation of the classical ECs, before considering a particular more specific formulation [17, 91].

Quantum WEC (QWEC): The energy density measured by any observer should not be *excessively negative*.

The QWEC, therefore, allows the energy density to be negative in semi-classical situations but its value has to be bounded from below. Now, assuming that this bound depends on characteristics of the system, such as the number of fields N, the system 4-velocity U^a, and a characteristic distance L, we can formulate the QWEC as

$$T^a{}_b\, V_a V^b \geq -\zeta\, \frac{\hbar N}{L^4}\, (U_a\, V^a)^2. \tag{9.42}$$

Here ζ is a parameter of order unity. For the QWEC we have:

Type I	$\rho \geq -\zeta\hbar N/L^4$	$\rho + p_i \geq -\zeta\hbar N/L^4$	—
Type II	$\mu \geq -\zeta\hbar N/L^4$	$p_i \geq -\zeta\hbar N/L^4$	$f \geq -\zeta\hbar N/L^4$
Type III	$\rho \geq -\zeta\hbar N/L^4$	$p \geq -\zeta\hbar N/L^4$	$\lvert f\rvert \leq \zeta\hbar N/L^4$
Type IV	$\rho \geq -\zeta\hbar N/L^4$	$p_i \geq -\zeta\hbar N/L^4$	$\lvert f\rvert \leq \zeta\hbar N/L^4$

In a similar way, other quantum (semi-classical) energy conditions have been formulated.

Quantum FEC (QFEC): The energy density measured by any observer either propagates in a causal way, or does not propagate *too badly* in an acausal way.

So, the QFEC allows the flux 4-vector to be (somewhat) space-like in semi-classical situations but its norm has to be bounded from above. It can be written as

$$F^a F_a \leq \zeta\, \left(\frac{\hbar N}{L^4}\right)^2\, (U_a\, V^a)^2. \tag{9.43}$$

Here ζ is again a parameter of order unity. For the QFEC we have:

Type I	$\rho^2 - p_i^2 \geq -\zeta \left(\hbar N/L^4\right)^2$	—	—
Type II	$\mu^2 - p_i^2 \geq -\zeta \left(\hbar N/L^4\right)^2$	$\mu f \geq -\zeta \left(\hbar N/L^4\right)^2$	—
Type III	$\rho^2 - p^2 \geq -\zeta \left(\hbar N/L^4\right)^2$	$\lvert\rho f\rvert \leq \zeta \left(\hbar N/L^4\right)^2$	$\lvert f\rvert \leq \zeta \hbar N/L^4$
Type IV	$\rho^2 - p_i^2 \geq -\zeta \left(\hbar N/L^4\right)^2$	$\lvert\rho f\rvert \leq \zeta \left(\hbar N/L^4\right)^2$	$\lvert f\rvert \leq \zeta \hbar N/L^4$

Analogously with the classical energy conditions, the quantum DEC (QDEC) would be satisfied in situations where both the QWEC and QFEC are fulfilled. That is, the QDEC states the following

Quantum DEC (QDEC): The energy density measured by any observer should not be *excessively negative*, and it either propagates in a causal way or does not propagate *too badly* in an acausal way. Specifically,

$$T^a{}_b\, V_a V^b \geq -\zeta_W \frac{\hbar N}{L^4}\, (U_a\, V^a)^2, \tag{9.44}$$

$$F^a F_a \leq \zeta_F \left(\frac{\hbar\, N}{L^4}\right)^2 (U_a\, V^a)^2. \tag{9.45}$$

In order to get the relevant inequalities for the QDEC to be satisfied for types I — IV stress–energy tensors, one needs just to combine the inequalities of the QWEC and QFEC tables, taking into account that the two ζ's should be kept distinct.

(For a recent rediscovery of a quantum energy condition along the lines investigated in Refs. [17, 91, 92] and presented here see Ref. [93]. For non-local quantum energy inequalities see Refs. [94, 95].)

Regarding the semi-classical quantum energy conditions it should be noted that:

- QECs are, of course, satisfied in classical situations where their classical counterparts are satisfied.
- The Casimir vacuum satisfies the QECs presented here [17].
- QFEC can be satisfied by the Boulware and Unruh vacuum even in situations where the QWEC is violated [91].
- The QECs can be used as a way of quantifying/minimizing the violation of the ECs.

Concerning the last point it should be clarified we are referring to quantifying the degree of violation of an energy condition for a given amount of matter [92, 96–98], and not to minimizing the quantity of matter violating the energy condition [99–101].

9.6 Discussion

As we have seen, the energy conditions (both classical and semi-classical) are numerous and varied, and depending on the context can give one rather distinct flavours of both qualitative and quantitative information — either concerning the matter content, or concerning the (attractive) nature of gravity. Variations on the original classical point-wise energy conditions are still under development and investigation, and the status of the energy conditions as fundamental physics should still be considered provisional.

There is no strict ordering on the set of energy conditions, at best a partial ordering, so there is no strictly "weakest" energy condition. Nonetheless, perhaps the weakest of the *usual* energy conditions (in terms of the constraint imposed on the stress energy) is the ANEC, which makes it the strongest energy condition in terms of proving theorems. Attempts at developing a general proof of the ANEC are ongoing — part of the question is exactly what one might mean by "proving an energy condition" from more fundamental principles. It should be noted, however, that even the ANEC can be violated by conformal anomalies, so to have any hope of a truly general derivation of the ANEC from more fundamental principles, one would need to enforce some form of conformal anomaly cancellation.

On the other hand, it should be emphasized that the FEC is completely independent of the NEC. Hence, there could be in principle realistic situations where the stress–energy tensor violates the ANEC but satisfies the FEC. Although, as we have reviewed, the FEC can be violated by semi-classical effects, its quantum counterpart is satisfied by the renormalized stress–energy tensor of quantum vacuum states.

An alternative approach is to formulate curvature conditions directly on the Ricci or Einstein tensors, and then use global analysis, (based, for instance, on the Raychaudhuri equation or its generalized variants) to extract information regarding curvature singularities and/or the Weyl tensor.

Acknowledgements PMM acknowledges financial support from the Spanish Ministry of Economy and Competitiveness through the postdoctoral training contract FPDI-2013-16161, and through the project FIS2014-52837-P. MV acknowledges financial support via the Marsden Fund administered by the Royal Society of New Zealand.

References

1. Hawking SW, Ellis GFR. The large scale structure of spacetime. England: Cambridge University Press; 1972.
2. Abreu G, Visser M. Some generalizations of the Raychaudhuri equation. Phys Rev D. 2011;83:104016.
3. Borde A. Geodesic focusing, energy conditions and singularities. Class Quant Grav. 1987;4:343.
4. Parikh M, van der Schaar JP. Derivation of the null energy condition. Phys Rev D. 2015;91(8):084002.
5. Parikh M. Two roads to the null energy condition. Int J Mod Phys D. 2015;24:1544030.

6. Parikh M, Svesko A. Thermodynamic Origin of the Null Energy Condition. arXiv:1511.06460 [hep-th].
7. Parikh M, Svesko A. Logarithmic corrections to gravitational entropy and the null energy condition. Phys Lett B. 2016;761:16.
8. Morris MS, Thorne KS. Wormholes in space-time and their use for interstellar travel: a tool for teaching general relativity. Am J Phys. 1988;56:395.
9. Morris MS, Thorne KS, Yurtsever U. Wormholes, time machines, and the weak energy condition. Phys Rev Lett. 1988;61:1446.
10. Hochberg D, Visser M. Dynamic wormholes, anti-trapped surfaces, and energy conditions. Phys Rev D. 1998;58:044021.
11. Borde A, Vilenkin A. Violations of the weak energy condition in inflating space-times. Phys Rev D. 1997;56:717.
12. Molina-París C, Visser M. Minimal conditions for the creation of a Friedman–Robertson–Walker universe from a bounce. Phys Lett B. 1999;455:90.
13. Barceló C, Visser M. Twilight for the energy conditions? Int J Mod Phys D. 2002;11:1553.
14. Bekenstein JD. If vacuum energy can be negative, why is mass always positive?: uses of the subdominant trace energy condition. Phys Rev D. 2013;88:125005.
15. Hayward G. Quasilocal energy conditions. Phys Rev D. 1995;52:2001.
16. Roman TA. Quantum stress energy tensors and the weak energy condition. Phys Rev D. 1986;33:3526.
17. Martín-Moruno P, Visser M. Semiclassical energy conditions for quantum vacuum states. JHEP. 2013;1309:050.
18. Nicolis A, Rattazzi R, Trincherini E. Energy's and amplitudes' positivity. JHEP. 2010;1005:095 Erratum: [JHEP. 2011;1111:128].
19. Deffayet C, Pujolas O, Sawicki I, Vikman A. Imperfect dark energy from kinetic gravity braiding. JCAP. 2010;1010:026.
20. Kobayashi T, Yamaguchi M, Yokoyama J. G-inflation: inflation driven by the Galileon field. Phys Rev Lett. 2010;105:231302.
21. Dubovsky S, Gregoire T, Nicolis A, Rattazzi R. Null energy condition and superluminal propagation. JHEP. 2006;0603:025.
22. Visser M, Bassett B, Liberati S. Perturbative superluminal censorship and the null energy condition. AIP Conf Proc. 1999;493:301.
23. Visser M, Bassett B, Liberati S. Superluminal censorship. Nucl Phys Proc Suppl. 2000;88:267.
24. Lobo F, Crawford P. Weak energy condition violation and superluminal travel. Lect Notes Phys. 2003;617:277.
25. Alcubierre M. The warp drive: hyperfast travel within general relativity. Class Quant Grav. 1994;11:L73.
26. Visser M. Traversable wormholes: some simple examples. Phys Rev D. 1989;39:3182.
27. Visser M. Traversable wormholes from surgically modified Schwarzschild space-times. Nucl Phys B. 1989;328:203.
28. Cramer JG, Forward RL, Morris MS, Visser M, Benford G, Landis GA. Natural wormholes as gravitational lenses. Phys Rev D. 1995;51:3117.
29. Ori A, Soen Y. Causality violation and the weak energy condition. Phys Rev D. 1994;49(8):3990.
30. Kar S. Evolving wormholes and the weak energy condition. Phys Rev D. 1994;49:862.
31. Hochberg D, Visser M. Geometric structure of the generic static traversable wormhole throat. Phys Rev D. 1997;56:4745.
32. Visser M, Hochberg D. Generic wormhole throats. Annals Israel Phys Soc. 1997;13:249.
33. Hochberg D, Visser M. The null energy condition in dynamic wormholes. Phys Rev Lett. 1998;81:746.
34. Hochberg D, Molina-París C, Visser M. Tolman wormholes violate the strong energy condition. Phys Rev D. 1999;59:044011.
35. Hochberg D, Visser M. General dynamic wormholes and violation of the null energy condition. arXiv:gr-qc/9901020.

36. Barceló C, Visser M. Brane surgery: energy conditions, traversable wormholes, and voids. Nucl Phys B. 2000;584:415.
37. Dadhich N, Kar S, Mukherji S, Visser M. R = 0 space-times and selfdual Lorentzian wormholes. Phys Rev D. 2002;65:064004.
38. Visser M. The Quantum physics of chronology protection. arXiv:gr-qc/0204022.
39. Lemos JPS, Lobo FSN, Quinet de Oliveira S. Morris–Thorne wormholes with a cosmological constant. Phys Rev D. 2003;68:064004.
40. Lobo FSN, Crawford P. Linearized stability analysis of thin shell wormholes with a cosmological constant. Class Quant Grav. 2004;21:391.
41. Lobo FSN. Energy conditions, traversable wormholes and dust shells. Gen Rel Grav. 2005;37:2023.
42. Roman TA. Some thoughts on energy conditions and wormholes. arXiv:gr-qc/0409090.
43. Lobo FSN, Visser M. Fundamental limitations on 'warp drive' spacetimes. Class Quant Grav. 2004;21:5871.
44. Lobo FSN. Phantom energy traversable wormholes. Phys Rev D. 2005;71:084011.
45. Lobo FSN. Chaplygin traversable wormholes. Phys Rev D. 2006;73:064028.
46. Lobo FSN. Exotic solutions in general relativity: traversable wormholes and 'warp drive' spacetimes. Classical and quantum gravity research. New York: Nova Science Publishers; 2008. p. 1–78 ISBN 978-1-60456-366-5 [arXiv:0710.4474 [gr-qc]].
47. Martín-Moruno P, González-Díaz PF. Thermal radiation from Lorentzian traversable wormholes. Phys Rev D. 2009;80:024007.
48. Visser M. Buchert coarse-graining and the classical energy conditions. arXiv:1512.05729 [gr-qc].
49. Bekenstein JD. Positiveness of mass and the strong energy condition. Int J Theor Phys. 1975;13:317.
50. Cattoën C, Visser M. Necessary and sufficient conditions for big bangs, bounces, crunches, rips, sudden singularities, and extremality events. Class Quant Grav. 2005;22:4913.
51. Cattoën C, Visser M. Cosmological milestones and energy conditions. J Phys Conf Ser. 2007;68:012011.
52. Starobinsky AA. Future and origin of our universe: modern view. Grav Cosmol. 2000;6:157.
53. Caldwell RR, Kamionkowski M, Weinberg NN. Phantom energy and cosmic doomsday. Phys Rev Lett. 2003;91:071301.
54. Yurov AV, Martin Moruno P, Gonzalez-Diaz PF. New bigs in cosmology. Nucl Phys B. 2006;759:320.
55. Bouhmadi-López M, González-Díaz PF, Martín-Moruno P. Worse than a big rip? Phys Lett B. 2008;659:1.
56. Bouhmadi-López M, González-Díaz PF, Martín-Moruno P. On the generalised Chaplygin gas: worse than a big rip or quieter than a sudden singularity? Int J Mod Phys D. 2008;17:2269.
57. Visser M. Energy conditions and galaxy formation. arXiv:gr-qc/9710010.
58. Visser M. Energy conditions in the epoch of galaxy formation. Science. 1997;276:88.
59. Visser M. General relativistic energy conditions: the Hubble expansion in the epoch of galaxy formation. Phys Rev D. 1997;56:7578.
60. Visser M, Barceló C. Energy conditions and their cosmological implications. arXiv:gr-qc/0001099.
61. Cattoën C, Visser M. Cosmodynamics: energy conditions, Hubble bounds, density bounds, time and distance bounds. Class Quant Grav. 2008;25:165013.
62. Kandrup HE. Violations of the strong energy condition for interacting systems of particles. Phys Rev D. 1992;46:5360.
63. Rose B. A matter model violating the strong energy condition-the influence of temperature. Class Quant Grav. 1987;4:1019.
64. Barceló C, Visser M. Scalar fields, energy conditions, and traversable wormholes. Class Quant Grav. 2000;17:3843.
65. Visser M. Gravitational vacuum polarization. arXiv:gr-qc/9710034.

66. Visser M. Gravitational vacuum polarization. 2: energy conditions in the Boulware vacuum. Phys Rev D. 1996;54:5116.
67. Visser M. Gravitational vacuum polarization. 1: energy conditions in the Hartle–Hawking vacuum. Phys Rev D. 1996;54:5103.
68. Visser M. Gravitational vacuum polarization. 4: energy conditions in the Unruh vacuum. Phys Rev D. 1997;56:936.
69. Visser M. Gravitational vacuum polarization. 3: energy conditions in the $(1 + 1)$ Schwarzschild space-time. Phys Rev D. 1996;54:5123.
70. Bellucci S, Faraoni V. Energy conditions and classical scalar fields. Nucl Phys B. 2002;640:453.
71. Baccetti V, Martín-Moruno P, Visser M. Null energy condition violations in bimetric gravity. JHEP. 2012;1208:148.
72. Capozziello S, Lobo FSN, Mimoso JP. Energy conditions in modified gravity. Phys Lett B. 2014;730:280.
73. Capozziello S, Lobo FSN, Mimoso JP. Generalized energy conditions in extended theories of gravity. Phys Rev D. 2015;91(12):124019.
74. Rubakov VA. The null energy condition and its violation. Phys Usp. 2014;57:128 [Usp Fiz Nauk. 2014;184(2):137].
75. Lobo FSN, Oliveira MA. Wormhole geometries in f(R) modified theories of gravity. Phys Rev D. 2009;80:104012.
76. Montelongo Garcia N, Lobo FSN. Nonminimal curvature-matter coupled wormholes with matter satisfying the null energy condition. Class Quant Grav. 2011;28:085018.
77. Boehmer CG, Harko T, Lobo FSN. Wormhole geometries in modified teleparralel gravity and the energy conditions. Phys Rev D. 2012;85:044033.
78. Klinkhammer G. Averaged energy conditions for free scalar fields in flat space-times. Phys Rev D. 1991;43:2542.
79. Ford LH, Roman TA. Averaged energy conditions and quantum inequalities. Phys Rev D. 1995;51:4277.
80. Yurtsever U. The averaged null energy condition and difference inequalities in quantum field theory. Phys Rev D. 1995;51:5797.
81. Ford LH, Roman TA. Averaged energy conditions and evaporating black holes. Phys Rev D. 1996;53:1988.
82. Flanagan EE, Wald RM. Does back reaction enforce the averaged null energy condition in semiclassical gravity? Phys Rev D. 1996;54:6233.
83. Fewster CJ, Roman TA. Null energy conditions in quantum field theory. Phys Rev D. 2003;67:044003 Erratum: [Phys Rev D. 2009;80:069903].
84. Graham N, Olum KD. Achronal averaged null energy condition. Phys Rev D. 2007;76:064001.
85. Roman TA. On the averaged weak energy condition and Penrose's singularity theorem. Phys Rev D. 1988;37:546.
86. Fewster CJ, Galloway GJ. Singularity theorems from weakened energy conditions. Class Quant Grav. 2011;28:125009.
87. Friedman JL, Schleich K, Witt DM. Topological censorship. Phys Rev Lett. 1993;71:1486 Erratum: [Phys Rev Lett. 1995;75:1872].
88. Friedman JL, Higuchi A. Topological censorship and chronology protection. Annalen Phys. 2006;15:109.
89. Visser M. Scale anomalies imply violation of the averaged null energy condition. Phys Lett B. 1995;349:443.
90. Abreu G, Barceló C, Visser M. Entropy bounds in terms of the w parameter. JHEP. 2011;1112:092.
91. Martín-Moruno P, Visser M. Classical and quantum flux energy conditions for quantum vacuum states. Phys Rev D. 2013;88(6):061701.
92. Bouhmadi-López M, Lobo FSN, Martín-Moruno P. Wormholes minimally violating the null energy condition. JCAP. 2014;1411(11):007.

93. Bousso R, Fisher Z, Koeller J, Leichenauer S, Wall AC. Proof of the quantum null energy condition. Phys Rev D. 2016;93(2):024017.
94. Fewster CJ, Verch R. Stability of quantum systems at three scales: passivity, quantum weak energy inequalities and the microlocal spectrum condition. Commun Math Phys. 2003;240:329.
95. Fewster CJ. Quantum energy inequalities and stability conditions in quantum field theory. In: Boutet de Monvel A, et al., editors. Rigorous quantum field theory. p. 95–111. arXiv:math-ph/0502002.
96. Bouhmadi-López M, Errahmani A, Martín-Moruno P, Ouali T, Tavakoli Y. The little sibling of the big rip singularity. Int J Mod Phys D. 2015;24(10):1550078.
97. Martín-Moruno P. Semiclassical energy conditions and wormholes. J Phys Conf Ser. 2015;600(1):012036.
98. Albarran I, Bouhmadi-López M, Cabral F, Martín-Moruno P. The quantum realm of the "Little Sibling" of the big rip singularity. JCAP. 2015;1511(11):044.
99. Visser M, Kar S, Dadhich N. Traversable wormholes with arbitrarily small energy condition violations. Phys Rev Lett. 2003;90:201102. arXiv:gr-qc/0301003.
100. Kar S, Dadhich N, Visser M. Quantifying energy condition violations in traversable wormholes. Pramana. 2004;63:859.
101. Garcia NM, Lobo FSN, Visser M. Generic spherically symmetric dynamic thin-shell traversable wormholes in standard general relativity. Phys Rev D. 2012;86:044026.

Chapter 10
Quantum Energy Inequalities

Christopher J. Fewster

10.1 Introduction

Energy conditions are restrictions on the stress–energy tensor, intended to express generic properties such as the tendency of matter to contract under its own gravity. A stress–energy tensor T_{ab} is said to obey

- the Weak Energy Condition (WEC) if $T_{ab}u^a u^b \geq 0$ for all timelike u^a;
- the Null Energy Condition (NEC) if $T_{ab}u^a u^b \geq 0$ for all null u^a;
- the Dominant Energy Condition (DEC) if $T_{ab}u^a v^b \geq 0$ for all future-pointing timelike u^a and v^b;
- and the Strong Energy Condition (SEC) if $T_{ab}u^a u^b - \frac{1}{n-2} g^{ab} T_{ab} \geq 0$ for all timelike unit u^a where n is the spacetime dimension.

These definitions were presented in the previous chapter, but are included here for self-completeness and self-consistency. Some of these conditions have direct physical interpretations: the WEC asserts that every observer perceives a non-negative energy density, while the DEC states that each observer encounters a causal, future-directed energy–momentum flux. For others the interpretation is less direct. The Raychaudhuri equation implies that the expansion of any irrotational null geodesic congruence is non-increasing (and typically decreasing) in any solution to the Einstein equations with stress–energy tensor obeying the NEC [65, Sect. 4.3]; the same holds for irrotational timelike geodesic congruences if the SEC holds (for vanishing cosmological constant). These facts underpin the proofs of the singularity theorems [65, 92] and many other important results in mathematical relativity. See [71] for a review of the Raychaudhuri equations and variants thereof.

It is therefore a surprise that quantum field theory (QFT), our most successful fundamental description of matter, is incompatible with the energy conditions. For

C.J. Fewster (✉)
Department of Mathematics, University of York, Heslington, York YO10 5DD, UK
e-mail: chris.fewster@york.ac.uk

F.S.N. Lobo (ed.), *Wormholes, Warp Drives and Energy Conditions*,
Fundamental Theories of Physics 189, DOI 10.1007/978-3-319-55182-1_10

instance, in any QFT on Minkowski spacetime obeying standard assumptions, each local average of the energy density takes negative expectation values in some physically acceptable states. Worse still, the energy density at a given point can be made unboundedly negative by varying the state. Similarly, vacuum energy densities in many curved spacetime situations are negative, and the Casimir effect provides an experimentally tested phenomenon in which negative energy densities arise. These facts have often been used to argue that QFT might support spacetime geometries, such as wormholes [98] or warp drives [2], that would be impossible for matter that obeys the classical energy conditions. However, the violation of the classical energy conditions is only one among a number of situations in which sharp classical bounds become blurred in quantum theory (tunnelling and diffraction are other examples). A common theme is that the uncertainty principle accounts for both the disease and its remedy: on one hand, classical limitations cannot be maintained, but on the other, transgressions are controlled in their scope. In our case, we may seek bounds on the extent to which a given local average of the energy density can be negative. These constraints, known as Quantum Energy Inequalities (QEIs) are the subject of this chapter.

QEIs (also called Quantum Inequalities) have been studied for nearly 40 years, following the realisation by Ford [52] that unfettered violation of the energy conditions could lead to macroscopic violations of the second law of thermodynamics. They have been derived, in many cases with full mathematical rigour, for a variety of free QFT models in both flat and curved spacetimes.[1] They are less well developed for interacting QFTs (and there are some problems in straightforwardly generalising the type of result that holds in the free case) but QEIs are known for conformal field theories in two dimensions [33] and for the massive Ising model [4]; it is also known that related bounds can be found in a general class of Minkowski QFT models in dimensions of at least 3 [5].

The structure of the chapter is as follows. Section 10.2 shows in detail how negative energy density states can arise in QFT, giving both general results and specific examples. Section 10.3 presents a QEI obeyed by the real scalar field in four-dimensional Minkowski spacetime, namely

$$\int \langle T_{ab} u^a u^b \rangle(\gamma(t))\, |g(t)|^2 dt \geq -\frac{1}{16\pi^2} \int_{-\infty}^{\infty} |g''(t)|^2 dt, \tag{10.1}$$

where γ is an inertial curve with 4-velocity u (a more stringent bound holds for fields of non-zero mass). Here g is any smooth function vanishing outside a bounded set. By a scaling argument it can be shown that an energy density below $\rho < 0$ can be maintained for a proper time τ only if $|\rho|\tau^4 \lesssim 3.17$ in units where $\hbar = c = 1$. This displays the uncertainty principle at work: negative energy densities of large magnitude can only persist over short timescales. This and other consequences of the QEI are discussed in Sect. 10.3.2. In particular, the phenomenon of 'quantum interest' is described and it is also shown how QEIs can provide constraints on

[1] See Sect. 10.3.3 for references.

the Casimir energy density in cavities of arbitrary shape. Section 10.4 explains the derivation of a QEI valid in a general class of curved spacetimes for averaging along any smooth timelike curve for any Hadamard state of the free real scalar field. The argument follows [22] and is fully mathematically rigorous; for ease of reading, the more technical parts (which use some methods from microlocal analysis) are explained in an appendix, while Sect. 10.4 focusses on the structure of the proof. Following that, the resulting QEI bounds are discussed in situations (e.g., stationary trajectories in stationary spacetimes) where there is a time translation symmetry. Two specific examples are studied (both in Minkowski spacetime) for averaging along an inertial curve and a uniformly accelerated curve. The former case yields the bound studied in Sect. 10.3 while in the latter case, the integrand in (10.1) is modified by additional terms proportional to $|g'|^2$ and $|g|^2$ depending on the proper acceleration. The 'uncertainty principle' analogue of the QEI becomes the statement that energy densities below that of the Rindler vacuum state are constrained: $|\rho - \rho_{\text{Rindler}}|\tau^4 \lesssim 3.17/\tau^4$ (for $\tau\alpha \ll 1$).

In Sect. 10.5 we survey some more recent developments in QEIs, focussing on QEIs for non-free QFTs and also recent work on the probability distribution of individual measurements of averaged energy densities. Finally, some applications of the QEIs are described in Sect. 10.6.

Summary of main conventions: We take $\hbar = c = G = 1$ and adopt $(- - -)$ geometric conventions: the metric has signature $+ - - - \cdots$, $(\nabla_a\nabla_b - \nabla_b\nabla_a)v^d = R_{abc}{}^d v^c$, $R_{ab} = R^d{}_{adb}$. Fourier transforms will be defined non-standardly by $\widehat{f}(k) = \int d^n x\, e^{ik\cdot x} f(x)$; and that will sometimes be displaced, e.g. $f^\wedge(k)$, for typographical reasons.

10.2 Violation of the Energy Conditions in QFT

It is helpful to begin with the classical situation. In many cases, classical matter models obey the energy conditions because the left-hand side of the relevant inequality can be written as a sum of squares of basic fields. For example, the minimally coupled scalar field obeying $(\Box + m^2)\phi = 0$ has stress–energy tensor

$$T_{ab} = (\nabla_a\phi)(\nabla_b\phi) - \frac{1}{2}g_{ab}g^{cd}(\nabla_c\phi)(\nabla_d\phi) + \frac{1}{2}g_{ab}m^2\phi^2.$$

Given any timelike unit vector u^a, choose a frame e_A $(0 \le A \le n-1)$ with $e_0 = u$. Then

$$T_{ab}u^a u^b = \frac{1}{2}\sum_{A=0}^{n-1}(e_A \cdot \nabla\phi)^2 + \frac{1}{2}m^2\phi^2 \ge 0 \tag{10.2}$$

so this theory obeys WEC due to the 'sum of squares' form; similarly it also obeys the NEC and DEC for the same reason. However, we also see that

$$T_{ab}u^a u^b - \frac{1}{n-2}T^a{}_a = (u^a\nabla_a\phi)^2 - \frac{1}{n-2}m^2\phi^2$$

so the SEC can fail even for this model if $m > 0$. The non-minimally coupled scalar field, obeying $(\Box + m^2 + \xi R)\phi = 0$, has stress energy tensor

$$T^{(\xi)}_{ab} = T^{(\xi=0)}_{ab} + \xi\left(g_{ab}\Box_g - \nabla_a\nabla_b - G_{ab}\right)\phi^2,$$

where $G_{ab} = R_{ab} - \frac{1}{2}Rg_{ab}$, the Einstein tensor. As the additional terms are not of the sum of squares form, even NEC can be violated: at points where $\nabla\phi = 0$, for example, this happens when the second derivative terms outweigh contributions proportional to ϕ^2.

In QFT, however, squares of fields require regularisation, replacing the square by a Wick square in free theories, for example. The formal square is positive, but infinite; regularisation restores finiteness at the cost of positivity. Let us see how this occurs in the theory of a real scalar field in four-dimensional Minkowski space with mass $m \geq 0$,

$$\Phi(x) = \int \frac{d^3\boldsymbol{k}}{(2\pi)^3\sqrt{2\omega}}\left(e^{-ik\cdot x}a(\boldsymbol{k}) + e^{ik\cdot x}a^*(\boldsymbol{k})\right),$$

where the 4-covector k is $k_\mu = (\omega, \boldsymbol{k})$, with $\omega = \sqrt{\|\boldsymbol{k}\|^2 + m^2}$, the annihilation and creation operators obey the commutation relations

$$[a(\boldsymbol{k}), a(\boldsymbol{k}')] = 0, \qquad [a(\boldsymbol{k}), a^*(\boldsymbol{k}')] = (2\pi)^3\delta^{(3)}(\boldsymbol{k} - \boldsymbol{k}')\mathbb{1}$$

and the vacuum vector is denoted Ω. We will show that if $f \in C_0^\infty(\mathbb{R}^4)$ is any smooth function of compact support (i.e., vanishing outside a bounded set) with $f \not\equiv 0$ then, no matter how large is the support of f, there are states in which the smeared Wick square

$$:\Phi^2:(f) = \int d^4x\, :\Phi^2:(x)f(x),$$

(with $:\Phi^2:(x)$ defined by normal ordering) has negative expectation value. In particular this holds if f is non-negative, when the corresponding smeared classical field squared is always non-negative. Noting that

$$:\Phi^2:(f)\Omega = \int \frac{d^3\boldsymbol{k}}{(2\pi)^3}\frac{d^3\boldsymbol{k}'}{(2\pi)^3}\frac{1}{2\sqrt{\omega\omega'}}\widehat{f}(k+k')a^*(\boldsymbol{k})a^*(\boldsymbol{k}')\Omega,$$

it is obvious that $\langle\Omega \mid :\Phi^2:(f)\Omega\rangle = 0$, and a short calculation gives

$$\|:\Phi^2:(f)\Omega\|^2 = \int \frac{d^3\boldsymbol{k}}{(2\pi)^3}\frac{d^3\boldsymbol{k}'}{(2\pi)^3}\frac{|\widehat{f}(k+k')|^2}{2\omega\omega'},$$

which is non-zero unless f vanishes identically.[2] Accordingly, the observable $:\Phi^2:(f)$ has vanishing expectation value but non-zero fluctuation in the state Ω; it must therefore have some negative spectrum and take on negative expectation values in suitable states. Indeed, if

$$\psi_\alpha = \cos\alpha\,\Omega + \sin\alpha :\Phi^2:(f)\Omega$$

(assuming f is chosen so $\|:\Phi^2:(f)\Omega\| = 1$) then

$$\langle\psi_\alpha \mid :\Phi^2:(f)\psi_\alpha\rangle = \sin(2\alpha) + \sin^2\alpha\langle\Omega \mid :\Phi^2:(f)^3\Omega\rangle = 2\alpha + O(\alpha^2)$$

giving negative expectation values for sufficiently small $\alpha < 0$. By a scaling argument [24] it may be shown that the expectation value of $:\Phi^2:$ at a point is unbounded from below as the state varies among physically reasonable (Hadamard) states.

The same conclusion may be reached in general QFTs. An argument due to Epstein, Glaser and Jaffe [18] proves that loss of positivity is unavoidable for Wightman fields with vanishing vacuum expectation values. The main thrust of their argument is the following. Suppose a local observable A, such as a local average of the energy density, has vanishing vacuum expectation value, $\langle\Omega \mid A\Omega\rangle = 0$. If A is positive, it has a square root, and we have

$$\|A^{1/2}\Omega\|^2 = \langle\Omega \mid A\Omega\rangle = 0$$

and therefore $A^{1/2}\Omega = 0$. Hence $A\Omega = 0$ and thus $A = 0$, because the Reeh–Schlieder theorem [64] entails that no non-zero local observable can annihilate the vacuum. (The Reeh–Schlieder theorem only applies to local observables, which is why the Hamiltonian can be positive and have vanishing vacuum expectation value.) Alternatively, one can argue as follows: individual measurements of A in state Ω constitute a random variable with vanishing expectation value; this implies *either* that zero is measured with probability 1, in which case $A\Omega = 0$ (impossible for non-zero local observables by the Reeh–Schlieder theorem) *or* that there is a non-zero probability for both positive and negative measurement values, so the spectrum of A extends into the negative half-line.

There are many physical situations in which negative energy densities arise in QFT. One of the main examples is provided by the Casimir effect, in which plane parallel conducting plates *in vacuo* experience an attractive force. This force can be predicted from QFT and agrees well with experiment; the same calculations also predict a violation of the weak energy condition between the plates. Actually, this conclusion may be reached simply from the existence of the attractive force and some physical reasoning. In the case of infinite plane plates, separated through distance L along the z-axis in standard (t, x, y, z) coordinates, one may deduce on

[2] As f is compactly supported, $\hat{f}(k)$ is analytic in each component of k. A necessary condition for the integral to vanish is that $\widehat{f}(k + k')$ is identically zero for all k', k on the mass-shell; as the set of 4-momenta of 2-particle states has non-empty interior, $\hat{f}$ and hence f vanish identically.

symmetry grounds and dimensional considerations that the stress–energy tensor of the electromagnetic field takes the form [7]

$$T_{\mu\nu} = \frac{C(z)}{L^4}\mathrm{diag}\,(-1, 1, 1, -3),$$

where $C(z)$ is dimensionless; here we have also used tracelessness of the stress–energy tensor. Conservation of the stress–energy tensor entails that $C(z)$ is constant except at the plates, so C may take different values C_0 and C_1 inside and outside the plates (by reflection symmetry the values on the two outer components should be equal). As there is no other length scale in the problem, C_1 and C_0 must be independent of the plate separation L. Now the two limits $L \to 0$ and $L \to \infty$ can both be regarded as describing a single plate alone in the world (as far as the outer regions are concerned). In the limit $L \to \infty$ one finds that the energy density must vanish to either side of the plate; for this also to happen in the limit $L \to 0$, it must be that $C_1 = 0$. Returning to the case of finite separation, the inward pressure on each plate is then $3C_0/L^4$, so we may deduce $C_0 > 0$ from an attractive Casimir force. Therefore, the energy density between the plates, $-C_0/L^4$, is negative, violating WEC. The full computation of the stress–energy tensor in QFT leads to the values $C_1 = 0$ and $C_0 = \pi^2/720$.

A noteworthy feature of the Casimir effect is the small magnitude of the leading coefficient $\pi^2/720 = 0.0137...$ in the stress–energy tensor. This is a typical feature—violations of the energy conditions are typically either small in magnitude, or short-lived, or when they are not, require disparate scales, highly non-inertial motion, or large positive energies somewhere in the system. Indeed, it has been argued that the classical energy conditions might be regarded as holding in an operational sense, once one takes account of the positive energies present in apparatus used to produce and detect negative energy densities [66].

Other well-known instances in which negative energy densities occur include moving mirror models in $1 + 1$ dimensions [62], and (portions of) the exterior of a Schwarzschild black hole in the Hartle–Hawking, Boulware or Unruh states (see [99–101], and [80] for recent numerical calculations).

It is clear that the pointwise energy conditions are not respected by QFT. To gain some insight into what conditions might hold instead, it is helpful to consider again the expectation values of the Wick square in a state

$$\Psi = \mathscr{N}\left[\Omega + \lambda \int d^3\boldsymbol{k}\, d^3\boldsymbol{k}'\, b(\boldsymbol{k}, \boldsymbol{k}')a^*(\boldsymbol{k})a^*(\boldsymbol{k}')\Omega\right],$$

where we assume for simplicity that b is real-valued and $\mathscr{N}$ is a normalisation constant. An easy calculation shows that

$$\langle \Psi \mid :\Phi^2:(x)\Psi\rangle \propto \int d^3\boldsymbol{k}\, d^3\boldsymbol{k}' \left(\lambda b(\boldsymbol{k},\boldsymbol{k}')\cos((k+k')\cdot x) + \lambda^2 c(\boldsymbol{k},\boldsymbol{k}')\cos((k-k')\cdot x)\right),$$

where c is given as an integral expression in b. If $b(\boldsymbol{k},\boldsymbol{k}') = 0$ unless both $\boldsymbol{k}$ and $\boldsymbol{k}'$ belong to a small neighbourhood of some $\boldsymbol{k}_0$, then the same is true of $c(\boldsymbol{k},\boldsymbol{k}')$. For small enough λ, the expectation value is approximately proportional to $\lambda\cos(2k_0\cdot x)$ and one has an oscillating pattern of positive and negative values. (See [40] for worked-out examples and plots in the case of energy density.) No worldline can remain in a negative 'trough', because $k_0\cdot u > 0$ for all timelike u, as k_0 is on-shell, so observers meet alternating positive and negative values. This suggests seeking constraints on local averages along timelike curves, and that is precisely what we will do.

10.3 An Example of a QEI and Its Consequences

10.3.1 QEIs Obeyed by a Free Scalar Field in Minkowski Spacetime

We consider weighted averages of the energy density expectation values for a free real scalar field in four-dimensional Minkowski spacetime with mass $m \geq 0$.

Let $\langle T_{ab}\rangle$ be the expectation value of the stress–energy tensor in an *arbitrary* Hadamard state. We will describe Hadamard states in detail later (Sect. 10.4 and the appendix)—for now it is enough to say that these are states whose two-point function has the same singularities as that of the Minkowski vacuum; this includes a dense subset of the Fock space $\mathscr{F}$ of the theory but also states that are not given by vectors in $\mathscr{F}$ (e.g., thermal equilibrium states at non-zero temperature). Choose any inertial curve γ in proper time parametrisation, with four-velocity $u^a = \dot{\gamma}^a$. It will be shown in Sect. 10.4.3 that the expected energy density along γ obeys the QEI

$$\int \langle T_{ab}u^a u^b\rangle(\gamma(t))\,|g(t)|^2 dt \geq -\frac{1}{16\pi^3}\int_m^\infty |\widehat{g}(u)|^2 u^4 Q\,(u/m)\,du, \tag{10.3}$$

where the averaging weight (or 'sampling function') $|g(t)|^2$ is the modulus-squared of an arbitrary smooth compactly supported test function g and the function $Q : [1,\infty) \to \mathbb{R}^+$ is

$$Q(v) = \left(1-\frac{1}{v^2}\right)^{1/2}\left(1-\frac{1}{2v^2}\right) - \frac{1}{2v^4}\ln(v+\sqrt{v^2-1}), \tag{10.4}$$

which obeys $0 \leq Q(v) \leq 1$ with $Q(v) \to 1$ as $v \to \infty$.

For massless fields, the bound simplifies to

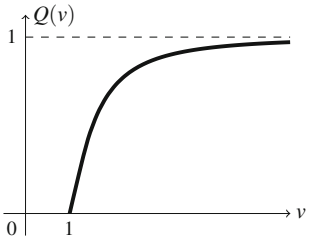

Fig. 10.1 The function Q

$$\int \langle T_{ab}u^a u^b\rangle(\gamma(t))\,|g(t)|^2 dt \geq -\frac{1}{16\pi^2}\int_{-\infty}^{\infty}|g''(t)|^2 dt, \tag{10.5}$$

which is also valid (but weaker than (10.3)) for $m > 0$ as well because $Q \leq 1$ (Fig. 10.1).

Note that the quantum energy inequalities (10.3) and (10.5) are valid for arbitrary (Hadamard) quantum states, and that their right-hand sides are state-independent in each case. They are not expected to be optimal bounds—in two-dimensions, the same method applied to the massless field gives a bound that is weaker by a factor than 3/2 than a bound that is optimal (see Sect. 10.5.1.1), while in four dimensions, numerical evidence suggests that the bound above could be improved by a factor of approximately 3 at $m = 0$, and somewhat more if $m\tau \gg 1$ [13]. The bounds remain true provided g, g' and g'' exist (in the distributional sense) and are square-integrable; in other words, if g belongs to the Sobolev space $W^{2,2}(\mathbb{R})$. However, the bound does not apply to g with lower regularity, in particular, to discontinuous g. By 'sharp switching', one could in principle trap arbitrarily large negative energy densities—of course, no physical device is capable of instantaneous switching, as a consequence of the uncertainty principle. We proceed to study the properties of (10.3).

10.3.2 Properties and Consequences of the QEI

10.3.2.1 Scaling

Putting $g_\tau(t) = \tau^{-1/2}g(t/\tau)$ in place of g in (10.5), the QEI becomes

$$\frac{1}{\tau}\int \langle T_{ab}u^a u^b\rangle(\gamma(t))\,|g(t/\tau)|^2 dt \geq -\frac{1}{16\pi^2\tau^4}\int_{-\infty}^{\infty}|g''(t)|^2 dt = -\frac{\text{const}}{\tau^4},$$

where the constant depends on g. In the short sampling time limit $\tau \to 0$, this bound is consistent with the fact that the expectation value of energy density at a point is unbounded below, while in the limit $\tau \to \infty$ it gives

$$\liminf_{\tau\to\infty} \int \langle T_{ab}u^a u^b\rangle(\gamma(t))\; g(t/\tau)^2 dt \geq 0$$

for any Hadamard state ω, so the WEC holds in this averaged sense (known as AWEC). In Sect. 10.4.3 we will see how these results are modified for non-inertial trajectories.

10.3.2.2 Bounds on the Duration of Negative Energy Density

Suppose that $\langle T_{ab}u^a u^b\rangle(\gamma(t)) < \rho$ for some interval $t \in [t_0, t_0+\tau]$ of proper time. Then, for any $g \in C_0^\infty((t_0, t_0+\tau))$, one has

$$\rho \int |g(t)|^2\, dt \geq \int \langle T_{ab}u^a u^b\rangle(\gamma(t))\; |g(t)|^2 dt \geq -\frac{1}{16\pi^2}\int_{-\infty}^{\infty} |g''(t)|^2 dt.$$

Rearranging and integrating by parts twice, this says that

$$\frac{\langle g \mid g''''\rangle}{\langle g \mid g\rangle} \geq -16\pi^2\rho,$$

where $\langle g \mid h\rangle$ denotes the standard L^2 inner product. As this inequality holds for all nontrivial $g \in C_0^\infty((t_0, t_0+\tau))$, we can replace the left-hand side by its infimum over all such g. This yields the minimum eigenvalue of the operator d^4/dt^4 on $[t_0, t_0+\tau]$, with boundary conditions at each end corresponding to vanishing of the function and its first derivative [45]. The upshot is that

$$\rho \geq -\frac{C}{\tau^4}, \tag{10.6}$$

where the numerical constant $C \sim 3.17$. Turning this around, in any time interval of duration τ, the energy density must at some instant exceed $-C/\tau^4$. Tighter results may be obtained for massive fields [20]. Inequality (10.6) resembles an uncertainty principle; note, however, that it is a rigorous consequence of the QEI rather than being injected as an additional assumption.

10.3.2.3 Quantum Interest

Developing the theme of the previous paragraph, let $\rho(t) = \langle T_{ab}u^a u^b\rangle(\gamma(t))$. Then the QEI can be regarded as asserting the positivity of the differential operator

$$P = \frac{d^4}{dt^4} + 16\pi^2\rho(t),$$

on any open interval of $\mathbb{R}$, with vanishing of the function and first derivative at any boundaries.[3] Here, positivity means that the operator has no negative spectrum, equivalently that $\langle \psi \mid P\psi \rangle \geq 0$ for all ψ in the domain of P (in particular, ψ obeys the boundary conditions). This leads to quite substantial restrictions on the possible form of ρ.

For example, suppose that ρ has an isolated pulse between proper times t_1 and t_2. As the pulse is isolated, we must have $\rho(t) = 0$ on $[t_1 - \tau_1, t_1]$ and $[t_2, t_2 + \tau_2]$ with $t_1 < t_2$ and $\tau_1, \tau_2 > 0$. Choose a test function $g \in C_0^\infty((t_1 - \tau_1, t_2 + \tau_2))$ that equals 1 on $[t_1, t_2]$. Then the quantum inequality gives

$$16\pi^2 \int_{t_1}^{t_2} \rho(t)\, dt \geq -\int |g''(t)|^2\, dt = -\int_{t_1-\tau_1}^{t_1} |g''(t)|^2\, dt - \int_{t_2}^{t_2+\tau_2} |g''(t)|^2\, dt.$$

Only the 'switch on' and 'switch off' intervals contribute and we can independently optimise over g in these intervals to give

$$\int_{t_1}^{t_2} \rho(t)\, dt \geq -\frac{A}{16\pi^2\tau_1^3} - \frac{A}{16\pi^2\tau_2^3} \geq -\frac{A}{8\pi^2 \min\{\tau_1, \tau_2\}^3},$$

where

$$A = \inf_g \int_0^1 |g''(t)|^2\, dt$$

with the infimum taken over smooth functions g that are equal to 1 near $t = 0$ and vanish near $t = 1$. This amounts to an Euler–Lagrange equation $g'''' = 0$ with $g(0) = 1, g'(0) = g(1) = g'(1) = 0$. The solution is $g(t) = 1 - 3t^2 + 2t^3$ and gives $A = 12$, so we find

$$\min\{\tau_1, \tau_2\}^3 \int_{t_1}^{t_2} \rho(t)\, dt \geq -\frac{3}{2\pi^2},$$

which gives a nontrivial constraint on the extent to which a pulse (of any shape) can be isolated if the integral is negative, namely

$$\min\{\tau_1, \tau_2\} \leq \left(\frac{3}{2\pi^2 |\int_{t_1}^{t_2} \rho(t)\, dt|} \right)^{1/3}. \tag{10.7}$$

In particular, if ρ is compactly supported, then we may take the τ_i arbitrarily large and conclude that ρ can only be compatible with the QEI restrictions if it has nonnegative integral (another version of AWEC). Abreu and Visser [1] have also shown that if ρ is the energy density compatible with the quantum inequalities and $\int \rho = 0$, then $\rho \equiv 0$.

[3] More precisely, the Friedrichs extension of P defined on the dense domain $C_0^\infty(I) \subset L^2(I)$ is positive for any interval I—the boundary conditions may be deduced from this [45].

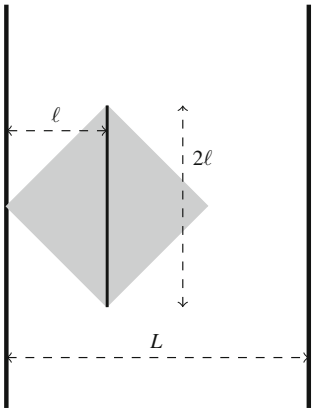

Fig. 10.2 Spacetime diagram of the Casimir plates and inertial trajectory

Ford and Roman [59] first described this type of behaviour and gave a financial analogy: nature allows you to 'borrow' negative energy density, but you must 'repay' it within a maximum loan term set by constraints such as (10.7). Moreover, excluding the case $\rho \equiv 0$, the amount repaid must always exceed the amount borrowed. This is the so-called *quantum interest* effect—one may also show in various ways that the interest rate diverges if one delays payment towards the maximum loan term. The argument above (which is new) is based on [45], further developments of which can be found in [1, 96]. A slightly earlier proof of some aspects of Ford and Roman's Quantum Interest Conjecture can be found in [88], but this is not as quantitative in nature as the bounds given here.

10.3.2.4 A Priori Bounds on Casimir Energy Densities

Experiments conducted in a causally convex[4] spacetime region ought not to yield any information regarding the geometry outside the region. This insight has been used to analyse the Casimir effect for a long time [72] and has also been at the root of much recent progress in QFT in CST following the work of Brunetti, Fredenhagen and Verch [9]. Here, we combine it with the quantum inequalities; what follows is based on [39] (see also [25]).

Consider a region between Casimir plates at $z = \pm L/2$ in otherwise flat spacetime and an inertial trajectory parallel to the plates, as illustrated in Fig. 10.2. Let ℓ be the distance from this trajectory to the nearest plate in the $t = 0$ surface. Then no experiment conducted along the trajectory in a time interval of less than 2ℓ can possibly know about the existence of the plates (and, *a fortiori*, what boundary conditions apply there); it should be as if the experiment was conducted in Minkowski space. In particular the quantum energy inequalities apply, and [as the energy density is supposed constant along the trajectory] (10.6) gives an *a priori* bound

[4] A set S is causally convex if every causal curve with endpoints in S lies completely within it.

$$T_{00} \geq -\frac{C}{(2\ell)^4} \sim -\frac{3.17}{(2\ell)^4} = -\frac{0.20}{\ell^4}. \tag{10.8}$$

By comparison, the known value of the Casimir energy density for the massless minimally coupled scalar field between parallel plates with Dirichlet conditions is [17, Sect. 2]

$$T_{00} = -\frac{\pi^2}{1140L^4} - \frac{\pi^2}{48L^4}\,\frac{3 - 2\cos^2(\pi z/L)}{\cos^4 \pi z/L},$$

which ranges between 3 and 7% of the bound (10.8) as z varies in $[-L/2, L/2]$.

Inequality (10.8) is valid for the Casimir effect in a cavity of any (time-independent) geometry, with ℓ as the minimum distance from the trajectory to any boundary. Clearly this includes situations where the exact calculation of the Casimir energy density would be difficult or impossible; it also applies to all stationary (Hadamard) states of the system and to all possible boundary conditions at the plates.

10.3.3 Some History and References

The study of QEIs began with a 1978 paper of Ford [52], in which he argued that a beam of negative energy (described by a pure quantum state) could be used to cool a hot body and decrease its entropy. Ford argued from the macroscopic validity of the second law of thermodynamics that violations of the energy conditions must be governed by bounds of uncertainty principle type. That was borne out in subsequent derivations of quantum inequalities by Ford in a series of papers written in conjunction with Roman and Pfenning [53, 55, 56, 58, 85, 87], concerning Minkowski space and some static spacetimes. These papers established lower bounds on weighted averages of the energy density[5] of the scalar and electromagnetic quantum fields along a static trajectory, where the weight is given by the Lorentzian function $f(t) = \tau/(\pi(t^2 + \tau^2))$. Here τ sets the timescale for the averaging. For example, the massless scalar field in 4-dimensions obeys a bound

$$\int \frac{\tau \langle T_{00}(t, \boldsymbol{x})\rangle}{\pi(t^2 + \tau^2)} dt \geq -\frac{3}{32\pi^2\tau^4}$$

for all sufficiently nice states and any $\tau > 0$.

The first QEI for general weighted averages was derived by Flanagan [48] for the special case of massless quantum fields in two-dimensional Minkowski space. His argument forms the basis of a general argument for two-dimensional conformal field theories [33] that will be discussed in Sect. 10.5.1.1.

[5] In fact, the earliest papers consider negative energy-momentum fluxes, but the energy density soon became the main object of interest.

The QEI (10.3) was derived in [27] for the scalar field of mass $m \geq 0$ in Minkowski space for averaging along inertial curves with general weight functions of sufficiently rapid decay. Analogous results were derived in arbitrary spacetime dimension. This was generalised to some static spacetimes [44] for averaging along static trajectories. With some modification, the method also applies to the electromagnetic [84], Dirac [14, 34] and Rarita–Schwinger fields [105]. The general approach of [27] (somewhat rephrased) formed the basis for the first fully rigorous QEI [22] for the scalar field, which was also much more general than the previously known results. We will discuss that argument in Sect. 10.4.2. Generalisations to the Dirac and electromagnetic fields are also known [15, 38, 46].

Some applications of the QEIs will be discussed in Sect. 10.6. To round off the present historical discussion, it is worth noting that the link between QEIs and thermodynamics, which originally motivated Ford [52], can be pursued abstractly (in a setting that includes the scalar field) [47]. It turns out that QEIs are part of a chain of links between stability conditions at three scales: the microscopic (conditions on the field in the ultraviolet such as the restriction to Hadamard states), mesocopic (QEIs) and macroscopic (thermodynamic stability expressed via the second law).

10.4 Derivation of a QEI

This section will give, in outline, the proof of a general QEI for the free real scalar field in a general globally hyperbolic spacetime (M, g) of dimension $n \geq 2$. The resulting bound will be computed in various situations. The derivation presented in this section contains most of the core ideas but is incomplete in important respects, which will be resolved in the appendix to this chapter.

10.4.1 Background and Preliminaries on QFT in Curved Spacetimes

Recall that a time-oriented Lorentzian spacetime is globally hyperbolic if it contains no closed-timelike curves and every intersection $J^+(p) \cap J^-(q)$ is compact, where $J^{+/-}(p)$ is the causal future/past of p. Equivalently the spacetime is globally hyperbolic if and only if it has a (global) Cauchy surface.

We consider the real scalar field on (M, g), with field equation $(\Box + m^2)\phi = 0$. The quantum field theory can be described elegantly using algebraic quantum field theory (see [8, 68] for recent surveys). Here, however, we only need some basic facts concerning the two-point function $W_2(x, x') = \langle \Phi(x)\Phi(y) \rangle$ of a quantum state:

- W_2 is a distribution on $M \times M$, and the distributional action $W_2(f, h)$ on a pair of test functions $f, h \in C_0^\infty(M)$, written formally as

$$W_2(f,h) = \int_{M\times M} W_2(x,y) f(x) h(y) d\mathrm{vol}(x)\, d\mathrm{vol}(y),$$

is the expectation value of the product of smeared fields $\langle \Phi(f)\Phi(h)\rangle$.

- W_2 is a (distributional) solution to the field equation in each of its variables

$$(\Box_x + m^2) W_2(x,y) = 0 = (\Box_y + m^2) W_2(x,y).$$

- W_2 obeys the *hermiticity* condition $\overline{W_2(f,h)} = W_2(\bar{h},\bar{f})$ for all test functions f, h.
- The antisymmetric part of the two-point function is

$$W_2(x,y) - W_2(y,x) = iE(x,y),$$

where $E(x,y) = E^-(x,y) - E^+(x,y)$ is the difference of the advanced and retarded Green functions. Here,

$$\phi^{\pm}(x) = \int_M E^{\pm}(x,y) f(y) d\mathrm{vol}(y)$$

is the unique solution to $(\Box + m^2)\phi^{\pm} = f$ that vanishes outside the causal future $(+)$ or past $(-)$ of the support of f – the closure of the set of points on which f is non-zero.

- W_2 has *positive type*, which means that $W_2(\bar{f},f) \geq 0$ for every test function f.

The positive type and hermiticity conditions can be understood easily by reference to a Hilbert space representation (or, more abstractly, to the algebra of smeared fields) in which the state of interest has state vector Ω and one has

$$W_2(f,h) = \langle \Phi(f)\Phi(h)\rangle = \langle \Omega \mid \Phi(f)\Phi(h)\Omega\rangle.$$

For a real scalar field one has $\Phi(f)^* = \Phi(\bar{f})$ and correspondingly

$$\overline{W_2(f,h)} = \langle \Phi(f)\Phi(h)\Omega \mid \Omega\rangle = \langle \Omega \mid \Phi(\bar{h})\Phi(\bar{f})\Omega\rangle = W_2(\bar{h},\bar{f}).$$

Similarly,

$$W_2(\bar{f},f) = \langle \Phi(\bar{f})\Phi(f)\rangle = \langle \Phi(f)\Omega \mid \Phi(f)\Omega\rangle \geq 0.$$

We emphasise that these properties hold for all states and not just states that are vacua in some sense. In order to construct a stress–energy tensor or other Wick powers it is necessary to restrict further to the class of Hadamard states, whose 2-point functions take a specific form for near-coincident points.

The Hadamard class was precisely described in [73] in the four-dimensional case. Briefly, near the diagonal $\{(x,x) : x \in M\}$ in $M \times M$ one may define a sequence of distributions $H^{(r)}$ taking the form

$$H^{(r)}(x,y) = \frac{U(x,y)}{4\pi^2\sigma_+(x,y)} + V^{(r)}(x,y)\log(\sigma_+(x,y)/\ell^2) + W^{(r)}(x,y),$$

where ℓ is a fixed length scale and $\sigma(x,y)$ is the signed squared geodesic separation of x and y, with a positive sign for spacelike separation.[6] The functions U, $V^{(r)}$ and $W^{(r)}$ are smooth; $V^{(r)}$ and $W^{(r)}$ take the form

$$V^{(r)}(x,y) = \sum_{k=0}^{r} v_k(x,y)\sigma(x,y)^k, \qquad W^{(r)}(x,y) = \sum_{k=0}^{r} w_k(x,y)\sigma(x,y)^k$$

where the coefficients v_k and w_k are recursively determined by the requirement that $P_x H^{(r)} = (P_x w_r)\sigma^r + (P_x v_r)\sigma^r \log\sigma_+$ together with $U(x,x) = 1$ and the convention that $w_0 = 0$.[7] Here, the subscript $+$ indicates a distributional regularisation, $f(\sigma_+(x,y)) = \lim_{\varepsilon\to 0+} f(\sigma(x,y) + 2i\varepsilon(T(x) - T(y)) + \varepsilon^2)$, where T increases to the future. With these definitions in place, we describe W_2 as being Hadamard if and only if $W_2 - H^{(r)}$ is r-times continuously differentiable in the neighbourhood of the diagonal where it is defined, for all $r \geq 0$. It is an important result that the difference of two Hadamard 2-point functions is smooth on $M \times M$, even though the Hadamard condition is stated only for nearby points. This was proved by Radzikowski [89, 90] using a much cleaner definition of the Hadamard condition based on microlocal analysis. This formulation is described briefly in the Appendix to this chapter, as it will be required in the rigorous proof of the QEI.

Quantities like the Wick square and stress–energy tensor can be defined using point-splitting (see, e.g. [104]). In general, let P be a r'th order partial differential operator on M with smooth real coefficients and consider a Hadamard state with two-point function W_2. By the Hadamard condition, the difference $W_2 - H^{(2r)}$ is $2r$-times continuously differentiable near the diagonal in $M \times M$, so $(P \otimes P)(W_2 - H^{(2r)})(x,y)$ (i.e., the result of acting with P in each variable) is continuous and we may take the points together to define

$$\langle (P\Phi)^2(x)\rangle = (P \otimes P)(W_2 - H^{(2r)})(x,x).$$

There are residual finite renormalisation freedoms but we will neglect them for now.

As the Hadamard series is cumbersome to work with directly, it is useful to consider quantities that are normal ordered with respect to a reference state, with 2-point function $W_{2,R}$, say. Here, we define

$$\langle :(P\Phi)^2:_R(x)\rangle = (P \otimes P)(W_2 - W_{2,R})(x,x).$$

[6] The function σ is well-defined and smooth in a neighbourhood of the diagonal in $M \times M$.

[7] Thus the $H^{(r)}$ satisfy the field equation in x to ever-increasing order in σ; however, the limit $r \to \infty$ does not necessarily exist, except in analytic spacetimes.

As $\langle (P\Phi)^2(x)\rangle = \langle :(P\Phi)^2:_R(x)\rangle + \langle (P\Phi)^2(x)\rangle_R$, where the last term is the expectation value in the reference state, a lower bound on the normal ordered quantity will imply the existence of a lower bound on $\langle (P\Phi)^2\rangle$.

10.4.2 The QEI Derivation

Let (M, g) be any globally hyperbolic spacetime of dimension $n \geq 2$ and let $\gamma : \mathbb{R} \to M$ be a smooth timelike curve, with proper time parametrisation. Let P be any partial differential operator with smooth real coefficients. We consider the quantity $:(P\Phi)^2:_R$, and seek a lower bound on

$$\int d\tau\, |g(\tau)|^2 \langle :(P\Phi)^2:_R\rangle(\gamma(\tau))$$

for $g \in C_0^\infty(\mathbb{R})$ where the expectation value is taken in an arbitrary Hadamard state and normal ordering is performed relative to a reference Hadamard state with two-point function $W_{2,R}$.

To start, we introduce a point-split quantity

$$G(\tau, \tau') = \langle P\Phi(\gamma(\tau))P\Phi(\gamma(\tau'))\rangle = ((P \otimes P)W_2)(\gamma(\tau), \gamma(\tau'))$$

and write G_R for the same quantity computed using $W_{2,R}$. There are immediate questions to address about whether these quantities are well-defined,[8] but we defer these for the moment. Both G and G_R are distributions, but their difference $F = G - G_R$ is a smooth function,

$$F(\tau, \tau') = ((P \otimes P)(W_2 - W_{2,R}))(\gamma(\tau), \gamma(\tau'))$$

because $W_2 - W_{2,R}$ is the difference of Hadamard 2-point functions and therefore smooth. Furthermore, F is symmetric in its arguments, because $W_2 - W_{2,R}$ is (recall that all two-point functions have the same antisymmetric part) and one has

$$F(\tau, \tau) = \langle :(P\Phi)^2:_R\rangle(\gamma(\tau)).$$

For any real-valued $g \in C_0^\infty(\mathbb{R})$ we now compute

$$\begin{aligned}\int d\tau\, |g(\tau)|^2 \langle :(P\Phi)^2:_R\rangle(\gamma(\tau)) &= \int d\tau\, |g(\tau)|^2 F(\tau, \tau) \\ &= \int_{-\infty}^{\infty} \frac{d\alpha}{2\pi} \int d\tau\, d\tau'\, g(\tau)g(\tau')e^{-i\alpha(\tau-\tau')}F(\tau, \tau')\end{aligned}$$

[8] For example, one cannot make sense of an expression like $u(f(t))$ if $u(x, y) = \delta(x)\delta(y)$ and $f(t) = (0, t)$, because $u(f(t)) = \delta(0)\delta(t)$.

(inserting the Fourier representation of a δ-function to 'unsplit' the points)

$$= \int_{-\infty}^{\infty} \frac{d\alpha}{2\pi} F(g_{-\alpha} \otimes g_\alpha)$$

(regarding F as a distribution and writing $g_\alpha(\tau) = g(\tau)e^{i\alpha\tau}$)

$$= \int_{0}^{\infty} \frac{d\alpha}{\pi} F(g_{-\alpha} \otimes g_\alpha) \tag{10.9}$$

using the symmetry of F, and hence $F(g_{-\alpha} \otimes g_\alpha) = F(g_\alpha \otimes g_{-\alpha})$ to make the final step. As g is real-valued, $g_{-\alpha}(\tau) = \overline{g_\alpha(\tau)}$ and so one may compute

$$\begin{aligned}\int d\tau\, |g(\tau)|^2 \langle :(P\Phi)^2:_R\rangle(\gamma(\tau)) &= \int_0^\infty \frac{d\alpha}{\pi} F(\overline{g_\alpha} \otimes g_\alpha) \\ &= \int_0^\infty \frac{d\alpha}{\pi} G(\overline{g_\alpha} \otimes g_\alpha) - \int_0^\infty \frac{d\alpha}{\pi} G_R(\overline{g_\alpha} \otimes g_\alpha) \\ &\geq -\int_0^\infty \frac{d\alpha}{\pi} G_R(\overline{g_\alpha} \otimes g_\alpha),\end{aligned}$$

where we have used $F = G - G_R$ and the positive type property $G(\overline{h}, h) \geq 0$ of G, which it inherits from W_2. Similarly, G_R is of positive type, so the integrand in the final expression is pointwise positive in α.

We summarise with a theorem (although there are some important points left to resolve—see below).

Theorem 10.1 *Let (M, g) be any globally hyperbolic spacetime of dimension $n \geq 2$, P be any partial differential operator with smooth real coefficients, γ be any smooth timelike curve in a proper-time parameterisation. For normal ordering performed relative to a Hadamard reference state with two-point function $W_{2,R}$, the inequality*

$$\int d\tau\, |g(\tau)|^2 \langle :(P\Phi)^2:_R\rangle(\gamma(\tau)) \geq -\int_0^\infty \frac{d\alpha}{\pi} G_R^{(P)}(\overline{g_\alpha} \otimes g_\alpha), \tag{10.10}$$

holds for any Hadamard state of the real scalar field and all real-valued $g \in C_0^\infty(\mathbb{R})$, where

$$G_R^{(P)}(\tau, \tau') = ((P \otimes P)W_{2,R})(\gamma(\tau), \gamma(\tau')).$$

The lower bound bound in (10.10) depends only on the reference two-point function together with P, γ and g.

This derivation provides a quantum inequality on $:(P\Phi)^2:$ and hence on any other quantity that can be expressed as a finite sum of such quantities, recalling that P is any partial differential operator with smooth real coefficients. For example:

- Taking P to be a multiplication operator (i.e., a zeroth order partial differential operator) we obtain bounds on averages of the Wick square $:\Phi^2:_R$.
- Taking $P = v^a\nabla_a$ where v is any smooth vector field gives bounds on $:(v^a\nabla_a\Phi)^2:_R$.
- Combining these ideas and using the decomposition in (10.2) we have a QEI on the energy density $:T_{ab}:_R u^a u^b$ by summing the bounds for $P = e_A^a\nabla_a$ $(0 \leq A \leq n-1)$ and $P = m$:

$$\int d\tau\, |g(\tau)|^2 \langle :u^a u^b T_{ab}:_R\rangle(\gamma(\tau)) \geq -\int_0^\infty \frac{d\alpha}{\pi} T_R(\overline{g_\alpha} \otimes g_\alpha), \tag{10.11}$$

  where

$$T_R(\tau,\tau') = \frac{1}{2}G_R^{(m)}(\tau,\tau') + \frac{1}{2}\sum_{A=0}^{n-1} G_R^{(e_A\cdot\nabla)}(\tau,\tau')$$

  is the point-split energy density in the reference state [22]. This QEI can be called a Quantum Weak Energy Inequality (QWEI).
- Taking $P = k^a\nabla_a$ where k is any smooth null vector field, we note that $:T_{ab}:_R k^a k^b = :(P\Phi)^2:_R$ and thereby obtain a Quantum Null Energy Inequality (QNEI) [40]

$$\int d\tau\, |g(\tau)|^2 \langle :k^a k^b T_{ab}:_R\rangle(\gamma(\tau)) \geq -\int_0^\infty \frac{d\alpha}{\pi} G_R^{(k\cdot\nabla)}(\overline{g_\alpha} \otimes g_\alpha). \tag{10.12}$$

- Similarly, one could obtain a Quantum Dominated Energy Inequality (QDEI); the classical field obeys the DEC precisely because $u^a v^b T_{ab}$ is a sum of squares, in the case that u and v are future-pointing causal vectors.

Two important questions must be resolved to complete the proof of Theorem 10.1. First, is it legitimate to restrict the differentiated two-point function to the worldline, as we did in defining $G$and G_R? Second, is the final integral in (10.10) finite? If not, the bound would be true, but useless! The (affirmative) answers to these questions are briefly explained in the Appendix (see also [22]), making use of microlocal analysis to provide the necessary deeper understanding of Hadamard states.[9] However, the reader who does not wish to delve into the details should at least note that neither is simply a matter of fine precision. For instance, the first question would be answered negatively for a null trajectory (and indeed there is no QEI bound in this case [40]). Regarding the second, had we restricted to the *negative* half-line in (10.9), the argument would have yielded a bound in which the final integral *diverges*—this does not contradict our theorem above, but simply provides no useful information.

Further remarks and extensions

1. Variants of Theorem 10.1 exist for averages over suitable Lorentzian submanifolds, instead of timelike curves (see, e.g. [43]). However, no such bounds can

[9] Indeed, it is far from obvious in the derivation above where the Hadamard condition enters at all.

exist for averages over spacelike surfaces (certainly above 2-dimensions) [54] or, as already mentioned, along null curves [40].

2. The argument above relies on 'classical positivity' of the quantity in question. This permits a number of related bounds to be proven by similar methods, e.g. see [38] for spin-1 fields. Nonetheless, there are also QEIs for the free Dirac field [15, 46, 94] despite the fact that the 'classical' Dirac energy density is symmetrical about zero and unbounded from below. It turns out that the analogue of the Hadamard condition also functions as a local version of the Dirac sea, and restores positivity [modulo a finite QEI lower bound] as well as renormalising the energy density. See Sect. 10.5.1 for discussion of nonminimally coupled scalar fields and the case of interacting QFT.
3. The expectation value in (10.10) may be written as $\langle (P\Phi)^2\rangle - \langle (P\Phi)^2\rangle_R$ and for this reason a bound of this type is sometimes called a 'difference quantum inequality'. It can be rewritten as

$$\int d\tau\, |g(\tau)|^2 \langle (P\Phi)^2\rangle(\gamma(\tau)) \geq \int d\tau\, |g(\tau)|^2 \langle (P\Phi)^2\rangle_R(\gamma(\tau)) - \int_0^\infty \frac{d\alpha}{\pi} G_R(\overline{g_\alpha} \otimes g_\alpha).$$

Schematically, $\langle (P\Phi)^2\rangle_R(\gamma(\tau))$ is the diagonal of a function $F_{\mathrm{ren}}(\tau,\tau') = G_R - G_{\mathrm{ren}}$, where G_{ren} is formed from the distribution $H^{(k)}$ (for sufficiently large k) and the operator P. So the dependence on the reference state actually cancels, and we obtain the 'absolute quantum inequality'

$$\int d\tau\, |g(\tau)|^2 \langle (P\Phi)^2\rangle(\gamma(\tau)) \geq -\int_0^\infty \frac{d\alpha}{\pi} G_{\mathrm{ren}}(\overline{g_\alpha} \otimes g_\alpha)$$

on the Hadamard-renormalised square $(P\Phi)^2$. Making this precise and quantitative takes a bit of work [43] and leads to a QEI expressed in terms of $H^{(5)}$ for averaging along timelike curves. (See [94] for similar analysis of the Dirac case.) Recently, Kontou and Olum have evaluated the resulting bounds to first order in the Ricci tensor and its derivatives [up to third order] in spacetimes with small curvature [79] for massless fields, averaging along timelike geodesics. In so doing, they showed that the QEI bounds of [43] could be simplified to require fewer terms of the Hadamard series (only $H^{(1)}$ is needed although the advanced-minus-retarded bi-distribution E must be computed separately). The resulting QEI takes the form (10.5) at leading order and involves other terms which are given as integral expressions bilinear in g and its derivatives (up to the second order), and involving the Ricci tensor and derivatives. Under rescaling, these additional terms are at worst of order τ^{-2} as $\tau \to 0$.

10.4.3 Specific Examples

We illustrate the quantum inequality bound (10.11) in some specific situations.

10.4.3.1 Stationary Trajectories in Stationary Spacetimes

Suppose that γ is an orbit of a timelike Killing vector field, defined at least in an open neighbourhood of γ. In particular this holds if (M, g) is stationary, and γ is a stationary trajectory. Choose a frame near γ with $e_0 = \dot{\gamma}$ and e_A invariant under the Killing flow. We also suppose that (M, g) admits Hadamard reference state with two-point function W_R that is also invariant under the flow near γ (for example, a stationary state). In this case, the point-split energy density T_R is translationally invariant

$$T_R(\tau, \tau') = \mathscr{T}_R(\tau - \tau')$$

and, writing $\mathscr{T}_R$ in terms of its Fourier transform, (10.11) becomes

$$\begin{aligned}\int d\tau\, |g(\tau)|^2 \langle{:}u^a u^b T_{ab}{:}_R\rangle(\gamma(\tau)) &\geq -\int_0^\infty \frac{d\alpha}{\pi} \int_{-\infty}^\infty \frac{dv}{2\pi}\, \widehat{\mathscr{T}_R}(v) |\widehat{g}(\alpha + v)|^2 \\ &\geq -\int_{-\infty}^\infty \frac{du}{\pi}\, |\widehat{g}(u)|^2 \mathscr{Q}(u), \end{aligned} \tag{10.13}$$

where

$$\mathscr{Q}(u) = \int_{(-\infty,u)} \frac{dv}{2\pi}\, \widehat{\mathscr{T}_R}(v).$$

Via the Bochner–Schwartz theorem, the positive type property of W_R implies that $\widehat{\mathscr{T}_R}$ is a polynomially bounded positive measure (cf. the appendix of [22]) so $\mathscr{Q}$ grows at most polynomially. Further, if W_R is the two-point function of a stationary ground state, then the $\widehat{\mathscr{T}_R}(v) = 0$ for $v < 0$ [22]. We note that (10.13) extends to complex-valued $g \in C_0^\infty(\mathbb{R})$ simply by applying the above argument to the real and imaginary parts separately. It is clear that a number of the general properties discussed in Sect. 10.3.2 will transfer *mutatis mutandis* to the present case. In particular, replacing g by $g_\lambda(\tau) = g(\tau/\lambda)/\sqrt{\lambda}$, one may show that

$$\liminf_{\lambda \to +\infty} \int d\tau\, |g(\tau/\lambda)|^2 \left(\langle{:}u^a u^b T_{ab}{:}_R\rangle(\gamma(\tau)) + \mathscr{Q}(0+) + \mathscr{Q}(0-)\right) \geq 0 \tag{10.14}$$

which gives a 'difference AWEC' relative to the reference state (a 'difference AWEC') if $\mathscr{Q}(0+) = \lim_{u \to 0+} \mathscr{Q}(u) = 0$ (which implies that $\mathscr{Q}(0-) = 0$ given the properties of $\widehat{\mathscr{T}_R}$), which would be expected if W_R is a ground-state two-point function with respect to the Killing flow. Section 10.4.3.3 gives an example in which these additional terms are nonzero.

Various examples have been worked out in detail; we give some instances here and refer to [44] for others.

10.4.3.2 Inertial Trajectory in Minkowski Space

Let γ be an inertial trajectory in n-dimensional Minkowski spacetime, choosing coordinates so that $\gamma(\tau) = (\tau, \boldsymbol{x})$ for fixed $\boldsymbol{x}$. Let P be a partial differential operator with constant real coefficients, so that $Pe^{ik\cdot x} = p(k)e^{ik\cdot x}$ for some polynomial p (which necessarily obeys $p(-k) = \overline{p(k)}$) and adopt the Minkowski vacuum as the reference state, with corresponding two-point function

$$W_{2,R}(x, x') = \int \frac{d^{n-1}\boldsymbol{k}}{(2\pi)^{n-1}} \frac{\mathrm{e}^{-ik\cdot(x-x')}}{2\omega},$$

where $k_\mu = (\omega, \boldsymbol{k})$, $\omega = \sqrt{|\boldsymbol{k}|^2 + m^2}$. With this choice, the normal ordering is precisely the conventional normal ordering of Minkowski space QFT (and indeed, one would normally adjust the full renormalised quantity to coincide with this as well). Then

$$G_R^{(P)}(\tau, \tau') = \int \frac{d^{n-1}\boldsymbol{k}}{(2\pi)^{n-1}} \frac{|p(k)|^2}{2\omega} \mathrm{e}^{-i\omega(\tau-\tau')}$$

from which the quantum inequality on $:(P\Phi)^2:$ can be computed. In particular, for the point-split energy density one has

$$\begin{aligned} T_R(\tau, \tau') &= \int \frac{d^{n-1}\boldsymbol{k}}{(2\pi)^{n-1}} \frac{\omega^2 + \boldsymbol{k}\cdot\boldsymbol{k} + m^2}{4\omega} \mathrm{e}^{-i\omega(\tau-\tau')} \\ &= \frac{\mathrm{vol}(\mathbb{S}^{n-2})}{2(2\pi)^{n-1}} \int_m^\infty d\omega\, \omega^2(\omega^2 - m^2)^{(n-3)/2} \mathrm{e}^{-i\omega(\tau-\tau')} \end{aligned}$$

leading ultimately to the QWEI

$$\int d\tau\, |g(\tau)|^2 \langle :u^a u^b T_{ab}:_R \rangle(\gamma(\tau)) \geq -\frac{\mathrm{vol}(\mathbb{S}^{n-2})}{n(2\pi)^n} \int_m^\infty du\, |\widehat{g}(u)|^2 u^n Q_{n-1}(u/m),$$

where

$$Q_{n-1}(x) = nx^{-n} \int_1^\infty dy\, y^2(y^2 - 1)^{(n-3)/2}.$$

Normalisation has been chosen so that $Q_{n-1}(x) \to 1$ as $x \to +\infty$; in the massless case, one may thus replace $Q_{n-1}(u/m)$ by 1. The above bounds were originally derived in a purely momentum-space framework in [27]—the case $n = 4$ corresponds to the bound stated as (10.3), with $Q = Q_3$.

10.4.3.3 Uniformly Accelerated Trajectory in $n = 4$ Minkowski for $m = 0$

Again we use the vacuum state as the reference, $W_{2,R}(x, x') = 1/(4\pi^2\sigma_+(x, x'))$. We consider the trajectory with uniform proper acceleration $\alpha_0 > 0$, given in inertial coordinates by $\gamma(\tau) = (\xi_0 \sinh(\tau/\xi_0), \xi_0 \cosh(\tau/\xi_0), 0, 0)$ in proper time parametrisation, where $\xi_0 = \alpha_0^{-1}$. In this case one may show [39] that

$$\mathscr{T}_R(\tau) = \lim_{\varepsilon\to 0+} \frac{3}{32\pi^2\xi_0^4} \operatorname{cosech}^4\left(\frac{\tau - i\varepsilon\xi_0}{2\xi_0}\right), \quad \text{with} \quad \widehat{\mathscr{T}}(u) = \frac{1}{2\pi}\left(\frac{u^3 + u\xi_0^{-2}}{1 - e^{-2\pi\xi_0 u}}\right)$$

and similar calculations to those above give

$$\int d\tau\, |g(\tau)|^2 \dot\gamma^a\dot\gamma^b \langle{:}T_{ab}{:}\rangle(\gamma(\tau)) \geq -\frac{1}{16\pi^3}\int_{-\infty}^{\infty} du\, |\widehat{g}(u)|^2 \Upsilon(\xi_0, u) \tag{10.15}$$

for any Hadamard state, where $\Upsilon(\xi_0, u) = (4\pi)^2\mathscr{Q}(u)$ in our previous notation. As $|\widehat{g}(u)|^2$ is even, we may replace $\Upsilon(\xi_0, u)$ by $\frac{1}{2}(\Upsilon(\xi_0, u) + \Upsilon(\xi_0, -u))$ in (10.15). Using the identity

$$\Upsilon(\xi_0, u) + \Upsilon(\xi_0, -u) = u^4 + 2\frac{u^2}{\xi_0^2} + \frac{11}{30\xi_0^4}, \tag{10.16}$$

the following QEI holds for all Hadamard states and all $g \in C_0^\infty(\mathbb{R})$:

$$\int d\tau\, |g(\tau)|^2 \dot\gamma^a\dot\gamma^b \langle{:}T_{ab}{:}\rangle(\gamma(\tau)) \geq -\frac{1}{16\pi^2}\int_{-\infty}^{\infty} d\tau \left(|g''(\tau)|^2 + 2\alpha_0^2|g'(\tau)|^2 + \frac{11\alpha_0^4}{30}|g(\tau)|^2\right). \tag{10.17}$$

Comparing with (10.5), we see that the acceleration leads to modifications to the QEI bound that are lower order in the number of derivatives applied to g.

In particular, the scaling behaviour discussed in Sect. 10.3 is modified; we have

$$\frac{1}{\tau}\int \dot\gamma^a\dot\gamma^b \langle{:}T_{ab}{:}\rangle(\gamma(t))|g(t/\tau)|^2 dt \geq -\frac{\|g''\|^2}{16\pi^2\tau^4} - \frac{\|g'\|^2\alpha_0^2}{8\pi^2\tau^2} - \frac{11\|g\|^2\alpha_0^4}{480\pi^2},$$

where the norm $\|\cdot\|$ is that of $L^2(\mathbb{R})$. For $\alpha_0\tau \ll 1$ the previous result is recovered to good approximation; however, for $\alpha_0\tau \gg 1$ it is the last term that dominates and, indeed, the AWEC fails—multiplied by τ, the right-hand side diverges to $-\infty$ as $\tau \to \infty$. By subtracting this troublesome term we can deduce that

$$\liminf_{\tau\to\infty} \int \left(\dot\gamma^a\dot\gamma^b \langle{:}T_{ab}{:}\rangle(\gamma(t)) + \frac{11\alpha_0^4}{480\pi^2}\right)|g(t/\tau)|^2\, dt \geq 0$$

holds for any Hadamard state. This is precisely an example of (10.14), noting that $\mathscr{Q}(0+) = \mathscr{Q}(0-) = 11/(960\xi_0^4\pi^2)$ by (10.16). At first sight it is remarkable that the integrand vanishes identically in the Rindler vacuum state, which has energy density $\rho = -11\alpha_0^4/(480\pi^2)$ along γ [67, Sect. 3]. From another viewpoint, however, it is just the difference AWEC that one would have obtained using the Rindler vacuum as the reference state on the right wedge $x > |t|$; even though our calculation was conducted entirely in Minkowski space. This is local covariance [9] in action—physics along the accelerated curve can know of nothing outside the wedge!

This example might suggest that a good way to experience long-lasting negative energy densities is to follow a uniformly accelerated trajectory. It is worth noting that the work required to maintain this motion grows exponentially with the proper time, and therefore the 'cost' in work done is growing much more rapidly than the 'benefit' of negative energy 'seen'. An alternative, studied by Ford and Roman [61] is for the observer to follow an oscillatory trajectory with the field in a suitably prepared state. They were able to find examples in which the integrated negative energy density 'seen' grows linearly with the sampling time just as we have at leading order in the accelerated case. This is not in contradiction with the QEIs; it simply shows that the bounds can become quite weak for long sampling times along non-inertial trajectories. The examples given in [61] avoid unphysically large velocities, but of course it remains the case that work must be done to maintain non-inertial motion.

10.5 Further Developments

10.5.1 Quantum Energy Inequalities Beyond Free QFT

10.5.1.1 Conformal Fields in 1 + 1 Dimensions

QEIs have been derived for a general class of conformal field theories (CFTs) in $1 + 1$ dimensions.[10] The basic idea was given by Flanagan [48] for massless scalar fields and was generalised to massless Dirac fields [102] before being turned into a general and rigorous argument in [33].

Recall that the stress tensor T^{ab} in CFT is traceless, and that

$$T^{00}(t,x) = T_R(t-x) + T_L(t+x), \qquad T^{01}(t,x) = T_R(t-x) - T_L(t+x),$$

where the left- and right-moving chiral components T_L and T_R commute and obey the spectrum condition

$$P_{L,R} = \int T_{L,R}(v)\, dv \geq 0.$$

[10] See [63] for a general reference on CFT in $1 + 1$ Minkowski space.

An important feature of CFTs is that suitable reparametrisations of null coordinates $v = t - x$, $u = t + x$ are unitarily implemented in the vacuum Hilbert space. Under the correspondence $v \mapsto z(v) := (i - v)/(i + v)$, the real-line is mapped to $\mathbb{T} \setminus \{-1\}$, where $\mathbb{T} \cong S^1$ is the unit circle in $\mathbb{C}$. If a reparametrisation $v \mapsto V(v)$ lifts to an orientation preserving diffeomorphism of S^1, then there is a unitary $U_R(V)$ such that

$$U_R(V)T_R(v)U_R(V)^{-1} = V'(v)^2 T_R(V(v)) - \frac{c_R}{24\pi}\{V, v\}\mathbf{1},$$

where c_R is the central charge (for right-movers) and

$$\{V, v\} = -2\sqrt{V'(v)}\frac{d^2}{dv^2}\frac{1}{\sqrt{V'(v)}}$$

is the Schwarzian derivative. The same is true for T_L and the U_L, U_R commute.

Consider one of the stress-tensor components, say, $T(v)$ and let f be a smooth compactly supported positive real-valued function. We define

$$T(f) = \int T(v)f(v)\,dv$$

and aim to show that there is a lower bound on the expectation values $\langle T(f)\rangle_\psi$.

The idea is to define $v \mapsto V(v)$ by $V'(v) = 1/f(v)$ and set $\psi' = U(V)\psi$. Then

$$\begin{aligned} f(v)\langle T(v)\rangle_\psi &= f(v)\langle U(V)T(v)U(V)^{-1}\rangle_{\psi'} \\ &= V'(v)\langle T(V(v))\rangle_{\psi'} - \frac{c}{24\pi}\{V, v\}f(v) \end{aligned}$$

so

$$\begin{aligned} \int \langle T(v)\rangle_\psi f(v)\,dv &= \int \langle T(V)\rangle_{\psi'}\,dV - \frac{c}{24\pi}\int \{V, v\}f(v)\,dv \\ &= \langle P\rangle_{\psi'} - \frac{c}{24\pi}\int \{V, v\}f(v)\,dv. \end{aligned}$$

Using the spectrum condition, and rearranging, we find

$$\int \langle T(v)\rangle_\psi f(v)\,dv \geq -\frac{c}{12\pi}\int \left(\frac{d}{dv}\sqrt{f(v)}\right)^2 dv$$

for all 'reasonable' ψ. The only problem is that the map $v \mapsto V(v)$ does not lift to a diffeomorphism of S^1, but this can be resolved by an approximation argument [33], in which all the above manipulations are justified and the class of 'reasonable' ψ is specified. The necessary assumptions on the theory are shown to hold for CFTs constructed from unitary, positive energy Virasoro representations. It was also proved

that the bound is sharp if the theory has a conformally invariant vacuum. Any non-negative $f \in \mathscr{S}(\mathbb{R})$ can be used for smearing. Combining the results from left- and right- movers, one has

$$\int \langle T_{00}(t,0)\rangle_\psi f(t)\,dt \geq -\frac{c}{6\pi}\int \left(\frac{d}{dt}\sqrt{f(t)}\right)^2 dt \tag{10.18}$$

for an average along a timelike inertial curve (assuming the central charges of left- and right movers take a common value c). The QEIs derived by Flanagan and Vollick for massless scalars and Dirac fields respectively [48, 102] correspond to $c = 1$, while the massless Majorana field, for example, has $c = 1/2$ and a tighter bound.

This argument is notable, partly as the first examples of QEIs for non-free fields, but also because it does not depend on a 'sum of squares' form of the energy density. It is also model-independent, applying to *all* unitary positive energy CFTs in one go. Further developments of these and related ideas can be found in [12]. These bounds have also been derived by holographic arguments [81] (based on a holographic proof of ANEC [74]).

10.5.1.2 The Ising Model and Other Integrable Theories

The massive Ising model is a very simple integrable QFT in $1+1$-dimensional Minkowski space.[11] It is a theory of massive bosons, but differs in essential ways from the free massive free field. In particular, it has nontrivial scattering (albeit simple: the two-particle S-matrix is minus the identity) and there are single particle states with negative energy density.[12] Moreover, the energy density of a multi-particle combination of such states is not the sum of their individual energy densities. A simplifying feature is that the Fock space of the theory also supports an auxiliary free Majorana field, whose stress–energy tensor generates the energy momentum operators (which are determined by the translation symmetry). Therefore the Majorana stress–energy tensor can be identified as the stress–energy tensor of the Ising model.[13] However, as the latter obeys a state-independent QEI, it follows that the Ising model does too, as was shown in [4]. One has, for any inertial curve γ with proper time parametrisation and 2-velocity u^a,

$$\int \langle T_{ab}u^a u^b\rangle(\gamma(t))\;|g(t)|^2 dt \geq -\frac{1}{4\pi^2}\int_m^\infty |\widehat{g}(u)|^2 u^2 Q_{\text{Ising}}\,(u/m)\,du,$$

where the expectation value is taken in any sufficiently regular state of the theory and $g \in C_0^\infty(\mathbb{R})$ as usual. Here, m is the boson mass and

[11] By Wick rotation it is related to a continuum limit of the statistical mechanical Ising model above the critical temperature.

[12] This cannot happen in the free scalar field, because the classical field obeys WEC.

[13] Note however that the Ising model is not equivalent to the Majorana theory.

$$Q_{\text{Ising}}(v) = \sqrt{1 - v^{-2}} - v^{-2} \log(v + \sqrt{v^2 - 1}).$$

This is the first example of a truly interacting theory in which QEIs have been established. One might wonder whether the same is true of other integrable QFTs and an investigation has been begun in [3] for a class of theories including the sinh-Gordon model. Generically, these models admit single-particle states with locally negative energy densities (an effect that become more pronounced as the interaction strength increases). In fact, there is some freedom in determining the stress–energy tensor of these models, which is constrained if QEIs are required to hold, in some cases leading to a unique stress–energy tensor. To date, the analysis of [3] is restricted to single-particle states, but it provides a basis for a full investigation of QEIs in integrable QFT.

10.5.1.3 Nonminimal Coupling

As already emphasised, the classical minimally coupled scalar field obeys the WEC by virtue of a decomposition of the energy density as a sum of squares. This is not true for the nonminimally coupled field, and indeed the energy density can be made arbitrarily negative at any given point (see, e.g. [60] for a discussion). It turns out that this behaviour is, nonetheless, constrained by locally averaged energy conditions reminiscent of the QEIs [36]. In spacetime dimensions $n \geq 2$, for example, let ϕ be any solution to the nonminimally coupled field equation $(\Box + m^2 + \xi R)\phi = 0$ with $\xi \in [0, 1/4]$. Then, if γ is any complete causal geodesic with affine parameter λ, the corresponding stress–energy tensor obeys

$$\int_\gamma \mathrm{d}\lambda \; T_{ab}\dot{\gamma}^a\dot{\gamma}^b |g|^2 \geq -2\xi \int_\gamma \mathrm{d}\lambda \; \left\{ |\partial_\lambda g|^2 + \frac{1}{2} R_{ab}\dot{\gamma}^a\dot{\gamma}^b |g|^2 - \left(\frac{1}{4} - \xi\right) R\dot{\gamma}^2 |g|^2 \right\} \phi^2$$

for any $g \in C_0^\infty(\mathbb{R})$. In particular this result includes the case of conformal coupling. Note that the left-hand side involves both the field and its derivatives (up to second order), while the right-hand side only involves the field: the bound exhibits a 'gain in derivatives'.

The corresponding quantum theory was discussed in [37], where it was shown that (in Minkowski space) the nonminimally coupled field can violate WEC very badly indeed. The argument is the following: the failure of classical WEC allows the existence of one-particle states with negative energy density near the origin, say. By a scaling argument these can be taken to have any desired spacetime extent; as tensoring N such states together multiplies the energy density by N, we see that states of arbitrarily negative energy density can be sustained over arbitrarily large spacetime volumes. However, there is a cost. The overall energy of these states is positive, and grows more rapidly than the scales characterising the negative energy density: the production of negative energy density is highly inefficient.

By modifying the argument in Sect. 10.4.2, one can establish QEI bounds for the nonminimally coupled field in general globally hyperbolic spacetimes that are

state-dependent [37]. In these bounds the averaged energy density is bounded below by state-independent terms together with terms that involve averages of the expectation value of the Wick square of the field in the state of interest—again demonstrating a 'gain in derivatives' phenomenon. One way of understanding this bound is to regard the Wick square as a thermal observable, specifically as a square of the local temperature. Similarly, the energy density could be regarded as a measure of the fourth power of the local temperature. This again shows how the lower bound is more stringent than any upper bound could be. The thermal interpretation makes best sense in the context of states of 'local thermal equilibrium' (LTE); Schlemmer and Verch have shown that one may also prove QEI-like results directly for such states, valid for any coupling constant and mass—see [91] for this and references to the LTE literature.

10.5.1.4 Interacting Fields

There is now a fairly complete theory of quantum energy inequalities for free fields in globally hyperbolic spacetimes of any dimension (although optimal bounds are lacking in general). As we have seen, similar results hold in a large class of conformal field theories in two dimensions. The situation for more general interacting QFTs is more complicated, of course, and less is known. The following remarks summarise the state of knowledge:

- One cannot expect state-independent QEIs to hold for worldline averaging; as mentioned, these can even fail in the nonminimally coupled theory. They also fail for theories with infinitely many minimally coupled fields, if the number of fields with mass below m grows exponentially in m [26]. Moreover, on physical grounds, we can expect that long-lasting negative energy densities can be sustained by quantum fields as shown by the example of the Casimir effect, modelling the plates as certain states of a full interacting theory. A computation along these lines was undertaken by Olum and Graham [83]; although there is a net positive energy density near the 'plates', their set-up maintains a negative energy density near the mid-point between them.
  However, it is possible that modified QEIs hold; for example, that suitable spacetime averages of the energy density can be bounded below when the scale of spatial averaging is comparable with that of temporal averaging (thus removing the objection posed by the Casimir example). This suggestion appears in [19, p. 176] and has been proposed as a spacetime averaged weak energy condition (SAWEC) in [21].
  The example of the nonminimally coupled scalar field shows that SAWEC cannot hold unconditionally. However, if there are interactions, the trick of tensoring together large numbers of single particle states to multiply up the energy density no longer works. Similarly, in the case of infinitely many fields, the mass spectra for which QEIs fail are essentially those for which other properties (nuclearity and the split property) also fail [26]. It is thus conceivable that well-behaved interacting models obey SAWEC or a similar condition.

- In terms of positive results, the averaged null energy condition is known to hold in general two-dimensional quantum field theories [97]. In spacetime dimension of 3 or more, it has been proved that for a wide class of theories obeying the 'microscopic phase space condition' there are (generally state-dependent) lower bounds on results on quantities that are 'classically positive', i.e. arise as composite fields in the operator product expansion of (sums of) squares [5]. For instance, one can obtain a bound on averages of the Wick square $:\Phi^2:$ because it is a composite field in the OPE of $\Phi(x)\Phi(y)$.[14] As yet, it is not known whether there are interacting theories in which the energy density can be
- A completely different and new direction is provided by the Quantum Null Energy Condition (QNEC) which asserts a state-dependent bound on the expectation value of the null-projected stress–energy tensor $T_{ab}k^ak^b$ *at a point*. The lower bound is provided by a second derivative of an entropy (non-uniquely) associated with the state and the null vector k. Such results have been established for super-renormalizable interacting theories [6] and also by holographic means for large-N (deformed) CFTs in Minkowski spacetime of general dimension [77].

10.5.2 Higher Moments and Probability Distributions

The discussion so far concerns the expectation value of the smeared stress–energy tensor or other similar quantities in arbitrary (physically reasonable) states. Here, we discuss what information can be gleaned concerning the underlying probability distribution of individual measurements of such quantities when the system is prepared in some specific state.

This has been worked out in detail for CFT in $1+1$ dimensions [30]. The idea is to study the probability distribution through its moment generating function

$$M[\mu f] = \sum_{n=0}^{\infty} \frac{\mu^n \langle \Omega \mid T(f)^n \Omega \rangle}{n!},$$

where Ω is the vacuum state and $T(f)$ is one of the chiral components of the stress–energy tensor averaged against test function f. In the special case where $f(u) = e^{-u^2/\tau^2}/(\tau\sqrt{\pi})$ it was shown that

$$M[\mu f] = \left[\frac{e^{-\mu/(\pi\tau^2)}}{1-\mu/(\pi\tau^2)}\right]^{c/24}.$$

Inverting a Laplace transform, the probability density for measurement values of $T(f)$ taken in the vacuum state is

[14] The fact that there is a state-independent lower bound in this case can be attributed to the fact that the only singular term in the OPE is a multiple of the identity.

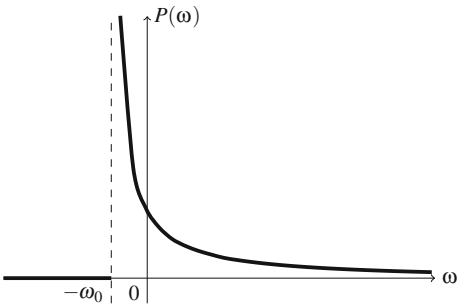

Fig. 10.3 The probability density $P(\omega)$ plotted for $c = 1$

$$P(\omega) = \vartheta(\omega + \omega_0)\frac{\beta^\alpha(\omega+\omega_0)^{\alpha-1}}{\Gamma(\alpha)}\exp(-\beta(\omega+\omega_0)),$$

(a shifted Gamma distribution) with parameters

$$\omega_0 = \frac{c}{24\pi\tau^2}, \qquad \alpha = \frac{c}{24}, \qquad \beta = \pi\tau^2,$$

which has an integrable singularity at lower limit for $c < 24$—see Fig. 10.3. Using the Hamburger uniqueness theorem [93] it may be shown that this is the only probability distribution corresponding to the moments $\langle\Omega \mid T(f)^n\Omega\rangle$.

The probability distribution is clearly highly skewed. We see that the lower bound of the support coincides precisely with the sharp lower bound on the expectation values of $T(f)$ for the Gaussian f, i.e. $-c/(24\pi\tau^2)$—as it should for general reasons [30]. Thus the QEI bound, originally conceived as a constraint on the *expectation value* of the smeared energy density, is also a constraint on the minimum value that can be achieved in an *individual measurement* of this quantity.

The probability of obtaining a negative value is given in terms of incomplete Γ-functions:

$$\text{Prob}(\omega < 0) = \int_{-\infty}^{0} P(\omega)d\omega = 1 - \frac{\Gamma(c/24, c/24)}{\Gamma(c/24)}.$$

For $c = 1$, this results in a value 0.89—an overwhelming likelihood of obtaining a *negative* value from a measurement in the vacuum state. This computation refers to just one of the chiral components of T_{ab}, and for averaging along the corresponding light-ray. For Gaussian averages of the energy density along an inertial curve and $c = 1$, as for the massless scalar field, the probability of obtaining a negative value is 0.84.

It is striking that negative energy densities occur with such high probability in individual measurements made in the *vacuum* state. It is not known with what probability negative energy densities occur in any other state, or for test functions other than a Gaussian, but it would be of interest to extend the CFT analysis further.

In four dimensions, similar questions have been studied in massless free field theory for averaging against Lorentzian sampling functions [31] (many of the results immediately transfer with slight modification to the electromagnetic field). Here, closed form results could not be obtained but strong numerical evidence was presented that the probability distribution for Lorentzian-smeared Wick square is again a shifted Gamma distribution): suitably normalised, all the moments turn out to be integers, and coincide with those of the fitted distribution *exactly* up to the 65th moment (calculations up to this level required some novel combinatorics [42]). The situation for the energy density is more complicated. The moments grow very rapidly $\sim(3n)!$ putting them beyond the scope of theorems on unique solution to the moment problem [93]. Nonetheless, every probability distribution consistent with the moments has a long tail

$$A(\upsilon/c)^{-7/6}e^{-(\upsilon/c)^{1/3}} \gtrsim \mathrm{Prob}(\omega > \upsilon) \gtrsim B(\upsilon/c)^{-4/3}e^{-(\upsilon/c)^{1/3}}$$

for constants A, B and c. Interestingly, this means that large positive QFT energy density fluctuations are more likely than comparable fluctuations from thermal noise, which may have implications for spontaneous nucleation of black holes [31].

What happens if the Lorentzian is replaced by a compactly supported function? The answer turns out to depends sensitively on the details of the sampling function as it switches on and off [29]. Averaging along the worldline results in even faster growth of the moments for the energy density on the order of $(3n/\alpha)!$, where the parameter α is associated with the fall-off in of the transform $\hat{f}(\omega) \sim e^{-\beta|\omega|^\alpha}$ (the previous result for Lorentzian sampling is consistent with the limiting case $\alpha = 1$). In the time domain, the switch-on is $f(t) \sim At^{-\mu}\exp(-Bt^{-\nu})$ for constants $A, B > 0$ where $\nu = \alpha/(1-\alpha)$, $\mu = (2-\alpha)/(2(1-\alpha))$ and we have supposed that the sampling function switches on at $t = 0$ for simplicity. The corresponding probability distribution must have an even more slowly decaying tail than before. On the other hand, averaging over spacetime volumes, rather than worldlines, results in moments that grow much more slowly, and might come within the scope of the Stieltjes uniqueness theorem in some cases [28] (see [70, Sect. II.D] for a summary). Even in these cases, the vacuum fluctuations dominate thermal fluctuations at high enough energy scale.

10.6 Applications of the QEIs

We have concentrated to a large extent on the QEI bounds themselves and their properties. By way of outlook, we briefly describe some of their applications.

10.6.1 Exotic Spacetimes

Any sufficiently smooth Lorentzian metric is a solution to the Einstein equations for *some* stress–energy tensor. Many exotic spacetime models (wormholes, warp drives, etc.) require stress–energy tensors that violate the classical energy conditions, and thus cannot be supported by for example a perfect fluid with positive energy density and pressure. Given that the energy conditions no longer hold in all circumstances in QFT, it is natural to consider whether exotic spacetimes can be supported by the expected stress–energy tensor in some quantum state.[15]

The QEIs can be used to provide strong constraints on the spacetime geometry in these scenarios (see, e.g. [41, 57, 86]): if the stress–energy tensor is supposed to be provided by a QFT, then it must obey the constraints that this entails. Of course this assumes that the QFTs involved obey QEIs at all. As described above, this is true for many free models, even in general curved spacetimes, and there is encouraging evidence that general interacting theories should obey related bounds with some caveats—almost certainly they do *not* obey state-independent worldline bounds, but a reasonable expectation is that they satisfy state-dependent QEIs (or possibly spacetime averaged conditions such as SAWEC), which make the long-term presence of large-magnitudes of negative energy density disproportionately expensive (in terms of the positive energy required overall).

A second problem is to determine the QEI bound. In principle the calculations can be done exactly, even in curved spacetimes [43] but tractable closed form expressions are not easily come by in general (except in weakly curved spacetimes [79] in a leading approximation). However, as one is typically interested only in order-of-magnitude estimates for the feasible parameters of the exotic spacetime (for example, the wormhole throat radius) one can be satisfied with approximations to the QEIs. The typical assumption made is that on sufficiently small scales, the spacetime can be assumed approximately Minkowskian and therefore the Minkowski QEIs apply for averages over sufficiently small scales. Therefore one can expect a results such as those of Sect. 10.3.2.2 to apply to the energy density along a timelike geodesic γ in a proper time parametrisation: that is, one has

$$\max \dot{\gamma}^a \dot{\gamma}^b T_{ab} \geq -\frac{C}{\tau^4},$$

where the maximum is taken over a proper time interval of duration τ and the constant $C \sim 3.17$. Alternatively, one can apply similar considerations to a QNEI (see (10.12)) to obtain

$$\max k^a k^b T_{ab} \geq -\frac{C'(\dot{\gamma}^a k_a)^2}{\tau^4},$$

[15] This sets important questions relating to fluctuations and back-reaction to the side but is at least a first step to understanding whether such spacetimes might be permitted in quantum gravity.

where γ is a timelike geodesic as before and k is a smooth null vector field so that $\dot{\gamma} \cdot k$ is approximately constant over the proper time interval in question. In this case, $C' \sim 4.23$—see [41, Sect. IV].

Via the Einstein equations, these bounds become geometric constraints and produce significant restrictions on wormhole geometry [41, 57] and on the Alcubierre warp drive spacetime [2, 86]. The reader is referred to these references for the specifics. An important aspect is to clarify what values of τ should be considered 'sufficiently small' for Minkowski bounds to apply. This can be worked out in detail for massless fields in two-dimensions [23] (based on the QEI derived in [49]) and it was shown that along an arbitrary timelike trajectory in proper time parametrisation with 2-velocity u^a one has

$$\int \langle T_{ab} u^a u^b \rangle |g(\tau)|^2 \, d\tau \geq -\frac{1}{6\pi} \int |\dot{g}(\tau)|^2 \, d\tau - \frac{1}{24\pi} \int |g(\tau)|^2 (R - a^c a_c) \, d\tau,$$

where R is the Ricci scalar and $a^c = u^a \nabla_a u^c$ is the acceleration of the trajectory. This bound holds provided that the region of γ where g is non-zero is contained in a single coordinate patch that can be conformally mapped to Minkowski space. The first term on the right-hand side is what would be expected for an inertial trajectory in Minkowski space, by the $c = 1$ case of (10.18). One sees that acceleration and positive Ricci scalar tend to weaken the bound (recall that $a^c a_c \leq 0$ in our conventions), but the Minkowski bound will be approximately valid provided that the sampling time is small in relation to both $\max\{R, 0\}^{-1/2}$ and $\max |a_c a^c|^{-1/2}$ over the sampling region (and so that the sampling fits inside a coordinate patch as described above).

In four dimensions, the rule of thumb used is that the sampling duration should be small in relation to the length scales set by suitable frame components of the Riemann tensor (and acceleration scales), but a rigorous proof that this suffices has not been given. At least in some cases, however, the rule of thumb is overconservative: for static wormholes one can consider QEIs relative to a static Hadamard ground state (assuming one exists) which are valid for sampling on arbitrarily large time scales. See [41, Sect. VIII], where the resulting bounds on Morris–Thorne wormholes were found to be more stringent by 5 orders of magnitude than those obtained by referring to Minkowski bounds in the small.

10.6.2 States of Low Energy

The QEIs show that local averages energy density of the free scalar field are bounded below on Hadamard states. Olbermann has turned this statement around in an interesting way [82]. In a Robertson–Walker spacetime, fix a local time average of the energy density along an isotropic worldline and minimise it over all homogeneous isotropic pure quasifree states. The minimising state is then called a state of low energy (SLE) and, crucially, is shown to be Hadamard. Of course, this state depends on the choice of the averaging function used. By contrast, adiabatic states, which

minimise instantaneous particle production, are not Hadamard in general. SLEs are of interest, because they provide a direct construction of Hadamard states, equipped with a good physical interpretation, in nonstationary backgrounds. They have been used as reference states to study particle production in cosmological models [16].

10.6.3 Averaged Null Energy Condition

We have already mentioned that the QEIs can be used to establish the 'difference' averaged weak energy condition (AWEC) in stationary situations—see (10.14). The situation for the averaged null energy condition (ANEC) is different, because of the lack of QEIs for averaging along null lines [40]. Direct proofs of (difference) ANEC exist in Minkowski space [50, 76, 97] and for suitable null geodesics in certain curved spacetimes [103, 106, 107]. Alternatively, one may consider QNEIs on a sequence of timelike curves that approach the given null.[16] This provides a proof of ANEC in spacetimes where the null geodesic is complete, achronal and surrounded by a tubular neighbourhood in which the metric is flat [35]. In fact, what is shown is that ANEC cannot be violated on a continuous family of timelike separated null geodesics in the tube. Finally, Kontou and Olum have combined their work on QEIs in spacetimes of small curvature [79] with the methodology of [35] to prove the ANEC on achronal geodesics in such spacetimes, under the additional assumption that the background satisfies the null convergence condition (i.e., the NEC holds for the background stress–energy tensor) [78]. Being based on the absolute QEI [43], this result is an absolute (rather than 'difference') form of ANEC.

10.6.4 Singularity Theorems

The energy conditions were originally introduced in GR to guarantee the focussing behaviour needed in the proofs of the singularity theorems. An important question is whether or not the QEI results provide sufficient control to guarantee that quantised matter also obeys singularity theorems.

Although this question is far from resolved, the hypotheses of the singularity theorems can be weakened to accommodate bounds motivated by the QEIs [32]. Unfortunately there is still a bit of a gap, because Hawking-style singularity theorems, concerning congruences of timelike geodesics, require the SEC (for which there is not a state-independent QEI) and Penrose-type results involve null geodesic congruences (which are not suitable for QEI bounds). Nonetheless, this is encouraging, and one can hope for more progress. For previous results along these lines see references in [32].

[16] One could also regard ANEC as a limiting case of AWEC [56], but only if the states and spacetime satisfy quite strong conditions at infinity.

10.6.5 Applications of the Probability Distribution

It has already been mentioned that the probability distribution of energy-density fluctuations appears to have a very slowly decaying tail for very large positive fluctuations. Therefore there is a possibility for vacuum fluctuation effects to stand out against a background of thermal or other relatively suppressed fluctuations. Recently, Ford and Huang have applied this idea to consider enhancements to quantum tunnelling [70]—the idea is that a rare vacuum pressure fluctuation might push a charged particle over a potential barrier thereby increasing the likelihood that it reaches the other side. In certain regimes these effects may be observable and might have interesting implications: simple calculations of nuclear fusion rates yield underestimates, and it is argued in [70] that the vacuum fluctuations are of a sufficient magnitude to account for the observed enhanced rate. It is also worth mentioning that, while negative energy densities themselves are difficult to observe directly, the related phenomenon of vacuum fluctuation suppression affects decay rates of excited atomic states [51].

In a different direction, Carlip, Mosna and Pitelli [11] argued that if the energy density fluctuations in two-dimensional dilaton quantum gravity are similar to those in CFT then the positive energy tail causes strong focussing of light cones near the Planck scale (outweighing the defocussing effects of negative energy densities) and resulting in 'asymptotic silence' – the inability of nearby regions to communicate. This may cast light on the physical mechanism for the dimensional reduction of quantum gravity at short distance scales; see also [10] for further discussion and references.

Acknowledgements This chapter is partly based on lectures given at the Albert Einstein Institute, Golm (March 2012) for graduate students enrolled in the IMPRS programme. I am grateful to the organisers and participants in those lectures for their interest and comments. I also thank Ko Sanders for detailed remarks on the lecture notes as written up in `arXiv:1208.5399`.

Appendix: Microlocal Analysis and the Proof of Theorem 10.1

As mentioned earlier, the rigorous proof of Theorem 10.1 requires techniques drawn from microlocal analysis [69], which provides detailed information on the singularities of distributions in a phase space perspective. We briefly summarise the main points as they apply to QEIs (see also [22], and the recent review of the Hadamard condition [75]).

Let $u \in \mathscr{D}'(X)$ be a distribution on a smooth n-dimensional manifold X. The *wavefront set* WF (u) of u is a subset of the cotangent bundle T^*X defined as follows. An element $(x, k) \in T^*X$ is called a *regular direction* for u if there exists a test

function $\phi \in C_0^\infty(X)$ with $\phi(x) \neq 0$ and a conic neighbourhood[17] V of k in T_x^*X so that for each $N \geq 1$, the quantity

$$(1 + \|\ell\|^N)|\widehat{\phi u}(\ell)|$$

is bounded on V. Here, $\|\cdot\|$ is an auxiliary norm on T_x^*X and the Fourier transform is taken with respect to a choice of coordinates x^α, so that

$$\widehat{\phi u}(\ell) = \int e^{i\ell_\alpha x^\alpha} \phi(x) u(x) d^n x.$$

(one requires that the support of ϕ is contained in the coordinate patch). It is a fundamental observation of the theory that this definition is independent of the choice of norm and coordinates. The wavefront set is then defined as

$$\mathrm{WF}(u) = \{(x, k) \in T^*X : k \neq 0 \text{ and } (x, k) \text{ is } \textit{not} \text{ a regular direction}\}.$$

Now suppose that (M, g) is a globally hyperbolic spacetime. The two-point function W_2 of a quantum state is a distribution on $M \times M$ and so $\mathrm{WF}(W_2) \subset T^*M \times M$. The remarkable fact is

Theorem 10.2 ([90, 95]) *The two-point function W_2 is Hadamard if and only if*

$$WF(W_2) \subset \mathcal{N}^+ \times \mathcal{N}^-$$

where $\mathcal{N}^{+/-}$ is the bundle of future/past directed null covectors on (M, g).

This neatly coincides with the idea that the two-point function $W_2(x, y)$ should be positive frequency in x and negative frequency in y. In fact, the wavefront set of a Hadamard two-point function can be given exactly [90], but this will not be needed here.

We can now resolve the remaining loose ends in the proof of Theorem 10.1. Suppose that W_2 is Hadamard, and let P be a partial differential operator on M with smooth coefficients. Then the wavefront set of $(P \otimes P)W_2$ obeys

$$\mathrm{WF}((P \otimes P)W_2) \subset \mathcal{N}^+ \times \mathcal{N}^-$$

because, in general, one has $\mathrm{WF}(Qu) \subset \mathrm{WF}(u)$ whenever Q is a partial differential operator with smooth coefficients (see [69, Chap. 8] for this and other general properties of wavefront sets stated below).

Next, we want to form the restriction $G^{(P)}(\tau, \tau') = (P \otimes P)W_2(\gamma(\tau), \gamma(\tau'))$ where γ is a smooth timelike curve. This amounts to taking a pull-back $(\gamma \times \gamma)^*(P \otimes P)W_2$. Microlocal analysis provides a sufficient criterion under which a pull-back $\varphi^* u$ can be defined, where $\varphi : X \to Y$ is smooth and $u \in \mathscr{D}'(Y)$. Namely, $\varphi^* u$ exists

[17] That is, V contains an open set around k and is a cone, i.e. if $\ell \in V$ then $\lambda\ell \in V$ for all $\lambda > 0$.

if there is no $(y, k) \in \mathrm{WF}(u)$ with the property that $y = \varphi(x)$ for some $x \in X$ and $\varphi^* k = 0$ (equivalently, that k annihilates the tangent space to $\varphi(X)$ at x). If this condition is met then $\varphi^* u$ can be defined (by extending the definition for pullbacks of smooth functions) so that

$$\mathrm{WF}(\varphi^* u) \subset \varphi^* \mathrm{WF}(u) := \{(x, \varphi^* k) \in T^*X : (\varphi(x), k) \in \mathrm{WF}(u)\}.$$

In our case of interest, $\varphi : \mathbb{R} \times \mathbb{R} \to M \times M$ by $\varphi(\tau, \tau') = (\gamma(\tau), \gamma(\tau'))$ and the tangent space to $\varphi(\mathbb{R}^2)$ at (τ, τ') consists of all tangent vectors of the form

$$(\mu\dot{\gamma}(\tau), \nu\dot{\gamma}(\tau')) \in T_{(\gamma(\tau),\gamma(\tau'))}M \times M,$$

where $\mu, \nu \in \mathbb{R}$. The crucial point is that no $(\gamma(\tau), k; \gamma(\tau'), k') \in \mathscr{N}^+ \times \mathscr{N}^-$ can simultaneously annihilate all such vectors, because this would entail

$$\mu k \cdot \dot{\gamma}(\tau) + \nu k' \cdot \dot{\gamma}(\tau') = 0$$

for all $\mu, \nu \in \mathbb{R}$ and hence $k \cdot \dot{\gamma}(\tau) = k' \cdot \dot{\gamma}(\tau') = 0$. But as k, k' are null (and non-zero) and $\dot{\gamma}$ is timelike this is impossible. Therefore the required pull-back $G^{(P)}$ exists, and one can compute further that

$$\mathrm{WF}(\varphi^*(P \otimes P)W_2) \subset \{(\tau, \zeta; \tau', \zeta') \in T^*\mathbb{R} \times \mathbb{R} : \zeta > 0,\ \zeta' < 0\} \tag{10.19}$$

simply because k and $\dot{\gamma}$ are future-pointing, while k' is past-pointing. All this holds both for our state of interest and for the reference state.

The second unresolved issue is to establish the finiteness of the bound in (10.10). For real-valued $g \in C_0^\infty(\mathbb{R})$, note that

$$G_R^{(P)}(\overline{g_\alpha}, g_\alpha) = \int d\tau\, d\tau' G_R^{(P)}(\tau, \tau') g(\tau) g(\tau') e^{-i\alpha\tau} e^{i\alpha\tau} \tag{10.20}$$

$$= \left((g \otimes g) G_R^{(P)}\right)^\wedge(-\alpha, \alpha) \tag{10.21}$$

according to our convention for the Fourier transform. A general result states that if u is a compactly supported distribution on $\mathbb{R}^n$, then the set $\Sigma(u) = \{k \in \mathbb{R}^n : (x, k) \in \mathrm{WF}(u)$ for some $x \in \mathbb{R}^n\}$ has the property that every non-zero k in its complement has a conic neighbourhood on which $(1 + \|\ell\|^N)|\hat{u}(\ell)|$ is bounded for every N. Applying this result to $(g \otimes g)G_R^{(P)}$ and using (10.19) we find

$$\Sigma\left((g \otimes g) G_R^{(P)}\right) \subset \mathbb{R}^+ \times \mathbb{R}^-$$

In particular, $(-1, 1) \notin \Sigma((g \otimes g)G_R^{(P)})$, and $((g \otimes g)G_R^{(P)})^\wedge(-\alpha, \alpha)$ decays rapidly as $\alpha \to +\infty$. By virtue of (10.21), the bound in (10.10) is therefore finite and the proof of Theorem 10.1 is complete.

References

1. Abreu G, Visser M. Quantum interest in (3 + 1)-dimensional Minkowski space. Phys Rev D. 2009;79:065004.
2. Alcubierre M. The warp drive: hyper-fast travel within general relativity. Class Quantum Gravity. 1994;11:L73–7.
3. Bostelmann H, Cadamuro D. Negative energy densities in integrable quantum field theories at one-particle level. Phys Rev D. 2016;93:065001.
4. Bostelmann H, Cadamuro D, Fewster CJ. Quantum energy inequality for the massive Ising model. Phys Rev D. 2013;88:025019.
5. Bostelmann H, Fewster CJ. Quantum inequalities from operator product expansions. Commun Math Phys. 2009;292:761–95.
6. Bousso R, Fisher Z, Koeller J, Leichenauer S, Wall AC. Proof of the quantum null energy condition. Phys Rev D. 2016;93:024017.
7. Brown LS, Maclay GJ. Vacuum stress between conducting plates: an image solution. Phys Rev. 1969;184:1272–9.
8. Brunetti R, Dappiaggi C, Fredenhagen K, Yngvason J, editors. Advances in algebraic quantum field theory. Mathematical physics studies. Cham: Springer; 2015.
9. Brunetti R, Fredenhagen K, Verch R. The generally covariant locality principle: a new paradigm for local quantum physics. Commun Math Phys. 2003;237:31–68.
10. Carlip S. Spontaneous dimensional reduction in quantum gravity. Int J Mod Phys D. 2016;25:1643003.
11. Carlip S, Mosna RA, Pitelli JPM. Vacuum fluctuations and the small scale structure of spacetime. Phys Rev Lett. 2011;107:021303.
12. Carpi S., Weiner M. Local energy bounds and representations of conformal nets. In preparation.
13. Dawson SP. Bounds on negative energy densities in quantum field theories on flat and curved space-times. PhD thesis, University of York (2006).
14. Dawson SP. A quantum weak energy inequality for the Dirac field in two-dimensional flat spacetime. Class Quantum Gravity. 2006;23:287–93.
15. Dawson SP, Fewster CJ. An explicit quantum weak energy inequality for Dirac fields in curved spacetimes. Class Quantum Gravity. 2006;23:6659–81.
16. Degner A, Verch R. Cosmological particle creation in states of low energy. J Math Phys. 2010;51:022302.
17. DeWitt BS. Quantum field theory in curved spacetime. Phys Rep. 1975;19:295–357.
18. Epstein H, Glaser V, Jaffe A. Nonpositivity of the energy density in quantized field theories. Il Nuovo Cim. 1965;36:1016–22.
19. Everett A, Roman T. Time travel and warp drives. Chicago: University of Chicago Press; 2012.
20. Eveson SP, Fewster CJ. Mass dependence of quantum energy inequality bounds. J Math Phys. 2007;48:093506.
21. Farnsworth K, Luty MA, Prilepina V. Positive energy conditions in 4d conformal field theory. J High Energy Phys. 2016;2016(10):1.
22. Fewster CJ. A general worldline quantum inequality. Class Quantum Gravity. 2000;17:1897–911.
23. Fewster CJ. Quantum energy inequalities in two dimensions. Phys Rev D. 2004;70:127501.
24. Fewster CJ. Energy inequalities in quantum field theory. In: Zambrini JC, editor. XIVth international congress on mathematical physics. Singapore: World Scientific; 2005. An expanded and updated version is available as arXiv:math-ph/0501073.
25. Fewster CJ. Quantum energy inequalities and local covariance. II. Categorical formulation. Gen Relativ Gravitat. 2007;39:1855–90.
26. Fewster CJ. The split property for quantum field theories in flat and curved spacetimes. Abh Math Semin Univ Hambg. 2016;86:153–75.

27. Fewster CJ, Eveson SP. Bounds on negative energy densities in flat spacetime. Phys Rev D. 1998;58:084010.
28. Fewster CJ, Ford LH. In preparation.
29. Fewster CJ., Ford LH. Probability distributions for quantum stress tensors measured in a finite time interval. Phys Rev D. 2015;92:105008.
30. Fewster CJ, Ford LH, Roman TA. Probability distributions of smeared quantum stress tensors. Phys Rev D. 2010;81:121901.
31. Fewster CJ, Ford LH, Roman TA. Probability distributions for quantum stress tensors in four dimensions. Phys Rev D. 2012;85:125038.
32. Fewster CJ, Galloway GJ. Singularity theorems from weakened energy conditions. Class Quantum Gravity. 2011;28:125009.
33. Fewster CJ, Hollands S. Quantum energy inequalities in two-dimensional conformal field theory. Rev Math Phys. 2005;17:577–612.
34. Fewster CJ, Mistry B. Quantum weak energy inequalities for the Dirac field in flat spacetime. Phys Rev D. 2003;68:105010.
35. Fewster CJ, Olum KD, Pfenning MJ. Averaged null energy condition in spacetimes with boundaries. Phys Rev D. 2007;75:025007.
36. Fewster CJ, Osterbrink LW. Averaged energy inequalities for the nonminimally coupled classical scalar field. Phys Rev D. 2006;74:044021.
37. Fewster CJ, Osterbrink LW. Quantum energy inequalities for the non-minimally coupled scalar field. J Phys A. 2008;41:025402.
38. Fewster CJ, Pfenning MJ. A quantum weak energy inequality for spin-one fields in curved spacetime. J Math Phys. 2003;44:4480–513.
39. Fewster CJ, Pfenning MJ. Quantum energy inequalities and local covariance. I: globally hyperbolic spacetimes. J Math Phys. 2006;47:082303.
40. Fewster CJ, Roman TA. Null energy conditions in quantum field theory. Phys Rev D. 2003;67:044003.
41. Fewster CJ, Roman TA. On wormholes with arbitrarily small quantities of exotic matter. Phys Rev D. 2005;72:044023.
42. Fewster CJ, Siemssen D. Enumerating permutations by their run structure. Electron J Combin. 2014;21(4.18):19.
43. Fewster CJ, Smith CJ. Absolute quantum energy inequalities in curved spacetime. Annales Henri Poincaré. 2008;9:425–55.
44. Fewster CJ, Teo E. Bounds on negative energy densities in static space-times. Phys Rev D. 1999;59:104016.
45. Fewster CJ, Teo E. Quantum inequalities and “quantum interest” as eigenvalue problems. Phys Rev D. 2000;61:084012.
46. Fewster CJ, Verch R. A quantum weak energy inequality for Dirac fields in curved spacetime. Commun Math Phys. 2002;225:331–59.
47. Fewster CJ, Verch R. Stability of quantum systems at three scales: passivity, quantum weak energy inequalities and the microlocal spectrum condition. Commun Math Phys. 2003;240:329–75.
48. Flanagan ÉÉ. Quantum inequalities in two-dimensional Minkowski spacetime. Phys Rev D. 1997;56:4922–6.
49. Flanagan ÉÉ. Quantum inequalities in two dimensional curved spacetimes. Phys Rev D. 2002;66:104007.
50. Folacci A. Averaged-null-energy condition for electromagnetism in Minkowski spacetime. Phys Rev D. 1992;46:2726–9.
51. Ford L, Roman TA. Effects of vacuum fluctuation suppression on atomic decay rates. Ann Phys. 2011;326:2294–306.
52. Ford LH. Quantum coherence effects and the second law of thermodynamics. Proc R Soc Lond A. 1978;364:227–36.
53. Ford LH. Constraints on negative-energy fluxes. Phys Rev D. 1991;43:3972–8.

54. Ford LH, Helfer AD, Roman TA. Spatially averaged quantum inequalities do not exist in four-dimensional spacetime. Phys Rev D. 2002;66:124012.
55. Ford LH, Pfenning MJ, Roman TA. Quantum inequalities and singular negative energy densities. Phys Rev D. 1998;57:4839–46.
56. Ford LH, Roman TA. Averaged energy conditions and quantum inequalities. Phys Rev D. 1995;51:4277–86.
57. Ford LH, Roman TA. Quantum field theory constrains traversable wormhole geometries. Phys Rev D. 1996;53:5496–507.
58. Ford LH, Roman TA. Restrictions on negative energy density in flat spacetime. Phys Rev D. 1997;55:2082–9.
59. Ford LH, Roman TA. The quantum interest conjecture. Phys Rev D. 1999;60:104018.
60. Ford LH, Roman TA. Classical scalar fields and the generalized second law. Phys Rev D. 2001;64:024023.
61. Ford LH, Roman TA. Negative energy seen by accelerated observers. Phys Rev D. 2013;87:085001.
62. Fulling SA, Davies PCW. Radiation from a moving mirror in two dimensional space-time: conformal anomaly. Proc R Soc Lond Ser A. 1976;348:393–414.
63. Furlan P, Sotkov GM, Todorov IT. Two-dimensional conformal quantum field theory. Riv Nuovo Cimento. 1989;12:1–202.
64. Haag R. Local quantum physics: fields, particles algebras. Berlin: Springer; 1992.
65. Hawking SW, Ellis GFR. The large scale structure of space-time. London: Cambridge University Press; 1973.
66. Helfer AD. "Operational" energy conditions. Class Quantum Gravity. 1998;15:1169–83.
67. Hill CT. One-loop operator matrix elements in the Unruh vacuum. Nucl Phys B. 1986;277:547–74.
68. Hollands S, Wald RM. Quantum fields in curved spacetime. Phys Rep. 2015;574:1–35.
69. Hörmander L. The analysis of linear partial differential operators I. Berlin: Springer; 1983.
70. Huang H, Ford LH. Vacuum radiation pressure fluctuations and barrier penetration. 2016. arXiv:1610.01252.
71. Kar S, Sengupta S. The Raychaudhuri equations: a brief review. Pramana. 2007;69:49–76.
72. Kay BS. Casimir effect in quantum field theory. Phys Rev D. 1979;20:3052–62.
73. Kay BS, Wald RM. Theorems on the uniqueness and thermal properties of stationary, nonsingular, quasifree states on space-times with a bifurcate Killing horizon. Phys Rep. 1991;207:49–136.
74. Kelly WR, Wall AC. Holographic proof of the averaged null energy condition. Phys Rev D. 2015;90:106003 Erratum, Phys Rev D 91, 069902 (2015).
75. Khavkine I, Moretti V. Algebraic QFT in curved spacetime and quasifree Hadamard states: an introduction. In: Advances in algebraic quantum field theory. Mathematical physics studies. Cham: Springer; 2015. pp. 191–251
76. Klinkhammer G. Averaged energy conditions for free scalar fields in flat spacetime. Phys Rev D. 1991;43:2542–8.
77. Koeller J, Leichenauer S. Holographic proof of the quantum null energy condition. Phys Rev D. 2016;94:024026.
78. Kontou EA, Olum KD. Proof of the averaged null energy condition in a classical curved spacetime using a null-projected quantum inequality. Phys Rev D. 2015;92:124009.
79. Kontou EA, Olum KD. Quantum inequality in spacetimes with small curvature. Phys Rev D. 2015;91:104005.
80. Levi A, Ori A. Versatile method for renormalized stress-energy computation in black-hole spacetimes. 2016. arXiv:1608.03806.
81. Levine AR. A holographic dual of the quantum inequalities. 2016. arXiv:1605.05751.
82. Olbermann H. States of low energy on Robertson-Walker spacetimes. Class Quantum Gravity. 2007;24:5011–30.
83. Olum KD, Graham N. Static negative energies near a domain wall. Phys Lett B. 2003;554:175–9.

84. Pfenning MJ. Quantum inequalities for the electromagnetic field. Phys Rev D. 2001;65:024009.
85. Pfenning MJ, Ford LH. Quantum inequalities on the energy density in static Robertson-Walker spacetimes. Phys Rev D. 1997;55:4813–21.
86. Pfenning MJ, Ford LH. The unphysical nature of 'warp drive'. Class Quantum Gravity. 1997;14:1743–51.
87. Pfenning MJ, Ford LH. Scalar field quantum inequalities in static spacetimes. Phys Rev D. 1998;57:3489–502.
88. Pretorius F. Quantum interest for scalar fields in Minkowski spacetime. Phys Rev D. 2000;61:064005.
89. Radzikowski MJ. A local-to-global singularity theorem for quantum field theory on curved space-time. Commun Math Phys. 1996;180:1–22. (With an appendix by Rainer Verch).
90. Radzikowski MJ. Micro-local approach to the Hadamard condition in quantum field theory on curved space-time. Commun Math Phys. 1996;179:529–53.
91. Schlemmer J, Verch R. Local thermal equilibrium states and quantum energy inequalities. Ann Henri Poincaré. 2008;9:945–78.
92. Senovilla JMM. Singularity theorems and their consequences. Gen Relat Grav. 1998;30:701–848.
93. Simon B. The classical moment problem as a self-adjoint finite difference operator. Adv Math. 1998;137:82–203.
94. Smith CJ. An absolute quantum energy inequality for the Dirac field in curved spacetime. Class Quantum Gravity. 2007;24:4733–50.
95. Strohmaier A, Verch R, Wollenberg M. Microlocal analysis of quantum fields on curved space-times: analytic wavefront sets and Reeh-Schlieder theorems. J Math Phys. 2002;43:5514–30.
96. Teo E, Wong KF. Quantum interest in two dimensions. Phys Rev D. 2002;66:064007.
97. Verch R. The averaged null energy condition for general quantum field theories in two dimensions. J Math Phys. 2000;41:206–17.
98. Visser M. Lorentzian wormholes: from Einstein to Hawking. AIP Series in Computational and Applied Mathematical Physics. AIP Press, American Institute of Physics; 1995.
99. Visser M. Gravitational vacuum polarization. I. Energy conditions in the Hartle-Hawking vacuum. Phys Rev D. 1996;54:5103–15.
100. Visser M. Gravitational vacuum polarization. II. Energy conditions in the Boulware vacuum. Phys Rev D. 1996;54:5116–22.
101. Visser M. Gravitational vacuum polarization. IV. Energy conditions in the Unruh vacuum. Phys Rev D. 1997;56:936–52.
102. Vollick DN. Quantum inequalities in curved two-dimensional spacetimes. Phys Rev D. 2000;61:084022.
103. Wald R, Yurtsever U. General proof of the averaged null energy condition for a massless scalar field in two-dimensional curved spacetime. Phys Rev D. 1991;44:403–16.
104. Wald RM. Quantum field theory in curved spacetime and black hole thermodynamics. Chicago: University of Chicago Press; 1994.
105. Yu H, Wu P. Quantum inequalities for the free Rarita-Schwinger fields in flat spacetime. Phys Rev D. 2004;69:064008.
106. Yurtsever U. Averaged null energy condition and difference inequalities in quantum field theory. Phys Rev D. 1995;51:5797–805.
107. Yurtsever U. Remarks on the averaged null energy condition in quantum field theory. Phys Rev D. 1995;52:R564–8.

Part III
Warp Drive

Chapter 11
Warp Drive Basics

Miguel Alcubierre and Francisco S.N. Lobo

11.1 Introduction

Recently much interest has been revived in superluminal travel, due to the research in wormhole geometries [1, 2] and superluminal warp drive spacetimes [3]. However, despite the use of the term superluminal, it is not possible to locally achieve faster than light travel. In fact, the point to note is that one can make a round trip, between two points separated by a distance D, in an arbitrarily short time as measured by an observer that remained at rest at the starting point, by varying one's speed or by changing the distance one is to cover. It is a highly nontrivial issue to provide a general global definition of superluminal travel [4, 5], but it has been shown that the spacetimes that permit "effective" superluminal travel generically suffer from several severe drawbacks. In particular, superluminal effects are associated with the presence of *exotic* matter, that is, matter that violates the null energy condition (NEC).

In fact, it has been shown that superluminal spacetimes violate all the known energy conditions and, in particular, it was shown that negative energy densities and superluminal travel are intimately related [6]. Although it is thought that most classical forms of matter obey the energy conditions, they are violated by certain quantum fields [7]. Additionally, specific classical systems (such as non-minimally coupled scalar fields) have been found that violate the null and the weak energy conditions [8, 9]. It is also interesting to note that recent observations in cosmology, such as the late-time cosmic speed-up [10], strongly suggest that the cosmological fluid violates the strong energy condition (SEC), and provides tantalizing hints that the NEC is violated in a classical regime [10–12].

In addition to wormhole geometries [1, 2], other spacetimes that allow superluminal travel are the Alcubierre warp drive [3] and the *Krasnikov tube* [13, 14],

M. Alcubierre (✉)
Instituto de Ciencias Nucleares, Universidad Nacional Autónoma de México,
Circuito Exterior C.U., A.P. 70-543, 04510 Mexico City, Mexico
e-mail: malcubi@nucleares.unam.mx

F.S.N. Lobo
Instituto de Astrofísica e Ciências do Espaço, Universidade de Lisboa,
Faculdade de Ciências, 1749-016 Campo Grande, Lisboa, Portugal
e-mail: fslobo@fc.ul.pt

F.S.N. Lobo (ed.), *Wormholes, Warp Drives and Energy Conditions*,
Fundamental Theories of Physics 189, DOI 10.1007/978-3-319-55182-1_11

which will be presented in detail below. Indeed, it was shown theoretically that the Alcubierre warp drive entails the possibility to attain arbitrarily large velocities [3], within the framework of general relativity. As will be demonstrated below, a warp bubble is driven by a local expansion of space behind the bubble, and an opposite contraction ahead of it. However, by introducing a slightly more complicated metric, Natário [15] dispensed with the need for expansion of the volume elements. In the Natário warp drive, the expansion (contraction) of the distances along the direction of motion is compensated by a contraction (expansion) of area elements in the perpendicular direction, so that the volume elements are preserved. Thus, the essential property of the warp drive is revealed to be the change in distances along the direction of motion, and not the expansion/contraction of space. Thus, the Natário version of the warp drive can be thought of as a bubble sliding through space.

However, an interesting aspect of the Alcubierre warp drive is that an observer on a spaceship, within the warp bubble, cannot create nor control on demand a superluminal Alcubierre bubble surrounding the ship [13]. This is due to the fact that points on the outside front edge of the bubble are always spacelike separated from the centre of the bubble. Note that, in principle, causality considerations do not prevent the crew of a spaceship from altering the metric along the path of their outbound trip, by their own actions, in order to complete a round trip from the Earth to a distant star and back in an arbitrarily short time, as measured by clocks on the Earth. To this effect, an interesting solution was introduced by Krasnikov, that consists of a two-dimensional metric with the property that although the time for a one-way trip to a distant destination cannot be shortened, the time for a round trip, as measured by clocks at the starting point (e.g. Earth), can be made arbitrarily short. Soon after, Everett and Roman generalized the Krasnikov two-dimensional analysis to four dimensions, denoting the solution as the *Krasnikov tube* [14]. Interesting features were analysed, such as the effective superluminal nature of the solution, the energy condition violations, the appearance of closed timelike curves and the application of the Quantum Inequality (QI) deduced by Ford and Roman [16].

Using the QI in the context of warp drive spacetimes, it was soon verified that enormous amounts of energy are needed to sustain superluminal warp drive spacetimes [17, 18]. However, one should note the fact that the quantum inequalities might not necessarily be fundamental, and anyway they are violated in the Casimir effect. To reduce the enormous amounts of exotic matter needed in the superluminal warp drive, van den Broeck proposed a slight modification of the Alcubierre metric that considerably improves the conditions of the solution [19]. It was also shown that using the QI, enormous quantities of negative energy densities are needed to support the superluminal Krasnikov tube [14]. This problem was surpassed by Gravel and Plante [20, 21], who in similar manner to the van den Broeck analysis, showed that it is theoretically possible to lower significantly the mass of the Krasnikov tube.

However, applying the linearized approach to the warp drive spacetime [22], where no a priori assumptions as to the ultimate source of the energy condition violations are required, the QI are not used nor needed. This means that the linearized restrictions derived on warp drive spacetimes are more generic than those derived using the quantum inequalities, where the restrictions derived in [22] hold regardless of whether

the warp drive is assumed to be classical or quantum in its operation. It was not meant to suggest that such a *reactionless drive* is achievable with current technology, as indeed extremely stringent conditions on the warp bubble were obtained, in the weak-field limit. These conditions are so stringent that it appears unlikely that the warp drive will ever prove technologically useful.

This chapter is organized in the following manner: In Sect. 11.2, we present the basics of the warp drive spacetime, showing the explicit violations of the energy conditions, and a brief application of the QI. In Sect. 11.3, using linearized theory, we show that significant constraints in the weak-field regime arise, so that the analysis implies additional difficulties for developing a "strong field" warp drive. In Sect. 11.4, we consider further interesting aspects of the warp drive spacetime, such as the "horizon problem", in which an observer on a spaceship cannot create nor control on demand a superluminal Alcubierre bubble. In Sect. 11.5, we consider the physical properties of the Krasnikov tube, that consists of a metric in which the time for a round trip, as measured by clocks at the starting point, can be made arbitrarily short. In Sect. 11.6, we consider the possibility of closed timelike curves in the superluminal warp drive and the Krasnikov tube, and in Sect. 11.7, we conclude.

11.2 Warp Drive Spacetime

Alcubierre proved that it is, in principle, possible to warp spacetime in a small *bubble-like* region, within the framework of general relativity, in a manner that the bubble may attain arbitrarily large velocities. The enormous speed arises from the expansion of spacetime itself, analogously to the inflationary phase of the early universe. More specifically, the hyper-fast travel is induced by creating a local distortion of spacetime, producing a contraction ahead of the bubble, and an opposite expansion behind it.

11.2.1 Alcubierre Warp Drive

In Cartesian coordinates, the Alcubierre warp drive spacetime metric is given by (with $G = c = 1$)

$$ds^2 = -dt^2 + dx^2 + dy^2 + [dz - v(t)\ f(x, y, z - z_0(t))\ dt]^2\ , \qquad (11.1)$$

where $v(t) = dz_0(t)/dt$ is the velocity of the warp bubble, moving along the positive z-axis. The form function $f(x, y, z)$ possesses the general features of having the value $f = 0$ in the exterior and $f = 1$ in the interior of the bubble. The general class of form functions, $f(x, y, z)$, chosen by Alcubierre was spherically symmetric: $f(r)$ with $r = \sqrt{x^2 + y^2 + z^2}$. Then $f(x, y, z - z_0(t)) = f(r(t))$ with $r(t) = \left\{[(z - z_0(t)]^2 + x^2 + y^2\right\}^{1/2}$.

We consider the specific case given by

$$f(r) = \frac{\tanh\left[\sigma(r+R)\right] - \tanh\left[\sigma(r-R)\right]}{2\tanh(\sigma R)}\,, \tag{11.2}$$

where $R > 0$ and $\sigma > 0$ are two arbitrary parameters. R is the radius of the warp bubble, and σ can be interpreted as being inversely proportional to the bubble wall thickness. If σ is sufficiently large, the form function rapidly approaches a *top hat* function, i.e. $f(r) = 1$ if $r \in [0, R]$, and $f(r) = 0$ if $r \in (R, \infty)$, for $\sigma \to \infty$.

It can be shown that observers with the four velocity

$$U^{\mu} = (1, 0, 0, v f)\,, \tag{11.3}$$

and $U_{\mu} = (-1, 0, 0, 0)$ move along geodesics, as their 4-acceleration is zero, i.e. $a^{\mu} = U^{\nu}\, U^{\mu}{}_{;\nu} = 0$. These observers are usually called "Eulerian observers" in the 3+1 formalism, as they move along the normal directions to the spatial slices [3]. The spaceship, which in the original formulation is treated as a test particle which moves along the curve $z = z_0(t)$, can easily be seen to always move along a timelike curve, regardless of the value of $v(t)$. One can also verify that the proper time along this curve equals the coordinate time, by simply substituting $z = z_0(t)$ in Eq. (11.1). This reduces to $d\tau = dt$, taking into account $dx = dy = 0$ and $f(0) = 1$.

Consider a spaceship placed within the Alcubierre warp bubble. The expansion of the volume elements, $\theta = U^{\mu}{}_{;\mu}$, is given by $\theta = v\ (\partial f/\partial z)$. Taking into account Eq. (11.2), we have

$$\theta = v\,\frac{z - z_0}{r}\,\frac{df(r)}{dr}. \tag{11.4}$$

The centre of the perturbation corresponds to the spaceship's position $z_0(t)$. The volume elements are expanding behind the spaceship, and contracting in front of it, as shown in Fig. 11.1.

11.2.2 Superluminal Travel in the Warp Drive

To demonstrate that it is possible to travel to a distant point and back in an arbitrary short time interval, consider two distant stars, A and B, separated by a distance D in flat spacetime. Suppose that, at the instant t_0, a spaceship moves away from A, using its engines, with a velocity $v < 1$, and finally comes to rest at a distance d from A. We shall, for simplicity, assume that $R \ll d \ll D$. Now, at this instant the perturbation of spacetime appears, centred around the spaceship's position, and pushing it away from A, and rapidly attains a constant acceleration, a. Consider that now at half-way between A and B, the perturbation is modified, so that the acceleration rapidly varies from a to $-a$. The spaceship finally comes to rest at a distance, d, from B, at

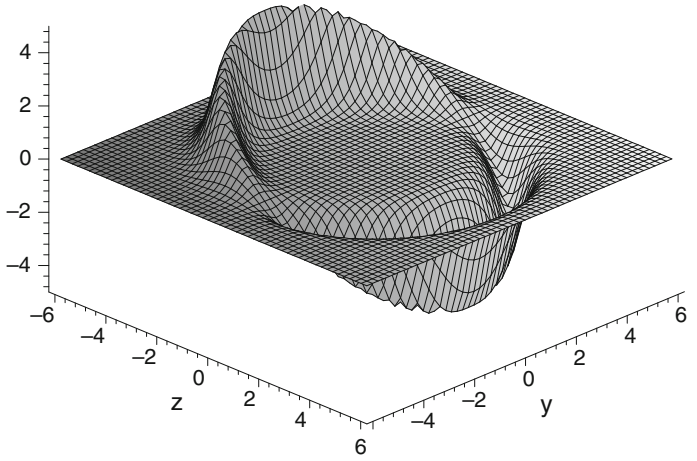

Fig. 11.1 The plot depicts the expansion of the volume elements of an Alcubierre warp bubble moving along the positive z-axis, with an arbitrary velocity $v(t)$. Note that the volume elements are expanding behind the spaceship, and contracting in front of it. See the text for more details

which point the perturbation disappears. The spaceship then moves to B at a constant velocity in flat spacetime. The return trip to A is analogous.

Consider that the variations of the acceleration are extremely rapid, so that the total coordinate time, T, in a one-way trip will be

$$T = 2\left(\frac{d}{v} + \sqrt{\frac{D-2d}{a}}\right). \tag{11.5}$$

The proper time of an observer, in the exterior of the warp bubble, is equal to the coordinate time, as both are immersed in flat spacetime. The proper time measured by observers within the spaceship is given by:

$$\tau = 2\left(\frac{d}{\gamma v} + \sqrt{\frac{D-2d}{a}}\right). \tag{11.6}$$

with $\gamma = (1-v^2)^{-1/2}$. The time dilation only appears in the absence of the perturbation, in which the spaceship is moving with a velocity v, using only its engines in flat spacetime.

Using $R \ll d \ll D$, we can then obtain the following approximation $\tau \approx T \approx 2\sqrt{D/a}$, which can be made arbitrarily short, by increasing the value of a. This implies that the spaceship may travel faster than the speed of light, however, it moves along a spacetime temporal trajectory, contained within its light cone, as light suffers the same distortion of spacetime [3].

11.2.3 The Violation of the Energy Conditions

11.2.3.1 The Violation of the WEC

As mentioned in the previous chapters, the weak energy condition (WEC) states $T_{\mu\nu}\,U^{\mu}\,U^{\nu} \geq 0$, in which U^{μ} is a timelike vector and $T_{\mu\nu}$ is the stress–energy tensor. As mentioned in Chaps. 9 and 10, its physical interpretation is that the local energy density is positive, and by continuity it implies the NEC. Now, one verifies that the WEC is violated for the warp drive metric, i.e.

$$T_{\mu\nu}\,U^{\mu}\,U^{\nu} = -\frac{v^2}{32\pi}\left[\left(\frac{\partial f}{\partial x}\right)^2 + \left(\frac{\partial f}{\partial y}\right)^2\right] < 0\,, \tag{11.7}$$

and by taking into account the Alcubierre form function (11.2), we have

$$T_{\mu\nu}\,U^{\mu}U^{\nu} = -\frac{1}{32\pi}\,\frac{v^2(x^2+y^2)}{r^2}\left(\frac{df}{dr}\right)^2 < 0\,. \tag{11.8}$$

By considering an orthonormal basis, we verify that the energy density of the warp drive spacetime is given by $T_{\hat{t}\hat{t}} = T_{\hat{\mu}\hat{\nu}}\,U^{\hat{\mu}}U^{\hat{\nu}}$, which is precisely given by Eq. (11.8). It is easy to verify that the energy density is distributed in a toroidal region around the z-axis, in the direction of travel of the warp bubble [18], as may be verified from Fig. 11.2. It is perhaps instructive to point out that the energy density for this class of spacetimes is nowhere positive.[1]

In analogy with the definitions in [25, 26], one may quantify the "total amount" of energy condition violating matter in the warp bubble, by defining the "volume integral quantifier"[2]

$$M_{\text{warp}} = \int \rho_{\text{warp}}\,d^3x = \int T_{\mu\nu}\,U^{\mu}\,U^{\nu}\,d^3x = -\frac{v^2}{12}\int\left(\frac{df}{dr}\right)^2 r^2\,dr. \tag{11.10}$$

---

[1] It is also interesting to note that the inclusion of a generic lapse function $\alpha(x,\,y,\,z,\,t)$, in the metric, decreases the negative energy density, which is now given by

$$T_{\hat{t}\hat{t}} = -\frac{v^2}{32\pi\,\alpha^2}\left[\left(\frac{\partial f}{\partial x}\right)^2 + \left(\frac{\partial f}{\partial y}\right)^2\right]. \tag{11.9}$$

One may impose that α may be taken as unity in the exterior and interior of the warp bubble, so that proper time equals coordinate time. In order to significantly decrease the negative energy density in the bubble walls, one may impose an extremely large value for the lapse function. However, the inclusion of the lapse function suffers from an extremely severe drawback, as proper time as measured in the bubble walls becomes absurdly large, $d\tau = \alpha\,dt$, for $\alpha \gg 1$.

[2] We refer the reader to [25, 26] for details.

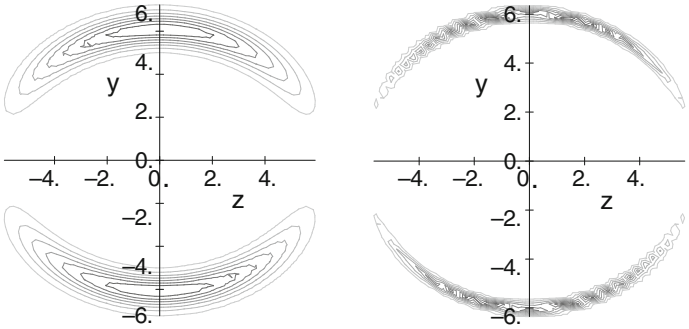

Fig. 11.2 The energy density is distributed in a toroidal region perpendicular to the direction of travel of the spaceship, which is situated at $z_0(t)$. We have considered the following values, $v = 2$ and $R = 6$, with $\sigma = 1$ and $\sigma = 4$ in the left and right plots, respectively. See the text for more details

This is not the total mass of the spacetime, but it characterizes how much (negative) energy one needs to localize in the walls of the warp bubble. For the specific shape function (11.2) we can estimate

$$M_{\text{warp}} \approx -v^2\ R^2\ \sigma, \tag{11.11}$$

so that one can readily verify that the energy requirements for the warp bubble scale quadratically with bubble velocity and with bubble size, and inversely as the thickness of the bubble wall [22].

11.2.3.2 The Violation of the NEC

As mentioned before in the previous chapters, the NEC states that $T_{\mu\nu}\,k^\mu\,k^\nu \geq 0$, where k^μ is *any* arbitrary null vector and $T_{\mu\nu}$ is the stress–energy tensor. The NEC for a null vector oriented along the $\pm\hat{z}$ directions takes the following form

$$T_{\mu\nu}\,k^\mu\,k^\nu = -\frac{v^2}{8\pi}\left[\left(\frac{\partial f}{\partial x}\right)^2 + \left(\frac{\partial f}{\partial y}\right)^2\right] \pm \frac{v}{8\pi}\left(\frac{\partial^2 f}{\partial x^2} + \frac{\partial^2 f}{\partial y^2}\right). \tag{11.12}$$

Note that if we average over the $\pm\hat{z}$ directions we have the following relation

$$\frac{1}{2}\left[T_{\mu\nu}\,k^\mu_{+\hat{z}}\,k^\nu_{+\hat{z}} + T_{\mu\nu}\,k^\mu_{-\hat{z}}\,k^\nu_{-\hat{z}}\right] = -\frac{v^2}{8\pi}\left[\left(\frac{\partial f}{\partial x}\right)^2 + \left(\frac{\partial f}{\partial y}\right)^2\right], \tag{11.13}$$

which is manifestly negative, and implies that the NEC is violated for all v. Furthermore, note that even if we do not average, the coefficient of the term linear in v

must be nonzero *somewhere* in the spacetime. Then at low velocities, this term will dominate and at low velocities the un-averaged NEC will be violated in either the $+\hat{z}$ or $-\hat{z}$ directions.

11.2.4 The Quantum Inequality Applied to the Warp Drive

It is of interest to apply the QI to the warp drive spacetimes [18], rather than deduce the QI in this section, we refer the reader to the chapter on the quantum energy inequalities. By inserting the energy density, Eq. (11.8), into the QI, one arrives at the following inequality

$$t_0 \int_{-\infty}^{+\infty} \frac{v(t)^2}{r^2} \left(\frac{df}{dr}\right)^2 \frac{dt}{t^2+t_0^2} \leq \frac{3}{\rho^2\, t_0^4}\,, \tag{11.14}$$

where the quantity $\rho = \left(x^2+y^2\right)^{1/2}$ is defined for notational convenience.

One may consider that the warp bubble's velocity is roughly constant, i.e. $v_s(t) \approx v_b$, by assuming that the time scale of the sampling is sufficiently small compared to the time scale over which the bubble's velocity is varying. Now, taking into account the small sampling time, the $(t^2+t_0^2)^{-1}$ term becomes strongly peaked, so that only a small portion of the geodesic is sampled by the QI integral. Consider also that the observer is situated at the equator of the warp bubble at $t=0$ [18], so that the geodesic is approximated by $x(t) \approx f(\rho) v_b t$, and consequently $r(t) = \left[(v_b t)^2 (f(\rho)-1)^2 + \rho^2\right]^{1/2}$.

For simplicity, without a significant loss of generality, and instead of taking into account the Alcubierre form function (11.2), one may consider a piece-wise continuous form of the shape function given by

$$f_{p.c.}(r) = \begin{cases} 1 & r < R - \frac{\Delta}{2} \\ -\frac{1}{\Delta}(r - R - \frac{\Delta}{2}) & R - \frac{\Delta}{2} < r < R + \frac{\Delta}{2} \\ 0 & r > R + \frac{\Delta}{2} \end{cases}\,, \tag{11.15}$$

where R is the radius of the bubble, and Δ the bubble wall thickness [18]. Note that Δ is related to the Alcubierre parameter σ by setting the slopes of the functions $f(r)$ and $f_{p.c.}(r)$ to be equal at $r=R$, which provides the following relationship $\Delta = \left[1+\tanh^2(\sigma R)\right]^2 / [2\,\sigma\ \tanh(\sigma R)]$.

Note that in the limit of large σR one obtains the approximation $\Delta \simeq 2/\sigma$, so that the QI-bound simplifies to

$$t_0 \int_{-\infty}^{+\infty} \frac{dt}{(t^2+\bar{\beta}^2)(t^2+t_0^2)} \leq \frac{3\Delta^2}{v_b^2\, t_0^4\, \bar{\beta}^2}\,, \tag{11.16}$$

where $\bar{\beta} = \rho/[v_b(1 - f(\rho))]$. Now, evaluating the integral in the left-hand side yields the following inequality

$$\frac{\pi}{3} \leq \frac{\Delta^2}{v_b^2\, t_0^4}\left[\frac{v_b t_0}{\rho}(1 - f(\rho)) + 1\right] . \tag{11.17}$$

It is perhaps important to note that the above inequality is only valid for sampling times on which the spacetime may be considered approximately flat. Considering the Riemann tensor components in an orthonormal frame [18], the largest component is given by

$$|R_{\hat{t}\hat{y}\hat{t}\hat{y}}| = \frac{3v_b^2\, y^2}{4\, \rho^2}\left[\frac{df(\rho)}{d\rho}\right]^2 , \tag{11.18}$$

which yields $r_{\min} \equiv 1/\sqrt{|R_{\hat{t}\hat{y}\hat{t}\hat{y}}|} \sim 2\Delta/\left(\sqrt{3}\, v_b\right)$, considering $y = \rho$ and the piecewise continuous form of the shape function. The sampling time must be smaller than this length scale, so that one may define $t_0 = 2\alpha\, \Delta/\left(\sqrt{3}\, v_b\right)$. Assuming $\Delta/\rho \sim v_b\, t_0/\rho \ll 1$, the term involving $1 - f(\rho)$ in Eq. (11.17) may be neglected, which provides

$$\Delta \leq \frac{3}{4}\sqrt{\frac{3}{\pi}}\, \frac{v_b}{\alpha^2} . \tag{11.19}$$

Taking a specific value for α, for instance, considering $\alpha = 1/10$, one obtains

$$\Delta \leq 10^2\, v_b\, L_{\text{Planck}} , \tag{11.20}$$

where L_{Planck} is the Planck length. Thus, unless v_b is extremely large, the wall thickness cannot be much above the Planck scale.

It is also interesting to find an estimate of the total amount of negative energy that is necessary to maintain a warp metric. It was found that the energy required for a warp bubble is on the order of

$$E \leq -3 \times 10^{20}\, M_{\text{galaxy}}\, v_b , \tag{11.21}$$

which is an absurdly enormous amount of negative energy,[3] roughly ten orders of magnitude greater than the total mass of the entire visible universe [18].

[3] Due to these results, one may tentatively conclude that the existence of these spacetimes is improbable. But, there are a series of considerations that can be applied to the QI. First, the QI is only of interest if one is relying on quantum field theory to provide the exotic matter to support the Alcubierre warp bubble. However, there are classical systems (non-minimally coupled scalar fields) that violate the null and the weak energy conditions, whilst presenting plausible results when applying the QI (See Chap. 10). Second, even if one relies on quantum field theory to provide exotic matter, the QI does not rule out the existence of warp drive spacetimes, although they do place serious constraints on the geometry.

11.3 Linearized Warp Drive

In this section, we show that there are significant problems that arise in the warp drive spacetime, even in the weak-field regime, and long before strong field effects come into play. Indeed, to ever bring a warp drive into a strong field regime, any highly advanced civilization would first have to take it through the weak-field regime [22]. We now construct a more realistic model of a warp drive spacetime where the warp bubble interacts with a finite mass spaceship. To this effect, consider the linearized theory applied to warp drive spacetimes, for non-relativistic velocities, $v \ll 1$.

Consider now a spaceship in the interior of an Alcubierre warp bubble, which is moving along the positive z axis with a non-relativistic constant velocity [22], i.e. $v \ll 1$. The metric is given by

$$\begin{aligned} ds^2 = &-dt^2 + dx^2 + dy^2 + [dz - v\, f(x, y, z - vt)\, dt]^2 \\ &- 2\Phi(x, y, z - vt)\left[dt^2 + dx^2 + dy^2 + (dz - v\, f(x, y, z - vt)\, dt)^2\right], \end{aligned} \tag{11.22}$$

where Φ is the gravitational field of the spaceship. If $\Phi = 0$, the metric (11.22) reduces to the warp drive spacetime of Eq. (11.1). If $v = 0$, we have the metric representing the gravitational field of a static source.

We consider now the approximation by linearizing in the gravitational field of the spaceship Φ, but keeping the exact v dependence. For this case, the WEC is given by

$$T_{\hat{\mu}\hat{\nu}}\, U^{\hat{\mu}} U^{\hat{\nu}} = \rho - \frac{v^2}{32\pi}\left[\left(\frac{\partial f}{\partial x}\right)^2 + \left(\frac{\partial f}{\partial y}\right)^2\right] + O(\Phi^2)\,, \tag{11.23}$$

and assuming the Alcubierre form function, we have

$$T_{\mu\nu}\, U^{\mu} U^{\nu} = \rho - \frac{1}{32\pi}\frac{v^2(x^2 + y^2)}{r^2}\left(\frac{df}{dr}\right)^2 + O(\Phi^2)\,. \tag{11.24}$$

Using the "volume integral quantifier", as before, we find the following estimate

$$\int T_{\mu\nu}\, U^{\mu} U^{\nu}\, d^3x = M_{\text{ship}} - v^2\, R^2\, \sigma + \int O(\Phi^2)\, d^3x\,, \tag{11.25}$$

which can be recast in the following form

$$M_{\text{ADM}} = M_{\text{ship}} + M_{\text{warp}} + \int O(\Phi^2)\, d^3x\,. \tag{11.26}$$

Now, demanding that the volume integral of the WEC be positive, then we have

$$v^2\ R^2\ \sigma \leq M_{\rm ship}\,, \tag{11.27}$$

which reflects the quite reasonable condition that the net total energy stored in the warp field be less than the total mass–energy of the spaceship itself. Note that this inequality places a powerful constraint on the velocity of the warp bubble. Rewriting this constraint in terms of the size of the spaceship $R_{\rm ship}$ and the thickness of the warp bubble walls $\Delta = 1/\sigma$, we arrive at the following condition

$$v^2 \leq \frac{M_{\rm ship}}{R_{\rm ship}}\ \frac{R_{\rm ship}\ \Delta}{R^2}. \tag{11.28}$$

For any reasonable spaceship this gives extremely low bounds on the warp bubble velocity.

One may analyse the NEC in a similar manner. Thus, the quantity $T_{\mu\nu}\,k^\mu k^\nu$ is given by

$$T_{\mu\nu}\,k^\mu k^\nu = \rho \pm \frac{v}{8\pi}\left(\frac{\partial^2 f}{\partial x^2} + \frac{\partial^2 f}{\partial y^2}\right) - \frac{v^2}{8\pi}\left[\left(\frac{\partial f}{\partial x}\right)^2 + \left(\frac{\partial f}{\partial y}\right)^2\right] + O(\Phi^2)\,. \tag{11.29}$$

Considering the "volume integral quantifier", we may estimate that

$$\int T_{\mu\nu}\,k^\mu k^\nu\ d^3x = M_{\rm ship} - v^2\ R^2\,\sigma + \int O(\Phi^2)\ d^3x\,. \tag{11.30}$$

which is [to order $O(\Phi^2)$] the same integral we encountered when dealing with the WEC. In order to avoid that the total NEC violations in the warp field exceed the mass of the spaceship itself, we again demand that

$$v^2\ R^2\ \sigma \leq M_{\rm ship}\,. \tag{11.31}$$

More specifically, it reflects that for all conceivably interesting situations the bubble velocity should be absurdly low, and it therefore appears unlikely that, by using this analysis, the warp drive will ever prove to be technologically useful.

Finally, we emphasize that any attempt at building up a "strong-field" warp drive starting from an approximately Minkowski spacetime will inevitably have to pass through a weak-field regime. Taking into account the analysis presented above, we verify that the weak-field warp drives are already very tightly constrained, which implies additional difficulties for developing a "strong field" warp drive.[4]

[4] See Ref. [22] for more details.

11.4 The Horizon Problem

Shortly after the discovery of the Alcubierre warp drive solution [3], an interesting feature of the spacetime was found. Namely, an observer on a spaceship cannot create nor control on demand an Alcubierre bubble, with $v > c$, around the ship [13]. It is easy to understand this, by noting that an observer at the origin (with $t = 0$), cannot alter events outside of his future light cone, $|r| \leq t$, with $r = (x^2 + y^2 + z^2)^{1/2}$. In fact, applied to the warp drive, it is a trivial matter to show points on the outside front edge of the bubble are always spacelike separated from the centre of the bubble.

The analysis is simplified in the proper reference frame of an observer at the centre of the bubble, so that using the transformation $z' = z - z_0(t)$, the metric is given by

$$ds^2 = -dt^2 + dx^2 + dy^2 + \left[dz' + (1 - f)v dt\right]^2 . \tag{11.32}$$

Now, consider a photon emitted along the $+z$ axis (with $ds^2 = dx = dy = 0$), so that the above metric provides $dz'/dt = 1 - (1 - f)v$. If the spaceship is at rest at the centre of the bubble, then initially the photon has $dz/dt = v + 1$ or $dz'/dt = 1$ (recall that $f = 1$ in the interior of the bubble). However, at a specific point $z' = z'_c$, with $f = 1 - 1/v$, we have $dz'/dt = 0$ [14]. Once photons reach z'_c, they remain at rest relative to the bubble and are simply carried along with it. This implies that photons emitted in the forward direction by the spaceship never reach the outside edge of the bubble wall, which therefore lies outside the forward light cone of the spaceship. This behaviour is reminiscent of an *event horizon*. Thus, the bubble cannot be created, or controlled, by any action of the spaceship crew, which does not mean that Alcubierre bubbles, if it were possible to create them, could not be used as a means of superluminal travel. It only implies that the actions required to change the metric and create the bubble must be taken beforehand by some observer whose forward light cone contains the entire trajectory of the bubble.

The appearance of an event horizon becomes evident in the two-dimensional model of the Alcubierre spacetime [27–29]. Consider that the axis of symmetry coincides with the line element of the spaceship, so that the metric (11.1), reduces to

$$ds^2 = -(1 - v^2 f^2)dt^2 - 2v f dz dt + dz^2 . \tag{11.33}$$

For simplicity, we consider a constant bubble velocity, $v(t) = v_b$, and $r = [(z - v_b t)^2]^{1/2}$. Note that the metric components of Eq. (11.33) only depend on r, which may be adopted as a coordinate, so if $z > v_b t$, we consider the transformation $r = (z - v_b t)$. Using this transformation, $dz = dr + v_b\, dt$, the metric (11.33) takes the following form:

$$ds^2 = -A(r)\left[dt - \frac{v_b(1 - f(r))}{A(r)}\, dr\right]^2 + \frac{dr^2}{A(r)} , \tag{11.34}$$

where $A(r)$, denoted by the Hiscock function, is defined by $A(r) = 1 - v_b^2 [1 - f(r)]^2$.

Now, it is possible to represent the metric (11.34) in a diagonal form, using a new time coordinate

$$d\tau = dt - \frac{v_b\,[1 - f(r)]}{A(r)}\,dr\,, \tag{11.35}$$

so that the metric (11.34) reduces to a manifestly static form, given by

$$ds^2 = -A(r)\,d\tau^2 + \frac{dr^2}{A(r)}\,. \tag{11.36}$$

The τ coordinate has an immediate interpretation in terms of an observer on board of a spaceship, namely, τ is the proper time of the observer, taking into account that $A(r) \to 1$ in the limit $r \to 0$. We verify that the coordinate system is valid for any value of r, if $v_b < 1$. If $v_b > 1$, we have a coordinate singularity and an event horizon at the point r_0 in which $f(r_0) = 1 - 1/v_b$ and $A(r_0) = 0$.

11.5 Superluminal Subway: The Krasnikov Tube

It was pointed out above, that an interesting aspect of the warp drive resides in the fact that points on the outside front edge of a superluminal bubble are always spacelike separated from the centre of the bubble. This implies that an observer in a spaceship cannot create nor control on demand an Alcubierre bubble. However, causality considerations do not prevent the crew of a spaceship from arranging, by their own actions, to complete a round trip from the Earth to a distant star and back in an arbitrarily short time, as measured by clocks on the Earth, by altering the metric along the path of their outbound trip. Thus, Krasnikov introduced a metric with an interesting property that although the time for a one-way trip to a distant destination cannot be shortened [13], the time for a round trip, as measured by clocks at the starting point (e.g. Earth), can be made arbitrarily short, as will be demonstrated below.

11.5.1 The Two-Dimensional Krasnikov Solution

The two-dimensional Krasnikov metric is given by

$$\begin{aligned} ds^2 &= -(dt - dx)(dt + k(t,x)dx) \\ &= -dt^2 + [1 - k(x,t)]\,dx\,dt + k(x,t)\,dx^2\,, \end{aligned} \tag{11.37}$$

where the form function $k(x,t)$ is defined by

$$k(t,x) = 1 - (2-\delta)\theta_\varepsilon(t-x)\left[\theta_\varepsilon(x) - \theta_\varepsilon(x+\varepsilon-D)\right], \tag{11.38}$$

with δ and ε are arbitrarily small positive parameters. θ_ε denotes a smooth monotone function

$$\theta_\varepsilon(\xi) = \begin{cases} 1, \text{ if } \xi > \varepsilon, \\ 0, \text{ if } \xi < 0. \end{cases}$$

One may identify essentially three distinct regions in the Krasnikov two-dimensional spacetime, which is summarized in the following manner:

The outer region: The outer region is given by the following set:

$$\{x < 0\} \cup \{x > D\} \cup \{x > t\}. \tag{11.39}$$

The two time-independent θ_ε-functions between the square brackets in Eq. (11.38) vanish for $x < 0$ and cancel for $x > D$, ensuring $k = 1$ for all t except between $x = 0$ and $x = D$. When this behaviour is combined with the effect of the factor $\theta_\varepsilon(t-x)$, one sees that the metric (11.37) is flat, i.e. $k = 1$, and reduces to Minkowski spacetime everywhere for $t < 0$ and at all times outside the range $0 < x < D$. Future light cones are generated by the following vectors: $r_O = \partial_t + \partial_x$ and $l_O = \partial_t - \partial_x$.

The inner region: The inner region is given by the following set:

$$\{x < t - \varepsilon\} \cap \{\varepsilon < x < D - \varepsilon\}, \tag{11.40}$$

so that the first two θ_ε-functions in Eq. (11.38) both equal 1, while $\theta_\varepsilon(x + \varepsilon - D) = 0$, giving $k = \delta - 1$ everywhere within this region. This region is also flat, but the light cones are *more open*, being generated by the following vectors: $r_I = \partial_t + \partial_x$ and $l_I = -(1-\delta)\partial_t - \partial_x$.

The transition region: The transition region is a narrow curved strip in spacetime, with width $\sim\varepsilon$. Two spatial boundaries exist between the inner and outer regions. The first lies between $x = 0$ and $x = \varepsilon$, for $t > 0$. The second lies between $x = D - \varepsilon$ and $x = D$, for $t > D$. It is possible to view this metric as being produced by the crew of a spaceship, departing from point A ($x = 0$), at $t = 0$, travelling along the x-axis to point B ($x = D$) at a speed, for simplicity, infinitesimally close to the speed of light, therefore arriving at B with $t \approx D$.

Thus, the metric is modified by changing k from 1 to $\delta - 1$ along the x-axis, in between $x = 0$ and $x = D$, leaving a transition region of width $\sim\varepsilon$ at each end for continuity. However, as the boundary of the forward light cone of the spaceship at $t = 0$ is $|x| = t$, it is not possible for the crew to modify the metric at an arbitrary point x before $t = x$. This fact accounts for the factor $\theta_\varepsilon(t-x)$ in the metric, ensuring a transition region in time between the inner and outer region, with a duration of $\sim \varepsilon$, lying along the wordline of the spaceship, $x \approx t$. The geometry is shown in the (x,t) plane in Fig. 11.3.

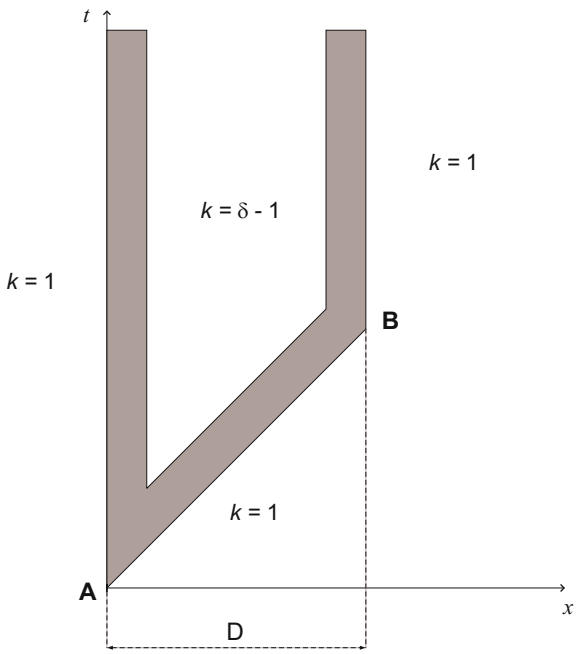

Fig. 11.3 The plot depicts the Krasnikov spacetime in the (x, t) plane, where the *vertical lines* A and B are the world lines of the stars A and B, respectively. The world line of the spaceship is approximately represented by the line segment AB. See the text for more details

11.5.2 Superluminal Travel Within the Krasnikov Tube

The factored form of the metric (11.37), for $ds^2 = 0$, provides some interesting properties of the spacetime with $\delta - 1 \leq k \leq 1$. Note that the two branches of the forward light cone in the (t, x) plane are given by $dx/dt = 1$ and $dx/dt = -k$. As k becomes smaller and then negative, the slope of the left-hand branch of the light cone becomes less negative and then changes sign. This implies that the light cone along the negative x-axis opens out, as depicted in Fig. 11.4.

The inner region, with $k = \delta - 1$, is flat because the metric (11.37) may be cast into the Minkowski form, applying the following coordinate transformations

$$dt' = dt + \left(\frac{\delta}{2} - 1\right) dx\,, \qquad dx' = \left(\frac{\delta}{2}\right) dx\,, \tag{11.41}$$

and one verifies that the transformation is singular at $\delta = 0$, i.e. $k = -1$. Note that the left branch of the region is given by $dx'/dt' = -1$.

From the above analysis, one may easily deduce the following expression:

$$\frac{dt}{dt'} = 1 + \left(\frac{2 - \delta}{\delta}\right) \frac{dx'}{dt'}\,. \tag{11.42}$$

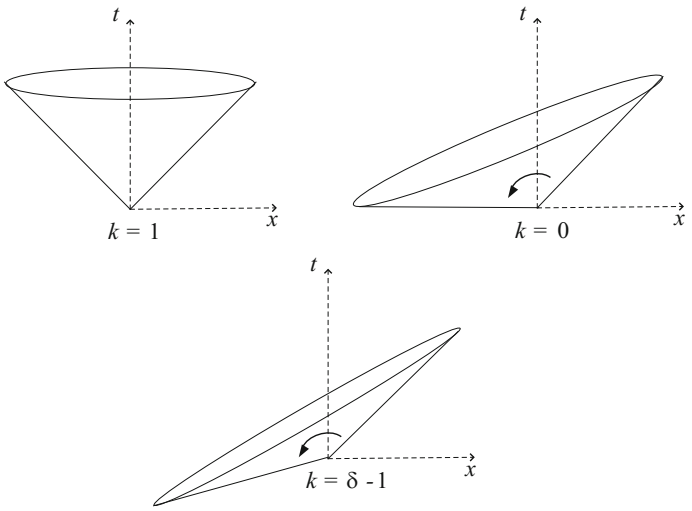

Fig. 11.4 Forward light cones in the two-dimensional Krasnikov spacetime for $k = 1$, $k = 0$ and $k = \delta - 1$

For an observer moving along the positive x' and x directions, with $dx'/dt' < 1$, we have $dt' > 0$ and consequently $dt > 0$, if $0 < \delta \leq 2$. However, if the observer is moving sufficiently close to the left branch of the light cone, given by $dx'/dt' = -1$, Eq. (11.42) provides us with $dt/dt' < 0$, for $\delta < 1$. Therefore we have $dt < 0$, which means that the observer traverses backward in time, as measured by observers in the outer region, with $k = 1$.

The superluminal travel analysis is as follows. Consider a spaceship departing from star A and arriving at star B, at the instant $t \approx D$. Along this journey, the crew of the spaceship modify the metric, so that $k \approx -1$, for simplicity, along the trajectory. Now imagine that the spaceship returns to star A, travelling with a velocity arbitrarily close to the speed of light, i.e. $dx'/dt' \approx -1$. Therefore, from Eq. (11.41), one obtains the following relation

$$v_{\text{return}} = \frac{dx}{dt} \approx -\frac{1}{k} = \frac{1}{1-\delta} \approx 1 \tag{11.43}$$

and $dt < 0$, for $dx < 0$. The return trip from star B to A is done in an interval of $\Delta t_{\text{return}} = -D/v_{\text{return}} = D/(\delta - 1)$. Note that the total interval of time, measured at A, is given by $T_A = D + \Delta t_{\text{return}} = D\delta$. For simplicity, consider ε negligible, so that superluminal travel is implicit, as $|\Delta t_{\text{return}}| < D$, if $0 < \delta < 1$, i.e. we have a spatial spacetime interval between A and B. Now, T_A is always positive, but may attain a value arbitrarily close to zero, for an appropriate choice of δ.

Note that for the case $\delta < 1$, it is always possible to choose an allowed value of dx'/dt' for which $dt/dt' = 0$, meaning that the return trip is instantaneous as seen by observers in the external region. This follows easily from Eq. (11.42), which implies that $dt/dt' = 0$ when dx'/dt' satisfies $dx'/dt' = -\delta/(2-\delta)$, which lies between 0 and -1 for $0 < \delta < 1$.

11.5.3 The Four-Dimensional Generalization

Shortly after the Krasnikov two-dimensional solution, the analysis was generalized to four dimensions by Everett and Roman [14], who denoted the solution as the *Krasnikov tube*. The latter four-dimensional modification of the metric begins along the path of the spaceship, which is moving along the x-axis, and occurs at the position x, at time $t \approx x$, which is the time of passage of the spaceship. Everett and Roman also assumed that the disturbance in the metric propagated radially outward from the x-axis, so that causality guarantees that at time t the region in which the metric has been modified cannot extend beyond $\rho = t - x$, where $\rho = (y^2 + z^2)^{1/2}$. The modification in the metric was also assumed to not extend beyond some maximum radial distance $\rho_{max} \ll D$ from the x-axis.

Thus, the metric in the four-dimensional spacetime, written in cylindrical coordinates, is given by [14]

$$ds^2 = -dt^2 + [1 - k(t, x, \rho)]\, dx\, dt + k(t, x, \rho) dx^2 + d\rho^2 + \rho^2 d\phi^2\,, \quad (11.44)$$

where the four-dimensional generalization of the Krasnikov form function is given by

$$k(t, x, \rho) = 1 - (2 - \delta)\theta_\varepsilon(\rho_{max} - \rho)\theta_\varepsilon(t - x - \rho)[\theta_\varepsilon(x) - \theta_\varepsilon(x + \varepsilon - D)]\,. \quad (11.45)$$

For $t \gg D + \rho_{max}$ one has a tube of radius ρ_{max} centred on the x-axis, within which the metric has been modified. It is this structure that is denoted by the *Krasnikov tube*, and contrary to the Alcubierre spacetime metric, the metric of the Krasnikov tube is static, once it has been created.

The stress–energy tensor element T_{tt} given by

$$T_{tt} = \frac{1}{32\pi(1+k)^2}\left[-\frac{4(1+k)}{\rho}\frac{\partial k}{\partial \rho} + 3\left(\frac{\partial k}{\partial \rho}\right)^2 - 4(1+k)\frac{\partial^2 k}{\partial \rho^2}\right], \quad (11.46)$$

can be shown to be the energy density measured by a static observer [14], and violates the WEC in a certain range of ρ, i.e. $T_{\mu\nu}U^\mu U^\nu < 0$. To this effect, consider the energy density in the middle of the tube and at a time long after its formation, i.e. $x = D/2$ and $t \gg x + \rho + \varepsilon$, respectively. In this region we have $\theta_\varepsilon(x) = 1, \theta_\varepsilon(x + \varepsilon - D) = 0$ and $\theta_\varepsilon(t - x - \rho) = 1$. With this simplification the form function (11.45) reduces to

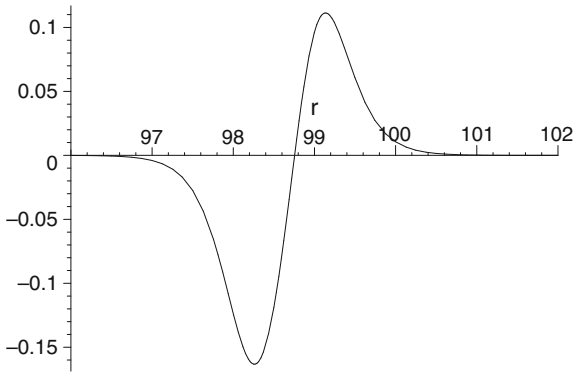

Fig. 11.5 Graph of the energy density, T_{tt}, as a function of ρ at the middle of the Krasnikov tube, $x = D/2$, and long after its formation, $t \gg x + \rho + \varepsilon$. We consider the following values for the parameters: $\delta = 0.1$, $\varepsilon = 1$ and $\rho_{max} = 100\varepsilon = 100$. See the text for details

$$k(t, x, \rho) = 1 - (2 - \delta)\theta_\varepsilon(\rho_{max} - \rho)\,. \tag{11.47}$$

A useful form for $\theta_\varepsilon(\xi)$ [14] is given by

$$\theta_\varepsilon(\xi) = \frac{1}{2}\left\{\tanh\left[2\left(\frac{2\xi}{\varepsilon} - 1\right)\right] + 1\right\}\,, \tag{11.48}$$

so that the form function (11.47) yields

$$k = 1 - \left(1 - \frac{\delta}{2}\right)\left\{\tanh\left[2\left(\frac{2\xi}{\varepsilon} - 1\right)\right] + 1\right\}\,. \tag{11.49}$$

Choosing the following values for the parameters: $\delta = 0.1$, $\varepsilon = 1$ and $\rho_{max} = 100\varepsilon = 100$, the negative character of the energy density is manifest in the immediate inner vicinity of the tube wall, as shown in Fig. 11.5.

11.6 Closed Timelike Curves

11.6.1 The Warp Drive

Consider a hypothetical spaceship immersed within a warp bubble, moving along a timelike curve, with an arbitrary value of $v(t)$. Due to the latter, the metric of the warp drive permits superluminal travel, which raises the possibility of the existence of CTCs. Although the solution deduced by Alcubierre by itself does not possess CTCs, Everett demonstrated that these are created by a simple modification of the Alcubierre metric [14], by applying a similar analysis as is carried out using tachyons.

The modified metric takes the form

$$ds^2 = -dt^2 + dx^2 + dy^2 + (dz - v f dt)^2 \,, \tag{11.50}$$

with $v(t) = dz_0(t)/dt$ and $r(t) = [(z - z_0(t))^2 + (y - y_0)^2 + z^2]^{1/2}$. As in Sect. 11.2.1 spacetime is flat in the exterior of a warp bubble with radius R, which now is centred in $(0, y_0, z_0(t))$. The bubble moves with a velocity v, on a trajectory parallel to the z-axis. Consider, for simplicity, the form function given by Eq. (11.2). We shall also impose that $y_0 \gg R$, so that the form function is negligible, i.e. $f(y_0) \approx 0$.

Now, consider two stars, S_1 and S_2, at rest in the coordinate system of the metric (11.50), and located on the z-axis at $t = 0$ and $t = D$, respectively. The metric along the z-axis is Minkowskian as $y_0 \gg R$. Therefore, a light beam emitted at S_1, at $t = 0$, moving along the z-axis with $dz/dt = 1$, arrives at S_2 at $t = D$. Suppose that the spaceship initially starts off from S_1, with $v = 0$, moving off to a distance y_0 along the $y-$axis and neglecting the time it needs to cover $y = 0$ to $y = y_0$. At y_0, it is then subject to a uniform acceleration, a, along the $z-$axis for $0 < z < D/2$, and $-a$ for $D/2 < z < D$. The spaceship will arrive at the spacetime event S_2 with coordinates $z = D$ and $t = 2\sqrt{D/a} \equiv T$. Once again, the time required to travel from $y = y_0$ to $y = 0$ is negligible.

The separation between the two events, departure and arrival, is $D^2 - T^2 = D^2(1 - 4/(aD))$ and will be spatial if $a > 4/D$ is verified. In this case, the spaceship will arrive at S_2 before the light beam, if the latter's trajectory is a straight line, and both departures are simultaneous from S_1. Inertial observers situated in the exterior of the spaceship, at S_1 and S_2, will consider the spaceship's movement as superluminal, since the distance D is covered in an interval $T < D$. However, the spaceship's wordline is contained within its light cone. The worldline of the spaceship is given by $z = vt$, while its future light cone is given by $z = (v \pm 1)t$. The latter relation can easily be inferred from the null condition, $ds^2 = 0$.

Since the quadri-vector with components $(T, 0, 0, D)$ is spatial, the temporal order of the events, departure and arrival, is not well defined. Introducing new coordinates, (t', x', y', z'), obtained by a Lorentz transformation, with a boost β along the z-axis, the arrival at S_2 in the (t', x', y', z') coordinates correspond to

$$T' = \gamma(2\sqrt{D/a} - \beta D) \,, \qquad Z' = \gamma(D - 2\sqrt{D/a}) \,, \tag{11.51}$$

with $\gamma = (1 - \beta^2)^{-1/2}$. The events, departure and arrival, will be simultaneous if $a = 4/(\beta^2 D)$. The arrival will occur before the departure if $T' < 0$, i.e.

$$a > \frac{4}{\beta^2 D} \,. \tag{11.52}$$

The fact that the spaceship arrives at S_2 with $t' < 0$, does not by itself generate CTCs. Consider the metric (11.50), substituting z and t by $\Delta z' = z' - Z'$ and $\Delta t' = t' - T'$, respectively; $v(t)$ by $-v(t)$; a by $-a$; and y_0 by $-y_0$. This new metric

describes a spacetime in which an Alcubierre bubble is created at $t' = T'$, which moves along $y = -y_0$ and $x = 0$, from S_1 to S_2 with a velocity $v'(t')$, and subject to an acceleration a'. For observers at rest relatively to the coordinates (t', x', y', z'), situated in the exterior of the second bubble, it is identical to the bubble defined by the metric (11.50), as it is seen by inertial observers at rest at S_1 and S_2. The only differences reside in a change of the origin, direction of movement and possibly of the value of acceleration. The stars, S_1 and S_2, are at rest in the coordinate system of the metric (11.50), and in movement along the negative direction of the z-axis with velocity β, relatively to the coordinates (t', x', y', z'). The two coordinate systems are equivalent due to the Lorentz invariance, so if the first is physically realizable, then so is the second. In the new metric, by analogy with Eq. (11.50), we have $d\tau = dt'$, i.e. the proper time of the observer, on board of the spaceship, travelling in the centre of the second bubble, is equal to the time coordinate, t'. The spaceship will arrive at S_1 in the temporal and spatial intervals given by $\Delta t' > 0$ and $\Delta z' < 0$, respectively. As in the analysis of the first bubble, the separation between the departure, at S_2, and the arrival S_1, will be spatial if the analogous relationship of Eq. (11.52) is verified. Therefore, the temporal order between arrival and departure is also not well defined. As will be verified below, when z and z' decrease and t' increases, t will decrease and a spaceship will arrive at S_1 at $t < T$. In fact, one may prove that it may arrive at $t < 0$.

Since the objective is to verify the appearance of CTCs, in principle, one may proceed with some approximations. For simplicity, consider that a and a', and consequently v and v' are enormous, so that $T \ll D$ and $\Delta t' \ll -\Delta z'$. In this limit, we obtain the approximation $T \approx 0$, i.e. the journey of the first bubble from S_1 to S_2 is approximately instantaneous. Consequently, taking into account the Lorentz transformation, we have $Z' \approx \gamma D$ and $T' \approx -\gamma\beta D$. To determine T_1, which corresponds to the second bubble at S_1, consider the following considerations: since the acceleration is enormous, we have $\Delta t' \approx 0$ and $\Delta t = T_1 - T \approx T_1$, therefore $\Delta z = -D \approx \gamma \Delta z'$ and $\Delta t \approx \gamma\beta\Delta z'$, from which one concludes that

$$T_1 \approx -\beta D < 0\,. \tag{11.53}$$

11.6.2 The Krasnikov Tube

As mentioned above, for superluminal speeds the warp drive metric has a horizon so that an observer in the centre of the bubble is causally separated from the front edge of the bubble. Therefore he/she cannot control the Alcubierre bubble on demand. In order to address this problem, Krasnikov proposed a two-dimensional metric [13], which was later extended to a four-dimensional model [14], as outlined in Sect. 11.5. A two-dimensional Krasnikov tube does not generate CTCs. But the situation is quite different in the four-dimensional generalization. Using two such tubes it is a simple matter, in principle, to generate CTCs [30]. The analysis is similar to that of the warp drive, so that it will be treated in summary.

Imagine a spaceship travelling along the x-axis, departing from a star, S_1, at $t = 0$, and arriving at a distant star, S_2, at $t = D$. An observer on board of the spaceship constructs a Krasnikov tube along the trajectory. It is possible for the observer to return to S_1, travelling along a parallel line to the x-axis, situated at a distance ρ_0, so that $D \gg \rho_0 \gg 2\rho_{max}$, in the exterior of the first tube. On the return trip, the observer constructs a second tube, analogous to the first, but in the opposite direction, i.e. the metric of the second tube is obtained substituting x and t, for $X = D - x$ and $T = t - D$, respectively in Eq. (11.44). The fundamental point to note is that in three spatial dimensions, it is possible to construct a system of two non-overlapping tubes separated by a distance ρ_0.

After the construction of the system, an observer may initiate a journey, departing from S_1, at $x = 0$ and $t = 2D$. One is only interested in the appearance of CTCs in principle, therefore the following simplifications are imposed: δ and ε are infinitesimal, and the time to travel between the tubes is negligible. For simplicity, consider the velocity of propagation close to that of light speed. Using the second tube, arriving at S_2 at $x = D$ and $t = D$, then travelling through the first tube, the observer arrives at S_1 at $t = 0$. The spaceship has completed a CTC, arriving at S_1 before its departure.

11.7 Summary and Conclusion

In this chapter, we have seen how warp drive spacetimes can be used as gedanken-experiments to probe the foundations of general relativity. Though they are useful toy models for theoretical investigations, we emphasize that as potential technology they are greatly lacking. We have verified that exact solutions of the warp drive spacetimes necessarily violate the classical energy conditions, and continue to do so for an arbitrarily low warp bubble velocity. Thus, the energy condition violations in this class of spacetimes are generic to the form of the geometry under consideration and are not simply a side effect of the superluminal properties. Furthermore, by taking into account the notion of the "volume integral quantifier", we have also verified that the "total amount" of energy condition violating matter in the warp bubble is negative.

Using linearized theory, a more realistic model of the warp drive spacetime was constructed where the warp bubble interacts with a finite mass spaceship. The energy conditions were determined to first and second order of the warp bubble velocity, which safely ignores the causality problems associated with "superluminal" motion. A fascinating feature of these solutions resides in the fact that such a spacetime appear to be examples of a "reactionless" drives, where the warp bubble moves by interacting with the geometry of spacetime instead of expending reaction mass, and the spaceship is simply carried along with it. Note that in linearized theory, the spaceship can be treated as a finite mass object placed within the warp bubble. It was verified that in this case, the "total amount" of energy condition violating matter, the "net" negative energy of the warp field, must be an appreciable fraction of the positive mass of the spaceship carried along by the warp bubble. This places an extremely stringent condition on the warp drive spacetime, in that the bubble velocity should

be absurdly low. Finally, we point out that any attempt at building up a "strong-field" warp drive starting from an approximately Minkowski spacetime will inevitably have to pass through a weak-field regime. Since the weak-field warp drives are already so tightly constrained, the analysis of the linearized warp drive implies additional difficulties for developing a "strong field" warp drive.

Furthermore, we have shown that shortly after the discovery of the Alcubierre warp drive solution it was found that an observer on a spaceship cannot create nor control on demand a superluminal Alcubierre bubble, due to a feature that is reminiscent of an event horizon. Thus, the bubble cannot be created, nor controlled, by any action of the spaceship crew. We emphasize that this does not mean that Alcubierre bubbles could not be theoretically used as a means of superluminal travel, but that the actions required to change the metric and create the bubble must be taken beforehand by an observer whose forward light cone contains the entire trajectory of the bubble. To counter this difficulty, Krasnikov introduced a two-dimensional metric in which the time for a round trip, as measured by clocks at the starting point (e.g. Earth), can be made arbitrarily short. This metric was generalized to four dimensions, denoting the solution as the *Krasnikov tube*. It was also shown that this solution violates the energy conditions is specific regions of spacetime. Finally, it was shown that these spacetimes induce closed timelike curves.

Acknowledgements FSNL acknowledges financial support of the Fundação para a Ciência e Tecnologia through an Investigador FCT Research contract, with reference IF/00859/2012, funded by FCT/MCTES (Portugal). MA also acknowledges support from UNAM through PAPIIT-IN103514 grant, and from CONACYT through infrastructure grant 253709.

References

1. Morris MS, Thorne KS. Wormholes in spacetime and their use for interstellar travel: a tool for teaching general relativity. Am J Phys. 1988;56:395.
2. Visser M. Lorentzian Wormholes: From Einstein to Hawking. New York: American Institute of Physics; 1995.
3. Alcubierre M. The warp drive: hyper-fast travel within general relativity. Class Quant Grav. 1994;11:L73–7.
4. Visser M, Bassett B, Liberati S. Perturbative superluminal censorship and the null energy condition. In: Proceedings of the eigth canadian conference on general relativity and relativistic astrophysics. AIP Press; 1999.
5. Visser M, Bassett B, Liberati S. Superluminal censorship. Nucl Phys Proc Suppl. 2000;88:267–70.
6. Olum K. Superluminal travel requires negative energy density. Phys Rev Lett. 1998;81:3567–70.
7. Barcelo C, Visser M. Twilight for the energy conditions? Int J Mod Phys D. 2002;11:1553.
8. Barcelo C, Visser M. Scalar fields, energy conditions, and traversable wormholes. Class Quant Grav. 2000;17:3843.
9. Barcelo C, Visser M. Traversable wormholes from massless conformally coupled scalar fields. Phys Lett B. 1999;466:127.
10. Riess AG, et al. Type Ia Supernova discoveries at $z>1$ from the hubble space telescope: evidence for past deceleration and constraints on dark energy evolution. Astrophys J. 2004;607:665–87.

11. Visser M. Jerk, snap, and the cosmological equation of state. Class Quant Grav. 2004;21:2603.
12. Caldwell RR, Kamionkowski M, Weinberg NN. Phantom energy and cosmic doomsday. Phys Rev Lett. 2003;91:071301.
13. Krasnikov SV. Hyper-fast interstellar travel in general relativity. Phys Rev D. 1998;57:4760 [arXiv:grspsqcsps9511068].
14. Everett AE, Roman TA. A superluminal subway: the krasnikov tube. Phys Rev D. 1997;56:2100.
15. Natário J. Warp drive with zero expansion. Class Quant Grav. 2002;19:1157.
16. Ford LH, Roman TA. Averaged energy conditions and quantum inequalities. Phys Rev D. 1995;51:4277.
17. Ford LH, Roman TA. Quantum field theory constrains traversable wormhole geometries. Phys Rev D. 1996;53:5496.
18. Pfenning MJ, Ford LH. The unphysical nature of warp drive. Class Quant Grav. 1997;14:1743.
19. Van Den Broeck C. A Warp drive with reasonable total energy requirements. Class Quant Grav. 1999;16:3973.
20. Gravel P, Plante J. Simple and double walled Krasnikov tubes: I Tubes with low masses. Class Quant Grav. 2004;21:L7.
21. Gravel P. Simple and double walled Krasnikov tubes: II. Primordial microtubes and homogenization. Class Quant Grav. 2004;21:767.
22. Lobo FSN, Visser M. Fundamental limitations on 'warp drive' spacetimes. Class Quant Grav. 2004;21:5871.
23. York JW. Kinematic and dynamics of general relativity. In: Smarr LL, editor. Sources of gravitational radiation. UK: Cambridge University Press; 1979. p. 83–126.
24. Alcubierre M. Introduction to 3+1 numerical relativity. UK: Oxford University Press; 2008.
25. Visser M, Kar S, Dadhich N. Traversable wormholes with arbitrarily small energy condition violations. Phys. Rev. Lett. 2003;90:201102.
26. Kar S, Dadhich N, Visser M. Quantifying energy condition violations in traversable wormholes. Pramana. 2004;63:859–64.
27. Hiscock WA. Quantum effects in the Alcubierre warp drive spacetime. Class Quant Grav. 1997;14:L183.
28. Clark C, Hiscock WA, Larson SL. Null geodesics in the Alcubierre warp drive spacetime: the view from the bridge. Class Quant Grav. 1999;16:3965.
29. González-Díaz PF. On the warp drive space-time. Phys Rev D. 2000;62:044005.
30. Everett AE. Warp drive and causality. Phys Rev D. 1996;53:7365.

Chapter 12
Probing Faster than Light Travel and Chronology Protection with Superluminal Warp Drives

Carlos Barceló and Stefano Liberati

12.1 Introduction

The possibility of "faster than light" (FTL) travel and time machines (TM) have been a fascinating theme for human beings since the dawn of storytelling and they are at the centre of many science fiction novels and movies. What is less known to the broad pubic is that these tantalising phenomena are definitely an open possibility in Einstein's general relativity (GR) theory. The very same "plasticity" of spacetime that is at the core of the Einstein's grand construction allows at the same time for extremely warped spacetimes where the causal structure can be subverted and realise these extreme features. In this chapter, we are going to see how FTL and TM are related and why they are so relevant in assessing the viability of GR as a fundamental theory of reality. We shall consider explicit examples allowing for these features, explain why the latter are so problematic for our understanding of reality, and focus on those spacetimes that seems so far not forbidden or evidently unphysical. In particular, we shall discuss a class of spacetimes called "warp drives", presented in the previous chapter—which allow for FTL travel and can be used to built a TM—and show that they will generically present a semiclassical instability just for the fact of allowing faster than light propagation.

The structure of this contribution will be the following. We shall first provide some technical definitions about what we mean by time travel. We shall then review some spacetimes which allow for TM and FTL travel. We shall then discuss in the next

C. Barceló (✉)
Instituto de Astrofísica de Andalucía (CSIC), Glorieta de la Astronomía,
18008 Granada, Spain
e-mail: carlos@iaa.es

S. Liberati
SISSA, Via Bonomea 265, 34136 Trieste, Italy

S. Liberati
INFN, sezione di Trieste, Italy
e-mail: liberati@sissa.it

F.S.N. Lobo (ed.), *Wormholes, Warp Drives and Energy Conditions*,
Fundamental Theories of Physics 189, DOI 10.1007/978-3-319-55182-1_12

section why FTL travel can be easily manipulated for building TMs. In Sect. 12.5, we shall consider why TM are paradoxical and which solutions have been devised to come out of these paradoxes and explain why so far it seems that for reaching a definitive conclusion one should go beyond the realm of semiclassical gravity. Finally, in Sect. 12.6 we shall consider the specific case of warp drives and show that a generic prediction about their instability can be reached by a quantum field theory calculation in curved spacetime. We shall argue that this result seems to strongly hint that structures allowing for FTL travel and hence TM building are intrinsically unstable even within the well-known framework of semiclassical gravity.

12.2 Time Machines: Basic Technical Definitions

Worldlines of observers/particles in spacetime are typically timelike curves if they have mass, and null curves if the particles are massless (respectively inside and on the border of light cones). A causal curve is defined to be a curve which is nowhere spacelike (i.e. lying outside of a light cone). A chronological curve is a curve which is everywhere timelike. So in layman language, the first kind of curves characterises the propagation of signals via massive or massless mediators while the second class pertains to massive objects/observers.

Time travelling notoriously requires a time machine (exactly like in the H.G. Well novel). A time machine is defined as some device able to provide closed causal or chronological curves, loops in propagation of signals or massive objects. Albeit closed timelike/chronological curves (CTC) imply automatically closed causal curves (CCC) the reverse is of course not true, i.e. one might have a spacetime where only massless particles can form loops but massive objects cannot. Of course this last case is also not seriously dangerous as it does not lead to the aforementioned paradoxes. So, the culprit of our search, the smoking gun of time travel, is the presence of a CTC in a given spacetime.

However we can imagine, and indeed we have many examples of spacetime which are almost everywhere "sane" except for regions where time travel is allowed, or alternatively spacetimes which in the past look globally hyperbolic but later develop a region with CTC and hence do not admit a well-posed Cauchy evolution. In order to describe precisely these situations, a first step is to characterise points within a chronology-violating region (a region with CTC). There are events p belonging to a chronology-violating region I_p^0 if

$$I_p^0 \equiv I^+(p) \bigcap I^-(p) \neq \emptyset,$$

in words, if the intersection of the chronological past and future for this set of events (i.e. the interiors of the past and future light cone stemming from these events) is not an empty set. As usual, we shall then define the total chronology-violating region in a given manifold $\mathscr{M}$ as the union of all these I_p^0, i.e.

$$I^0(\mathscr{M}) = \bigcup_{p\in\mathscr{M}} I^0_p.$$

Of course in the same way we can define causality violating regions by just replacing in the above formulas chronological future and past $I^{\pm}$ with causal future and past $J^{\pm}$.

We can now define the onset of a time machine region, its border, as the *future chronological horizon* which is technically characterised as

$$H^+(I) \equiv \partial\left[I^+\left(I^0(\mathscr{M})\right)\right].$$

Of course we can also straightforwardly define a *past chronological horizon* (the border in the past of a time machine region) by the same definition replacing the chronological future with the chronological past. Similarly, the definition for a past/future causal horizon can be obtained replacing the chronological past/future with their causal counterparts.

It is worth stressing that chronological horizons are always generated by null geodesics [33] and that while they do not need to coincide mathematically with causal horizons, they do so in many cases. Finally, it is easy to see that chronological horizons are just a special case of Cauchy horizons as they also characterise a breakdown of the Cauchy evolution of data and a lack of global hyperbolicity of the spacetime (the other typical case of Cauchy horizons being those associated to missing points in spacetime e.g. due to timelike singularities).

12.3 Causality Challenging Spacetimes

The list of spacetimes in GR which are problematic from the point of view of the causal structure is quite long and basically splits in two big families. The first family is made by what we might call "time machine rotating solutions". For all these solutions rotation is the key ingredient as the swirling of spacetime and frame dragging tilts the light cones till they eventually include closed orbits around the rotation axis. These are spacetimes which self-evidently include regions with CTC and hence TMs. The second family of spacetimes is in a sense milder. These spacetimes do not per se entail CTCs but, as we shall see in the following sections, can be easily manipulated so to form them.

12.3.1 Time Machine Rotating Solutions

A succinct (incomplete) list of this kind of solutions includes (see [33] for a more complete treatment)

- **van Stockum spacetimes**: Infinitely long cylinders of spinning dust with density increasing with radii. Tipler cylinders are included in this family (with a massive cylinder replacing the cylindrical distribution of dust).
- **Gott's spacetimes**: these are spacetimes, e.g. with two infinitely long, parallel, cosmic strings longitudinally spinning around each other.
- **Gödel universe**: this is the famous solution found by Kurt Gödel in 1949 which describes a globally rotating spacetime filled with (homogeneously distributed) dust and a (positive) cosmological constant fine-tuned to match the energy density of the dust. The solution is not isotropic due to the rotation, however the homogeneity implied by the matter distribution requires that the direction but not the position of the rotation "axis" is determined. Indeed, any event in the spacetime can be considered at the origin of the rotating frame and lies on some CTCs.
- **Kerr–Newman black holes**: Rotating (neutral or charged) black holes are endowed with a region, inside the Cauchy horizon, where the Killing vector associated to invariance under rotations about the spin axis becomes timelike. Given that the orbits of this vector are necessarily closed curves this implies the presence of CTCs.

The first three items of this list are often (somewhat irreverently) characterised as GIGO, i.e. as solutions "garbage in-garbage out", which means that these are solutions characterised by somewhat unphysical matter/energy distributions (e.g. infinitely long cylinders or strings) and/or global rotation (e.g. Gödel universe). In the case of the rotating black hole solutions, the common objection is instead that the chronology-violating region is located well within the inner/Cauchy horizon. The well-known instability associated to this global structure (infinite blueshift) is per se a warning bell that this (classical) instability might lead to an internal geometry very different from the one predicted by the Kerr family of solutions. There is however a second class of dangerous spacetimes that are not as easily dismissed because they "per se" do not posses CTC and can be grouped under the name of "superluminal travel allowing" spacetimes.

12.3.2 Faster than Light Travel Spacetimes

There are two well-known kinds of spacetimes in general relativity which allow for faster than light travel, these are warp drives and traversable wormholes. Let us summarise their main features here.

Warp drives: Warp drives (where the most known declination is the Alcubierre warp drive (see the previous chapter) discovered in 1994 [1]) are a different sort of spacetimes where a spherical region with flat (or almost flat) geometry, a bubble, can move at arbitrary speed thanks to the simultaneous contraction and expansion of spacetime respectively at its front and rear. Of course such a geometry does not violate local Lorentz invariance as this still holds locally around each point of spacetime. However, geometrically speaking general relativity does not pose any

bound on the relative motion of different regions of spacetime. Noticeably, these geometries need exotic matter for being realised, i.e. matter which violates some energy condition (typically the null one).

Traversable wormholes: The concept of a "spacetime shortcut", a sort of tunnel connecting points of spacetime which might be otherwise separated by long distances arose several times in the literature. The first to be discovered was the so-called Schwarzschild wormhole often called Einstein–Rosen bridge (after the name of the authors of the 1935 paper [12] that brought it to the general attention albeit it was already discovered in 1916 by Flamm [14]). The latter connects two asymptotically flat regions in an eternal black hole spacetime. Unfortunately this class of wormholes is not traversable. Indeed if they connect two parts of the same universe, it was shown [16] that they will pinch off too quickly for light (or any massive particle) to travel from one exterior region to the other. However, traversable wormhole solutions were found in 1988 by Morris and Thorne [26, 27] (and later developed by several authors, see e.g. [33, 34] and references therein). These are wormhole structures whose throat is held open by variably large amounts of exotic matter.

Let us consider more in detail one solution for each of these classes.

12.3.2.1 The Alcubierre Warp Drive in a Nutshell

The Alcubierre warp drive geometry was introduced by Miguel Alcubierre in 1994 (see Ref. [1]) and represents a bubble containing an almost flat region, moving at arbitrary speed within an asymptotically flat spacetime. Mathematically its metric can be written as

$$ds^2 = -c^2dt^2 + [dx - v(r)dt]^2 + dy^2 + dz^2 \,, \tag{12.1}$$

where $r \equiv \sqrt{[x - x_c(t)]^2 + y^2 + z^2}$ is the distance from the centre of the bubble, $\{x_c(t), 0, 0\}$, which is moving in the x direction with arbitrary speed $v_c = dx_c/dt$. Here $v(r) = v_c f(r)$ and f is a suitable smooth function satisfying $f(0) = 1$ and $f(r) \to 0$ for $r \to \infty$. To make the warp drive travel at the speed $v_c(t)$, the spacetime has to contract in front of the warp drive bubble and expand behind it. It is easy to see that the worldline $\{x_c(t), 0, 0\}$ is a geodesic for the above metric. Roughly speaking, if one places a spaceship at $\{x_c(t), 0, 0\}$, it is not subject to any acceleration, while moving faster than light with respect to someone living outside of the bubble (here the spaceship is basically treated as a test particle, see Ref. [23] for a more general treatment). The spaceship inside the warp drive bubble is, as a matter of fact, isolated from the spacetime surroundings and cannot interact with them, however one could in principle conceive to build a sort of "interstellar railway" running from Earth to a distant planet which by a coordinated generation of energy violating matter could

locally produce and move a warp drive, with a spaceship inside, at superluminal speeds.

A curious characteristic of the Alcubierre warp drive geometry, which is seldom mentioned, is that in a superluminal travel between two events in spacetime A and B, the proper time as measured by the traveller inside the bubble is not subject to the standard relativistic time slowdown. This is due to the fact that the observer inside the warp drive finds itself at rest in a basically flat portion of spacetime and (classically) does not perceive the bubble motion. Indeed, observers at rest outside, as well as internal travellers, will measure essentially the same amount of travel duration in terms of their proper times (see Eq. (12.1)). This contrasts with what normally happens in standard special relativity. From the traveller's point of view if one approaches the speed of light, the proper time duration to go from A to B becomes arbitrarily short. Instead, using a warp drive to shorten this time duration one would need to increase the warp drive velocity to larger and larger speeds which will not affect the relation between the proper time of the warp drive traveller and that of some observer outside at rest.

12.3.2.2 Traversable Morris–Thorne Wormholes in a Nutshell

Traversable Morris–Thorne wormholes [26, 27] are time independent, non-rotating and spherically symmetric solutions of general relativity describing a bridge/passage between two asymptotically flat regions (not necessarily in the same universe albeit this is the case we are interested in here). They are described by a simple metric

$$ds^2 = -e^{2\Phi(\ell)}dt^2 + d\ell^2 + r^2(\ell)\left[d\theta^2 + \sin^2\theta d\phi^2\right], \tag{12.2}$$

where one requires $\ell \in (-\infty, +\infty)$, absence of event horizons and metric components at least C^2 in ℓ. Furthermore asymptotic flatness for $\ell \to \pm\infty$ is imposed by requiring

$$\lim_{\ell\to\pm\infty}\left\{\frac{r(\ell)}{|\ell|}\right\} = 1 \qquad \text{i.e.} \quad r(\ell) = |\ell| + O(1) \quad \text{for} \quad \ell \to \pm\infty \tag{12.3}$$

for space asymptotic flatness and

$$\lim_{\ell\to\pm\infty} \Phi(\ell) = \Phi_{\pm} = \text{constant and finite} \tag{12.4}$$

for spacetime asymptotic flatness. The radius at the wormhole throat is $r_0 \equiv \min\{r(\ell)\}$ which can always be chosen to be at $\ell = 0$.

This metric is a solution of the Einstein equations but requires a stress–energy tensor (SET) $T^{\mu}{}_{\nu} = \text{diag}(-\rho(r), \tau(r), p_\theta(r), p_\phi(r))$ with radial tension $\tau(r) = -p_r(r)$ which violates the null energy condition (NEC) which states the positivity of the product $T_{\mu\nu}k^\mu k^\nu$ for any null-like vector k^μ. More precisely there is always

some r_* such that for any $r \in (r_0, r_*)$ one has $\rho(r) - \tau(r) < 0$ which is tantamount to NEC violation (which also implies the violation of the weak, strong and dominant energy conditions, see e.g. [33]). Of course this implies that also at the throat the NEC is violated and specifically one finds

$$\tau(r_0) = \frac{1}{8\pi G r_0^2} \approx 5 \cdot 10^{36} \left(\frac{10\ \mathrm{m}}{r_0}\right)^2 \frac{\mathrm{N}}{\mathrm{cm}^2}\,, \tag{12.5}$$

so that as anticipated a huge tension is required for keeping a macroscopic wormhole open.

12.3.2.3 Objections and Answers

The common objections against these spacetimes are twofold. One consists in noticing that this "superluminal travel allowing" spacetimes generically require large amounts of exotic (energy violating) matter (e.g. for a traversable wormhole with a throat of about one metre one would need about one Jupiter of matter with negative energy density), at least within GR (in alternative theories of gravity this does not need to be the case). The other objection has to do with the way such structures could be formed in the first place. For example, forming from nowhere a wormhole would imply a change in topology which is forbidden in classical GR and anyway is known to lead to unacceptable large particle production from the vacuum [2, 25]. However, such objections could be seen as engineering challenges, in the sense that no no-go theorem tells us that we cannot generate exotic matter in a given region (indeed we can do so, in small quantities, e.g. with the Casimir effect) or that in principle one cannot "grow" macroscopic wormholes from those expected to be spontaneously produced at the Planck scale in the so-called Wheeler spacetime foam.

So in conclusion, within GR nothing seems to prevent, at least in principle, the possibility of superluminal travel at the moderate cost to solve few (daunting) engineering problems and to produce and control sufficiently large amounts of exotic matter. Of course this sounds pretty exciting but on second thoughts also very worrisome. Indeed, it is quite easy to transform any superluminal travel capable structure into a time machine. This is what we shall analyse in the following section.

12.4 Time Machines from Faster than Light Travel

Wormholes and warp drives are two ways in which one could travel faster than light (FTL). As we shall see, within the GR framework the existence of CTCs is strongly linked with the seemingly milder concept of FTL travel.

Probably the question that lay public asked more frequently to specialists in relativity is "why is it not possible to travel faster than light". We do not know why

but, leaving aside for the moment the cosmological realm, we have not observed any counterexample. Moreover, the theory of special relativity was born out of requiring this as a postulate and after one hundred years of development we can say with confidence that the number of predictions and verifications of this theory are quite robust (at least at currently explored energies, see e.g. [21] for a recent review).

In special relativity, the proper time of an observer freezes out when the observer approaches the speed of light. Beyond that, travelling in a spacelike trajectory amounts to having your proper time running backwards in time, the seed of time travel. But these trajectories are precisely the ones not allowed for real massive particles. By allowing the deformation of the light-cone structure, general relativity opens new venues into the connection between CTC and FTL travel.

As we already mentioned general relativity is constructed so that locally nothing can travel outside the light cone, so locally nothing can travel faster than light. However, somewhat surprisingly general relativity can indeed accommodate FTL travel. The cleanest situation one can think of is the following. Consider an asymptotically flat spacetime. In the asymptotic limit a light ray will traverse this spacetime in a straight line and at the speed of light. However, geometrically the light-cone structure deep in the spacetime can be such that a light ray could traverse this region faster than it would be done by his homologous at infinity.

This is possible because there is a tight connection between this sort of formulation of FTL travel and the existence of violations of the energy conditions. While the presence of positive distributions of energy results in Shapiro time delays, when light rays traverse negative energy distributions they are advanced. For instance, K. Olum [28] proved that to produce a FTL configuration one needs to violate the Weak Energy Condition. Related investigations were carried over in [35] dealing with weak fields. This association between ray advancement and negative energy has also been used to produce a slightly different formulation and proof of a positive mass theorem [29].

From this perspective, the problem of FTL travel is transmuted in general relativity into the problem of understanding the nature of the possible sources of gravity. In fact, without restricting the possible matter content general relativity allows in principle all imaginable Lorentzian geometries.

Leaving aside the energy-condition-violations issue, how can one manipulate FTL configurations such as warp drives or wormholes to build a time machine?

12.4.1 The Warp Drive Case

Before any warp drive is operating, consider an inertial reference frame in which two locations A and B are at rest. At some point, we arrange a warp drive so that someone in the bubble travels from A and B in a time interval $0 < t_B - t_A < |x_B - x_A|$ as measured from this inertial frame. From the perspective external to the warp drive the trajectory of the bubble seems to be spacelike (although it is not). Now, make a change of inertial frame to describe the same configuration, one travelling with a velocity

close to the speed of light in the same direction of the warp drive. In this inertial frame the trajectory of the warp drive will be such that $t'_B - t'_A < 0$, it is as if the warp drive was running backwards in time. Then, in this frame one just needs to arrange another warp drive to travel back from B to A so that $0 < t'_{AB} - t'_B < |t'_B - t'_A|$. In this way the time t'_{Ab} can be made smaller than t'_A, that is, one can come back to the initial position before the very forth and back journey has started: CTCs and a chronological horizon have been formed. Of course, the discussed warp drive is just a special case, as the above reasoning would apply to any device allowing faster than light propagation at arbitrary speeds while special relativity holds (see e.g. [22] for an extensive discussion).

12.4.2 The Wormhole Case

The same type of time machine configuration can be produced using a wormhole. Consider one mouth of the wormhole to be always at rest in one inertial frame. Then, in principle one can make time to run slower in the other mouth, for instance by making this mouth to travel towards the other at a certain velocity (a special relativistic effect) or by placing it close to a very compact object (a general relativistic effect). In the first case, if we wait long enough since the second mouth starts moving, a light ray produced in the first mouth and sent through the throat will come up again in the inertial frame in the past. This travel back in time can be strong enough so that the ray now travelling from the second mouth to the first through the standard path in spacetime arrives earlier than it was sent in the first place. Again, CTCs and a chronological horizon have been formed.

12.4.3 Some Analogue Gravity Lessons

One can build warp drive geometries in analogue gravity systems, such as a flowing fluid [5]. Is it then possible to build a time machine using a fluid? No, definitely it is not. From the perspective of the lab one of the two warp drives needs to be running backwards in time. From the same perspective one can perfectly tilt the sound cones (by producing background flows) so that the sound travels quicker or slower than in a fluid at rest. However, to tilt a sound cone so that it runs backwards in time needs to pass through a configuration in which the sound velocity becomes infinite (and beyond). This is clearly not possible as the background fluid flow cannot be arranged to reach an infinite velocity. So although an internal observer could follow the same line of reasoning leading from warp drives to time machines the existence of an external and more fundamental causality forbids to perform this step. Any proper manipulation of the system in terms of initial data developments will show that no causal paradoxes can occur. The fundamental causality of the Minkowskian lab is the one that controls the evolution of the system and that is always running forward in time.

If the general relativity causality were not the only one in reality, a similar argument could be in place. The fact that there is a hand waving argument to build a time machine does not imply that this can be realised as a well-defined initial data problem. There might be deeper layers of reality, with a perfectly well-defined causality but possessing FTL characteristics, fooling us (a nice discussion of these possibilities can be found in [18]). Nature shows that indeed there are many different causalities operating for different degrees of freedom. To this day it is a well-supported hypothesis that the general relativity causality encompassed all of the rest. It is this fundamentality that allows to think about FTL travel and time machines. However, it is clear that whether the general relativity causality is the ultimate causality and whether one could build this type of configurations can only be ultimately distinguished by experiments.

An example of the previous discussion is provided by dispersive modifications of the general relativity behaviour. A superluminal dispersion can produce FTL travel without the need *per se* of allowing the construction of time machines. It will all depend on the specific causal characteristics of the final system of differential equations. Superluminal modifications of the dispersion relations could be obtained as a semiclassical result of an underlying theory of quantum gravity (see e.g [17]). Also, it was shown by Scharnhorst [31] that in a Casimir vacuum photons travelling perpendicular to the plate boundaries could achieve FTL (although the suppossed effect is too small to be measured in current experimental setups). In this case, it has been shown that even if this effect existed it will not break the tenets of special relativity [22] maintaining the existence of a constant c which is invariant under Lorentz transformations. On the other hand, they also show that the Scharnhorst effects cannot be used to build a time machine in the form described above. In this sense, the Scharnhorst effect would exhibit a mild violation of the speed of light limit.

But even before reflecting onto more or less speculative possibilities based on beyond general relativity effects, the very construction of a time machine has to be examined at the light of a well-defined initial value problem within the very framework of general relativity. As is conjectured to happen with Cauchy horizons, it might be that the formation of a chronological horizon is non-generic and unstable to perturbations. The analysis of possible classical instabilities has to be complemented by one of semiclassical instabilities in a hierarchy of possibilities. One of these semiclassical instabilities will be discussed later on in this chapter.

12.5 Time Travel Paradoxes and Possible Solutions

We have seen in the previous sections that GR seems to entail the possibility of time travel and that at the classical level nothing seems to forbid a priori the production of CTCs in otherwise healthy spacetimes, especially by making a careful use of the superluminal travel allowed by some solution with exotic matter.

The reason why the possibility of time travel is per se considered a deeply worrying weakness of the theory is that time travel to the past is per se logically paradoxical (apart from being a limit to the predictive power of the theory as e.g. singularities are as well). Indeed, the possibility to travel back in time (there is no logical paradox with travelling into the future, which is anyway already allowed by special relativity, think about the *apparent* twin paradox often quoted in text books) is *logically* paradoxical in two ways:

Grandfather paradox: The first way is related to the fact that when travelling back into the past our actions can affect what was supposed to stem from that past. So, for example, we could end up killing our grandfather and in this way prevent our own birth. Then how can we exist and change the past in the first place?

Bootstrap paradox: If we could travel back in time we could generate information from nothing. For example, someone could copy a mathematical theorem proof from a textbook, then travel back in time to find the mathematician who first published the proof before he published it, and simply pass the proof to the mathematician. In this case, the information in the proof has no origin.

So it is easy to see that time travel is a quite dangerous feature to have built in within your theory of spacetime dynamics. In what comes next we shall analyse why GR allows for this feature. But before doing this, we need to have the mathematical tools for being precise about what we mean by time travel.

In order to avoid such paradoxes, several approaches have been proposed in the past. We shall here summarise them briefly.

- **Bifurcating reality**: The most radical approach consists in accepting the possibility of modifying the past so creating a bifurcation in the future. This obviously requires also a radical rewriting in physics and possibly stepping from pseudo-Riemannian manifolds to non-Hausdorff ones.[1]
- **Multiverse/many-worlds reality**: This alternative is much in line with the one above but is based on quantum rather than classical reasoning. Reality would be made of several (possibly infinite) copies of our universe corresponding to all the possible outcomes of the many choices/measurements continuously performed. In this sense, changing the past does not produce any paradox as it would just correspond to take a pre-existing parallel reality while all the realities in which we never changed the past continue to exist.
- **Novikov's consistency conjecture**: In this case, one postulates CTCs never lead to paradoxes because only periodic solutions are really allowed. More rigorously, one conjectures a principle of self-consistency, which states that the only solutions to the laws of physics that can occur locally in the real Universe are those which are globally self-consistent [15]. That means that if you go back in time and attempt any action to change the past you will not only be unable to succeed but any of these actions will have to be there in first place for things to unfold the

[1] A Hausdorff manifold is a manifold for which for any two different points x_1 and x_2 belonging to the manifold admit open sets O_1 and O_2, with $x_1 \in O_1$ and $x_2 \in O_2$, such that $O_1 \cap O_2 = \emptyset$.

way they did in your past. You had to travel back in time and do what you had to do. A strict consistency without escape. The conjecture has been subject of debate with attempts to prove it in simple systems such as billiard balls moving in spacetimes with traversable wormholes [11]. The upshot from this and other studies is that there seems to exist self-consistent solutions for every possible billiard ball initial trajectory. However, this only applies to initial conditions outside of the chronology-violating region of spacetime, which is, as said, bounded by a Chronological/Cauchy horizon and moreover it is very difficult to extend to more complex, realistic, systems.

- **Hawking Chronology protection conjecture**: Finally a more orthodox solution to the paradoxes entailed by time machines is that the latter are always unstable due to quantum effects. More precisely, the chronology protection conjecture says that the laws of physics will always prevent the formation of CTCs [19]. Much work was put in the last 25 years for proving this conjecture on the base of calculations using QFT in curved spacetime (see e.g. [32, 34] and references therein). Generically, all these calculations confirm that the renormalized stress–energy tensor (SET) tends to blow up in the proximity of a chronological horizon. Nonetheless, no conclusive proof up to date can be provided due to the fact that generically the Green functions fail to be Hadamard on a Chronological/Cauchy horizon [20]. Given that the Hadamard behaviour of two points Green functions is a crucial requirement for deriving a renormalised SET and hence the semiclassical Einstein equations that would predict the evolution of spacetime, we are hence obliged to accept that no definitive proof is derivable from this framework. Actually, the behaviour of the Green functions close to a chronological horizon seems to indicate that contributions for Planck scale physics will always be non-negligible in its proximity and that consequently a full quantum gravity framework will be the only hope to prove the conjecture.

So it looks like no conclusive answer is available for how to cope with the widespread possibility of spacetimes with CTCs in GR missing a deeper understanding of spacetime as it should be provided by full-fledged quantum gravity. Nonetheless, a more humble approach can sometimes be taken. As we have seen most of the "rotation-based" time machines can be discarded on physical grounds (including the interior of a Kerr black hole). So, much more dangerous is the appearance of spacetimes such as wormholes and warp drives that would "only" require sufficiently large amounts of exotic matter. In particular, we have also seen that it is very debatable if a macroscopic wormhole can be created (problems with topology change) from nothing or growth from a hypothetic spacetime foam. No such objection though are present for a superluminal warp drive (the type that could be used to build a time machine). So is there anything forbidding the formation of such structures? Can semiclassical gravity provide at least in this case a definitive prediction? In what follows, we shall show that the answer to this question is in fact affirmative.

12.6 Superluminal Warp Drive Instabilities: A Pre-emptive Chronology Protection at Work?

We are going to discuss now the instability associated with a superluminal warp drive. In the actual computation, we shall restrict our attention to the $1+1$ dimensions case (since in this case one can carry out a complete analytic treatment). Changing coordinates to those associated with an observer at the centre of the bubble, the warp drive metric (12.1) becomes

$$ds^2 = -c^2 dt^2 + [dr - \bar{v}(r)dt]^2\,, \qquad \bar{v} = v - v_c\,, \tag{12.6}$$

where $r \equiv x - x_c(t)$ is now the signed distance from the centre. Let us consider a dynamical situation in which the warp drive geometry interpolates between an initial Minkowski spacetime [$\hat{v}(t,r) \to 0$, for $t \to -\infty$] and a final stationary superluminal ($v_c > c$) bubble [$\hat{v}(t,r) \to \bar{v}(r)$, for $t \to +\infty$]. To an observer living inside the bubble this geometry has two horizons, a *black horizon* $\mathscr{H}^+$ located at some $r = r_1$ and a *white horizon* $\mathscr{H}^-$ located at $r = r_2$. Here, let us just add that from the point of view of the Cauchy development of $\mathscr{I}^-$ these spacetimes possess Cauchy horizons.

12.6.1 Light Ray Propagation

Let us now consider light ray propagation in the above-described geometry. Only the behaviour of right-going rays determines the universal features of the renormalised stress–energy tensor (RSET), just like outgoing modes do in the case of a black hole collapse (see Refs. [3, 4, 13]). Therefore, we need essentially the relation between the past and future null coordinates U and u, labelling right-going light rays. There are two special right-going rays defining, respectively, the asymptotic location of the black and white horizons. In terms of the right-going past null coordinate U, let us denote these two rays by $U_{\rm BH}$ and $U_{\rm WH}$, respectively. The finite interval $U \in (U_{\rm WH}, U_{\rm BH})$ is mapped to the infinite interval $u \in (-\infty, +\infty)$ covering all the rays travelling inside the bubble. For rays which are close to the black horizon, the relation between U and u can be approximated as a series of the form [13]

$$U(u \to +\infty) \simeq U_{\rm BH} + A_1 e^{-\kappa_1 u} + \frac{A_2}{2} e^{-2\kappa_1 u} + \dots\,. \tag{12.7}$$

Here A_n are constants (with $A_1 < 0$) and $\kappa_1 > 0$ represents the surface gravity of the black horizon. This relation is the standard result for the formation of a black hole through gravitational collapse. As a consequence, the quantum state which is vacuum on $\mathscr{I}^-$ will show, for an observer inside the warp drive bubble, Hawking radiation with temperature $T_H = \kappa_1/2\pi$.

Equivalently, we find that the corresponding expansion in the proximity of the white horizon is [13]

$$U(u \to -\infty) \simeq U_{\rm WH} + D_1 e^{\kappa_2 u} + \frac{D_2}{2} e^{2\kappa_2 u} + \dots \,, \tag{12.8}$$

where $D_1 > 0$ and κ_2 is the white hole surface gravity and is also defined to be positive. The interpretation of this relation in terms of particle production is not as clear as in the black horizon case and a full study of the RSET is required.

12.6.2 Renormalized Stress–Energy Tensor

In past null coordinates U and W the metric can be written as

$$ds^2 = -C(U, W) dU dW \,. \tag{12.9}$$

In the stationary region at late times, we can use the previous future null coordinate u and a new coordinate $\tilde{w}$, defined as

$$\tilde{w}(t, r) = t + \int_0^r \frac{dr}{c - \bar{v}(r)} \,. \tag{12.10}$$

In these coordinates the metric is expressed as

$$ds^2 = -\bar{C}(u, \tilde{w}) du d\tilde{w} \,, \quad C(U, W) = \frac{\bar{C}(u, \tilde{w})}{\dot{p}(u)\dot{q}(\tilde{w})} \,, \tag{12.11}$$

where $U = p(u)$ and $W = q(\tilde{w})$. In this way, $\bar{C}$ depends only on r through u, $\tilde{w}$.

For concreteness, we refer to the RSET associated with a quantum massless scalar field living on the spacetime. The RSET components for this case acquire the well-known expressions [6, 10]

$$T_{UU} = -\frac{1}{12\pi} C^{1/2} \partial_U^2 C^{-1/2} \,, \tag{12.12}$$

$$T_{WW} = -\frac{1}{12\pi} C^{1/2} \partial_W^2 C^{-1/2} \,, \tag{12.13}$$

$$T_{UW} = T_{WU} = \frac{1}{96\pi} C \; R \,. \tag{12.14}$$

Using the relationships $U = p(u)$, $W = q(\tilde{w})$ and the time independence of u and $\tilde{w}$, one can calculate the RSET components in the stationary (late times) region (see [13]).

Let us here focus on the energy density inside the bubble, in particular at the energy density ρ as measured by a set of free-falling observers, whose four velocity is $u_c^\mu = (1, \bar{v})$ in (t, r) components. For these observers neglecting transient terms one obtains [13] $\rho = T_{\mu\nu} u_c^\mu u_c^\nu = \rho_{\rm st} + \rho_{\rm dyn}$, where we define a static term $\rho_{\rm st}$, depending only on the r coordinate through $\bar{v}(r)$,

$$\rho_{\rm st} \equiv -\frac{1}{24\pi}\left[\frac{\left(\bar{v}^4 - \bar{v}^2 + 2\right)}{\left(1-\bar{v}^2\right)^2}\bar{v}'^{\,2} + \frac{2\bar{v}}{1-\bar{v}^2}\bar{v}''\right], \tag{12.15}$$

and a, time-dependent, dynamic term

$$\rho_{\rm dyn} \equiv \frac{1}{48\pi}\frac{\mathscr{F}(u)}{(1+\bar{v})^2}, \quad \text{where} \quad \mathscr{F}(u) \equiv \frac{3\ddot{p}^2(u) - 2\dot{p}(u)\dddot{p}(u)}{\dot{p}^2(u)}. \tag{12.16}$$

12.6.3 Physical Interpretation

Let us start by looking at the behaviour of the RSET in the centre of the bubble at late times. Here $\rho_{\rm st} = 0$, because $\bar{v}(r=0) = \bar{v}'(r=0) = 0$. One can evaluate $\rho_{\rm dyn}$ from Eq. (12.16) by using a late-time expansion for $\mathscr{F}(u)$, which gives $\mathscr{F}(u) \approx \kappa_1^2$, so that $\rho(r=0) \approx \kappa_1^2/(48\pi) = \pi T_H^2/12$, where $T_H \equiv \kappa_1/(2\pi)$ is the usual Hawking temperature. This result confirms that an observer inside the bubble measures a thermal flux of radiation at temperature T_H. Thus, apart from the energy-condition-violating mass distribution engineered to create the warp drive, the semiclassical calculation shows that one would need to add to the configuration an energy supply to maintain the unavoidable Hawking flux.

Let us now study ρ on the horizons $\mathscr{H}^+$ and $\mathscr{H}^-$. Here, both $\rho_{\rm st}$ and $\rho_{\rm dyn}$ are divergent because of the $(1+\bar{v})$ factors in the denominators. Using the late time expansion of $\mathscr{F}(u)$ in the proximity of the black horizon (see Ref. [13]) one gets

$$\lim_{r\to r_1}\mathscr{F}(u) = \kappa_1^2\left\{1 + \left[3\left(\frac{A_2}{A_1}\right)^2 - 2\frac{A_3}{A_1}\right]e^{-2\kappa_1 t}\,(r-r_1)^2 + \mathscr{O}\left((r-r_1)^3\right)\right\}, \tag{12.17}$$

and expanding both the static and the dynamic terms up to order $\mathscr{O}(r-r_1)$, one obtains that the diverging terms ($\propto (r-r_1)^{-2}$ and $\propto (r-r_1)^{-1}$) in $\rho_{\rm st}$ and $\rho_{\rm dyn}$ exactly cancel each other [13]. It is now clear that the total ρ is $\mathscr{O}(1)$ on the horizon and does not diverge at any finite time. By looking at the subleading terms,

$$\rho = \frac{e^{-2\kappa_1 t}}{48\pi}\left[3\left(\frac{A_2}{A_1}\right)^2 - 2\frac{A_3}{A_1}\right] + A + \mathscr{O}(r-r_1), \tag{12.18}$$

where A is a constant, we see that on the black horizon the contribution of the transient radiation (different from Hawking radiation) dies off exponentially with time, on a time scale $\sim 1/\kappa_1$.

Close to the white horizon, the divergences in the static and dynamical contributions cancel each other, as in the black horizon case. However, something distinctive occurs with the subleading contributions. In fact, they now become

$$\rho = \frac{e^{2\kappa_2 t}}{48\pi}\left[3\left(\frac{D_2}{D_1}\right)^2 - 2\frac{D_3}{D_1}\right] + D + \mathscr{O}(r - r_1) \ . \tag{12.19}$$

This expression shows an exponential increase of the energy density with time. This means that ρ grows exponentially and eventually diverges along $\mathscr{H}^-$. In a completely analogous way, one can study ρ close to the Cauchy horizon. Performing an expansion at late times ($t \to +\infty$) one finds that the RSET diverges also there [13].

Note that the above-mentioned divergences are very different in nature. The divergence at late times on $\mathscr{H}^-$ stems from the untamed growth of the transient disturbances produced by the white horizon formation. The Hawking radiation produced in the black hole will be accumulating at the white horizon. The RSET divergence on the Cauchy horizon is due instead to the well-known infinite blueshift suffered by light rays while approaching this kind of horizon. While the second can be deemed inconclusive because of the Kay–Radikowski–Wald theorem, the first one is inescapable. Apart from the energy supply necessary to maintain the Hawking fluxes, one would have to compensate an ever-increasing accumulation of energy at the white horizon.

The appearance of event horizons can of course be avoided if the superluminal travel does not last forever. However, these two exponentially fast accumulations of energy will still occur. The exponential increase will be controlled by $1/\kappa = \Delta/c$, where Δ represents the thickness of the warp drive walls. Note that, in order to get a time scale of even 1s, one would need $\Delta \sim 3 \times 10^8$ m.

Another way of taming the exponential accumulations of energy could be to travel in non-straight trajectories.[2] But also this solution seems impractical. First of all, to reach B starting from A in a superluminal manner with a wiggling trajectory would require faster velocities than in the straight trajectory case. Furthermore, one might avoid the problem of energy accumulation at the cost of introducing additional devices to produce the wiggling. At the semiclassical level, it is to be expected that the fast wiggling would also produce additional energy fluxes that one would also have to sustain (a sort of analogue of superradiant particle production).

Summarising, although not logically impossible, finite duration superluminal warp drive configurations will be very costly to produce and probably technically extremely hard to realise in practice.

[2] A possibility brought to us by E. Martín-Martínez and L.J. Garay in a personal communication.

12.7 Warp Drive Instabilities Under Dispersion

The semiclassical instability described above stems from standard, relativistic, QFT in curved spacetimes. One might wonder if the story could be different in scenarios, where a UV completion of the theory is provided by some quantum gravity (QG) scenario. This is the case of analogue gravity inspired Lorentz breaking scenarios (see e.g. Ref. [5]), where generically one expects the standard relativistic dispersion relation for the matter field to be replaced by $E^2 = c^2(p^2 + p^n/M_{\rm LIV}^{n-2})$, where $M_{\rm LIV}$ is normally assumed to be of the order of the Planck mass and n is some integer greater than two.

Indeed, this is a modification that could potentially stabilise the warp drive, as it is by now understood that modified LIV dispersion relations are able to remove Cauchy horizons instabilities and tame the divergence of fluxes at white hole horizons. The reason for this is simple, UV rays in the above dispersion relations are faster or slower than light, in both cases light rays will not accumulate at the horizons (past or forward in time depending on the black or white nature of the horizon) as they normally do. Hence no built-up of divergences can take place.

Can this be a scenario where a quantum gravity inspired UV completion/ regularisation could appear? This problem was dealt with in Ref. [9] and surprisingly it leads to a negative answer, i.e. not even the breakdown of Lorentz invariance can stabilise superluminal warp drives. Let us see how this works.

For the sake of simplicity, we work in $1 + 1$ dimensions and consider a stationary situation. We can define a new spatial coordinate $X = x - v_c t$ (we use a different notation to avoid confusion between the two calculations) so the warp drive metric becomes

$$ds^2 = -c^2 dt^2 + [dX - V(X)dt]^2 \,, \tag{12.20}$$

where $V(X) = v_c(f(X) - 1)$ is negative. In this spacetime, ∂_t is a globally defined Killing vector field whose norm is given by $c^2 - V^2$: it is timelike within the bubble, its norm vanishes on the two horizons, and it is spacelike outside. In a fluid flow analogy, this would correspond to two superluminal asymptotic regions separated by a black and a white horizon from a compact internal subluminal region [9].

We can now consider a massless scalar field with a quartic dispersion relation. In covariant terms, its action reads

$$S_\pm = \frac{1}{2}\int d^2x\sqrt{-g}\left[g^{\mu\nu}\partial_\mu\phi\partial_\nu\phi \pm \frac{(h^{\mu\nu}\partial_\mu\partial_\nu\phi)^2}{M_{\rm LIV}^2}\right], \tag{12.21}$$

where $h^{\mu\nu} = g^{\mu\nu} + u^\mu u^\nu$ is the spatial metric in the direction orthogonal to the unit timelike vector field u^μ which specifies the preferred frame used to implement the dispersion relation. The sign $\pm$ in Eq. (12.21) holds for superluminal and subluminal dispersion, respectively.

Using Eq. (12.20) and taking $u^\mu = (1, V)$ in the t, X frame, the wave equation is

$$\left[(\partial_t + \partial_X V)(\partial_t + V\partial_X) - \partial_X^2 \pm \frac{1}{M_{\rm LIV}^2}\partial_X^4\right]\phi = 0. \tag{12.22}$$

and $V(x)$ can be shaped so to mimic the warp drive geometry. Because of stationarity, the field can be decomposed in stationary modes $\phi = \int d\omega e^{-i\omega t}\phi_\omega$, where ω is the conserved (Killing) frequency. Correspondingly, at fixed ω the dispersion relation reads

$$(\omega - Vk_\omega)^2 = k_\omega^2 \pm \frac{k_\omega^4}{M_{\rm LIV}^2} \equiv \Omega_\pm^2, \tag{12.23}$$

where $k_\omega(X)$ is the spatial wave vector, and Ω the *comoving* frequency, *i.e.* the frequency in the aether frame. The quartic nature of the dispersion relations allows up to four solutions/modes and the problem in the end reduces to solve a Bogoliubov matrix of coefficients relating the mode in the asymptotic regions (assuming $M_{\rm LIV}$ to be larger than any other scale in the problem) [9].

The upshot is that in the case of subluminal dispersion relation there is an instability related to the well-known "laser effect" [8]. In the case of superluminal dispersion relations there is an infrared divergence that leads to a linear growth in time of the energy density proportional to $M_{\rm LIV}$ and the square of the warp drive wall surface gravity κ (we are assuming $\kappa_1 = \kappa_2 = \kappa$) [9]. Using quantum inequalities, Ref. [30], one can argue that κ must be of the order of the Planck scale, which implies that the growth rate is also of that order (unless $M_{\rm LIV}$ is very different from that scale). So, even in the presence of superluminal dispersion, warp drives would be unstable on short time scales. This instability, although not logically impossible to compensate for, would be extremely costly making it technologically implausible.

In conclusion with or without local Lorentz invariance FTL travel via warp drives seems inherently extremely problematic. This might seem a very depressing piece of news to science fiction fans, however let us stress that still any subluminal propagation (even just at 99.999% of the speed of light) seems to be free of most of the superluminal problems, of course, if the daunting engineering problems related to the very formation of the warp drive will be solved in a (possibly distant) future. Not too bad for novels and movies...

12.8 Conclusions

In summary, the above-discussed warp drive case shows that the very formation of the spacetime structure, allowing for a TM built up via FTL travel, can be very problematic—to say the least—well within the realm of semiclassical gravity. Remarkably, this conclusion still holds even when one allows for high energy deviations from local Lorentz invariance as inspired by analogue models of gravity. So, this "pre-emptive" chronology protection seems to strongly suggest that FTL travel will be always forbidden by the underlying structure of spacetime and gravity.

Interestingly enough, there are hints how this might work in some QG models. For examples in Causal Set Theory [7], the discrete structure replacing spacetime is made of sets of points which must be acyclic, meaning that no element in a causal set can causally precede itself. This in turn implies that CTCs are ruled out a priori. Actually, there is concrete evidence that generically Planck scale approaches based only on the causal structure of a spacetime cannot permit CTCs in the continuous classical limit (neither a corresponding phenomenon in their quantum counterparts) [24].

Looking forward it would be interesting to see if the warp drive analysis presented here could be extended to the formation of a traversable wormhole. As we have said in this chapter there are already hints that the very formation, e.g. with an otherwise flat spacetime, might be forbidden due to a divergent particle production generated by the topology change [2, 25] but it is not so clear if quantum gravity (via Wheeler spacetime foam "harvesting" or by allowing relic wormholes from the big bang era) could not get around this apparent obstruction.

In any case, whatever the final answer on the viability of FTL travels and TM might be, let us stress that it will be very relevant to our understanding of the fabric of reality as it might very well tell us crucial features that will have to be embedded in our models of the spacetime at the Planck scale and beyond. So this research is not just a fun field for sci-fi fans, but should be considered a very crucial aspect of general relativity which might teach us the way forward. We hence hope that this humble contribution would stimulate further research in this field.

Acknowledgements The authors wish to acknowledge that the research reported here was done also in collaboration with A. Coutant, S. Finazzi and R. Parentani. S.L. also wish to acknowledge the John Templeton Foundation for the supporting grant #51876. C.B. acknowledge support provided by the Spanish MINECO through the project FIS2014-54800-C2-1 (with FEDER contribution), and by the Junta de Andalucìa through the project FQM219.

References

1. Alcubierre M. The warp drive: hyperfast travel within general relativity. Class Quant Grav. 1994;11:L73–7.
2. Anderson A, DeWitt B. Does the topology of space fluctuate? Found Phys. 1986;16(2):91–105.
3. Barcelo C, Liberati S, Sonego S, Visser M. Quasi-particle creation by analogue black holes. Class Quant Grav. 2006;23:5341–66.
4. Barcelo C, Liberati S, Sonego S, Visser M. Fate of gravitational collapse in semiclassical gravity. Phys. Rev. 2008;D77:044,032.
5. Barcelo C, Liberati S, Visser M. Analogue gravity. Living Rev. Rel. 2005;8:12 [Living Rev. Rel.14,3(2011)].
6. Birrell ND, Davies PCW. Quantum fields in curved space., Cambridge monographs on mathematical physicsCambridge: Cambridge Univ. Press; 1984. http://www.cambridge.org/mw/academic/subjects/physics/theoretical-physics-and-mathematical-physics/quantum-fields-curved-space?format=PB.
7. Bombelli L, Lee J, Meyer D, Sorkin R. Space-time as a causal set. Phys Rev Lett. 1987;59:521–4.
8. Corley S, Jacobson T. Black hole lasers. Phys Rev. 1999;D59:124,011.

9. Coutant A, Finazzi S, Liberati S, Parentani R. Impossibility of superluminal travel in Lorentz violating theories. Phys Rev. 2012;D85:064,020.
10. Davies PCW, Fulling SA, Unruh WG. Energy momentum tensor near an evaporating black hole. Phys Rev D. 1976;13:2720–3.
11. Echeverria F, Klinkhammer G, Thorne KS. Billiard balls in wormhole spacetimes with closed timelike curves: classical theory. Phys Rev D. 1991;44:1077–99.
12. Einstein A, Rosen N. The particle problem in the general theory of relativity. Phys Rev. 1935;48:73–7. http://link.aps.org/doi/10.1103/PhysRev.48.73.
13. Finazzi S, Liberati S, Barcelo C. Semiclassical instability of dynamical warp drives. Phys Rev. 2009;D79:124,017.
14. Flamm L. Beiträge zur Einsteinschen Gravitationstheorie. Hirzel (1916)
15. Friedman J, Morris MS, Novikov ID, Echeverria F, Klinkhammer G, Thorne KS, Yurtsever U. Cauchy problem in spacetimes with closed timelike curves. Phys Rev D. 1990;42:1915–30.
16. Fuller RW, Wheeler JA. Causality and multiply connected space-time. Phys Rev. 1962;128:919–29.
17. Gambini R, Pullin J. Nonstandard optics from quantum space-time. Phys Rev. 1999;D59:124,021.
18. Geroch R. Faster Than Light? AMS/IP Stud Adv Math. 2001;49:59–70.
19. Hawking SW. Chronology protection conjecture. Phys Rev D. 1992;46:603–11.
20. Kay BS, Radzikowski MJ, Wald RM. Quantum field theory on space-times with a compactly generated Cauchy horizon. Commun Math Phys. 1997;183:533–56.
21. Liberati S. Tests of Lorentz invariance: a 2013 update. Class Quant Grav. 2013;30:133,001.
22. Liberati S, Sonego S, Visser M. Faster than c signals, special relativity, and causality. Ann Phys. 2002;298:167–85.
23. Lobo FSN, Visser M. Fundamental limitations on 'warp drive' spacetimes. Class Quant Grav. 2004;21:5871–92.
24. Malament D. Causal theories of time and the conventionality of simultaneity. Noûs. 1977;11(3):293–300.
25. Manogue CA, Copeland E, Dray T. The trousers problem revisited. Pramana. 1988;30:279–92.
26. Morris MS, Thorne KS. Wormholes in spacetime and their use for interstellar travel: a tool for teaching general relativity. Am J Phys. 1988;56(5):395–412.
27. Morris MS, Thorne KS, Yurtsever U. Wormholes, time machines, and the weak energy condition. Phys Rev Lett. 1988;61(13):1446.
28. Olum KD. Superluminal travel requires negative energies. Phys Rev Lett. 1998;81:3567–70.
29. Penrose R, Sorkin RD, Woolgar E. A Positive mass theorem based on the focusing and retardation of null geodesics. 1993.
30. Roman TA. Some thoughts on energy conditions and wormholes. In: Proceedings, 10th Marcel Grossmann Meeting On recent developments in theoretical and experimental general relativity, gravitation, and relativistic field theories. MG10, Rio de Janeiro: Brazil; 2004. 20-26 July 2003. pp. 1909–1922
31. Scharnhorst K. On Propagation of light in the vacuum between plates. Phys. Lett. B. 1990;236:354–9.
32. Visser M. Hawking's chronology protection conjecture: Singularity structure of the quantum stress energy tensor. Nucl. Phys. B. 1994;416:895–906.
33. Visser, M.: Lorentzian wormholes: From Einstein to Hawking. Springer (1995)
34. Visser, M.: The Quantum physics of chronology protection. In: Workshop on Conference on the Future of Theoretical Physics and Cosmology in Honor of Steven Hawking's 60th Birthday Cambridge, England, January 7-10, 2002, pp. 161–176 (2002). URL http://alice.cern.ch/format/showfull?sysnb=2303505
35. Visser M, Bassett B, Liberati S. Superluminal censorship. Nucl. Phys. Proc. Suppl. 2000;88:267–70.

Index

F.S.N. Lobo (ed.), *Wormholes, Warp Drives and Energy Conditions*,
Fundamental Theories of Physics 189, DOI 10.1007/978-3-319-55182-1